

Sugars and organic acids separation by preparative chromatography with strong anionic resins: model-based three-fraction process design

Séparation de sucres et d'acides organiques par chromatographie préparative avec des résines anioniques fortes : conception d'un procédé à trois fractions par modélisation

Thèse de doctorat de l'université Paris-Saclay

École doctorale n°579 : sciences mécaniques et énergétiques, matériaux et géosciences (SMEMaG)

Spécialité de doctorat : Génie des procédés

Graduate School : Sciences de l'ingénierie et des systèmes. Référent : CentraleSupélec

Thèse préparée dans l'unité de recherche **Laboratoire de Génie des Procédés et Matériaux (LGPM)**,

Chaire de Biotechnologie (Saclay, CentraleSupélec), 51110 Pomacle, France

Sous la direction de **Patrick PERRE**, Professeur,
le co-encadrement de **Julien LEMAIRE**, maître de conférence

Thèse soutenue à Pomacle, le 08/02/2022, par

Wuyang ZHONG

Composition du Jury

Marie-Odile SIMONNOT

Professeure, Université de Lorraine (EEIGM)

Présidente

Laurence MUHR

Professeure, Université de Lorraine (ENSIC)

Rapporteure &

Examinateuse

Nabil GRIMI

Professeur, Université de Technologie de Compiègne (UTC)

Rapporteur &

Examinateur

Claire FARGUES

Maître de Conférences HDR, Université de Paris-Saclay (IUT Orsay)

Examinateuse

Patrick PERRE

Professeur, Université de Paris-Saclay (CentraleSupélec)

Directeur de thèse

Julien LEMAIRE

Maître de Conférences, Université de Paris-Saclay
(CentraleSupélec)

Co-encadrant

Sugars and organic acids separation by preparative chromatography with strong anionic resins: model-based three-fraction process design

Wuyang ZHONG

Under the direction of

Patrick PERRE and Julien LEMAIRE

Doctoral thesis defense on February 8, 2022

This work was carried out in the “Centre Européen de Biotechnologie et de Bioéconomie” (CEBB), supported by the Chair of Biotechnology of CentraleSupélec.

Acknowledgments

I would first like to thank my parents for supporting me during my whole 8 years in France.

I would like to thank my supervisor, M. Julien LEMAIRE and M. Patrick PERRE, whose expertise was invaluable in formulating the research questions and methodology. Your insightful feedback pushed me to sharpen my thinking and brought my work to a higher level.

I would like to acknowledge my colleagues from these years at CentraleSupélec for their wonderful collaboration.

Titre : Séparation de sucres et d'acides organiques par chromatographie préparative avec des résines anioniques fortes : conception d'un procédé à trois fractions par modélisation

Mots clés : Lit mobile simulé, Résines échangeuses d'ions, Chromatographie, Acides organiques

Résumé : Cette étude porte sur l'utilisation d'une résine anionique forte pour séparer des molécules biosourcées par chromatographie préparative. Deux sucres (glucose et xylose) et cinq acides organiques (acides formique, acétique, lactique, succinique et citrique) ont été étudiés, en tant que produits communs issus de l'hydrolyse de la biomasse lignocellulosique ou de procédés biotechnologiques. Les principaux objectifs de ce travail sont i) l'acquisition d'une meilleure compréhension des mécanismes de rétention et ii) le développement d'un outil de simulation prédictif, pour aider à la conception et à l'optimisation de procédés de chromatographie multi-colonne, plus particulièrement à trois fractions.

Une approche combinée d'expériences (élution simple et analyse frontale) et de modélisation (formulation continue non linéaire et hors équilibre) a été utilisée pour atteindre cet objectif. Un modèle de rétention plus prédictif, appelé "modèle hybride", a été développé pour les acides organiques, en combinant une adsorption compétitive de type Langmuir avec de l'échange d'ions. De plus, un modèle continu, résolu par la méthode CE/SE (*conservation element / solution element*), a été utilisé pour mieux prédire l'élution et la dispersion des composés.

Les propriétés du lit et les coefficients de dispersion axiale et de vitesse de transfert ont été estimés en effectuant des élutions simples avec des solutions pures. Les isothermes d'adsorption ont été établis pour chaque composé par analyse frontale, afin d'estimer les coefficients d'équilibre correspondants. Ensuite, des élutions simples avec un mélange binaire ont été réalisés pour valider notre modèle hybride de rétention.

Finalement, ce modèle hybride a d'abord été utilisé pour simuler et optimiser un procédé multi-colonne à deux fractions bien connus, appelé ISMB (Improved Simulated Moving Bed). Le résultat remarquable de ce travail de modélisation, a été de pouvoir ensuite concevoir un nouveau procédé à trois fractions plus efficaces que le procédé habituel utilisant deux ISMB en cascade, à la fois en termes de productivité et de facteur de dilution.

Title: Sugars and organic acids separation by preparative chromatography with strong anionic resins: model-based three-fraction process design.

Keywords: Simulated moving bed, Ion exchange resins, Chromatography, Organic acids

Abstract: This study investigates the use of strong anionic resin to separate biosourced molecules by preparative chromatography. Two sugars (glucose and xylose) and five organic acids (formic, acetic, lactic, succinic, and citric acids) were studied, as common products of lignocellulosic biomass hydrolysis or biotechnological processes. The main objectives of the work are i) to get a better understanding of retention mechanisms and ii) to develop a predictive simulation tool, to support design and optimization of multi-column chromatography processes, more particularly for three-fraction separation.

A combined approach of experiments (pulse tests and frontal analysis) and modelling (continuous non-linear and non-equilibrium formulation) was used to achieve these objectives. A more predictive retention model, called "hybrid model", was developed for organic acids, by combining competitive Langmuir adsorption with ion-exchange. Moreover, a continuous model, solved by the CE/SE (conservation element / solution element) method, was used to better predict compounds elution and dispersion.

Bed properties, axial dispersion and transfer rate coefficients were estimated by performing pulse tests with pure solutions. Adsorption isotherms were established for each compound by frontal analysis, to estimate corresponding equilibrium coefficients. Then, pulse tests with binary mixture were performed to validate our retention hybrid model.

Finally, this hybrid model was used first to simulate and optimize the well-known two-fraction multi-column process, called ISMB (Improved Simulated Moving Bed). Then, as an outstanding achievement, it was used to design a new three-fraction process more efficient than the usual process using two ISMB in cascade, both in terms of productivity and dilution factor.

Table of contents

Table of contents	2
List of figures	4
List of tables	7
List of symbols	9
List of abbreviations.....	11
Introduction	14
Chapter I. Literature review.....	21
1 Context	21
1.1 Lignocellulosic biomass	21
1.2 Sugars, organic acids and their valorization	24
1.3 Hemicellulose hydrolysis.....	32
2 Chromatography separation	34
2.1 Different chromatography processes	34
2.2 Pulse tests and frontal analysis.....	37
2.3 Preparative chromatography	40
3 Modeling of chromatography	51
3.1 Column models.....	51
3.2 Physico-chemical formulation of the chromatography system.....	52
3.3 Numerical methods.....	58
4 Objectives of the thesis	64
Chapter II. Materials and methods.....	66
1 Experimental devices	66
2 Protocols of pure component column tests	72
2.1 Determination of bed properties	72
2.2 Mass transfer coefficients determination: van Deemter curve	73
2.3 Langmuir adsorption coefficients estimation: frontal analysis	75
2.4 Uncertainty range determination	76
3 Chromatography modeling.....	76
3.1 Continuous column model.....	76
3.2 Formulation and computational strategy of the continuous model.....	81
3.3 The discontinuous model.....	85
4 Simulation of multi-column system: 3C-ISMB process	86
Chapter III. Estimation of components physico-chemical properties and bed parameters.....	90
1 Bed property determination	90
1.1 Bed porosity	90
1.2 Resin ion exchange capacity.....	93
2 Frontal analysis.....	93
2.1 Glucose and xylose	93
2.2 Organic acids	94
3 Pulse tests.....	99
3.1 Presentation of van Deemter curves.....	99

3.2	Estimation of van Deemter coefficients	101
Chapter IV. Batch chromatography simulation (pulse tests).....	104	
1	Influence of ka , D , K_{iex} and Langmuir coefficients	104
1.1	Influence of global mass transfer coefficient ka and axial dispersion coefficient D	104
1.2	Influence of Langmuir coefficients and K_{iex}	106
2	Identification of Langmuir and ion-exchange coefficients	107
3	Validation of coefficients for binary mixture and comparison with Langmuir model	112
4	Comparison between continuous column model and discontinuous column model	113
Chapter V. Multi-column process simulation and development.....	116	
1	Introduction	116
2	3C-ISMB simulation for binary separation (formic and succinic acids)	116
2.1	Estimation of V_{ssx} and adjustments of concentration profiles	117
2.2	System tuning and simulation with the hybrid model	119
2.3	Comparison with Langmuir model	123
3	Development of ternary SMB system (glucose, formic acid and succinic acid)	126
3.1	3C-ISMB in cascade.....	126
3.2	A new SSMB ternary separation process (3F4C SSMB).....	131
Conclusion and recommendations	134	
Bibliography	137	
Appendices.....	155	
Appendix I:.....	156	
Frontal analysis curves and isotherms.....	156	
Appendix II:.....	161	
Pulse tests and van Deemter curves:	161	
Appendix III:	168	
SBA (strong base anion) resin selectivity coefficients	168	
Appendix IV:	169	
CE/SE method proof	169	
Appendix V:	173	
Curve-fitting results.....	173	
Appendix VI:	176	
Synthèse de la manuscrit	176	

List of figures

Introduction

Figure 0-1. The number of scientific publications from 1998-2022 where the words “simulated moving bed” are included. Data extracted from sciencedirect.com.15

Chapter I

Figure 1-1. Presentation of lignocellulosic biomass [Isikgor et al. 2015].	21
Figure 1-2. The structure of cellulose [D. Klemm, 1998].....	22
Figure 1-3. An example of hemicelluloses pattern [Himme M.E., 2009].	23
Figure 1-4. Glucose molecule (ring form).....	25
Figure 1-5. Molecule of xylose, linear chains [Hongzhan C., 2017].....	26
Figure 1-6. D and L structure of Arabinose [Hongzhan C. 2017].....	28
Figure 1-7. Citric acid molecule.....	29
Figure 1-8. Molecule of succinic acid.	30
Figure 1-9. Formic acid molecule.	30
Figure 1-10. Lactic acid molecule.	31
Figure 1-11. Acetic acid molecule.	31
Figure 1-12. Chromatography classification.....	35
Figure 1-13. Example of pulse test chromatographic profile.....	37
Figure 1-14. Frontal analysis chromatography profile..	39
Figure 1-15. True moving bed [Abdelemoumen et al., 2006]	41
Figure 1-16. Schematic of four-zone SMB chromatography for binary separations. Column positions are periodically switched in opposite direction of liquid flow [Q. Lehe, 2018].	42
Figure 1-17. Sorbex (UOP) system with SMB technique [Lianming S., 2005].	42
Figure 1-18. The working principles of ISMB system.	45
Figure 1-19. (a) Schematic diagram of a six-column SMB system. (b) Principle of operation of SMBR and four-subinterval Varicol (port switching schedule) [Hariprasad et al., 2003]..	46
Figure 1-20. An example of sequential SMB process [K. K. Jeung, 2003].	48
Figure 1-21. The two sub-steps of J.O. process [G. Vera, 2001].	49
Figure 1-22. A simplified schema of a six-column MCSGP process.....	49
Figure 1-23. A simplified schema of the concentration profile inside the system shown in Figure 1-22.....	50
Figure 1-24. A simplified schema of BioSC process with profile obtained from the official site of Novasep (https://www.novasep.com/media/articles-and-publications/18multicolumn-chromatography-bioprocess.pdf).	51
Figure 1-25. Mass transfer resistance in the scale of bead.....	54
Figure 1-26. Example of van Deemter curve that measured experimentally.....	56
Figure 1-27. The SE (solution element, gray part) and CE (conservation element, green and blue part) at position j and time n. Values at point A are calculated from point C and E at n-1/2, values at C or E are obtained from points at n-1 via the CE and SE at the point at n-	

1/2.....	63
----------	----

Chapter II

Figure 2-1. Schema of experimental installations.....	66
Figure 2-2. The volumetric pump MasterFlex.....	67
Figure 2-3. The YMC-ECO 25 column with UMA 150 resin inside.....	68
Figure 2-4. The VETIRY 1810 Conductivity and pH monitor, 159 UV detector.....	68
Figure 2-5. The FC-203B fraction collector.....	69
Figure 2-6. The pressure-drop of the resin bed (from datasheet of resin).....	71
Figure 2-7. The physical model in the scale of bed and resin. D the axial dispersion coefficient (in $\text{m} \cdot \text{s}^{-2}$), v the interstitial velocity (in $\text{m} \cdot \text{s}^{-1}$).	77
Figure 2-8. Retention mechanisms of a strong anion IEX resin [Lemaire et al. 2016].....	79
Figure 2-9. Schematic illustration of organic acid adsorption by hydrogen bonding on sulfate or hydrogen sulfate counter-anions. Each SO_4^{2-} or HSO_4^- has eight lone pair elections....	80
Figure 2-10. Schema of cascade reactor, with Q the flowrate and X_n the concentration in mobile phase of component X at the end of reactor n.....	85
Figure 2-11. Process scheme of the 3C-ISMB process studied in the present work.	87

Chapter III

Figure 3-1. Residence time distribution in the system (resin bed + pump + tubing + fitting) ...	91
Figure 3-2. Residence time distribution in the system without the column.....	92
Figure 3-3. Part of resin bed (1/4 of a cylinder sample with 2mm of height) scanned by Tomography.....	92
Figure 3-4. Frontal analysis of glucose with UMA 150 resin in sulfate form at pH 1.5 and 20°C.	93
Figure 3-5. Isotherm of glucose and xylose with UMA 150 resin in sulfate form at pH 1.5 and 20°C.	94
Figure 3-6. Frontal analysis of acetic acid with UMA 150 resin in sulfate form at pH 1.5 and 20°C.	94
Figure 3-7. Isotherm of acetic acid with UMA 150 resin in sulfate form at pH 1.5 and 20°C....	95
Figure 3-8. Isotherm of acetic acid – linear relation between $1/q$ and $1/c$	95
Figure 3-9. Langmuir isotherms of all organic acids with UMA 150 resin in sulfate form at pH 1.5 and 20°C. Experimental results correspond to points and regression curves correspond to continuous lines.....	96
Figure 3-10. Pulse tests of glucose at different flowrates with UMA 150 resin in sulfate form at pH 1.5.	99
Figure 3-11. Van Deemter curve of glucose with UMA 150 resin in sulfate form at pH 1.5....	100
Figure 3-12. Pulse test of succinic acid at different flowrates with UMA 150 resin in sulfate form at pH 1.5.....	100
Figure 3-13. Van Deemter curve of succinic acid with UMA 150 resin in sulfate form at pH 1.5.	101

Chapter IV

Figure 4-1. Impact of global mass transfer coefficient (Fig. A at the top) and dispersion coefficient (Fig. B at the bottom) on the chromatography profile.....	105
Figure 4-2. Influence of k_s (Fig.A on the top) and K_{iex} (Fig. B at the bottom) on organic acid outlet profile.....	107
Figure 4-3. Fitting curves to experimental points in the case of citric acid.....	108
Figure 4-4. Influence of ion-exchange on the outlet profile of formic (Fig.9-A), succinic (Fig.9-B) and citric acids (Fig.9-C).....	111
Figure 4-5. Multi-component pulse test to compare predictions of the model which considers only Langmuir adsorption to the hybrid model which also considers ion-exchange.....	112
Figure 4-6. Multi-component pulse test to compare predictions of continuous model to discontinuous model.....	114

Chapter V

Figure 5-1. Moving of concentration profiles inside a 3C-ISMB system during one step (composed of four substeps).....	117
Figure 5-2. Elution curve and breakthrough curve of formic acid and succinic acid as well as approximative positions of V_{minS} , V_{maxS} , V_{minF} , V_{maxF} , obtained from simulation at pH 1.5 and 25°C.....	118
Figure 5-3. Concentration profiles after each substep, with the initial V_{ssx} estimation, in steady state.....	121
Figure 5-4. Concentration profiles after each substep with the best V_{ssx} tuning, in steady state (there is no substep 3 because $Velu2$ is set to 0).....	122
Figure 5-5. Optimized concentration profiles after each substep, in steady state, simulated with Langmuir model.....	124
Figure 5-6. Concentration profiles after each substep, in steady state, simulated with the hybrid model, but with the best V_{ssx} tuning obtained from the Langmuir model.....	125
Figure 5-7. Elution and breakthrough curves of glucose, formic acid and succinic acid, and approximative position of V_{minF} , V_{maxF} , V_{minM} , V_{maxM} , V_{minS} and V_{maxS} (Obtained from simulation at pH 1.5 and 25°C).....	127
Figure 5-8. Concentration profiles after each substep, in steady state, after optimization of the first 3C-ISMB unit.....	128
Figure 5-9. Concentration profiles after each substep, in steady state, after optimization of the second 3C-ISMB unit	129

List of tables

Chapter I

Table 1-1. Composition of different lignocellulosic biomass.....	22
Table 1-1. Composition of hemicellulose hydrolysis	24
Table 1-2. Examples of purification methods used during hemicellulose hydrolysis treatment.....	34
Table 1-4. A list of some SMB process and its developments in recent years.	43

Chapter II

Table 2-1. Specifications of the159- UV detector.....	69
Table 2-2. Main characteristics of the strong anionic resin used in this work (DIAION UMA 150). By convention, SBA resins produced with trimethylamine are called Type 1. When amine is dimethylethanalamine, it is called Type 2.....	70
Table 2-3. Chemical Materials used in experiments.....	71
Table 2-4. Operating conditions of pulse tests.....	73
Table 2-5. Experimental conditions of frontal analysis.	75

Chapter III

Table 3-1. Uncertainty range of affinity coefficient K_s for glucose and xylose.	94
Table 3-2. qSO_4tot range estimation as a function of eluent composition at different pH (H_2SO_4 solution).	97
Table 3-3. Langmuir coefficients of five organic acids with UMA 150 resin in sulfate form at pH 1.5 and 20°C.....	97
Table 3-4. Refined Langmuir coefficients assuming only NHA values which make sense for the five organic acids studied with UMA 150 resin in sulfate form at pH 1.5 and 20°C..	99
Table 3-5. Van Deemter coefficients for all compounds with UMA 150 resin in sulfate form at pH 1.5.....	102
Table 3-6. Impact of theoretical B values on axial dispersion coefficient D	102

Chapter IV

Table 4-1. Operating conditions of single component pulse tests.....	108
Table 4-2. Experimental uncertainty ranges of ka , D and their refined values.....	109
Table4-3. The comparison of ks , Ni between the refined values and experimental results.	109
Table 4-4. Comparison of K_{iex} estimated from pulse tests to the value given by the resin supplier.....	110

Table 4-5. Parameters used for multi-component pulse test simulation.....	112
Table 4-6. Parameters used for multi-component pulse test simulation with discontinuous model.....	113

Chapter V

Table 5-1. The input and output configuration of each column during a complete cycle ...	120
Table 5-2. Simulation parameters for 3C-ISMB process with binary mixture.....	120
Table 5-3. 3C-ISMB performance before and after optimization.....	123
Table 5-4. 3C-ISBM performance simulated with Langmuir model.....	124
Table 5-5. 3C-ISMB performance with the hybrid model (corresponding to experimental expectation) with the best tuning obtained from simulations with the Langmuir model.	125
.....	
Table 5-6. Two strategies to separate ternary mixture with two ISMB units.....	126
Table 5-7. Glucose parameters for 3C-ISMB process simulation with ternary mixture.....	127
Table 5-8. Performance of the first 3C-ISMB unit for ternary separation.....	128
Table 5-9. Performance of the second 3C-ISMB unit for ternary separation.....	129
Table 5-10. Global performance of the 2 ISMB process for ternary separation.....	130
Table 5-11. Purity requirements for the separation.....	131
Table 5-12. Optimum performance of the 3F4C SSMB process.....	132

List of symbols

α = liquid side local mass transfer coefficient (in s^{-1})

β = packing characterization factor

b = linear equilibrium constant between two phases

C_p = pore concentration in solution

C_s = pore concentration in solid phase

c_i = concentration at the interface in the mobile phase (in mol/L)

c = concentration in the mobile phase (in mol/L)

c_j^i = concentration of the component j at the interface (in $mol.m^{-3}$)

d_p = mean particle diameter (in m)

D = axial dispersion coefficient (in $m.s^{-2}$)

D_{ext} = external diffusion coefficient (in m^2/s)

D_{eff} = effective diffusion coefficient (in m^2/s)

D_m = molecular diffusion coefficient (in m^2/s)

ε = effective porosity of the bed

ε_b = total bed porosity

ε_p = inner porosity of bead

F = volume ratio between stationary and mobile phases = $(1-\varepsilon)/(\varepsilon)$

F_A = dilution factor of compound A

J = flux (mol/m^2)

k_{sj} = adsorption constant of component j

k_f = local mass transfer coefficient (in m/s)

N_{tot} = number of lone electron pairs on each counter anion ($N_{tot} = 8$)

N_{column} = number of columns

N_j = number of lone electron pair occupied by each adsorbed molecule.

n = number of experimental points

ρ = mass density

Pe = Peclet number

Pe_p = Peclet number based on the particle size

p = number of coefficients to estimate

q = concentration in the stationary phase (in mol.m⁻³_{resin})

q_j^{eq} = theoretical concentration of component j in the stationary phase (in mol.m⁻³)

$q_{SO_4}^{tot}$ = total amount of sulfate and hydrogen sulfate counter-anions on resin surface (in mol/L_{res}),

Q = volumetric flow rate (in BV/h)

R_A = recovery rate of compound A

r = particle radius

S = surface area of the cross-section (in m²)

Sc = Schmidt number

Sh = Sherwood number

τ = tortuosity

T_{step} = step time

μ = dynamic viscosity

V = eluted volume (in BV)

V_{ssx} = Eluted volume in substep X (in BV)

V_R = mean retention volume (in BV)

v = interstitial velocity (in m/s)

ω = stripping power per mass unit of liquid

W/F = volume ratio between the eluent (Water) and the product (Feed)

W_h = width at half peak height (= 2.355 σ for a Gaussian peak),

δ = film thickness (m)

θ_{min} = minimum relative error

σ^2 = variance

$\chi_{\alpha,n-p}$ = critical Chi-squared value with α risk (set to 5%) and $n - p$ degrees of freedom

List of abbreviations

3C-ISMB = three-column Improved Simulated Moving Bed

3F4C-SSMB = three-fraction four-column Sequential Simulated Moving Bed

A.A. = acetic acid

AHA = alpha-hydroxy acid

BV = bed volume

C.A. = citric acid

CE/SE = conservation element/solution element

ECP = elution by characteristic points

F.A. = formic acid

FACP = frontal analysis by characteristic points

FAST = Finnsugar applexion separation technology

HBV = hepatitis B virus

HETP = height equivalent to a theoretical plate

HFCS-55 = high fructose corn syrup with a fructose content of 55% in the dry mass

IC or IXC = ion chromatography

ISMB = Improved/Intermittent Simulated Moving Bed

J.O. process = Japan-Organo process

L.A. = lactic acid

L-FMAU = 1-(2-fluoro-5-methyl-beta, L-arabinofuranosyl)-uracil

LLC = partition or liquid–liquid chromatography

LSC = liquid-solid chromatography

M.F. = multiFeed

NET = number of theoretical plates

NMCI = Nippon Mitsubishi Chromatography Improved

NPC = normal-phase chromatography

ODE = ordinary differential equations

OSS = outlet Streams Swing

PBS = polybutylene succinate

PC = paper chromatography

PDE = partial differential equation

PLA = polylactic acid

RPC = reversed-phase chromatography

S.A. = succinic acid

SEC = size-exclusion chromatography

SMB = simulated Moving Bed

SS = sub-steps

SSMB = Sequential Simulated Moving Bed

SSR = sum of squared residuals

SST = sum of squared totals

TLC = thin-layer chromatography

TMB = true moving bed

VAM = vinyl acetate monomer

Introduction

Background

Chromatography is a widely used separation method based on the contrasted adsorption affinity to the solid of each component involved in a system. Chromatographic methods are characterized by their high selectivity and ability to separate components of very similar physical and chemical properties.

Chromatography is commonly seen as an analytical method used in environment protection, biology, medicine, pharmaceutics, foodstuff control, and quality control in the chemical, petrochemical, gas and other industries [Lauren V. & Marcia E., 2021]. Meanwhile, chromatography satisfies the growing demand for high purity products. Thus, it is also used as a commercial separation process known as preparative chromatography.

Preparative chromatography consists in pushing a mixture (generally liquid) through a column filled with a porous solid phase using a mobile phase called the eluent. Its principle is to separate different compounds according to their affinities towards both phases, affecting their travel speed and retention time inside the column [David et al., 2020]. The solid phase can be composed of dense or microporous resin beads. Hundreds of resin types exist on the market to separate ions or organic molecules, depending on their structures and retention mechanisms.

Batch chromatography was the first preparative chromatography technique which is limited by its low productivity and significant dilution rate. Later, true moving bed was invented to overcome the shortcomings of batch chromatography. However, it was soon abandoned because of various problems such as particle attrition, bed porosity variation, and the unstable flow rate.

In order to overcome these disadvantages, SMB (simulated moving bed) process was developed and first applied by Broughton and Gerhold in 1961 [Broughton D.B. & Gerhold C.G., 1961]. SMB simulates the continuous counter-current movement of the solid phase by the simultaneous switch of all injection/collection points along successive columns or column sections. High productivity, purity, and simple operation control can be accomplished due to the continuous operating mode.

The current industrial applications of SMB mainly include extraction of p-xylene [Minceva, M. & Rodrigues, A.E., 2002; Minceva, M. & Rodrigues, A.E., 2005], corn wet milling [Pynnonen B., 1998], and fructose/glucose separation [Azevedo D.C.S., & Rodrigues A.E., 2001]. Recently, its applications have been extended to the separation of fine and complicated chemicals, such as chiral drugs and biological components [Ribeiro et al., 2011; Faria, R.P.V. & Rodrigues, A.E., 2015].

Introduction

A typical SMB process contains 4-zones. Each zone has its specific function represented by injection/collection points located at inlet and outlet. At the end of a step, all zones are connected and form a closed loop. Recently, SMB process has been developed for better performance while changing various conditions such as flowrate, operating procedure, temperature/pressure, feed concentration. A literature search on words “simulated moving bed” indicates that many scientific papers, including the two words, have been published over the last 20 years, as depicted in Figure 1. During the period 1998-2008, many kinds of research works or developments were conducted on the operating conditions of SMB, such as temperature/pressure gradient, flowrate, feed concentration, etc. From 2010, a tremendous increase of published papers can be observed that can partly be explained by the invention of new processes or the optimization of the existing processes.

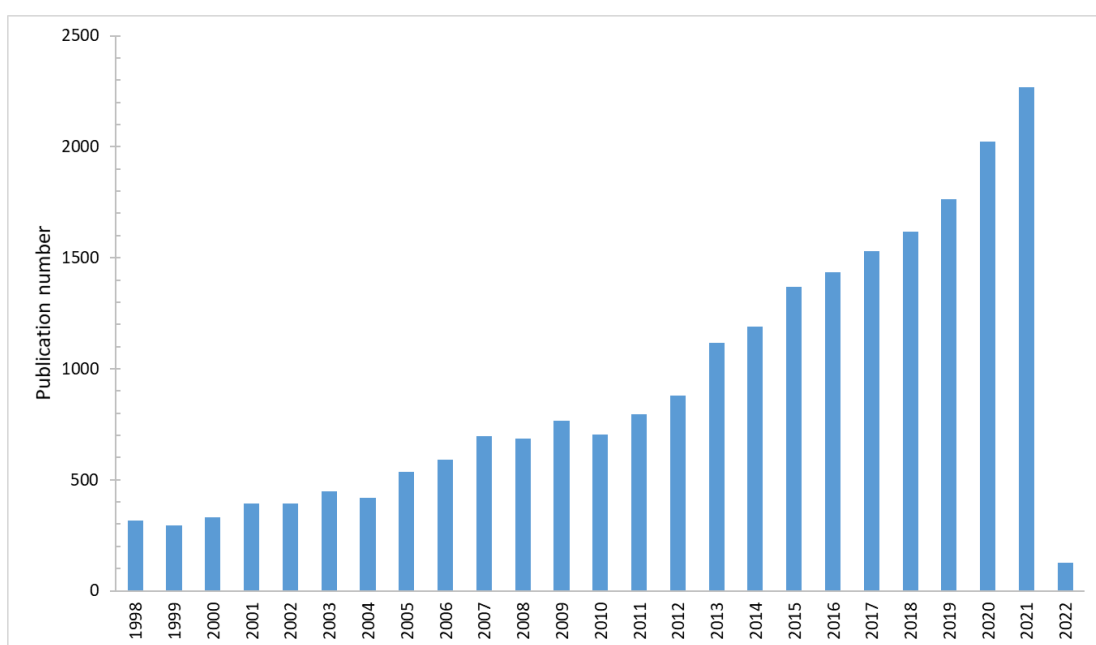


Figure 0-1. The number of scientific publications from 1998-2022 where the words “simulated moving bed” are included. Data extracted from sciencedirect.com.

A common weakness of these SMB-type processes is that they allow only binary separation. Repetitive usage of these units is required to separate ternary mixture, which increases dilution and production costs. Ternary processes with fewer columns have been invented and applied to the industry. Meanwhile, their application is limited because of their weak performance or manipulation complexity.

Another common default of these multi-column processes is that it takes a long time to stabilize. As concentration profiles in the system are not visible, this brings difficulty during optimization. Numerical simulation allows operating conditions to be tuned before real experiments, thus reducing experimental costs in material and time. Development of accurate and reliable mathematical models for chromatography is thus necessary for efficient optimization of the design and operation of such a complex process of ternary mixture separation.

Introduction

Research motivation and objectives

Preparative chromatography is known as an attractive separation technique due to its high selectivity and purity. Development of a ternary SMB process is an appealing research subject due to its industrial interest. However, as explained above, a detailed and predictive mathematical modeling is necessary to obtain insight into the dynamics and equilibria of chromatographic separations in order to reduce the time and effort required when developing new chromatographic processes. It is important to develop a numerical tool with an appropriate model to represent the process dynamics without excessive computational time.

A previous work [Lemaire *et al.*, 2016] shows that the Langmuir adsorption model is unsuitable for organic acid separation with strong anionic ion exchange resin. Both retention time and peak shape are not well predicted by the Langmuir model.

In addition, although ternary separation could be accomplished in a cascade of SMB units or other ternary processes, the system complexity and the large amount of expensive stationary phases represent significant drawbacks. Processes with fewer columns were proposed in recent decades. However, their performance is barely satisfying. It would then be attractive if we could develop an SMB-typed ternary process with fewer columns with better performance.

To address this challenge, this PhD work first addresses the need for a predictive model. At first, to address this issue raised for strong anionic resins, a new retention model was proposed which could predict the tailing of succinic acid and citric acid. Secondly, an accurate numerical tool for chromatography simulation was developed. Finally, a ternary SMB-typed process with fewer columns is proposed. It has a better performance than two binary SMB processes in cascade. Accordingly, the research work is divided into four parts as detailed below.

A comparison between chromatography models and their formulations

The first part of the study is to select a chromatography model and define its corresponding mathematical formulations. Selecting an appropriate model requires a compromise between accuracy and computational time. This task contains three steps:

- a) An overview of existing models
- b) A study of the current ion-exchange problem
- c) The choice of the most appropriate model

Determination of required physico-chemical parameters in the developed retention model

Numerical simulation requires physico-chemical parameters as input. Some come from literature with good accuracy, but others need to be determined. Specific experiments were performed and analyzed to determine unknown parameters or refine values provided by suppliers or literature. This strategy involves three kinds of parameters:

Introduction

- a) Bed properties characterization,
- b) Langmuir coefficients determination by frontal analysis,
- c) Mass transfer and dispersion coefficients estimation by tracing the van Deemter curve.

Simulation of single component tests and multi-component tests

As stated before, numerical simulation is likely to reduce experimental costs, namely for multi-column process development. It also identifies unknown parameters and refines experimental results. Chromatography modelling and simulation contain four steps:

- a) Physical formulation,
- b) Numerical strategy,
- c) Identification of unknown parameters or refining parameters from experiments by curve fitting,
- d) Binary mixture pulse test simulation to validate the developed model and parameters.

Development of a ternary multi-column process

Binary ISMB process was simulated firstly with both hybrid model and Langmuir model to show the importance of model precision during multi-column process simulation. Then, a working principle was first defined to develop a new ternary process. From this, an adapted optimization strategy was done by simulation. Finally, a comparison with other technologies allowed its competitiveness to be clearly stated.

- a) ISMB process simulation with both hybrid model and Langmuir model for binary mixture separation
- b) Ternary SMB process development and optimization strategy
- c) Simulation and comparison with an existing ternary process

Outline of the thesis

This work aims to develop a reliable numerical tool that is supposed to be implemented in a multi-column chromatography simulation program, and to predict and optimize the performance of a newly developed ternary simulated moving bed process with strong anionic ion exchange resin. Two sugars (glucose and xylose) and five organic acids (formic, acetic, lactic, succinic, and citric acids) were selected for the case study, which are commonly seen during hydrolysis or fermentation of hemicellulose.

In chapter I, the context and history of chromatography are examined. Retention mechanisms, along with their formulations, are detailed in this chapter. SMB and its various developments are presented. Different formulations and numerical strategies that are commonly used in chromatography are briefly introduced.

Introduction

In chapter II, experimental materials and devices are presented. Protocols used during frontal analysis and pulse tests are detailed. The non-linear non-ideal ion-exchange chromatography modeling is chosen for the study, with both continuous and discontinuous column models. A new model (called hybrid model) which combines detailed Langmuir adsorption and ion exchange effect was presented. The application of CE/SE (conservation element/solution element) method is presented in detail. 3C-ISMB (three columns improved simulated moving bed) is briefly presented at the end of this chapter.

In chapter III, experimental results are presented to determine parameters required in the hybrid model. Firstly, bed properties such as porosity and maximum ion exchange capacity are presented. Then, coefficients in the Langmuir equation and van Deemter curve were obtained by non-linear regression. Experimental results were analyzed to support retention mechanisms proposed in the hybrid model.

In chapter IV, pulse tests are simulated with the hybrid model and the numerical method presented in chapter II. Roles of Langmuir coefficients and ion exchange constant on the chromatography profile are first identified. Simulated profiles were then fitted to experimental profiles to refine parameters measured in chapter III. The hybrid model, along with its parameters, was then validated by a binary mixture simulation. The same binary separation was also simulated with the discontinuous column model and compared with the profile simulated with the continuous model.

In chapter V, multicolumn processes simulation and optimization are studied. A binary separation with 3C-ISMB is firstly simulated. Then a new 3F4C-SSMB (three-fractions-four-columns sequential simulated moving bed) process was developed and optimized. Its performance was compared with two 3C-ISMB in cascade to prove its competitiveness.

The main contribution of this thesis

The two major contributions of this project are:

- i) a reliable computational tool, predictive even with strong anionic ion exchange resins, that could be employed in the optimization.
- ii) an innovative multi-column chromatography process for ternary mixture. In order to achieve these goals, several steps were needed.

At first, compounds adsorption mechanisms were studied by frontal analysis. It revealed a very different behavior for the two types of compounds: the sugar adsorption is quite linear, while the organic acid adsorption is strongly non-linear and follows a Langmuir model. Then, the influence of velocity on peak shape and thus dispersion and mass transfer between two phases was studied.

It was shown that the efficiency of the column decreases linearly with the elution speed, according to the van Deemter model. Dispersion and mass transfer coefficients were then deducted from parameters in the van Deemter equation and then validated. Results showed that the van Deemter equation still has good precision.

Introduction

A new retention model was developed to better predict organic acid separation with strong anionic resin. This model combines a refined Langmuir adsorption model and an ion-exchange model. The adsorption coefficient evolution with molecular size and acid group number supports the hypothesis that the organic acid adsorption is due to hydrogen bonding with sulfate and hydrogen sulfate groups on the resin. It is also proved in numerical simulation that the tailing in chromatography profiles of some organic acids is caused by ion exchange effect and cannot be reproduced by Langmuir adsorption. The continuous column model used in this work considers different dispersion coefficient for each compound, which is advantageous compared to discontinuous column model (theoretical plate model).

The CE/SE method has never been applied to an ion exchange system in the literature. The present work proposes a generic and accurate modeling approach (continuous column model with mass balance equations solved by the conservation element/solution element (CE/SE) method), which could also be applied to other chromatography systems.

Finally, a new ternary SSMB process was successfully applied and appeared an attractive performance. Comparing two ISMB in cascade and the new 3F4C SSMB process shows that both can separate ternary mixture with high purity. However, the innovative process proposed in this work has a lower eluent consumption, which is important, especially when organic or supercritical fluid is used. Its lower dilution factor reduces concentration cost, which is an energy-consuming stage. Finally, its lower column number reduces investment and maintenance costs.

Chapter I. Literature review

1 Context

1.1 Lignocellulosic biomass

The lignocellulosic biomass, also called lignocellulose, is a composite material whose principal macromolecular components are cellulose, hemicelluloses, and lignins (Figure 1-1). It is drawing an incredible level of attention which is related to their important feedstock and their potential usages. It can find applications in the biomedical field, reinforcement of polymer matrix, biosourced materials, packaging, energy, and environment. It is also the most abundantly available raw organic material on the Earth to produce bio-ethanol, syngas/hydrogen etc. Inside this biomass, depending on the type of lignocellulosic biomass, these three polymers are organized in complex non-uniform three-dimensional structures to different degrees and varying relative composition.

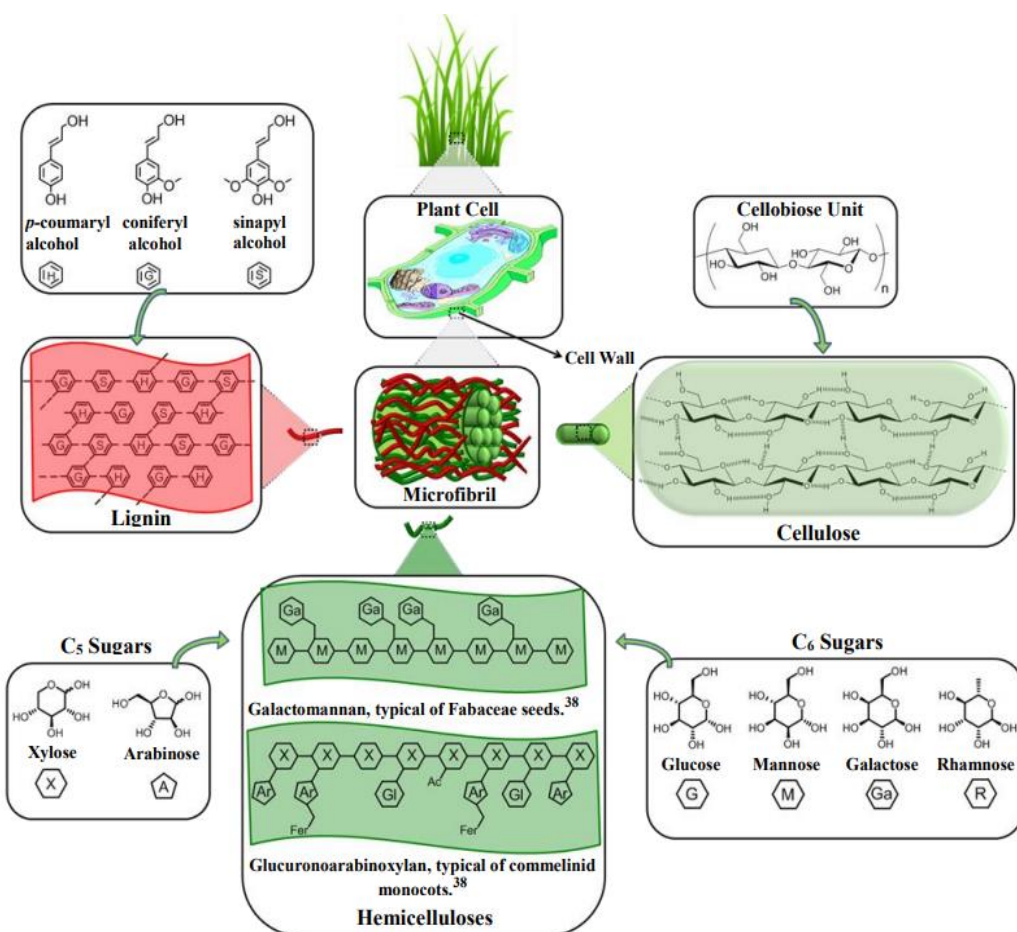


Figure 1-1. Presentation of lignocellulosic biomass [Isikgor et al. 2015]

Chapter I. Literature review

Cellulose, hemicelluloses, and lignins are not uniformly distributed within the cell walls. The structure and the quantity of these plant cell wall components vary according to species, tissues, and maturity of the plant cell wall. Generally, lignocellulosic biomass consists of 35–50% cellulose, 20–35% hemicelluloses, and 10–25% lignins. Proteins, oils, and ash make up the remaining fraction [Saha B.C., 2005]. Table 1-1 summarizes the types of lignocellulosic biomass and their chemical composition.

Table 1-1. Composition of different lignocellulosic biomass [Cherubini et al., 2010; Menon et al., 2012].

Lignocellulosic Biomass	Cellulose (%)	Hemicellulose (%)	Lignin (%)
Hardwood	Poplar	50.8-53.3	26.2-28.7
	Oak	40.4	35.9
	Eucalyptus	54.1	18.4
Softwood	Pine	42.0-50.0	24.0-27.0
	Douglas fir	44.0	11.0
	Spruce	45.5	22.9
Agricultural Waste	Wheat Straw	35.0-39.0	12.0-16.0
	Barley Hull	34.0	13.8-19.0
	Barley Straw	36.0-43.0	6.3-9.8
	Rice Straw	29.2-34.7	17.0-19.0
	Rice Husks	28.7-35.6	15.4-20.0
	Oat Straw	31.0-35.0	10.0-15.0
	Ray Straw	36.2-47.0	9.9-24.0
	Corn Cobs	33.7-41.2	6.1-15.9
	Corn Stalks	35.0-39.6	7.0-18.4
	Sugarcane Bagasse	25.0-45.0	15.0-25.0
Grasses	Sorghum Straw	32.0-35.0	15.0-21.0
	Grasses	25.0-40.0	10.0-30.0
	Switchgrass	35.0-40.0	15.0-20.0

1.1.1. Cellulose

Cellulose is the principal component of lignocellulosic biomass, consisting of 35 to 50% of the vegetal biomass. Unlike glucose in other glucan polymers, the repeating unit of the cellulose chain is the disaccharide cellobiose. Cellulose is a polymer of glucose comprising of numerous β -1,4-linked D-glucose subunits joined together by glycosidic linkages, van der Waals forces and hydrogen bonds [Nanda et al., 2015]. The polymerization degree is about 10,000 in the wood and could reach 15,000 in cotton [Fengel et al., 1983], [Gibson et al., 2012].

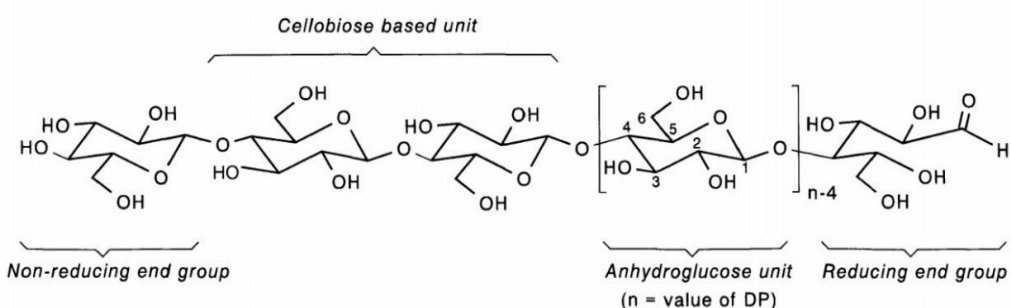


Figure 1-2. The structure of cellulose [D. Klemm, 1998]

1.1.2. Hemicelluloses

Hemicelluloses are the second most abundant polymer. Hemicelluloses are a branched biopolymer in lignocellulosic biomass that comprises a mixture of polysaccharides, such as pentose sugars (e.g. xylose and arabinose), hexose sugars (e.g. glucose, mannose and galactose) and sugar acids (e.g. glucuronic acid and galacturonic acid). Based on the structural difference, like backbone linkages and side groups, as well as other factors, like abundance and distributions in plants, hemicelluloses could be categorized into four groups as following [Thomas H., 2005]: xylans, mannans, mixed linkage β -glucans, and xyloglucans. Hemicelluloses consist of a relatively short-chained matrix of polysaccharide typically made up of 50–200 sugar monomers with acidic groups [Gibson L.J., 2012]. In the plant cell walls, hemicelluloses form a complex network of bonds, which provides structural strength by linking cellulose microfibrils and crosslinking with lignin. In contrast to cellulose, hemicelluloses can be degraded easily in an acidic or hot aqueous medium. The solubility and susceptibility to hydrolysis of hemicelluloses are also greater than cellulose due to its lower degree of polymerization (50–200) and amorphous structure [Chen H., 2014].

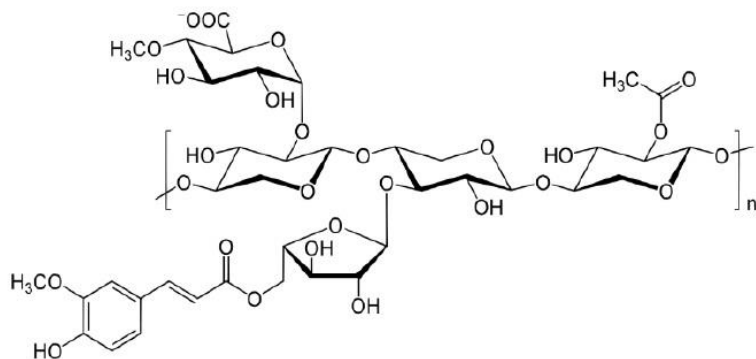


Figure 1-3. An example of hemicelluloses pattern [Himme M.E., 2009]

1.1.3. Lignins

Lignins are a class of complex organic polymers that form necessary structural materials in the support tissues of vascular plants and some algae [Martone Pt. 2008]. Lignins reinforce the secondary cell walls and hold the wood cells together and provides the extraordinary composite strength characteristics of a piece of wood. Due to their hydrophobic nature, lignins play an important role in the vascular system of plants and are insoluble in water under ambient conditions. By their roles in plants, they also inhibit the enzymatic hydrolysis of cellulose and hemicellulose in native cell walls [Nanda S., 2014]. Lignins are soluble in alkaline solutions, ionic liquids and appropriate extraction solvents when using organosolv technologies. Alkaline solutions cleave the ferulic acid cross-link between lignins and hemicelluloses and degrade lignins [Lawther J.M., 1996]. Its most commonly noted function is the support through the strengthening of wood (mainly composed of xylem cells and lignified sclerenchyma fibers) in vascular plants, which gives it the potential to become a source of specialty chemicals. Still, fuel for co-firing with coal to produce electricity at the biorefining site seems to be its only application.

1.2 Sugars, organic acids and their valorization

When lignocellulosic biomass is fractionated to produce valuable chemicals, generally by hydrolysis treatments, sugars and organic acids are the most commonly valorized fractions. Glucose obtained from the decomposition of cellulose or hemicelluloses is the main sugar produced and valorized after biomass hydrolysis. Other hexoses such as Mannose, Fructose or Galactose, or pentoses such as Xylose or Arabinose are extracted from hemicelluloses and separated for various applications. Finally, depending on the lignocellulosic biomass and the hydrolysis process, some valuable organic acids can also be recovered and valorized. They can be produced from hemicellulose decomposition or come from their use as a solvent (OrganoSolv® method) or as a chemical reagent (acid cooking) to improve hydrolysis efficiency.

A previous work [Lemaire et al., 2017] showed that wheat bran hydrolysis is a complicated solution with pH 1.4 and mainly sulfate (175.2 g/L) as inorganic anion. It contains mainly glucose (11.4 g/L), xylose (25.5 g/L) and arabinose (14.6 g/L) as sugars and acetic acid (6g/L), lactic acid (0.5g/L) and succinic acid (39g/L) as organic acids. Formic acid and citric acid are also chosen for this study to better understand the link between retention mechanisms and molecular size (or acid function number).

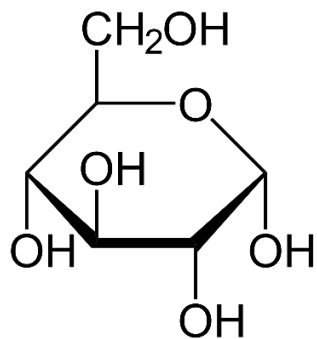
Table 1-2. Composition of hemicellulose hydrolysis [Lemaire et al., 2017].

Sugar		Anion		Organic acid	
Glucose	11.4	Chloride	2.0	Acetic	6.0
Xylose	25.5	Phosphate	24.3	Lactic	0.5
Arabinose	14.6	Sulfate	175.2	Succinic	39

1.2.1 Glucose

Description

Glucose is a mono-saccharide (simple sugar) with six carbon atoms. Its molecular formula C₆H₁₂O₆ corresponds to a molecular weight of 180 g/mol. Glucose is the most abundant monosaccharide on the earth [Domb A.J., 1998]. It is mainly made by plants and most algae during photosynthesis from water and carbon dioxide, using energy from sunlight, where it is used to make cellulose in cell walls and to store energy in starch, which is the most abundant carbohydrate [Kamide K. 2005]. Glucose is a monosaccharide containing six carbon atoms and one aldehyde group, and is therefore an aldohexose. The glucose molecule can exist in an open-chain (acyclic) as well as ring (cyclic) form. Glucose is naturally occurring and is found in fruits and other parts of plants in its free state.

**Figure 1-4.** Glucose molecule (ring form)

Glucose is produced industrially from starch by hydrolysis using glucose amylase or acids. The result is glucose syrup (>90% dry matter) [Fellows P.J., 2016] with an annual worldwide production volume of 20 million tons (as of 2011) [Thomas B., 2011]. This is the reason for the former common name "starch sugar". Many corps can be used as the source of starch. Rice, wheat, cassava, potato, barley, sweet potato, corn husk and beets are all used in various parts of the world [Alan D., 2014].

Application

Glucose is mainly used for the production of fructose, sucrose and in the production of glucose-containing foods.

In foods, it is used as a sweetener, humectant, to increase the volume and to create a softer mouthfeel [P. J. Fellows, 2016]. Various sources of glucose, such as grape juice (for wine) or malt (for beer), are used for fermentation to ethanol during the production of alcoholic beverages. Most soft drinks in the US use HFCS-55 (High Fructose Corn Syrup with a fructose content of 55% in the dry mass), while most other HFCS-sweetened foods in the US use HFCS-42 [High, 2018].

In addition, glucose syrup is used, inter alia, in the production of confectionery such as candies, toffee and fondant [T. Steve, 2017]. Typical chemical reactions of glucose when heated under water-free conditions are the caramelization and, in presence of amino acids, the Maillard reaction.

Various organic acids can be biotechnologically produced from glucose, for example by fermentation with *Zymomonas mobilis* to produce acetic acid [Tetsuya et al. 1996], with *Penicillium notatum* for the production of Erythorbic acid [Juichiro et al. 1967,], with *Candida brumptii* to produce isocitric acid, with *Lactobacillus delbrueckii* for the production of lactic acid, with *Lactobacillus brevis* for the production of malic acid, with *Propionibacterium shermanii* for the production of propionic acid, with *Pseudomonas aeruginosa* for the production of pyruvic acid and with *Gluconobacter suboxydans* for the production of tartaric acid [A. James 2013].

1.2.2 Pentoses

A pentose is a mono-saccharide with five carbon atoms. The chemical formula of all pentoses is $C_5H_{10}O_5$ which corresponds to a molecular weight 150 g/mol. Depending on its structure, it could be divided into aldopentose whose carbonyl is at carbon 1, and ketopentose whose carbonyl is at carbon 2 or 3.

Lignocellulosic raw materials, in particular hardwood and agricultural raw materials, can contain 5%–20% (or more) of the pentose sugars xylose and arabinose. Xylose is by far the most abundant pentose sugar, whereas arabinose can constitute as much as 14%–15% in corncob hulls and wheat bran, respectively [Andrea et al. 2020].

1.2.2.1 Xylose

Description

Xylose was first isolated from wood, which gave its name. It is a colorless or white solid that is soluble in water. Its solubility in water at 20 °C is 117 g per 100 ml of water and its crystals are white [Karl J. 2000].

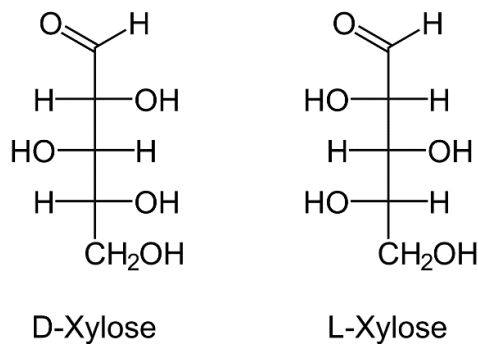


Figure 1-5. Molecule of xylose, linear chains [Hongzhan C., 2017].

Industrial production of xylose started with lignocellulosic biomass from which xylan is extracted from raw biomass materials include hardwoods, softwoods, and agricultural waste from processing maize, wheat, or rice. The xylan polymers can be hydrolyzed into xylose, which is catalytically hydrogenated into xylitol. The conversion changes the sugar (xylose, an aldehyde) into the primary alcohol, xylitol. Impurities are then removed. The processing uses standard industrial methods that involve fermentation with bacteria, fungi, or yeast, especially *Candida tropicalis*, which are common but are not as efficient [H. Jain, 2014]. Pentoses could also be separated and purified by chromatography or crystallization, for higher value added applications.

Application

In daily life it is commonly seen in the form of xylitol which is the sugar alcohol of xylose. The use of manufactured products containing xylitol may reduce tooth decay [Ur-rehman et al., 2015]. Xylose and xylitol are useful in many domains:

Chapter I. Literature review

Food industry

Wrigley Ltd. produced a new chewing gum which includes a xylitol coating. Xylitol is the product of xylose hydrogenation and includes impurities such as other sugars or sugar alcohols, which are the natural byproducts of the xylitol production process [Daniel J., 2017].

Xylitol is used to produce yogurt. The preparation technology provided by the invention can decompose lactose and protein in the milk, enabling the yogurt to be more easily digested and absorbed by a human body. The yogurt has the effects of promoting gastric secretion, improving appetite, and enhancing digestion. The lactic acid bacteria can reduce the generation of certain cancerogenic substances, thus having a function of preventing cancers. The yogurt can inhibit the proliferation of spoilage bacteria in the intestinal tract and weaken the toxins produced by the spoilage bacteria in the intestinal tract. The yogurt has a cholesterol-lowering effect, thus being especially suitable for people with hyperlipidemia to drink [Xiaoguang H., 2016].

Xylose is added to fruit jelly. Xylitol utilizes its non-fermentability, inhibits bacterial growth and reproduction, reduces bacterial acid production on tooth surfaces, and thus has significant prevention of tooth decay [Mingchuan *et al.*, 2017].

Daily necessities

Xylitol presents in an appetite suppressant toothpaste. The toothpaste composition includes toothpaste base ingredients; and at least one of appetite suppressant and appetite depressant herbs. Xylitol is one of its base ingredients. Alternatively, the toothpaste composition may be in the form of a dental cream or mouth spray [Shubham *et al.* 2000].

Serpelloni invented an improved hard coating process using a polyol in powder form, enabling easy, speedy creation of a hard coating on the surface of a product. This process consists essentially of the application of a syrup containing at least 90% of a polyol to a product. The polyol can be sorbitol, maltitol, mannitol, xylitol, etc. [Michel *et al.* 1999]

A hair composition suitable for repairing damaged hair and suppressing damage caused by heat treatment is invented by adding trehalose, xylose, xylitol, and maltitol to polyethylene glycol. [F. Momoko 2017]

Pharmaceutical industry

Daniel [Daniel G., 2000] found that xylitol can help the storage of blood platelets. When micromolar or nanomolar amounts of pentose is added to the solution, blood platelets can retain function after ten days. The preferred pentoses are D-Ribose, xylulose-5-phosphate, and pentose-related alcohol xylitol.

Romeo invented a pharmaceutical composition for the prevention or treatment of upper respiratory infections, including otitis media, by nasal administration of xylitol. Xylitol inhibits the growth of some bacteria during its exponential growth phase. The nose is a reservoir for infectious agents. Thus, a nasal administration of xylitol can treat respiratory infections and otitis media in a mammal, especially human [D. Vincent, 1999].

Chapter I. Literature review

Kuppusamy used xylose to reduce elevated blood glucose level in a subject typically having (pre-) diabetes, steatohepatitis, obesity, and metabolic syndrome when orally administered. Other saccharides like arabinose, galactose, and mannose also showed the same effect [Nallagounder et al., 2018].

1.2.2.2 Arabinose

Description

Arabinose is a monosaccharide. L-arabinose is more common than D-arabinose in nature and is found in nature as a component of biopolymers such as hemicellulose and pectin. Arabinose gets its name from gum arabic, from which it was first isolated [M.T. Holtzapple, 2003]. It is a colorless or white solid that is soluble in water. It is highly soluble in water: 70 g per 100 ml of water at 20°C.

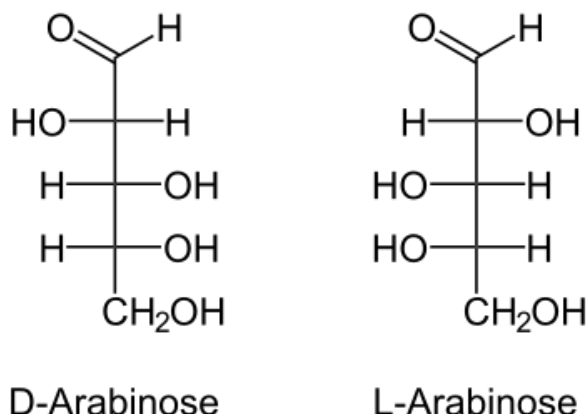


Figure 1-6. D and L structure of Arabinose [Hongzhan C. 2017].

As a newly developed functional sugar, L-arabinose is generally produced by hydrolysis of biomass such as vegetable gums, corncob, beet pulp, bagasse and other materials [Hu et al., 2018]. L-arabinose can also be prepared by chemical or biological synthesis methods, but both methods have shortcomings of high costs, difficult to separate, so it is rarely used in commercial production [Ahmed Z., 1999].

Applications

Arabinose has physical characteristics similar to sucrose, meanwhile it does not have too many calories. As a functional sweetener and pharmaceutical intermediate, L-arabinose presents gradually often in the food processing industry and the pharmaceutical and chemical industry:

Food industry

Liquid soda drinks such as Coca-Cola are one of the main causes of excessive consumption of sugar by humans. Wenbiao invented an herbal tea containing L-arabinose [Wenbiao Y., 2012]. This herbal tea can regulate blood sugar level, reduce blood fat and relieve lipogenesis, solves the problem that the conventional herbal tea with high sugar and heat and low nutrition.

Chapter I. Literature review

Pharmaceutical industry

Yoshihiro used arabinose to produce a Blood sugar level rising inhibitor [Yoshihiro *et al.*, 2004]. This blood sugar level rising inhibitor comes from dissolving hardly digestible dextrin (fiber sol 2 having 90% dextrin content) and L-arabinose syrup in water. The test shows that it can decrease the sucrose level in human blood by 40% to 60%.

L-FMAU (1-(2-fluoro-5-methyl-beta, L-arabinofuranosyl) uracil) is one of the most promising agents against HBV (Hepatitis B Virus). L-FMAU showed low toxicity in rats and woodchucks and no significant virus rebound up to 36 weeks after cessation of the drug treatment. Arabinose can be a raw material of an efficient and inexpensive synthesis of L-FMAU [Du *et al.*, 1999].

Telbivudine is an antiviral drug used in the treatment of hepatitis B infection. Industry synthesizes telbivudine L-arabinose with a 6-step process [Zhao-wen L., 2009].

1.2.3 Organic acids

An organic acid is an organic compound with acidic properties. The most common organic acids are the carboxylic acids, whose acidity is associated with their carboxyl group –COOH. Sulfonic acids, containing the group –SO₃OH, are relatively stronger acids. Alcohols, with –OH, can act as acids but they are usually very weak. The relative stability of the conjugate base of the acid determines its acidity. Main carboxylic acids that can be found in biomass or produced by fermentation are given below.

1.2.3.1 Citric acid

The citric acid (C.A., or 2-hydroxy-propane-1,2,3-tricarboxylic acid) is one of the most industrially used organic acids with different applications. Its pKa are 3.1, 4.7, and 6.4 at 25°C. The production for 2020 is estimated at 2 million tons [Ciriminna *et al.*, 2017] with a global market estimated at 3.6 billions US\$ in 2025.

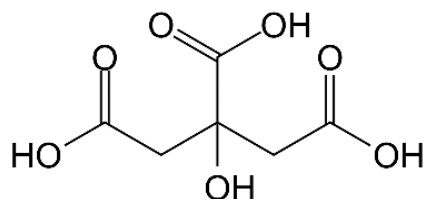


Figure 1-7. Citric acid molecule.

C.A. is a weak organic acid that has the molecular formula C₆H₈O₇. It occurs naturally in citrus fruits. C.A. is one of the main active ingredients of lemon. It is often used to balance basic pH of cosmetics. It is also present in some bath products (bath bombs, bath pebbles, or "magic powders") because of its effervescent properties. In the food industry, C.A. is the main food acidulant used to prevent oxidative deterioration of the taste and color of products, such as jellies, sweets, and soft drinks.

In the pharmaceutical industry, sodium citrate is used as an anticoagulant in blood transfusions. C.A. also has applications in the cosmetic and chemical industry, being used in astringent lotions, such as aftershave, due to its low pH. Besides, C.A. properties have been explored for use in new

Chapter I. Literature review

53 applications, such as components of biodegradable packaging, due to its crosslinking capacity, disinfectant agent, extracting agent, fruit preservative component, and 55 environmental remediation [Mores *et al.*, 2020; Umemura *et al.*, 2012].

1.2.3.2 Succinic acid

Succinic acid (S.A.) is a dicarboxylic acid. Its pKa are 4.21 and 5.64 at 25°C. In living organisms, succinic acid takes the form of an anion, succinate, which has multiple biological roles. It is an approved additive which is also known as E363. Its global production of 16,000–30,000 tons and records an annual growth of 10% in 2014 [Succinic 2018].

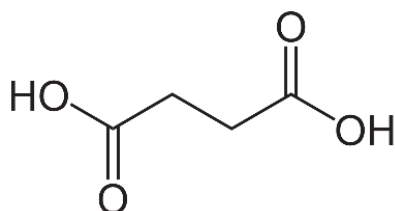


Figure 1-8. Molecule of succinic acid.

S.A. has been known traditionally as amber acid in Europe for centuries and used as a curative agent. Currently, S.A. is being recognized as the building block of many essential chemicals applied in food, chemical, and pharmaceutical industries. It has great potential in the manufacturing of polybutylene succinate (PBS), surfactant detergents, flavors and fragrances, herbicides and fungicides, and food additives. In the future, S.A. may be seen as an essential precursor used for the production of bio-based chemicals such as biodegradable plastic (e.g., Polybutylene succinate, PBS), polyester polyols, plasticizers, and polyurethanes (a replacement of petroleum-based adipic acid), and 1,4-butanediol. [Ramesh *et al.*, 2020] In 2004, succinate was placed on the U.S. Department of Energy's list of top 12 platform chemicals from biomass.

1.2.3.3 Formic acid

Formic acid (F.A.), systematically named methanoic acid, is the smallest carboxylic acid. Its pKa is 3.74 at 20°C. F.A. is an important intermediate in chemical synthesis and occurs naturally, most notably in some ants. The word "formic" comes from the Latin word for ant, formica, referring to its early isolation by the distillation of ant bodies. Esters, salts, and the anion derived from formic acid are called formates. Industrially, formic acid is produced from methanol. The formic acid market was valued at around 600 kilotons in 2020, and the market is projected to register a CAGR (compound annual growth rate) of over 3% during the forecast period (2021-2026).

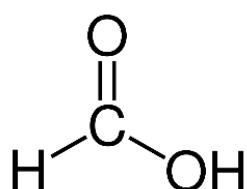


Figure 1-9. Formic acid molecule.

Chapter I. Literature review

A major use of F.A. is as a preservative and antibacterial agent in livestock feed. In Europe, it is applied on silage, including fresh hay, to promote the fermentation of lactic acid and to suppress the formation of butyric acid; it also allows fermentation to occur quickly and at a lower temperature, reducing the loss of nutritional value [W. Reutemann, 2000]. F.A. arrests certain decay processes and causes the feed to retain its nutritive value longer, and so it is widely used to preserve winter feed for cattle [Maria *et al.*, 2010]. F.A. is also significantly used in the production of leather, production of cleaning products [Bhat *et al.*, 2001]. Moreover, Beekeepers use formic acid as a miticide against other mites [Hoppe *et al.*, 1989] and it can be used as a fuel cell (it can be used directly in formic acid fuel cells and indirectly in hydrogen fuel cells) [Ha *et al.*, 2005].

1.2.3.4 Lactic acid

Lactic acid (L.A.) is an alpha-hydroxy acid (AHA) due to the presence of a hydroxyl group adjacent to the carboxyl group. Its pKa is 3.6 at 25°C, which means it has a remarkable acidity. Global lactic acid production is approximatively 270 000 t per year, as it presents a broad range of applications in food industry, cosmetics and also in pharmaceuticals [Klotz *et al.*, 2017].

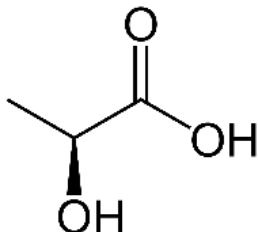


Figure 1-10. Lactic acid molecule.

L.A. is one of the essential products in green chemistry, and it has widespread applications, mainly in the pharmaceutical, cosmetic, chemical, and food industries. About 70% of the lactic acid produced is utilized in the food production sector due to its crucial role in manufacturing yogurt and cheese [Martinez *et al.*, 2013]. Additionally, polylactic acid (PLA) polymers are widely used as a raw material in packaging and fibers and foams [E. Ismail, 2018]. Lactate esters can be applied as emulsifiers and improving agents in food products [Gao *et al.*, 2011].

1.2.3.5 Acetic acid

Acetic acid (A.A), also named ethanoic acid, is a colorless liquid organic compound. Its pKa is 4.75 at 25°C. In 2018, the global production capacity of acetic acid reached almost 18 million metric tons, and it is forecast to increase to some 21.66 million metric tons by 2023 [Lucía *et al.*, 2021].

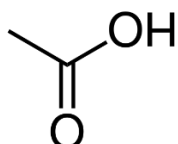


Figure 1-11. Acetic acid molecule.

A.A. is a major essential chemical product, being an important chemical reagent used primarily in the production of cellulose acetate, vinyl acetate monomer and polyvinyl acetate, acetic

Chapter I. Literature review

anhydride, monochloroacetic acid, acetate esters, terephthalic acid, and synthetic fibers and fabrics. [Le Berre *et al.*, 2014]. It is often used in descaling agents or as a food additive [Dimian A.C., 2020].

The primary use of A.A is the production of vinyl acetate monomer (VAM), which can be polymerized to polyvinyl or other polymers, which are components in paints and adhesives. [Bienewald *et al.*, 2018]. The major esters of acetic acid are commonly used as solvents for inks, paints and coatings. The worldwide production of acetic anhydride, which is an acetylation agent, uses approximately 25% to 30% of the global production of acetic acid. Glacial (water-free) acetic acid is an excellent polar protic solvent, as noted above. It is frequently used as a solvent for recrystallization to purify organic compounds [Malveda M., 2003].

1.3 Hemicellulose hydrolysis

During hydrolysis of biomass, the cellulose and hemicellulose are converted into glucose, pentoses and other compounds through the chemical reactions or the combined action of cellulolytic enzymes. The hydrolysate is then treated by the purification module.

The product can be fermented, usually into ethanol, to obtain biobased products. They can also be transformed by conventional chemical processes into other molecules of interest.

The hydrolysis of biomass involves two steps: pretreatment and degradation. Hemicellulose, which is less stable than cellulose, could be decomposed in both of these steps depending on experimental conditions, while the second step is mainly motivated by the hydrolysis of cellulose.

1.3.1 Biomass pretreatment

A first step of pretreatment of the biomass is necessary. The biomass is subjected to a pretreatment unit that aims to separate the major components of the biomass and increase the accessibility of the cellulose and hemicellulose.

This pre-treatment is based on different actions, often simultaneous [Ballerini *et al.*, 2011]: physical destruction of the matrix, removal of lignin and/or hemicelluloses and chemical or biological attack initiating cellulose decrystallization.

Several types of pretreatments are currently being studied. They can be classified into three categories [M, S. Haghghi, 2013]:

Physical processes: These processes involve the mechanical or thermal decomposition of organic compounds. In general, these techniques have the advantage of not producing effluents. However, they are often very costly in energy. The most common techniques are grinding, extrusion and microwave irradiation [Chen *et al.*, 2017].

Biological processes: These processes involve using microorganisms to degrade organic compounds. Most studies conducted on this topic focus on the use of fungi [Sindhu *et al.*, 2016]. This type of pretreatment is interesting because it does not require environmentally toxic products and it consumes very little energy. However, this process is not widely used because it is time consuming and requires continuous monitoring.

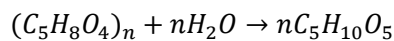
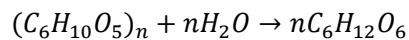
Chapter I. Literature review

Chemical processes: These processes consist in attacking the biomass with chemical agents with adapted conditions (mainly residence time and temperature level). The most used agents are acid, basic and organic solvent [Ballesteros *et al.*, 2008]. Acid cooking, acid catalysis or dilute acid pretreatment belongs to this category, which is one of the most effective methods for the destructure of lignocellulosic biomass. It is also possible to combine different methods. In any case, the aim of this pre-treatment step is to increase the interaction surface between the biomass and the reactant in charge of the hydrolysis of complex sugars.

Among all the existing processes, acid cooking, possibly followed by steam explosion, is the mostly used because of its efficiency. Indeed, it allows not only to obtain high yields of fermentable sugars but also to recover an aqueous phase rich in hemicelluloses [Hsu *et al.*, 2010]. It most often involves sulfuric acid or hydrochloric acid at low concentrations and temperatures above 140°C [Lee *et al.*, 1999]. Under these conditions, hemicelluloses, which are less stable than cellulose, could be depolymerized.

1.3.2 Hemicelluloses decomposition

The hydrolysis of biomass could be expressed as following reactions:



Hemicellulose can be decomposed by thermochemical or biochemical processes. Thermochemical processes produce gaseous or liquid compounds that are easier to handle and transform afterwards. The biochemical processes treat hemicellulose with an enzyme cocktail. For example, hemicellulase can decompose biomass at moderate conditions. However, no single enzyme is able to completely decompose hemicellulose [Wyman C.E., 2001; Torget *et al.*, 1990; Torget *et al.*, 1991].

In a chemical hydrolysis process, diluted acid catalyzes the transformation of long chains into short chains or monomers. Generally, hemicelluloses decompose at a temperature lower than cellulose since they are amorphous [Robert *et al.*, 1999]. Some alkalis could also catalyze the decomposition, for example, alkaline, NaOH [Fan *et al.*, 1987], and ammoniac [Kim *et al.*, 2011]. Some process using oxidant like diluted H₂O₂ were proven to be feasible [Shen *et al.*, 2009].

Instead of using chemical products like acids and bases, the enzyme process uses enzymes like hemicellulases to hydrolyze biomass. Hemicellulases (an enzyme that catalyzes depolymerizing of hemicellulose) exist in many species of bacteria and fungus [Uttam K.J., 2021]. Today the most commonly used hemicellulase is produced by a strain of *Trichoderma* or *Aspergillus*, which are genetically modified fungus [Xiaoling *et al.*, 2020]. Most of them are active at a pH between 4 and 7, with a temperature below 70°C. Thermophile enzymes have been discovered from thermophiles bacteria which allows hydrolysis reaction to take place at a higher temperature. For example, xylanase can stay active till 95°C within pH from 6 to 8. [H.D Simpson, 1991].

The separated hydrolysate is a solution of pentoses, hexoses, organic acids, salts and other macromolecules. It is then either fermented for the production of bioethanol or sent to a separation and purification module for the production of sugar and organic acids.

2 Chromatography separation

Many industrial methods such as distillation, liquid-liquid extraction or crystallization could be an alternative for the separation of molecules. Table below shows some examples of current possible separation techniques:

Table 1-3. Examples of purification methods used during hemicellulose hydrolysis treatment.

Process	Advantages	Disadvantages
Crystallization	Less dilution	Weak selectivity and purity
Electrodialysis	High purity and recovery rate	High equipment and maintenance costs
Ion exchange	High purity	High dilution and equipment costs
Chromatography	High purity and selectivity	High dilution

However, preparative chromatography is the best generic method today for the purification of small drugs and valuable chemical components at a small production rate [Torgny *et al.*, 2017].

Initially, chromatography was invented as a separative technique at a laboratory scale. The mixture is dissolved in a fluid (gas, solvent...) called the mobile phase, which carries it through a system (a column, a capillary tube, a plate, or a sheet) on which is fixed a material called the stationary phase. The choice of mobile phase, material of stationary phase, environmental factors and physico-chemical properties of molecules lead to different affinities of the molecule in the mobile phase to the stationary phase. Molecules that have more interactions with the stationary phase will travel slower than molecules less interactive. As a result of their different apparent velocities, sample components will be collected at different times at the end of the column.

Chromatography proposes a precise separation and purification. Many variations of chromatography were developed to reach different separation targets.

2.1 Different chromatography processes

Based on the physical state of the mobile phase, chromatography can be categorized into three major types: gas chromatography, liquid chromatography, and supercritical chromatography. Chromatography could also be subdivided into many other types depending on the separation mechanism or material of stationary phase:

Thin-layer Chromatography (TLC): TLC uses an absorbent material on flat glass or plastic plates. This is a simple and rapid method to check the purity of an organic compound. It is used to detect pesticide or insecticide residues in food. Thin-layer chromatography is also used in forensics to analyze the dye composition of fibers.

Chapter I. Literature review

Paper Chromatography (PC): PC is one of the most common types of chromatography. It uses a strip of paper as the stationary phase. Capillary action is used to pull the solvents up through the paper and separate the solutes.

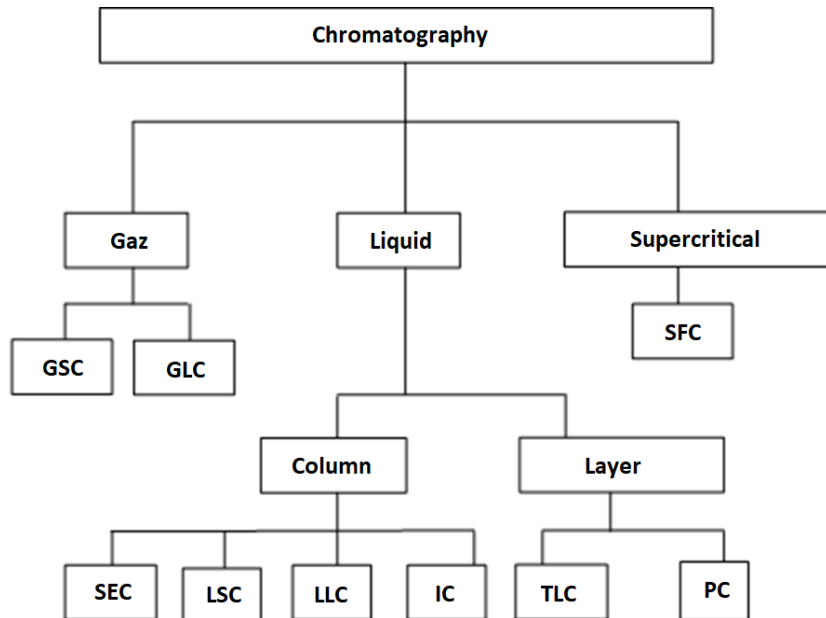


Figure 1-12. Chromatography classification.

Size-exclusion chromatography (SEC): SEC, also known as molecular sieve chromatography [Garrett *et al.*, 2013], is a chromatographic method in which molecules in solution are separated by their size, and in some cases molecular weight [Paul *et al.*, 2007]. It is usually applied to large molecules or macromolecular complexes such as proteins and industrial polymers.

The chromatography column is packed with fine, porous beads which are composed of dextran polymers (Sephadex), agarose (Sepharose), or polyacrylamide (Sephacryl or BioGel P). SEC works by trapping smaller molecules in the pores of the adsorbent ("stationary phase"), while large molecules follow the mobile phase: the larger the particles, the faster the elution. SEC is a widely used polymer characterization method because of its ability to provide good molar mass distribution results for polymers.

Liquid-solid chromatography (LSC): LSC was initially carried out by Tswett in the early 1900s, using columns packed with polar, inorganic particles such as calcium carbonate and a less-polar solvent as the mobile phase. Today, this technique is referred to as normal-phase chromatography (NPC) or adsorption chromatography (in contrast to reversed-phase chromatography (RPC), where a nonpolar stationary phase is used with a polar mobile phase).

Liquid-solid or normal-phase chromatography is used for the separation of nonionic solutes by adsorption onto the surface of an inorganic oxide stationary phase and displacement by competition with the components of the mobile phase. It has particular advantages for compound-class separations and the separation of diastereomers and geometrical isomers soluble in organic solvents [Lloyd *et al.*, 2017].

Chapter I. Literature review

Partition or liquid–liquid chromatography (LLC): LLC is a powerful separation technique which has been successfully used for the separation and analysis of a wide variety of sample types, including water-soluble and oil-soluble compounds, ionic and nonionic compounds, as well as biopolymers such as nucleic acids and proteins. The basis of LLC is the distribution of sample molecules between two immiscible phases: a stationary phase and a mobile phase. The liquid stationary phase fully fills the column and retains molecules in injected product. Retained molecules are then desorbed by injected eluent. In LLC, the mobile phase is pushed through the column by either density difference, or centrifuge. In conventional LLC, the stationary phase offers unique selectivity for various samples since a wide range of liquid phases can be used [Wingren *et al.*, 2000].

Ion chromatography (IC or IXC): IC has been in common use for more than 50 years, especially during the separation and purification of proteins. It separates ions and polar molecules based on their affinity to the ion exchanger. It works on almost any kind of charged molecule—including large proteins, small nucleotides, and amino acids. However, ion chromatography must be done in conditions that are one unit away from the isoelectric point of a protein [Ninfa *et al.*, 2010].

There are two types of ion chromatography: anion-exchange and cation-exchange. Cation-exchange chromatography is used when the molecule of interest is positively charged. The stationary phase is negatively charged and positively charged molecules are attracted to it. Anion-exchange chromatography is used when the stationary phase is positively charged and negatively charged molecules are loaded to be attracted on the surface. IC is often used in protein purification, water analysis, and quality control [Handbook 2016, Dąbrowski *et al.*, 2004].

Most IEX resins consist of small spherical particles and are microporous. Ions and other macromolecules can diffuse into the particle and bind to the ion exchange groups fixed on the inside and outside surface. Nonporous ion exchangers also exist in ion-exchange chromatography, where the ion exchange process occurs only at the external surface of these particles. It is only applied to analytical chromatography because of its high resolution but low capacity.

The resin matrix can be constructed in many materials. The classical ion exchange matrix, which is usually applied in water treatment, is a hydrophobic styrene polymer which has a small diameter of pore and a significant capacity of exchange [Samsonov *et al.* 1973; Vedeneeva *et al.* 1974; Yaskovich *et al.* 1974]. Exchanger based on cellulose came out in the 1950s and still plays an important role today. The matrix could be natural fibers or cellulose-based grains [C.S. Knight 1967]. Exchanger of dextran or agarose is initially invented for the gel filtration. This type of matrix is hydrophilic and has an outstanding capacity for proteins [Tsai *et al.* 1990]. Exchangers based on silicon are small particles with strong mechanical resistance and do not inflate. However, the silane function (SiH_4) on his surface makes the adsorption of macromolecules becoming irreversible. Hydrophilic polymer grafting and pore coating were also alternatives ways to develop new exchangers. These materials play an important role, especially in plasma fractionation [Mirabel *et al.*, 1980; Vanderwiel *et al.*, 1989; Stoltz *et al.* 1987].

2.2 Pulse tests and frontal analysis

Pulse tests and frontal analysis are two major methods to study column chromatography whatever its type. They involve solute migration through the entire system and solute detection as it emerges from the column. The detector continuously monitors the amount of solute in the emerging mobile phase and transduces the signal to the voltage, which is registered as a peak on a strip chart recorder. The recorder trace where the solute is absent is the baseline. The detector here can be pH, conductivity, absorbance etc. depending on the solute molecule and the required precision [Anna *et al.* 2009].

2.2.1 Pulse test

A pulse test consists of injecting a small volume of product (0.05 BV for example) then the eluent at a constant flow rate until all compounds get out of the column. The concentration at the end of column is analyzed and traced as a function of time over the injected volume. The curve obtained is called chromatography profile or chromatogram. For a linear chromatography, the profile is a Gaussian peak. It is one of the most common methods used in chromatography [Vincent *et al.*, 2018]. The bed properties and solute behavior are reflected by the retention volume and the dispersion of the peak.

As shown in Figure 1-13, the peak width and the retention volume V_R are main characters of the peak. V_R is represented approximatively by the eluted volume from the injection to the peak's midpoint. In the case of a dissymmetric peak, V_R is the weighted mean retention volume. The peak width gives the dispersion inside the column, in the case of a dissymmetric peak, the left and right-side peak width give the asymmetry factor As .

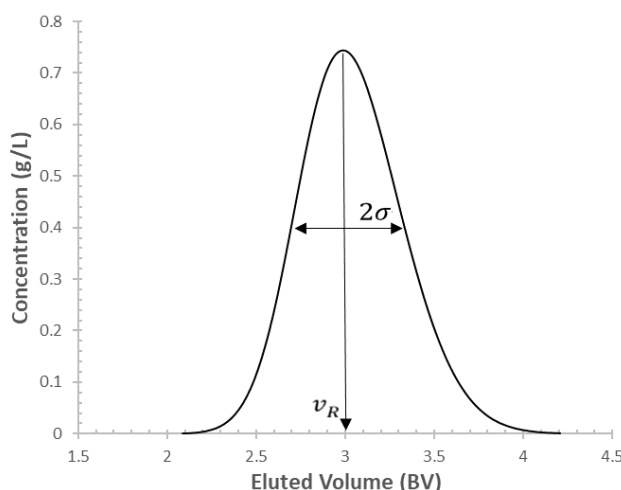


Figure 1-13. Example of pulse test chromatographic profile.

The global efficiency of the column is usually characterized by the Height Equivalent to a Theoretical Plate (HETP). Martin and Synge [Martin, A. J. P. & Synge, R. L. M. 1941] has proved that with the theoretical plate model proposed in their work, the solution of an ideal linear chromatography equation is a gaussian peak. The number of theoretical plates (NET) in the column could be deducted as:

Chapter I. Literature review

$$NET = \left(\frac{V_R}{\sigma} \right)^2 = 5.54 \left(\frac{V_R}{W_h} \right)^2 \quad (1 - 1)$$

where W_h is the width at half peak height ($=2.355 \sigma$ for a Gaussian peak), σ^2 is the variance of retention volume and V_R is the mean retention volume. This half-height method enables to estimate the number of theoretical plates even if the peak is not entirely separated from a neighboring peak. The HETP is therefore:

$$HETP = \frac{L}{NET} \quad (1 - 2)$$

where L is the column length.

The Peak Asymmetry Factor As is defined by the following equation:

$$As = \frac{b}{a} \quad (As > 1: tailing, As < 1: fronting) \quad (1 - 3)$$

Where b is the distance from the peak midpoint (corresponds to its highest point) to the trailing edge of the peak measured at 10% of peak height and a is the distance from the leading edge of the peak to the peak midpoint measured at 10% of peak height.

When the peak is not symmetric and not continuous (presented by a set of experimental points), it is difficult to define the width at half peak height. Separation parameters could be estimated by moment analysis from V_R and σ^2 estimation.

$$V_R = \frac{\int_0^\infty V \cdot c \cdot dV}{\int_0^\infty c \cdot dV} \quad (1 - 4)$$

$$\sigma^2 = \int_0^\infty (V - V_R)^2 \cdot c \cdot dV / \int_0^\infty c \cdot dV \quad (1 - 5)$$

$$HETP = \frac{L \cdot \sigma^2}{V_R^2} \quad (1 - 6)$$

where V is the eluted volume, and c is the component concentration in the mobile phase at column output (concentration unit does not matter).

In the current work V and V_R are expressed in bed volume (BV), which is the total volume of material, both solid and liquid, in the column. The interest of using BV is that calculations are not impacted by the column size, which is helpful for system up-scaling.

The estimation of HETP, or As at different interstitial velocity, allows to determinate many column properties such as mass transfer coefficient k_a and axial dispersion coefficient D , which will be introduced later in detail (chapter II, section 3).

2.2.2 Frontal analysis (F.A.)

During a frontal analysis, a solution is continuously injected into the column until the column is saturated. This method, proposed by James and Phillips [James *et al.* 1954], is usually used to determine the capacity of resin and the adsorption isotherm [F. Gritti, 2002].

Chapter I. Literature review

Figure 1-14 is an example of a concentration profile at the end of the column. The chromatography profile of frontal analysis resembles a stepped curve where the concentration rises from the initial concentration C_0 and stabilizes at the concentration of product C .

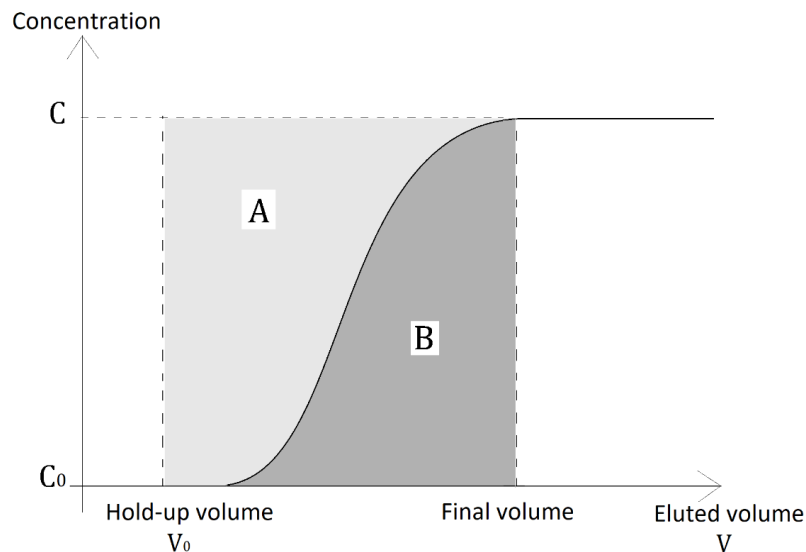


Figure 1-14. Frontal analysis chromatography profile.

At the final volume, the total rectangle area under the horizontal line, corresponding to product concentration C , is the total amount of product injected into the whole system. The right-side striped area **B** is the integration of the outlet concentration over eluted volume, which corresponds to the collected amount of product. The hold-up volume V_0 is the volume of liquid in the whole system (bed porosity, tubing and fitting)) and the rectangle on the left side, before V_0 , correspond to the variation of product amount in the whole liquid phase. Consequently, the striped area on the left side (**A**), which corresponds to the product amount adsorbed by the stationary phase, can be expressed as the total injected amount minus the collected amount minus the amount variation in liquid phase in the whole system. Thus, the concentration of product retained in the stationary phase $q(c)$, in equilibrium with its concentration c in the mobile phase, can be deducted from Figure (1-14) by the following equation:

$$q(c) = \frac{1}{(1 - \varepsilon)} \int_0^c (V - V_0) dc \quad (1 - 7)$$

where q is the concentration in the stationary phase.

To trace the isotherm, a series of products is prepared with different concentrations. The product is switched to a higher concentration after each injection. The final result show the relation between the concentration in the mobile phase and in the stationary phase.

There are some other arrangement methods like FACP (frontal analysis by characteristic points) where the product is injected from the highest concentration to the lowest, or ECP (elution by characteristic points) where the product is injected always to an empty column [Glueckauf E., 1955]. These methods are still less used because of the influence of the axial dispersion, and the requirement of detector calibration [Cavazzini *et al.*, 2003].

2.3 Preparative chromatography

Chromatography is a technique mostly used in analytical chemistry. Its applications to industrial separation are called preparative chromatography. The first column of chromatography was invented in 1903 by Tswett [Savidan L., 1963]. For almost 100 years, it has been always considered a separation technology comparable to distillation, especially for unstable molecules. The optimization and scale-up of preparative chromatography has never stopped remaining an active research topic.

Compared to analytical chromatography, preparative chromatography separates molecules at a larger scale. For example, Pharmacia Fine Chemicals and Amicon (now part of W R Grace), in order to support and complement their interests in the biotechnology field, built supply acrylic, glass, or stainless-steel columns with diameters of up to 1.8 m. These columns have been proved useful in affinity chromatography applications. Finnish Sugar Co. Ltd of Helsinki, Finland, is the leading company in batch liquid chromatography applications with specific interests in the carbohydrate field. They have constructed several large-scale systems worldwide and recently have commissioned a plant in Germany consisting of seven 3.6 m x 12 m high columns used to devulgarize 60 000 tons of molasses per year [Ganetsos G., 1992].

Batch chromatography was the first industrial application. It has several inconvenient: firstly, a long column is needed if components have similar physical and chemical properties. Then, it has a limited productivity since it works in a discontinuous way. Its most significant weakness is the dilution during separation which increases the concentrating cost afterwards. Nowadays it is still applied in pharmaceutical industries for high valued molecule separation.

2.3.1 True moving bed

A common shortcoming of batch chromatography is low productivity, high dilution factor, and its discontinuous working mode. To make the separation continuous, a countercurrent operation could be implemented through the True Moving Bed (TMB) technique shown in Figure (1-17).

In a TMB system, the stationary phase sediments because of gravity and is in countercurrent with the mobile phase, and a standard four-section configuration is used for the separation of a binary mixture which is injected in the middle of the column. The eluent, which is commonly the solvent constituting the mobile phase, is fed continuously into zone 1, and the fresh resin is fed in the zone 4. The extract (the fraction enriched with the slower component) is collected at the bottom of zone 2, meanwhile the raffinate (the fraction enriched with the faster component) is collected at the top of zone 3. The resin and eluent are recycled between zone 1 and zone 4.

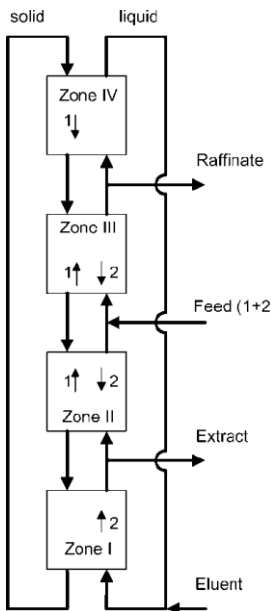


Figure 1-15. True moving bed [Abdelmoumen et al., 2006].

The TMB process possesses unique advantages compared to batch chromatography. Firstly, in the TMB process, the necessary column length for a perfect separation is much less than batch chromatography because of countercurrent.

Secondly, the TMB process allows continuous processing of the feed and therefore has better productivity. However, TMB also has several shortcomings. Firstly, non-homogeneous distribution of resin makes it difficult to characterize the bed. Secondly, the moving solid beads could break into pieces, blocking valves and tubes. Finally, the mobile phase speed is limited by the low fluidization speed due to small size of beads [N. Hideyuki, 1999].

2.3.2 Simulated moving bed

The countercurrent flow maximizes column efficiency. However, the moving stationary phase results in most of the inconveniences of TMB. A multiple column (or multiple sections) fixed-bed system could simulate the countercurrent with an appropriate column switching sequence. The Simulated Moving Bed technology (SMB) comprises at least 4 columns corresponding to 4 zones, as shown in Figure (1-16). One zone could contain more than one column depending on separation requirements. The two inputs (product and eluent) and the two outputs (the extract enriched with the slower compound, and the raffinate enriched with the faster compounds) are sequentially shifted by one column increment in the direction of flow according to a defined time step [I. Mueller, 2021]. This shifting of inputs/outputs simulates the movement of the solid phase, following the movement of compound profiles in the columns. Thus, the product is always injected in the most concentrated zone, and the collection is only carried out in the zones where the compounds are sufficiently pure. The SMB process approximates the TMB process, and the discrepancy between them can be reduced by using more columns that are shorter and proportionally increasing the switching frequency [B.R. Idelfonso, 2020].

Chapter I. Literature review

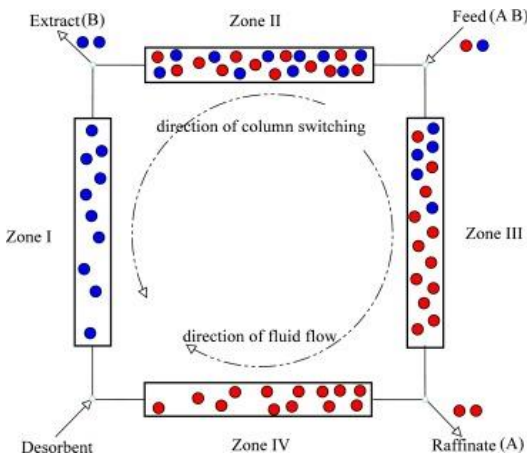


Figure 1-16. Schematic of four-zone SMB chromatography for binary separations. Column positions are periodically switched in liquid flow direction [Q. Lehe, 2018].

The SMB can separate one class of chemical compounds from one or more chemical compounds at a lower cost than batch chromatography and TMB. Meanwhile, it cannot separate compounds that cannot be separated by batch chromatography.

Initial SMB processes were applied in the petrochemical and sugar industries. The first SMB process was invented by UOP (Universal Oil Products) for petrol separation [D.B. Broughton, 1961]. Later, IFP developed the Eluxyl process for the separation of isomers and xylenes. Then enantiomer separation appeared feasible with SMB [M. Negawa, 1992; C.B. Ching, 1993; R.M. Nicoud, 1993]. In 1997 UCB Pharma installed a multi-ton SMB unit for large-scale chiral separation. [McCoy *et al.*, 2000]. In recent decades, the SMB process has been increasingly used in fine chemistry applications, mainly within the pharmaceutical industry. In this area, separations of enantiomers have been performed with great success via the SMB process, giving rise to pure enantiomeric products being commercialized, whereas once they were available only in a racemic mixture that could sometimes be highly undesirable [José *et al.*, 2015].

This technique could also find itself in the petrol oil industry. For example, simulated countercurrent adsorption systems are commercialized by UOP [Jason *et al.*, 2012], Axens [Michel *et al.*, 2015], and Aromax [Otani *et al.*, 1973]. Here is an example of UOP's adsorption system (Sorbex), where the simulated countercurrent technology is applied in an adsorption column.

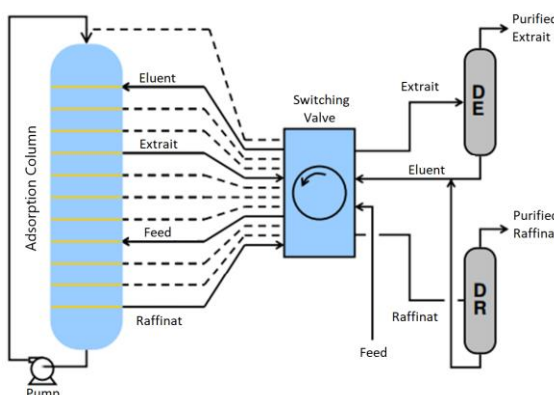


Figure 1-17. Sorbex (UOP) system with SMB technique [Lianming S., 2005].

Chapter I. Literature review

Instead of being contained in discrete beds, the adsorbent is contained in a single bed divided into many sections. A specially designed valve allows fluid to be introduced (or withdrawn) at each section. The flow circuit is completed by a pump that recirculates fluid from the bottom to the top of the column. At any time, only four of the connections to the column are utilized. Flow switching is accomplished by a single, sophisticated rotary valve which, at each switch, advances the eluent extract, feed, and raffinate points by one section in the direction of fluid flow. At the same time the extract and raffinate stream passes to the ancillary distillation column [M.G. Mónica, 2021].

The simulated moving bed process overcomes TMB's weaknesses. However, since the system consists of at least four columns, the installation cost is much higher than batch chromatography or TMB. The developments of SMB will focus on the improvements in the consummation of eluent, dilution rate and productivity.

2.3.3 Developments of SMB

Based on the traditional SMB technology that moves the inputs/outputs simultaneously, many variants of SMB have been developed and patented over the last 30 years. These processes reach their targets by changing operational parameters such as step time, feed concentration, liquid flowrate, valve switching, temperature and concentration gradient, etc. In parallel, three-fraction processes have been developed.

Table 1-4. A list of some SMB process and its developments in recent years (part I).

	Year	Inventor	Comments
Traditional SMB for binary separation			
Sorbex	1961	Universal Oil Products, USA	The first patented SMB applied majorly in petrochemistry and sugar industry.
Eluxyl	1990	IFP	The largest SMB unit in the world (South Korea) applied to xylene isomers
Multition SMB	1997	UCB Pharma	The first industrial application for chiral molecules production
Non-traditional SMB for binary separation			
ISMB	1991	Ryoka Techno Engineering & Construction Co. Tokyo Japan	An optimized process from Varicol
M3C	2006	LSGC & Novasep	A Multicolumn process integrating a concentration step
Varicol	2000	Novasepe	Adjustable length of each zone.
Powerfeed	1991	The Amalgamated Sugar Company, Utah, USA	Variation of feed flowrate.

Chapter I. Literature review

Multifeed	2005	School of Chemical Engineering, Purdue University, USA	SMB with more than one entry.
Modicon	2002	Max-Planck-Institute Dynamics of Complex Technical Systems,	Modulation of feed concentration from 0 to 2 times the initial concentration.
FAST	1998	Finnsugar and Applexion	Two or more dissolved material profiles in the system
Outlet stream swing	2007	University of Porto, Portugal	Raffinate and extract recovery in different steps.
Supercritical SMB	1992 to 2016	University of Porto, Portugal University of Degli, Padova, Italie	Supercritical fluid is used as the mobile phase

Table 1-4. A list of some SMB process and its developments in recent years (part II).

Non-conventionnel SMB for ternary separation			
JO process	2001	University of Porto, Portugal	Pseudo-SMB process with 2 sub-steps
BioSC	2003	Novasep	Eluent gradient process
SMB process	2010	Hanyang University, Seoul, South Korea	A four zone SMB process with two desorbent ports, without partial recycle
MCSGP	2007	ETH Zurich, Institute for Chemical and Bioengineering, Suisse	A process which uses solvent gradient
3W-ISMB 3S-ISMB	2012	ETH Zurich, Institute for Chemical and Bioengineering, Suisse	Ternary ISMB process which contains two substeps
SMB in cascade	1998 to 2015	Novasep France Purdue UniVersity USA	Sequential SMB process from 1 column to 15 or even more.

Table 1-2 shows some examples of variants of SMB that have already been applied to the industry. These non-conventional SMB processes are more used in industries than conventional SMB, yet a lot of work is needed to their optimization.

2.3.3.1 ISMB

The ISMB (Improved/Intermittent Simulated Moving Bed) process is based on the classical SMB process. It was invented in the 1990s then commercialized by Nippon Rensui society. In some articles, it is also called the NMCI (Nippon Mitsubishi Chromatography Improved) process. It contains two steps [Rajendran *et al.*, 2009; T. Masatake, 1989], as shown in figure 1-18.

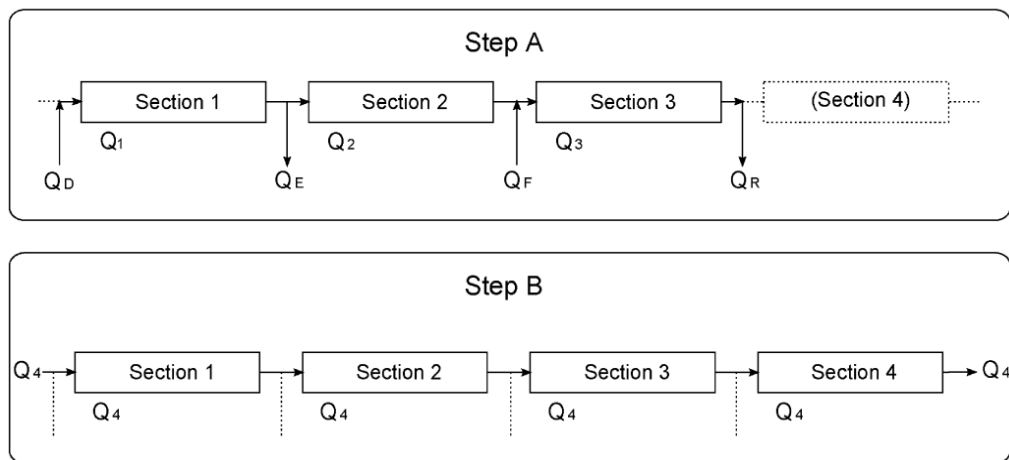


Figure 1-18. The working principles of ISMB system.

During step 1, ISMB works like a traditional SMB with two inlets and two outlets. Only three sections are used during this step. In step 2, all inlets and outlets are closed the fluid circulates with an inside loop. At the end of step 2, the ports are switched in the fluid flow direction, and step 1 is repeated.

In an ISMB process, only 3 of 4 sections are used. The non-used section serves as insurance for separation quality. Thus, if the process is well programmed, the size of ISMB could be reduced to 3C-ISMB (3 column ISMB). Compared to conventional ISMB, the installation cost is reduced without compromising product purity and productivity. Due to the smaller number of columns concerning conventional ISMB, higher internal flow rates can be achieved without pressure drop constraints. The productivity (given in terms of treated product per unit time and unit volume of the stationary phase) will increase significantly [Jermann *et al.*, 2014].

2.3.3.2 Varicol

Invented by Novasep company [P. Adam, 2000], the Varicol process introduces the operation of a continuous unit by the advance of feed and withdraw streams in an asynchronous mode. With this procedure, the column length and configuration are not maintained constant during the period. Therefore, its productivity depends mainly on the feed concentration, size, and the number of the used columns.

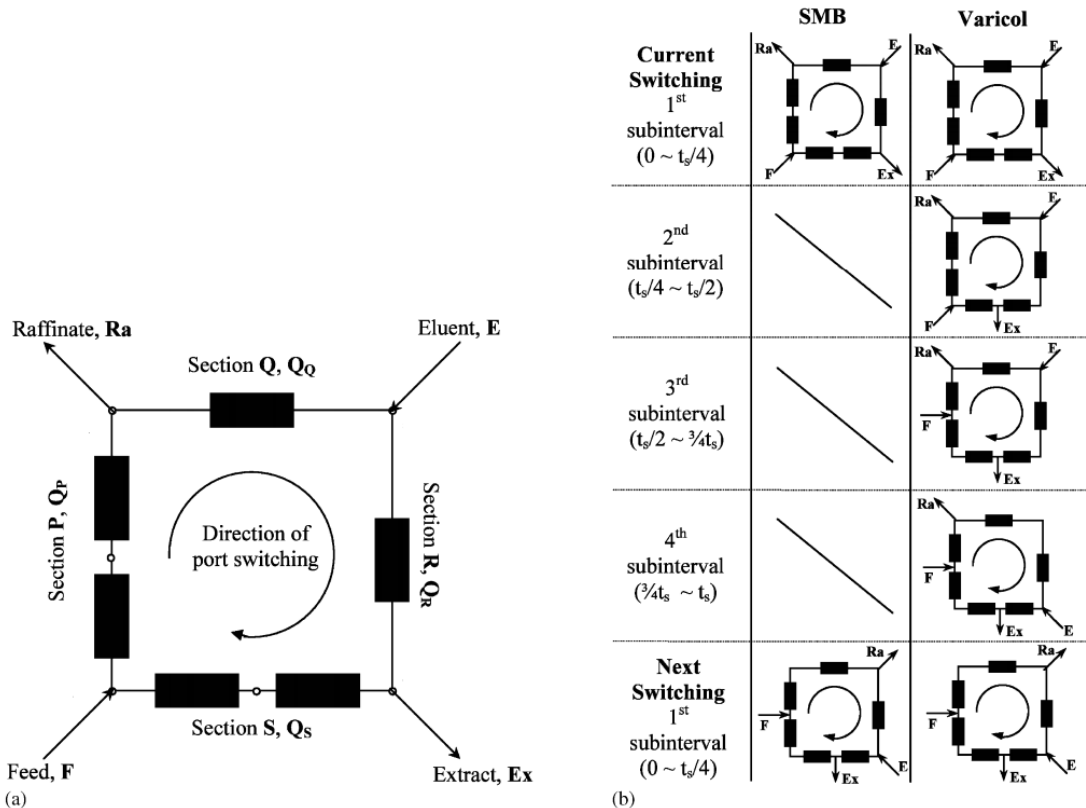


Figure 1-19. (a) Schematic diagram of a six-column SMB system. (b) Principle of operation of SMBR and four-subinterval Varicol (port switching schedule) [Hariprasad et al., 2003].

Figure 1-19 shows the difference of operation modes between SMB and Varicol process. Study shows that Varicol performances are better than those of conventional SMB process. For example, a 5-columns Varicol permits the same purities as a 6-columns SMB with the same productivity. The interest of the process was validated experimentally. Both SMB and Varicol are optimized to reach the highest achievable productivity for given outlet purities. The productivity of a 5-columns system can be improved by 18.5% by using the VARICOL process. [Ludemann *et al.*, 2000].

2.3.3.3 Powerfeed

Like the Varicol process, which allows for the asynchronous movement of ports, the PowerFeed process exhibits more degrees of freedom than the classical SMB process by changing the feed flow rate and allows more room for optimization. This modulation of the feed flow rate was firstly proposed by Morbidelli and Hongzhang [Morbidelli *et al.*, 2002; Hongzhang *et al.*, 2003].

In this operation mode, the internal and external liquid flowrates are modified during the switching period to improve the system's performance. It is found that PowerFeed and Varicol provide substantially equivalent performances, which are, however, significantly superior to those of the classical SMB process [Z. Ziyang, 2003].

Chapter I. Literature review

2.3.3.4 FAST technology

The Finnsugar Applexion Separation Technology (known as FAST) is used for many years in the sugar industry. The main difference between the FAST technologies and SMB is that the FAST process has two or more dissolved material profiles compared to only one in conventional SMB systems. This enables much efficient use of the resin, resulting in higher capacity at a given product recovery, purity and resin volume [Hyoky et al., 1999]. This system was installed in the early 1990s in the Renville and Scotts Bluff factories in the United States and in several factories around the world with satisfactory operations [Mosen et al., 2006].

Other non-conventional SMB operating modes could be found in various articles. The variable feed concentration was suggested by Schramm et al. [Shramm et al., 2002; Shramm et al., 2003] in the Modicon operation mode. The M3C process is patented by Nicoud et al. [M. Nicoud et al., 2004], in which a portion of the extracted product is concentrated and then re-injected into the SMB at the same collection point. The semi-continuous two-zone SMB/chromatography was proposed by J. Hur [Hur et al., 2005], and one-column Chromatography with recycling analogous to a four-zone SMB [N. Abunasser, 2005; Mota et al., 2005]. The introduction of multi-feed streams in the SMB area by analogy with distillation columns led to the formulation of the M.F. (MultiFeed) operating mode presented by Kim et al. [Kim et al., 2005], also called Outlet Streams Swing (OSS) in the work of Sa Gomes and Rodrigues [Sa Gomes et al., 2006].

2.3.4 Multi-component SMB process

Despite various research works on the optimization of SMB processes, ternary separation or more complex mixtures remains a big challenge of SMB-typed process. Generally, the use of SMB process has to be repeated twice to separate ternary mixture, which will at least double the installation cost. The development of an efficient multi-component SMB process is an attractive direction of research. Researchers have already proposed several possible solutions.

2.3.4.1 Sequential SMB (SSMB) process

An SMB process, either conventional or not, can only separate the binary system. Putting 2 SMB in cascade or adding extra columns while keeping the valve switching of SMB, are the most evident approach. For example, Wooley [R. Wooley, 1998] has combined two SMBs and obtained a system of SMB with nine zones. His experiments of separation of 3 components in hemicellulosic hydrolysates: sugars, acetic acid, and sulfuric acid, proved that this system is theoretically feasible.

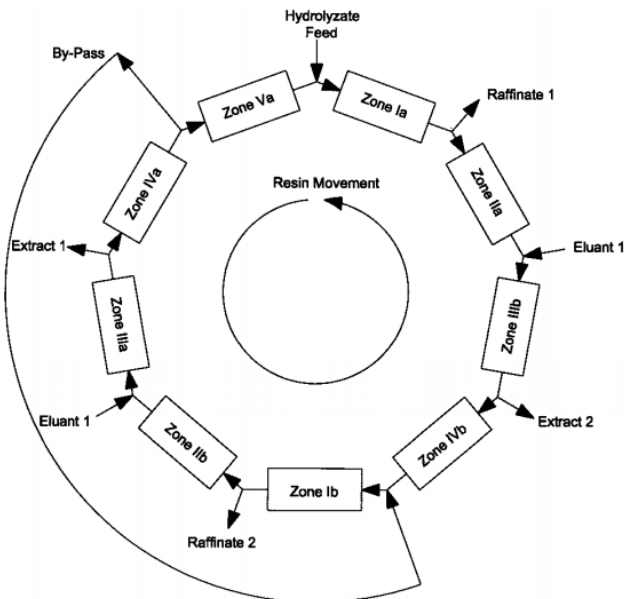


Figure 1-20. An example of sequential SMB process [K. K. Jeung, 2003].

Jeung Kun Kim [K. K. Jeung, 2003] studied the possibility of separating a ternary mixture by a 5-zone SMB followed by 2 SMB in parallel. The results show that, if the mixture does not contain a component that is strongly adsorbed by the bed, this kind of SSMB system could be applied to the industry. In another article [K. K. Jeung, 2004], SSMB systems from 12 zones to 60 zones have been tested for the separation of the quaternary system. Only a few of them are cost-effective.

In other works, 2-zone SMB [Jin S. H. & Phillip C. W., 2005], 3-zone SMB [Simon et al., 2012], 4-Zone SMB [Se-Hee et al., 2010], 5-zone SMB, [Massuda et al., 1993b; Navarro et al., 1997; Beste and Arlt, 2002], and 8-zone SMB [A. S. T. Chiang, 1998] are also studied. The results show that neither of them permits a total separation of a ternary system [Y. A. Beste, 2002]. These research shows that, increasing zones or columns from SMB will make ternary separation easier, yet, it won't help optimizing its performance.

2.3.4.2 Pseudo-SMB Japan-Organic Process (J.O. process)

The pseudo-SMB J.O. process is commercialized by the Japan Organic Company (Fig. 1-23). In contrast to the classic SMB process, it allows the separation of a ternary mixture with the same configuration of 4-column SMB. This SMB-typed chromatography system contains two sub-steps:

- In the first sub-step, the feed (Q_F) and eluent (Q_{E1}) streams enter the system and the component B with inter-phase medium affinity is recovered (Q_i). This step is modeled as a series of preparative chromatographic columns.
- In the second sub-step, there is only one inlet flow 2 of eluent (Q_{E2}) and no feed. The most retained component is recovered in the extract (Q_x) and the less adsorbed species is recovered in the raffinate (Q_R). This step is modeled as a pseudo simulated moving bed with no feed. At the end of this step, the intermediate species B is located downstream of the feed point. Zones and injection/collection points are then switched to simulate countercurrent as in the traditional SMB process.

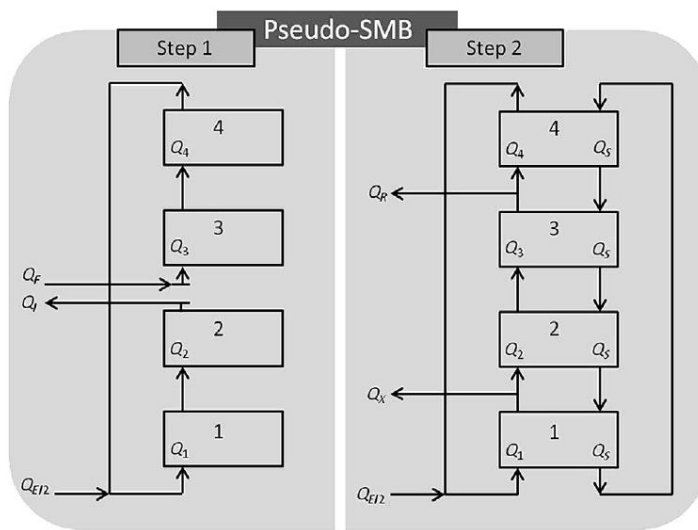


Figure 1-21. The two sub-steps of J.O. process [G. Vera, 2001].

The zone 4 here is an empty column for the assurance of the separation quality. The flowrates in each zone are different which gives more freedom of optimization.

G. Vera et al. [Vera et al., 2001] compared J.O. process and two SMB in cascade during a ternary separation. The results shows that purity, recovery rate, productivity and solvent consumption are similar in both systems. However, the investment in two SMBs is higher than in one J.O. system.

2.3.4.3 MCSGP process

The MCSGP process was invented by Swiss Federal Institute of Technology in Zurich [A. Lars, 2007], which can separate three components represented by S(strong), P(product), and W(weak). This SMB-typed chromatography system can be divided into five zones, which corresponds to columns 1 to 5 in Figure 1-22. Column 6 contains nothing but eluent. The concentration in each zone is roughly represented in Figure 1-23.

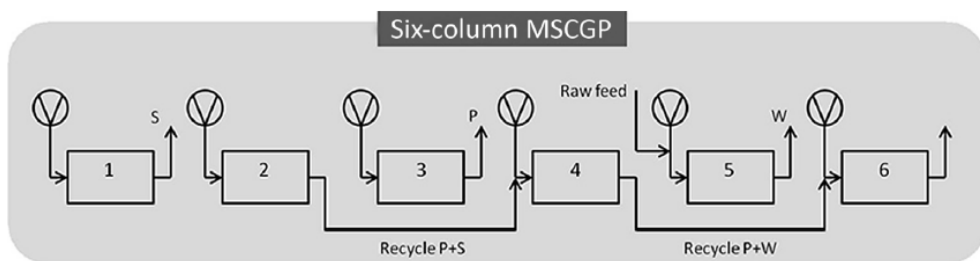


Figure 1-22. A simplified schema of a six-column MCSGP process.

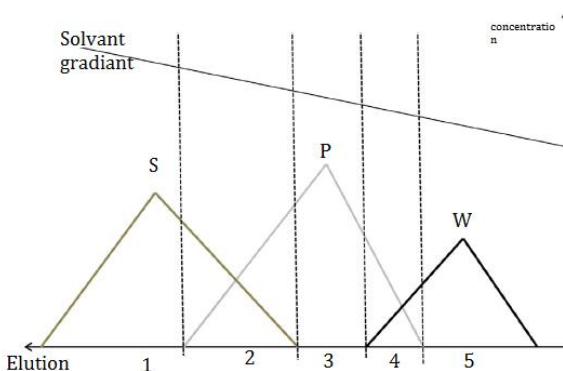


Figure 1-23. A simplified schema of the concentration profile inside the system shown in Figure 1-22.

The mixed product is recycled at the exit of columns 2 and 4 and then injected into columns 4 and 6. The strong fraction exits at the end of column 1, and the fast fraction exits at column 5. Column 3 contains the product only. After a predetermined time-sequence, valve positions will be shifted by one column as for the traditional SMB process. The MCSGP process is a complicated process and is often operated with eluent gradient technology, where different types of eluents are used depending on the target affinity to the resin.

At least 6 columns are required in the original MCSGP process. Later, an improved version reduces this number to 3 in 2010 [C. Grossmann, 2010] then 2 in 2015 [Papathanasiou et al., 2015]. Yet, the high dilution rate remains its weakness to overcome. Thus, it is preferred in pharmaceutical industry where molecules are high value-added such as proteins and polypeptides.

2.3.4.4 BioSC Process

The BioSC multicolumn chromatographic process developed by Novasep is applied mainly in separation problems associated with biopharmaceutical downstream processing. The BioSC process was designed to be a continuous process that allows a better use of the capacity of the stationary phase.

The BioSC is a sequential multicolumn system composed of two to six columns connected in series. The process working principle is the same as that illustrated in Figure 1-24. It was shown that the use of Novasep's BioSC technology, in the purification of mAb (monoclonal antibody) using protein A media, leads to a significant improvement in both productivity and economic savings relatively to the batch chromatography process [Rodrigues A.E., 2015].

Compared to binary separation, ternary separation with SMB-typed process remains a discussed topic. Industrial processes are capable to reach the ternary separation target, yet their performance need to be further optimized. The examples presented above show that most of ternary processes need more than 4 columns and propose limited applications. This fact motivated part of this PhD work, with the objective of developing a new ternary process with better performance and wider application range, together with the required experimental and modeling tools needed to achieve this goal.

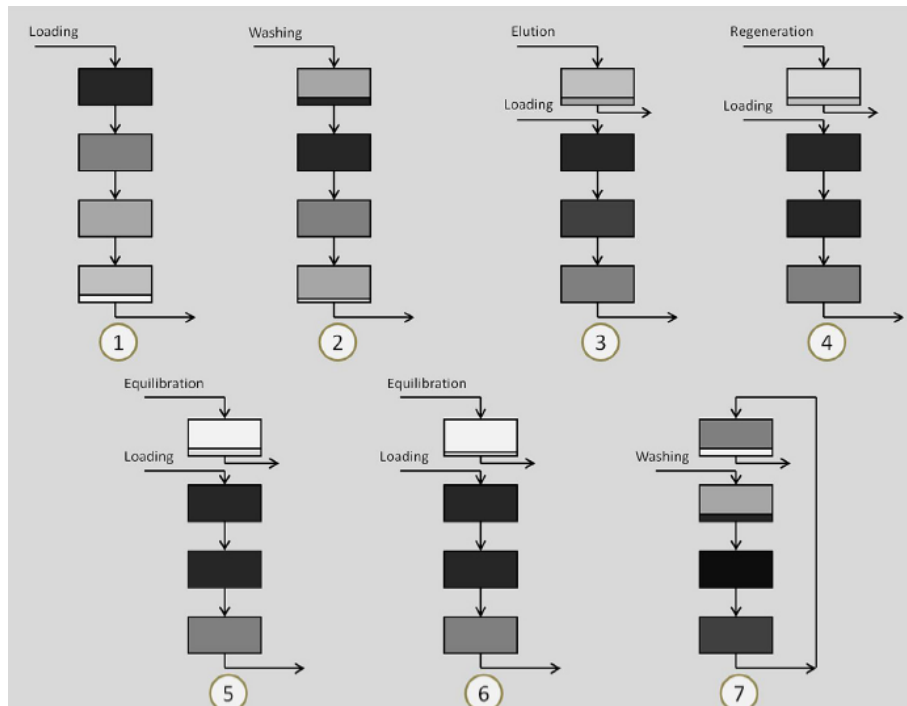


Figure 1-24. A simplified schema of BioSC process with profile obtained from the official site of Novasep (<https://www.novasep.com/media/articles-and-publications/18multicolumnchromatography-bioprocess.pdf>).

3 Modeling of chromatography

Experimentally, a long time is required, sometimes days, for a multi-column SMB system to reach the permanent regime. Tests at industrial scale is thus consuming in both energy and materials. Modeling of chromatography helps to determine critical experimental parameters before experiments, therefore, reduces experimental cost. It also enables studying under extreme conditions which are not easy to reach in reality.

Chromatography modeling involves two aspects: the column model and the physico-chemical model. The chromatography column could be treated either as a continuous packed column or a plate column and the column model determine the expression of the mass balance in the mobile phase. The physico-chemical model defines equilibrium and mass transfer equations, and amend mass balances. Finally, a computational method is required to solve the system of equations and perform simulations.

3.1 Column models

Generally, two types of unidimensional column model are used to describe mass transfers inside a chromatography column [Guiochon et al., 2006]:

- Continuous models, solved by usual finite methods, where the column is discretized into a large number of very small elements. The continuous model treats the distribution of the solute between the mobile and the stationary phases as a continuum. In this case, the axial dispersion depends on the axial dispersion coefficient D and the global mass transfer coefficient k_d .

Chapter I. Literature review

- Discontinuous models where the chromatography column is assimilated to a plate column. Each theoretical plate acts as a perfectly stirred reactor. In this case, the axial dispersion becomes an emerging property of the theoretical plate number NET.

Discontinuous models are easy to code and to solve and require low CPU time. However, since the axial dispersion is an indirect effect of the plate number NET, this model imposes the same axial dispersion for all compounds. Thus, this model is not appropriate for multi-component chromatography simulation if their axial dispersion coefficients D are not similar.

3.2 Physico-chemical formulation of the chromatography system

Chromatography can be roughly divided into linear and non-linear chromatography, or ideal and non-ideal chromatography depending on the type of isotherm and mass transfer effects (mass transfer resistance and axial dispersion). The non-ideal non-linear chromatography is closest to the reality, yet also the most complicated system to solve. The ideal and linear chromatography considers an instantaneous mass transfer, no axial dispersion and a linear isotherm. It is often used to model analytical chromatography, but it is less adequate, so rarely used, for preparative chromatography [Bingchang et al., 2004].

3.2.1 Linear and non-linear chromatography

The adsorption isotherm presents the relation between the concentration in the stationary phase and the concentration in the mobile phase when equilibrium is reached. Most of chromatography separation have a nonlinear isotherm except in analytical chromatography, where the isotherm is usually almost linear due to the low concentration of the injected sample. In preparative chromatography, the concentration is maintained at a high level to increase the productivity. Thus, nonlinear isotherms became the standard [Martin G., 2020].

In linear chromatography, the equilibrium concentrations of a component in two phases are connected with a linear function. For example

$$q = b \cdot c \quad (1 - 8)$$

Where

q : Concentration in stationary phase in mol/L of resin

b : Equilibrium coefficient

c : Concentration in the mobile phase in mol/L

Linear chromatography suits well for most of the phenomena observed in analytical chromatography if the concentration of the injected sample component is sufficiently low. In such case, it is possible to mathematically solve the chromatography mass balance even with a continuous column model. It can be proved that the individual band shapes and the retention volume are independent of the sample composition and its amount. The peak height is proportional to the amount of each component in the injected sample [Shamsul et al. 2016].

Nonlinear chromatography is more often seen in industry. The nonlinearity usually happens at

Chapter I. Literature review

high concentration in the mobile phase or low adsorption capacity in the stationary phase. In most cases, the adsorption is governed by a Langmuir mechanism:

$$q_i = q^{max} \cdot \frac{b_i \cdot c_i}{1 + \sum b_i \cdot c_i} \quad i = 1:k \quad (1 - 9)$$

The Langmuir-type adsorption has several assumptions [Sircar *et al.*, 2017]:

- The surface containing adsorbing sites is perfectly flat with no corrugations (homogeneous).
- The adsorbing molecules adsorb into an immobile state.
- All sites are equivalent.
- Each site can hold at most one molecule of A (mono-layer coverage only).
- There are no interactions between adsorbate molecules on adjacent sites.

When the concentration c_i or affinity coefficient b_i is too small, and the term $b_i \cdot c_i$ is negligible compared to 1, the Langmuir isotherm equation turns into a linear isotherm:

$$q_i = q^{max} \cdot b_i \cdot c_i \quad i = 1:k \quad (1 - 10)$$

Moreover, if the stationary phase contains two different adsorption sites, a bi-Langmuir adsorption isotherm could be used:

$$q_i = q_1^{max} \cdot \frac{b_i \cdot c_i}{1 + \sum b_i \cdot c_i} + q_2^{max} \cdot \frac{\beta_i \cdot c_i}{1 + \sum \beta_i \cdot c_i} \quad i = 1:k \quad (1 - 11)$$

For multi-stage adsorption, BET equation (Brunauer, Emmett et Teller) [Brunauer *et al.* 1938] is the most commonly used isotherm:

$$q_i = \frac{q^{max} \cdot b_i \cdot x_i}{(1 - x_i)(1 + (b_i - 1) \cdot x_i)} \quad i = 1:k \quad (1 - 11)$$

Where x_i is the saturation degree, which is the ratio between the actual concentration and saturation concentration in the mobile phase.

Other nonlinear isotherms are available such as Freundlich [Ng *et al.*, 2002], GAB [Timmermann E.O. & Chirife J., 1991; Roos Y.H., 1993], Halsey [Halsey G., 1951] or Oswin [Oswin C., 1946].

3.2.2 Ideal and Non-Ideal Chromatography

Chromatography can be classified into ideal and non-ideal chromatography depending on the importance of mass transfer phenomena. In an ideal chromatography the axial dispersion is ignored and there is no mass transfer resistance between two phases. In reality, these phenomena are unavoidable no matter which type of resin or mobile phase. Various factors (material and size of bead, column size, fluid temperature etc.) could impact mass transfer [Artak *et al.* 2015]. Therefore, there is no universal correlation which can calculate precisely the dispersion and the mass transfer coefficient.

In the continuous column model, the dispersion term is expressed by a second ordered partial differential term which increases the difficulty to solve the mass balance. Thus, sometimes the dispersion term is ignored, or compensated by other terms.

Chapter I. Literature review

The mass transfer from the mobile phase to the stationary phase involves four mechanisms placed in series: i) The convection in the mobile phase. ii) The diffusion through the film. iii) The diffusion from the surface to the inside of particle. iv) The reaction between solute and functional group fixed on the surface of the particle. The diffusion terms are always the limiting mechanisms of mass transfer [Pranay G., 2013].

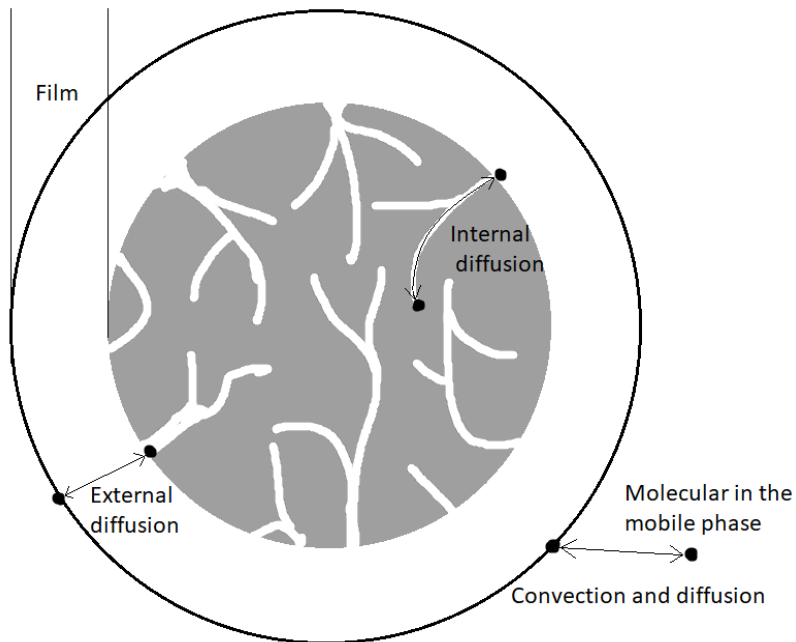


Figure 1-25. Mass transfer resistance in the scale of bead.

The internal mass transfer depends mainly on particles structure. Even though convection can happen inside some particles, it is usually ignored due to the small size of the pore [Carta et al., 1993; Rodrigues et al., 1996]. The mass transfer inside these pores is then driven only by molecular diffusion. The coefficient of diffusion inside pore should be redefined by following equation:

$$D_p = \frac{\varepsilon_p D_{ext}}{\tau} \quad (1 - 13)$$

where D_{ext} is the external diffusion coefficient, τ is the tortuosity and ε_p is the inner porosity of the bead. This equation is based on 4 assumptions:

- The particles are spherical and have a uniform density. The functional groups are uniformly attached on the surface of particles.
- The inside pore diffusion coefficient does not depend on the solute concentration and the charge of ion exchange resin.
- The porosity of particle ε is constant during ion exchange step.
- The resistant of external mass transfer is negligible.

In the stationary phase the mass balance reads:

Chapter I. Literature review

$$\varepsilon_p \frac{\partial C_p}{\partial t} + (1 - \varepsilon_p) \frac{\partial C_s}{\partial t} = D \left(\frac{\partial^2 C_p}{\partial r^2} + \frac{2}{r} \frac{\partial C_p}{\partial r} \right) \quad (1 - 14)$$

Where ε_p is the inner porosity of bead, C_p is the pore concentration in solution, C_s is the pore concentration in solid phase, r is the particle radius. C_p and C_s are in equilibrium described by adsorption isotherms.

In the mass transfer film outside the stationary phase, the gradient of concentration is the driving force for mass transfer and the flux is assumed to be proportional to this driving force. The external diffusion flux is calculated by Fick's law:

$$J = -D_{ext} * \frac{\partial c}{\partial x} = -\frac{D_{ext}}{\delta} * (c - c_i) = k_f * (c - c_i) \quad (1 - 15)$$

where J is the flux (mol/m^2), c the concentration in the mobile phase, c_i the concentration at the interface (mol/L), δ film thickness (m), k_f the local mass transfer coefficient and D_{ext} the external diffusion coefficient (m^2/s).

3.2.3 Calculation of dispersion coefficients and van Deemter curve

3.2.3.1 Empirical correlations

The determination of the two main parameters for mass transfer (external diffusivity D_{ext} and mass transfer coefficient k_f), is a challenging issue of chromatography simulation. Researchers have proposed many empirical equations with dimensionless numbers that suit different situations. For example [Armenante et al., 1989]:

$$Sh = 2 + 0.52 * \left(\frac{\omega^{-1/3} d_p^{4/3} \rho}{\mu} \right) * Sc^{1/3} \quad (1 - 16)$$

where ω is the stripping power per mass unit of liquid, ρ and μ are mass density and dynamic viscosity of the solution. Sc is the Schmidt number and Sh is the Sherwood number which are defined by following equations:

$$Sh = \frac{k_f d_p}{D_{ext}} \quad Sc = \frac{\mu}{\rho * D_{ext}} \quad (1 - 17)$$

In a packed bed, the Peclet number Pe is a very useful non-dimensional number. It reflects the characteristic ratio of convective transport rate to diffusive transport rate. Many researchers have tried to give an estimation of Pe from other dimensionless constants. The most known is the correlation proposed by Chung et al. [Chung et al., 1968]. This equation does not consider molecular diffusion since, in most cases, the resistance due to molecular diffusion is at least ten times smaller than other resistances:

$$\varepsilon_b Pe_p = 0.2 + 0.011 Re^{0.468} \quad (1 - 18)$$

where Pe_p is the Peclet number based on the particle size ($= v \cdot d_p / D_{ext}$), ε_b is the total bed porosity and v is the interstitial velocity.

While ignoring mass transfer resistance, de Ligny [C. L. de Ligny, 1970] proposed another correlation that combines eddy diffusion and molecular diffusion.

Chapter I. Literature review

$$\frac{1}{Pe_p} = \frac{D_{eff}}{d_p \cdot v} = \frac{\lambda}{1 + C \cdot D_m / (d_p \cdot v)} + \frac{\gamma \cdot D_{ext}}{d_p \cdot v} \quad (1 - 19)$$

where λ , γ , and C are dimensionless constants, which depend on the geometry of particle and packed bed and the flow rate. D_{eff} is effective diffusion coefficient, accounting for both convective and diffusive dispersion and D_m is the molecular diffusion coefficient.

Based on the work of Chung, and de Ligny, Seyed [O. R. Seyed 2017] fitted experimental data sets and added the effect of molecular diffusion to propose a new correlation:

$$\frac{1}{Pe_p} = \frac{0.7 \cdot D_{ext}}{2 \cdot r \cdot v} + \frac{\varepsilon_b}{0.18 + 0.008 \cdot Re^{0.59}} \quad (1 - 20)$$

where r is the particle radius.

Many other empirical equations exist in literature. They are either too complicated or do not have better accuracy [A.M. Athalye, 1992; J.J. Gunn, 1987; D.L. Koch, 1985].

3.2.3.2 The van Deemter curve

Instead of empirical equations based on dimensionless numbers, the dispersion effect could be evaluated by tracing the van Deemter curve of the packed column. The van Deemter curve describes the relationship between HETP (inversely proportional to the global dispersion) and the interstitial velocity v (in $m \cdot s^{-1}$). The column efficiency is represented by height equivalent of theoretical plate HETP, which also symbolizes the dispersion in the column.

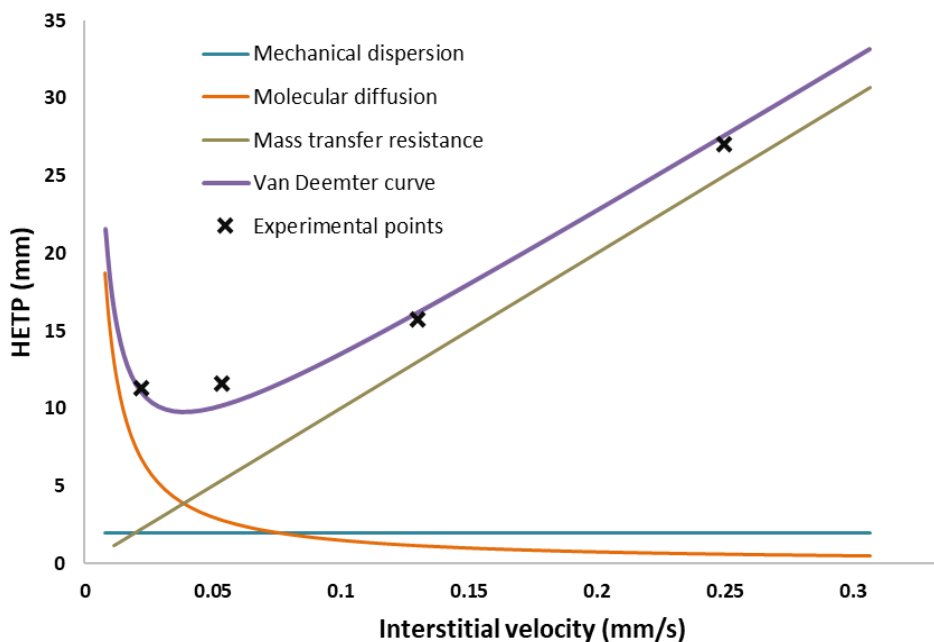


Figure 1-26. Example of van Deemter curve of succinic acid with a strong anionic resin.

The mathematical expression of van Deemter curve is also called the plate height equation. The most known is the van Deemter equation, which expresses the plate height as the sum of three terms corresponding to three contributions mentioned above:

Chapter I. Literature review

$$H = A + \frac{B}{v} + C \cdot v \quad (1 - 21)$$

Where:

- A is the Eddy diffusion (mechanical dispersion). The column packing consists of particles with flow channels between them. Due to the difference in packing and particle shape, the speed of the mobile phase in the various flow channels differs, and molecules travel along different flow paths through the channels. Factors such as particle size, shape, structure, roughness are all influencing by factor A . Even though the Eddy diffusion is usually considered independent of the flow velocity, this is not entirely true at low flow rates.
- B/v is the longitudinal diffusion: it refers to the diffusion of individual molecules in the mobile phase along the longitudinal direction of a column. It represents the sole source of dispersion which still exists when the flow is switched off. It encompasses the combined effect of the molecular species diffusion in the mobile zone (= zone outside particles) and in the stagnant mobile phase liquid inside the particles with the diffusion they experience when being in the retained state [H. Song *et al.*, 2018].
- $C \cdot v$ is the resistance to mass transfer: a chromatographic system is in dynamic equilibrium. As the mobile phase is moving continuously, the system has to restore this equilibrium continuously. Since it takes some time to restore equilibrium (resistance to mass transfer), the concentration profiles of sample components between the mobile and stationary phases are always slightly shifted, which results in additional peak broadening [Siouffi A. M., 2006].

The mathematical expressions of A , B and C are commonly discussed research subject. The original article of van Deemter proposed the following expression [van Deemter J.J., 1956]:

$$A = 2 \cdot \beta \cdot d_p \quad B = 2 \cdot \frac{D_m}{\tau} \quad C = 2 \cdot \left[\frac{\varepsilon/\alpha}{(1 + \frac{1}{F \cdot b})^2} \right] \quad (1-22)$$

where F is the phase ratio $(1-\varepsilon)/(\varepsilon)$, b is the linear equilibrium constant between two phases, D_{eff} is the effective dispersion coefficient (in m^2/s) and α is the liquid side local mass transfer coefficient (in s^{-1}).

In the original article, the axial dispersion effect, represented by a coefficient D_{eff} , is expressed as the sum of molecular diffusion and mechanical dispersion. It could be calculated *via* the values of A and B in the Langmuir equation:

$$D_{eff} = \frac{D_m}{\tau} + \beta * d_p \cdot v = \frac{A}{2} * v + \frac{B}{2} \quad (1 - 23)$$

where τ is the tortuosity of the bed, β is a packing characterization factor, d_p is the mean particle diameter (in m) given by the resin producer.

Researchers have proposed other mathematical expressions of three terms in van Deemter equation for better accuracy. These equations have different application conditions. For example, while the mobile phase is porous silica, Katz and al. (E. Katz, 1983) proposed the following precise expression of van Deemter equation:

Chapter I. Literature review

$$H = 2\lambda d_p + 2\gamma \frac{D_m}{v} + \left[\frac{d_p^2(1 + bk + ck^2)}{24(1 + k)^2 D_m} \right] * v \quad (1 - 24)$$

Where v is the interstitial velocity, d_p is the particle size, D_m is the molecular diffusion coefficient in the mobile phase, λ is the tortuosity factor (around 0.5), γ is the obstructive factor (0.6–0.8) and k is the retention factor. a , b and c are empirical constants that equal to 0.37, 4.69 and 4.04.

Instead of the van Deemter equation, many other plate equations were also published and appeared to have a good agreement with experimental data, such as:

1965: Giddings [J.C. Giddings, 1960]

$$H = \frac{A}{1 + E/v} + \frac{B}{v} + C \cdot v \quad (1 - 25)$$

1976: Horvath [Horvath et al., 1976]

$$H = \frac{1}{1/A + 1/(C \cdot v^{1/3})} + \frac{B}{v} + D \cdot v^{2/3} + E \cdot v \quad (1 - 26)$$

1977: Knox [J.H Knox, 1976]

$$H = A \cdot v^{1/3} + \frac{B}{v} + C \cdot v \quad (1 - 27)$$

1983: Knox [J.H Knox, 1983]:

$$H = \left[\frac{1}{A} + \frac{1}{Dv^n} \right]^{-1} + \frac{B}{v} + C \cdot v \quad (1 - 28)$$

Like in van Deemter equation, mass transfer and dispersion coefficients are calculated with A , B , C and sometimes D terms. Karyn et al. [Karyn et al., 2008] has compared these equations and find out that all these equations fit experimental data well. By visual inspection, it is difficult to tell which equation fits better than others. Fifty years after its introduction, the van Deemter equation still remains an accurate representation of band-broadening processes.

Other chromatography models exist such as Houghton model which suits for non-linear chromatography considering pressure drop [Houghton J., 1960], Haarhoff–van der Linde model for overload conditions [Cretier et al., 1984], Thomas model which assumes Langmuir kinetics of adsorption-desorption and no axial dispersion [Sadroddin G. S., 1992], and exponentially modified Gaussian model which is a good model for typical liquid chromatography peaks [Naish P. J., 1988].

3.3 Numerical methods

The mass balance of a non-linear non-ideal mono component chromatography equation (demonstration in chapter II) writes as:

$$-F \frac{\partial f(c)}{\partial t} = \frac{\partial c}{\partial t} + v \frac{\partial c}{\partial x} - D \frac{\partial^2 c}{\partial x^2} \quad (1 - 29)$$

Chapter I. Literature review

Where c and q are the concentration of component in the mobile phase (in mol.m⁻³) and stationary phase (in mol.m⁻³_{res}), D is the axial dispersion coefficient (in m².s⁻¹), v is the interstitial velocity (in m.s⁻¹) and F is the phase ratio $(1 - \varepsilon)/\varepsilon$.

Danckwertz conditions is a commonly used boundary condition in chemical engineering:

$$vc - D \frac{\partial c}{\partial x}_{x=0} = \theta(t), \quad \frac{\partial c}{\partial x}_{x=L} = 0 \quad (1 - 30)$$

Initially, chromatography column contains only eluent. Supposing that the column is long enough, in the zone that the peak has not reached yet, concentration in mobile phase is always zero. Thus, a fictive boundary condition is introduced:

$$c(x = \infty, t) = 0 \quad (1 - 31)$$

Four types of mathematical methods are majorly used nowadays to solve the chromatography differential equations: Finite difference, Galerkin, orthogonal collocation, and conservation element / solution element (CE/SE) method. The choice of numerical methods depends on the column model and physical formulation.

3.3.1 Finite-difference methods (FDM)

FDM are numerical methods for solving differential equations by approximating them with difference equations, in which finite differences approximate the derivatives. FDMs are thus discretization methods [Kaczmarski *et al.*, 1996].

In a 1-D case, assuming the function whose derivatives are to be approximated is properly-behaved, by Taylor's theorem, a Taylor series expansion can be expressed around point x_i :

$$u_{i+1} = u(x_i + \Delta x) = u_i + \Delta x \left(\frac{\partial u}{\partial x} \right)_i + O(\Delta x^2) \quad (1 - 32)$$

Therefore, the order-one derivative reads:

$$\frac{\partial u}{\partial x_i} = \frac{u_{i+1} - u_i}{\Delta x} + O(\Delta x^2) \quad (1 - 33)$$

By developing the Taylor expansion to higher order, the derivative of order 2 can be expressed in many ways. For example, the centralized expression:

$$\frac{\partial u}{\partial x_i} = \frac{u_{i+1} - u_{i-1}}{2\Delta x} + O(\Delta x^3) \quad (1 - 34)$$

The same Taylor expansion is used for both space and time. After the discretization of the chromatography equation, an implicit equation system is usually obtained. The iteration method, like Newton-Raphson, is commonly used here.

3.3.2 Galerkin methods

The Galerkin Finite Element method of lines is one of the most popular and powerful numerical techniques for solving transient partial differential equations of parabolic type. In principle, it is

Chapter I. Literature review

the equivalent of applying the method of variation of parameters to function space by converting the equation to a weak formulation [Kristian *et al.*, 2019].

While applying the Galerkin method to chromatography problems, the concentration in the mobile phase $C(x, t)$ is approximated over the basis function $\varphi_j(x)$ using the weighting values $A_j(t)$:

$$c(x, t) \approx \sum_{j=0}^M A_j(t) \varphi_j(x) \quad (1 - 35)$$

Where M is the number of nodes.

With Danckwerts boundary conditions, by choosing an appropriate basis function, the chromatography equation can be transformed into an ordinary differential equation:

$$\mathbf{P} \frac{d\mathbf{A}}{dt} + \frac{d\mathbf{Q}\mathbf{A}}{dt} - \mathbf{R}\mathbf{A} = \boldsymbol{\phi} \quad (1 - 36)$$

Where $\mathbf{P}, \mathbf{Q}, \mathbf{R}$ are matrix and \mathbf{A} is a vector. Their expressions depend on isotherm.

3.3.3 Orthogonal Collocation

Invented by Villadsen and Finlayson [Carey G.F., 1975], this method nowadays is widely applied in chemical engineering. The solution is expressed on a basis of orthogonal functions. Orthogonal polynomials, such as Tchebychev, Legendre or Laguerre can be used for that purpose. This method uses collocation at a set of points over the studied interval to transform the partial differential equation (PDE) to a set of ordinary differential equations (ODEs).

It has been shown that it is usually advantageous to choose the collocation points as the zeros of the corresponding Jacobi polynomial (independent of the PDE system) [KaczmarSKI et al., 1996].

For example. Supposing $x_i (i = 1: n + 1)$ are zero points of displaced Legendre polynomial in interval $[0,1]$. Using $x_i (i = 1: n + 1)$ as nodes, we construct Lagrange polynomial:

$$y(x) = L_n(x) = \sum_{i=1}^{n+1} l_i(x) y(x_i) \quad (1 - 37)$$

$$l_i(x) = \frac{\pi(x)}{(x - x_i)\pi'(x_i)}$$

Where $\pi(x) = (x - x_1)(x - x_2) \dots (x - x_{n+1})$, $\pi'(x_i) = (x_i - x_1)(x_i - x_2) \dots (x_i - x_{i-1})(x_i - x_{i+1}) \dots (x_i - x_{n+1})$

The 1st and 2nd order derivative of y can be deducted:

$$\frac{dy(x_j)}{dx} = \left(l_1^{(1)}(x_j), l_2^{(1)}(x_j), l_3^{(1)}(x_j) \dots l_{n+1}^{(1)}(x_j) \right) \mathbf{Y} = (\mathbf{A})\mathbf{Y} \quad (1 - 38)$$

Chapter I. Literature review

$$\frac{d^2y(x_j)}{dx^2} = \left(l_1^{(2)}(x_j), l_2^{(2)}(x_j), l_3^{(2)}(x_j) \dots l_{n+1}^{(2)}(x_j) \right) Y = (B)Y \quad (1 - 39)$$

When $x = x_i$,

$$l_i^{(1)}(x_j) = \frac{1}{2} \frac{\pi^{(2)}(x_i)}{\pi'(x_i)} \quad l_i^{(2)}(x_j) = \frac{1}{3} \frac{\pi^{(3)}(x_i)}{\pi'(x_i)} \quad (1 - 40)$$

When $x = x_j \neq x_i$,

$$l_i^{(1)}(x_j) = \frac{1}{x_j - x_i} \frac{\pi^{(2)}(x_i)}{\pi'(x_i)} \quad (1 - 41)$$

$$l_i^{(2)}(x_j) = \frac{1}{x_j - x_i} \left(\frac{\pi^{(2)}(x_i)}{\pi'(x_i)} - 2l_i^{(1)}(x_j) \right) = 2l_i^{(1)}(x_j) \left(l_i^{(1)}(x_j) - \frac{1}{x_j - x_i} \right)$$

This method applies in interval [0,1], meanwhile chromatography equation should be solved from 0 to column length L . We take step length h to divide interval [0, L] into N ($= L/h$) finite elements. Nodes are: $S_i = (i - 1).h$ ($i = 1, 2, 3, \dots, N + 1$). The variable S in the finite element (S_i, S_{i+1}) is then:

$$S = \frac{x - S_i}{h}, S \in [0, 1] \quad (1 - 42)$$

Which is a transformation of $x = S_i + Sh = (i - 1 + S).h$. 1st and 2nd order derivatives are then:

$$\frac{\partial c}{\partial x} = \frac{\partial c}{\partial s} \frac{\partial s}{\partial x} = \frac{1}{h} \frac{\partial c}{\partial s} \quad \frac{\partial^2 c}{\partial x^2} = \frac{1}{h^2} \frac{\partial^2 c}{\partial s^2} \quad (1 - 43)$$

At each finite element (S_i, S_{i+1}) , Lagrange polynomials are constructed at zero points of N_P order Legendre polynomial along with two ends 0 and 1, to approach the concentration $c(x, t)$.

Derivatives on space ($\frac{\partial c}{\partial x}$ and $\frac{\partial^2 c}{\partial x^2}$) are discretized as follows:

$$\frac{\partial c}{\partial x}_{c=c_{ji}} = \frac{1}{h} \sum_{k=1}^{N_P+2} A_{jk} c_{ki} = \frac{1}{h} (A)(c) \quad (1 - 44)$$

$$\frac{\partial^2 c}{\partial x^2} = \frac{1}{h^2} \sum_{k=1}^{N_P+2} B_{jk} c_{ki} = \frac{1}{h^2} (B)(c) \quad (1 - 45)$$

Where c_{ji} is the concentration at j^{th} collocation point in i^{th} finite element, (A) and (B) are matrix mentioned in Eq. 1-38 and 1-39.

Chapter I. Literature review

At each time step, left endpoint of the 1st finite element is decided by boundary condition. On the connection between elements, the function and its 1st order derivative are continuous, which means c and $\frac{\partial c}{\partial x}$ at the right endpoint of element i is equal at the left endpoint $i + 1$.

While applying this method to the chromatography equation, the equation is transformed into a first-order ordinary differential equation and could be solved by methods such as nth order Runge-Kutta method.

3.3.4 CE/SE Method

The CE/SE (Conservation Element / Solution Element) method, proposed by NASA in 1995 [S.C. Chang, 1995], has been applied for simulation of explosion [Wei *et al.*, 2014; Shen *et al.*, 2012], crystallization [Orkomi *et al.*, 2014] or chemical reaction [Qamar *et al.*, 2012; Sadighi *et al.*, 2012].

Based on Gauss's divergence theorem, this method is initially used to obtain highly accurate numerical solutions for one-to-three space dimensional conservation laws involving shocks, boundary layers, or contacting discontinuities. It was first used to simulate chromatography with Langmuir adsorption model in 2004 [Yong *et al.*, 2004].

CE/SE method allows simultaneous treatment of space and time integration. In the case of packed bed chromatography [Lan *et al.*, 2009], global performances of CE/SE method showed a better trade-off between accuracy, stability, and calculation speed compared to traditional methods using an upwind scheme.

The CE/SE (conservation element/solution element) method was chosen in the present work for its ability to deal with space and time integral simultaneously [Chuanyi *et al.*, 2015]. The integral is calculated between normal mesh points and intermediate mesh points, and it takes two integrals to move 1 step forward in space or time. For PDE like:

$$\frac{\partial u}{\partial t} + \frac{\partial f}{\partial x} = p \quad (1 - 46)$$

The Green's theorem tells that the line integral along a closed curve ∂D of a function equals to the integral of the derivative over the plane region D :

$$\oint_C -udx + fdt = \iint_D \left(\frac{\partial u}{\partial t} + \frac{\partial f}{\partial x} \right) dxdt = \iint_D p dxdt \quad (1 - 47)$$

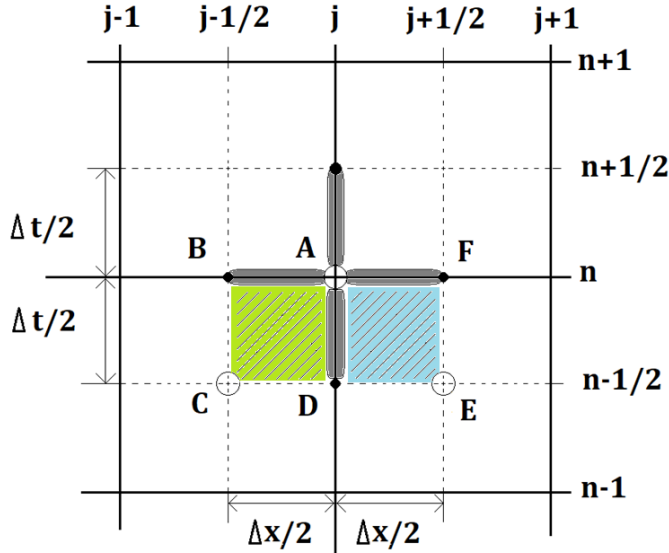


Figure 1-27. The SE (solution element, gray part) and CE (conservation element, green and blue part) at position j and time n . Values at point A are calculated from point C and E at $n-1/2$, values at C or E are obtained from points at $n-1$ via the CE and SE at the point at $n-1/2$.

Figure 1-27 shows the space and time discretization used and the mesh points where all variables are estimated. By definition, the solution element SE (j,n) is the gray space-time interior region centered at point A (j,n) . It includes a horizontal line segment, a vertical line segment, and their immediate neighborhood points (B, D, F).

In this solution element, we chose to approximate u and f values by a first-order Taylor formula from its center point A (j,n) :

$$u^*(j,n) \sim u_j^n + u_{xj}^n(x - x_j) + u_{tj}^n(t - t_n) \quad (1-48)$$

$$f^*(j,n) \sim f_j^n + f_{xj}^n(x - x_j) + f_{tj}^n(t - t_n) \quad (1-49)$$

$$p^*(j,n) \sim p_j^n + p_{xj}^n(x - x_j) + p_{tj}^n(t - t_n) \quad (1-50)$$

Where u_{xj}^n , f_{xj}^n and p_{xj}^n correspond to the space derivative of u , f and p at the mesh point (j,n) , and u_{tj}^n , f_{tj}^n and p_{tj}^n correspond to the time derivative of u , f and p at the mesh point (j,n) .

Equation (1-48) to (1-50) could also be developed to other orders. For example, the source term p could be approximated by the zero-order Taylor formula, which means the value of p is treated as a constant in each solution element:

$$p^*(j,n) \sim p_j^n \quad (1-51)$$

The conservation element CE (j,n) corresponds to the rectangle FADE and ABCD, where the source term p is considered equal at mesh points A, B, D, and F, but different at mesh points C ($p_{j-1/2}^{n-1/2}$) and E ($p_{j+1/2}^{n-1/2}$).

Finally, the Green's theorem applied within the rectangle FBCE by approximating u , f and p leads to the following explicit equation, which enables to estimate u_j^n from values of u , f and p at the previous semi-time step:

Chapter I. Literature review

$$u_j^n = \frac{1}{2} [u_{j+\frac{1}{2}}^{n-\frac{1}{2}} + u_{j-\frac{1}{2}}^{n-\frac{1}{2}}] - s_{j+\frac{1}{2}}^{n-\frac{1}{2}} + s_{j-\frac{1}{2}}^{n-\frac{1}{2}} + p_{j+\frac{1}{2}}^{n-\frac{1}{2}} + p_{j-\frac{1}{2}}^{n-\frac{1}{2}} \quad (1-52)$$

where

$$s_{j\pm\frac{1}{2}}^{n-\frac{1}{2}} = \left(\frac{\Delta t}{2.\Delta x}\right) \cdot f_{j\pm\frac{1}{2}}^{n-\frac{1}{2}} + \left(\frac{\Delta x}{8}\right) \cdot u_x_{j\pm\frac{1}{2}}^{n-\frac{1}{2}} + \left(\frac{\Delta t^2}{8.\Delta x}\right) \cdot f_t_{j\pm\frac{1}{2}}^{n-\frac{1}{2}} \quad (1-53)$$

Proof of Eq. 1-52 is presented in appendix. CE/SE method applies to a first-order partial differential equation. A few modifications are made before applying to the non-ideal chromatography-mass balance, which will be discussed in detail in the next chapter.

4 Objectives of the thesis

A previous work [Lemaire *et al.*, 2016] shows that the Langmuir adsorption model is unsuitable for organic acid separation with strong anionic ion exchange resin, namely in the case of succinic acid and citric acid where the chromatography peak presents an abnormal tailing. Both retention time and peak shape are not well predicted by the Langmuir model.

Another challenge while developing preparative chromatography is multi-component separation. Additional columns are added to SMB system to separate more than 2 fractions, resulting weak productivity and more significant dilution. An increase of system size also makes it longer to achieve permanent regime.

Facing these difficulties, this thesis aims to develop a precise numerical tool which is suited for organic acid separation over strong anionic resin. The abnormal behavior of succinic acid and citric acid is supposed to be explained by integrating ion exchange effect into the model.

3 fraction process such as J.O. process or 3W-ISMB are not largely applied to the industry due to the limit of their performance. Other 3F processes like MCSGP are limited in application domain. Three-fraction mixture is separated mainly by repeating the usage of 2F SMB process.

With the help of this numerical tool, it will be easier to develop a new multi-fraction chromatographical process. The new process will be based on ISMB by modifying its sequence without special conditions such as eluent gradient, thus could be largely applied. Its performance will be compared with 2 3C-ISMB in cascade to show its competitiveness.

Chapter II. Materials and methods

This chapter presents experimental devices and methods used in this PhD work. Numerical simulation of chromatography is a helpful tool to develop multi-column process which reduces experimental cost in both economic and time. However, several physico-chemical properties of the components are required to supply data to the simulation code, namely the axial dispersion coefficient D , the global mass transfer coefficient k_a , and Langmuir coefficients of adsorption isotherms. These coefficients were estimated by frontal analysis and pulse tests.

The first part of this chapter presents the equipments and protocols used. These experiments were carried out on three main types of value-added components produced by hydrolysis of hemicellulose: hexose represented by glucose, pentose represented by xylose, and organic acids represented by formic, acetic, lactic, succinic, and citric acids.

In the second part, the physico-chemical model and the numerical methods used are presented in detail. To model the chromatography column, it could be divided into a certain number of perfectly stirred batch reactors or treated continuously as a packed bed. Each method has its own mass balance formulation and involves different computational strategies. The discontinuous column model was solved by finite difference method and the continuous column model was solved by the CE/SE method. The 3C-ISMB process is briefly explained at the end of the chapter. More details about its tuning and optimization will be given in chapter V.

1 Experimental devices

Separation of sugar and organic acids by chromatography with strong anionic resin was studied by means of the experimental setup detailed in Figure 2-1.

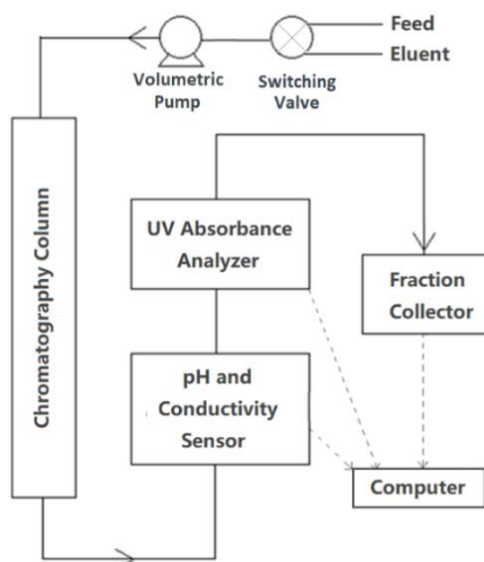


Figure 2-1. Schema of experimental installations.

Chapter II. Materials and methods

The product (feed) or the eluent is injected into the column by a volumetric pump. The liquid phase passes through the column, meanwhile compounds interact with the resin. The output liquid goes successively through a pH/conductivity sensor, an UV absorbance analyzer, and finally, goes to a fraction collector for offline analysis by HPLC. All sensors and the fraction collector are connected to a computer to monitor on-line pH, conductivity, UV absorbance and sample collection.

The eluent is H_2SO_4 solution at pH 1.5 (around 0.02 mol/L) for all experiments. The flowrate was set at 0.5 BV/h (BV represents the total bed volume, pores + solid, equal to 0.35 L). The internal column diameter was 2.5 cm, and bed length was 70 cm. The column was filled with the strong anion resin DIAION UMA 150 (manufactured by Mitsubishi Chemical), whose characteristics are summarized in Table 2-2.

Pump

The pump used here is MasterFlex L/S combined with Easyload head model 7518-10.



Figure 2-2. The volumetric pump MasterFlex.

The pump allows a Rotating speed ranging from 1 to 100 rpm (round per minute), which corresponds to a flow rate of ca. 0.06 to 3400 mL/min depending on pump head and tubing size. The motor is reversible, which allows pumping fluid in both directions. The screen on the pump shows the rpm value. The volumetric flow rate in ml/min depends on the tubing size and was measured manually.

The pump head Easyload 7518-10 was matched with the pump. It is adjustable for multiple tubing sizes. The unique over-center cam design and adjustable tubing retention allow quick tubing changes and significantly reduced maintenance time.

Column

The column used here is the ECO25 model manufactured by YMC Europe Ltd. It has an inner diameter of 25 mm, length of 1 m and an adjustable bed volume (BV) from 330 to 450 mL. It is suitable for all types of soft gels and supports a pressure up to 15 bar. Two adjustable length pistons allow dead zones inside the column to be avoided. The column has a heating-cooling jacket and, in our experiments, the temperature was always set at 25°C. The piston used here is made of PVC and present a good resistance to sulfuric acid at pH 1.5.

Chapter II. Materials and methods



Figure 2-3. The YMC-ECO 25 column with UMA 150 resin inside.

pH , Conductivity and UV measurements

The pH, conductivity and UV sensors are installed at the column output before the collector. These sensors are connected to the computer. Organic acid peaks were shown by the UV absorbance variation. The pH and conductivity sensor monitor variation of pH and conductivity during experiments. In the case of significant variation of pH or conductivity, simulation should be conducted on activity instead of concentration.

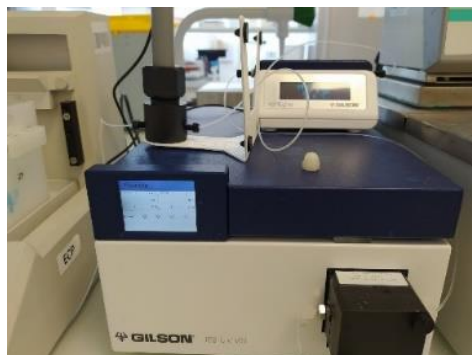


Figure 2-4. The VERITY 1810 Conductivity and pH monitor, 159 UV detector.

The VERITY 1810 Conductivity / pH monitor is used in the present work. It is connected to the computer and measurement results are instantly shown and saved in the computer.

The conductivity sensor works at a pressure up to 13 bar with a readable range from 1 $\mu\text{S}/\text{cm}$ to 999 mS/cm . It acquires a maximum of 10 points per second when connected with Trilution LC software. The dead volume of the detector is 54.1 μL .

The pH sensor works at pressure up to 6.9 bar. At 25°C, its accuracy is ± 0.1 unit. The readable range on the screen is 0-14 pH, but the specification range is from 2 to 12 pH for better accuracy. The dead volume of the chamber is 49.2 μL .

Chapter II. Materials and methods

The UV detector used here is 159 UV-VIS Detector which offers high sensitivity and baseline stability for HPLC applications, including fast LC methods. With an 80 Hz high-speed scanning design, up to four different wavelengths can be monitored simultaneously while acquiring spectral data from 190 to 750 nm. A wide range of flow cells is available for practically any LC application, including PEEK flow cells for analytical and preparative HPLC and pilot-scale flow cells for flow rates up to 1 L/min. Some specifications are listed below:

Table 2-1. Specifications of the 159-UV detector.

Wavelength range	190-750 nm
Wavelength accuracy	+/- 1.5 nm
Bandwidth	5 nm
Data rate	Up to 80 Hz
The volume of the flow cell	10 µL

Fraction collector

The FC 203B Fraction collector by Gilson Inc is used in this work. It has a three-way valve that contains only 3.5 µL dead volume and supports a maximum of 20 psi (1.4 bar) or 20 mL/minute flowrate. The collection schedule can be programmed through its panel or by Gilson software installed in the connected PC.



Figure 2-5. The FC-203B fraction collector.

The collector supports four collection modes used for different situations. The time mode is the most used: the collection time per fraction is specified up to 100 minutes. In this study, it was set to 3 min per tube when working at 0.5 BV/h flowrate, to obtain 7 mL sample per tube.

Other modes are available for different situations, such as the drop mode, where we specify the number of drops (up to 20) collected per fraction, the manual mode, where we launch the collection of samples manually by pushing the start/stop button. In the peak mode, if the fraction collector is connected to a detector, we can instruct the collector to collect only peaks. A peak can be subdivided by drops or time.

A 4 x 11 rack is joined to the collector to support tubes. After each experiment, collected samples are immediately filtrated into HPLC vials. The rest of samples are covered and conserved at 4°C in case of double analysis.

Chapter II. Materials and methods

HPLC

All samples are analyzed by HPLC (Ultimate 3000, Dionex). It is equipped with a pump, a sample collector, a cooler at the column outlet, and a refractometer RI-101 (Shodex) at 35°C. The analytical column is an Aminex HPX-87H (Biorad) connected to a guard column (Micro-Guard cartridge Biorad). It is kept at 45°C within an oven. The mobile phase is a H₂SO₄ solution prepared with Milli-Q water (Direct 8, Millipore) degassed by an online degasser. The Milli-Q water is previously degassed by a vacuum stirring system. Its flow rate is set to 0.5 mL/min, and the injection volume is 10 µL.

X-ray tomography

An EasyTom XL CT Scanner, manufactured by RX-Solutions, was used to obtain a 3D image of the packed bed. EasyTom XL is equipped with two X-ray sources, a high-power micro focus 230 kV and a high-resolution nano focus 160 kV and two imagers, a CCD camera and a flat panel. This allows any combinations from an ultimate resolution down to 0.4 µm to the inspection of very large samples. This CT System is designed to address the 3D applications ranging from material research to industrial applications in R&D. 3D images can be further processed to visualize, measure and analyze samples up to 600 mm in diameter and 720 mm in height.

Consumables used in the experiments

Resin:

A strong anionic exchange resin with a quite uniform particle size, DIAION UMA150, was used in this work. It has standard cross-linkages and solid resistance to acid and base. It has a wide range of applications, especially in manufacturing and pure water processes. Its main characteristics are listed in Table 2-2.

Table 2-2. Main characteristics of the strong anionic resin used in this work (DIAION UMA 150). By convention, SBA resins produced with trimethylamine are called Type 1. When amine is dimethylethanolamine, it is called Type 2.

Matrix	Styrene-DVB Gel
Functional Group	quaternary ammonium (Type 1)
Anion Form	Cl ⁻
Whole Bead Count	95% minimum
Salt Splitting Capacity	1.4 eq/L minimum
Water Content	37-47 %
Uniform Coefficient	1.1 max
Mean Particle Size	220-260 um
Particle density	1.09 g/ml

Originally, the resin is in Cl⁻ form but was put in sulfate form before experiments, by injecting 2 BV of 1 mol/L Na₂SO₄ at 1 BV/h, then 8 BV of eluent to wash bed resin and reach pH equilibrium.

Chapter II. Materials and methods

As provided by the supplier, the approximate pressure drop at various temperatures and flow rates for each meter of bed depth of DIAION™ UMA 150 resin in regular downflow operation is shown in the Figure 2-6 below.

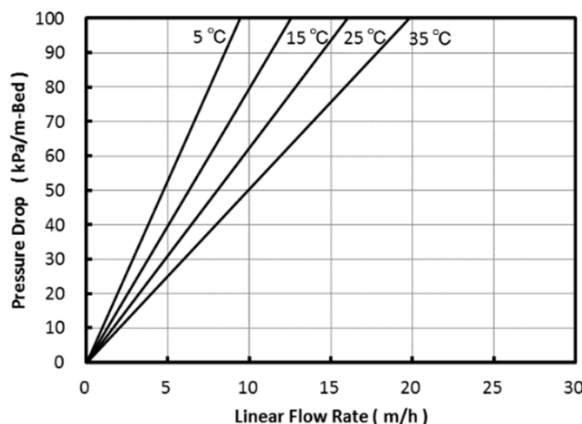


Figure 2-6. The pressure-drop of the resin bed (from datasheet of resin).

In the current work, the range of flowrate is around 1 m/h at 25°C. Therefore, the pressure-drop of the bed is less than 10 kPa/mBed. With a column length of 0.7 m and a working pressure of ca. 1 bar, the system can then be considered as isobar.

Chemical products

Table 2-3 gives the information about chemical products used in this work:

Table 2-3. Chemical Materials used in experiments.

	Producer	N° CAS	Purity
Glucose	Acros Organics	450740050	99%
Xylose	BioChemica	A2241,0500	99.9%
Acetic acid	Fisher scientific	64-19-7	glacial
Formic acid	Sigma-Aldrich	64-18-6	>98%
Lactic acid	Acros Organics	79-33-4	90%
Succinic acid	Acros Organics	110-15-6	99%
Citric acid	Acros Organics	5949-29-1	99.5%
Sulfuric acid	VWR PROLABO	7664-93-9	95%
NaOH	CARLO ERBA	1310-73-2	99+%
Na₂SO₄	Acros Organics	7757-82-6	99+%

2 Protocols of pure component column tests

Some physico-chemical parameters of the packed bed and components are required for the numerical simulation, namely maximum ion exchange capacity q_{max}^{ei} , porosity ε , global mass transfer coefficient k_a , dispersion coefficient D , and Langmuir coefficients N and k_s . These parameters were measured by pure component frontal analysis or pulse tests. All experiments were conducted at pH 1.5 at 25°C: pH 1.5 is a common pH of hemicellulose hydrolysis when treated by H₂SO₄, and a low temperature will facilitate adsorption process (exothermic).

2.1 Determination of bed properties

The packed bed could be characterized in many aspects, among which the most used are porosity and tortuosity. For the ion exchange resin, the maximum ion exchange capacity is also an important parameter.

Porosity, or void fraction, quantifies the void spaces in a porous material. It is simply obtained as the volume of voids over the total volume, which is necessarily between 0 and 1. In the present work, it was measured by the mean residence time of a tracer (1 mol/L Na₂SO₄ solution) with the device depicted in Figure 2-1. The column was initially in SO₄ form and rinsed with eluent (ca. 0.025 mol/L H₂SO₄ solution at pH 1.5). Then 10 mL of the 0.1 mol/L Na₂SO₄ solution was injected then eluted with the eluent at 1 BV/h.

The variation of conductivity at the column output was monitored. The mean residence time was calculated based on the outlet conductivity curve and allows to evaluate the total effective volume of liquid inside the system, called V_{total} .

Then, the column was bypassed from the system, and the same protocol was performed again to measure the volume of other materials, called V_{other} . The difference between these two volumes is then the volume of the effective liquid phase in the column. The porosity calculated by this method is then the effective porosity:

$$\varepsilon = \frac{V_{total} - V_{other}}{V_{bed}} \quad (2-2)$$

For comparison, a small part of the resin bed was sampled and scanned by EasyTomXL (Ultra 150-160, RX Solutions) with a voxel size of 3 μm³ using a nano-focus vacuum tube for X-ray emission at a working voltage of 75 kV and working current of 100 μA. A total of 1100 radiographs were obtained, each with an exposure time of 0.9 s and an average of 5 frames, using a CCD detector of 2016 x 1344 pixels. Avizo 2019.2 software (Thermo ScientificTM) was used to generate 3D volume.

The tortuosity was also estimated by 3D tomograph scan. The void space in the sample was scanned and divided into 100 stages. The centroid of each stage was calculated, and the tortuosity was defined as the ratio between the total lined-up distance of centroids and the thickness of the scanned bed.

Chapter II. Materials and methods

The maximum ion exchange capacity q_{max}^{ei} represents the quantity of quaternary ammonium group NR_4^+ sites on the surface of the resin. This value is crucial for the mass balance of anion in the stationary phase. It is estimated by the following protocol:

The resin in the column was put into OH^- form by injecting 5 BV of 1 mol/L NaOH (C_{NaOH}). Then, 10 mL of resin bed (V_{bed}) in OH^- form was taken out from the column to a beaker, along with its mobile phase (1 mol/L NaOH). 6 mL (V_{rinse}) of 1 mol/L NaOH was added to flush the resin on beaker wall. Then 40 mL (V_{HCl}) of 1 mol/L HCl (C_{HCl}) was mixed with the resin during 10 min. Finally, a liquid sample from the beaker is titrated (without resin) with 1 mol/L NaOH. Its remaining H^+ concentration (C_{final}) was measured at 0.37 ± 0.01 mol/L. The initial OH^- -concentration on resin, which correspond to q_{max}^{ei} , is then deduced with Eq. 2-3:

$$q_{max}^{ei} = \frac{(C_{\text{HCl}} \cdot V_{HCl} - C_{final} \cdot (V_{HCl} + V_{bed} \cdot \varepsilon + V_{rinse}) - C_{\text{NaOH}} \cdot (V_{bed} \cdot \varepsilon + V_{rinse}))}{V_{bed} \cdot (1 - \varepsilon)} \quad (2 - 3)$$

2.2 Mass transfer coefficients determination: van Deemter curve

Mass transfer properties of each component are studied by tracing their van Deemter curve. During a pulse test, 10 mL of the product (0.033 BV) is injected and then pushed through the column by the eluent (H_2SO_4 pH 1.5). The HETP in van Deemter curve is then calculated by analyzing the standard deviation σ of the chromatography profile (cf. Eq. 1-6).

Pulse tests were conducted at different flowrates. These flowrates are supposed to be distributed at both curly part and linear part on the van Deemter curve. From a previous study, 1 BV/h is sure to be in the linear part [Claire-Line B., 2015]. Besides, 0.1 BV/h is the lowest flowrate that we can reach with the minimum frequency of the pump (1 tour/min). Thus, single component pulse tests were conducted at 25°C at four different flow rates: 0.1 BV/h, 0.2 BV/h, 0.5 BV/h, and 1 BV/h.

Each product was prepared with H_2SO_4 pH 1.5 eluent to avoid pH variation. The pH of the product might be slightly different from 1.5 because of the presence of organic acid. The collector at the end of the system allows continuous or discrete collection. At 0.5 BV/h (around 3 mL/min), the collection time is set to 3 min, corresponding to 9 mL sample (0.025 BV).

Table 2-4. Operating conditions of pulse tests.

Product	Concentration (g/L)	Flowrate (mL/min)	pH product	Injected volume (mL)
Glucose	45.4	0.8; 1.7; 3.9; 7.8	1.5	10
Xylose	35.4	0.8; 1.7; 4; 8.2	1.5	10
Acetic acid	37.0	0.7; 1.5; 3.7; 8.9	1.4	10
Formic acid	27.0	0.7; 1.6; 3.8; 7.6	1.4	10
Lactic acid	28.5	0.8; 1.6; 3.7; 7.6	1.4	10
Succinic acid	31.9	0.7; 1.6; 3.9; 7.5	1.3	10
Citric acid	107.8	0.7; 1.4; 2.8; 8.2	1.3	5.5

Chapter II. Materials and methods

Because at least 2 BV (around 700 mL) of eluent was injected which corresponds to 80 tubes, the discrete collection is used in this work to avoid unnecessary sampling. Since the pH meter works less precisely at pH below 2, only UV absorbance was used to locate the peak. Because sugars do not absorb UV, their peaks were located with a Brix analyzer. Tubes corresponding to peak location were analyzed by HPLC. At the end of each pulse test the column was rinsed by 1 BV of eluent before the next pulse test. Operating conditions are detailed right below:

Each pulse test gives a chromatography profile. It is mainly characterized by its retention volume V_R and standard deviation σ , as explained in chapter 1 (section 2.2):

$$V_R = \frac{\int_0^\infty V c dV}{\int_0^\infty c dV} \quad (2 - 4)$$

$$\sigma^2 = \frac{\int_0^\infty (V - V_R)^2 c dV}{\int_0^\infty c dV} \quad (2 - 5)$$

Where V is the eluted volume (in BV) and c is the component concentration in the mobile phase at column output (concentration unit does not matter).

The volume of product injected into the column (< 0.05 BV) is small enough to have a negligible influence on the shape of the pulse test profile. In addition, dead volumes were minimized to limit their influence on dispersion. The global dispersion is usually characterized by the Height Equivalent to a Theoretical Plate (HETP), as a function of V_R , σ^2 and the bed length L :

$$HETP = \frac{L\sigma^2}{V_R^2} \quad (2 - 6)$$

Van Deemter equation is used to describe the relation between $HETP$ and interstitial velocity v :

$$HETP = A + \frac{B}{v} + C \cdot v \quad (2 - 7)$$

The mathematical expressions to obtain the values of A , B , and C are of importance for prediction purposes. The original article by van Deemter gives the following expressions:

$$A = 2 \cdot \beta \cdot d_p \quad B = 2 \cdot \frac{D_m}{\tau} \quad C = 2 \cdot \left[\frac{\varepsilon/\alpha}{(1 + b \cdot F)^2} \right] \quad (2 - 8)$$

Where β is a packing factor which equals 1 for homogeneous packed bed, d_p the mean particle diameter (in m), D_m the molecular diffusion coefficient (in $m^2 \cdot s^{-1}$), τ the bed tortuosity, ε the bed porosity, $F = \varepsilon/(1 - \varepsilon)$ the volumetric ratio of mobile phase to stationary phase, b the linear equilibrium constant defined as the ratio between concentration in the mobile phase and concentration in the stationary phase, and α the liquid-side local mass transfer coefficient (s^{-1}).

From experimental points, the values of A and C can be estimated by a linear regression on the linear part of the van Deemter curve. The value of B can subsequently be estimated by a least square method on the whole set of experimental points.

Chapter II. Materials and methods

In this work, the axial dispersion, represented by its coefficient D , is expressed as the sum of molecular diffusion and mechanical dispersion. Thus D is calculated from values of A and B as shown in chapter I section 3.2.3:

$$D = \frac{D_m}{\tau} + \beta \cdot d_p \cdot v = \frac{A}{2} \cdot v + \frac{B}{2} \quad (2 - 9)$$

2.3 Langmuir adsorption coefficients estimation: frontal analysis

In the physico-chemical model, the separation is driven by two retention mechanisms: ion exchange and Langmuir adsorption. Ion exchange coefficients are given in the datasheet of the resin manufacturer listed in the appendix, while Langmuir adsorption coefficients depends on the resin form and require experimental determination.

In the present work, Langmuir adsorption isotherms were measured by frontal analysis. During a frontal test, the product is continuously injected into the system shown in Figure 2-1, without the switch to eluent. A smaller column is used here ($1 \text{ BV} = 75 \text{ mL}$) to minimize chemical product consumption. The chromatography profile is monitored at the end of column as in pulse test by UV analyzer or Brixmeter. Each frontal test allows to determinate a pair of concentrations in equilibrium between two phases, which is one point on the adsorption isotherm. Langmuir equation was supposed to be the mathematical expression of the curve. After several frontal tests with product at different concentrations, the parameters in the Langmuir equation were obtained by non-linear regression. Details are presented in chapter III section 2.2.

Frontal tests were carried out at pH 1.5, where organic acids are mostly in molecular form, to minimize the ion exchange effect. The temperature is kept at 25°C with a jacketed column linked to a thermostatic bath. Each compound was prepared at 4 concentrations, and experiments were performed from the lowest to the highest concentration. The end of each injection was given by the UV absorbance or Brix variation, where the value rises and stabilizes at a certain level. The collected samples were then analyzed by HPLC. Unlike pulse tests, samples collected here are usually of high concentration and need to be diluted before being analyzed by HPLC. The complete set of experiments is listed below:

Table 2-5. Experimental conditions of frontal analysis.

Product	Concentration (g/L)	pH of product	Flowrate (mL/min)
Glucose	28.9; 56.3; 153.8; 229.3; 332.1	1.5	1.4
Xylose	15.4; 27.4; 74.2; 119.7; 174.7	1.5	1.4
Acetic acid	96.6; 203.4; 413.5; 526.6	1.4	1.4
Formic acid	93.8; 179.1; 293.6; 388.6	1.4	1.3
Lactic acid	49.1; 102.2; 181.3; 334.3	1.4	1.3
Succinic acid	10.6; 21.4; 30.7; 41.4	1.3	1.8
Citric acid	26.5; 46.4; 157.5; 289.4	1.3	1.3

Chapter II. Materials and methods

The curve obtained during such a frontal test is a stepped curve. Each step allows to obtain a concentration in the stationary phase $q(c)$ in equilibrium with the feed concentration c :

$$q(c) = \frac{1}{(1 - \varepsilon).BV} \int_{c_{initial}}^{c_{final}} (V - V_{Liq}^{tot})dc \quad (2 - 10)$$

Where V is the injected volume.

2.4 Uncertainty range determination

When performing non-linear regression to estimate coefficients of van Deemter curves or adsorption isotherms, coefficients were adjusted to minimize the sum of squared difference (also called SSR for Sum of Squared Residuals) between experimental result x_{exp} and theoretical value x_{th} according to following equation.

$$SSR = \sum_i (x_{exp} - x_{th})^2 \quad (2 - 11)$$

Coefficient ranges were estimated by finding all combinations that result in SSR lower than SSR_{max} , which is a statistical estimation of the maximum SSR value which cannot be explained only by experimental uncertainty (corresponding to the null hypothesis rejection with α risk). SSR_{max} is estimated by using Eq. 2-12:

$$SSR_{max} = \chi_{\alpha,n-p} \cdot max \left(\frac{\sum_i (\theta_{min} \cdot x_{exp})^2}{n}, \frac{SSR_{min}}{n-p} \right) \quad (2 - 12)$$

Where $\chi_{\alpha,n-p}$ is the critical Chi-squared value with α risk (set to 5%) and $n - p$ degrees of freedom, n is the number of experimental points, p is the number of coefficients to estimate, θ_{min} is the minimum relative error (set to 2.5% for q and $HETP$) and SSR_{min} is the minimum SSR value that is estimated when adjusting coefficients.

3 Chromatography modeling

Different physico-chemical formulations were introduced in chapter I. Based on the column model, chromatography models can be roughly divided into continuous or discontinuous. It can be subdivided into ideal or non-ideal, linear or non-linear and instant mass transfer or non-instant mass transfer model depending on the details of mass transfer and retention mechanisms. In this study, a non-ideal, non-linear and non-instant mass transfer model with a continuous column model was developed, and compared with a non-ideal, non-linear and non-instant mass transfer model with a discontinuous column model.

3.1 Continuous column model

Figure 2-7 details the mass balance in scale of bed and resin. A 1-D column model is used, assuming negligible radial velocity gradient. The bed packaging is supposed uniform: all bed

Chapter II. Materials and methods

parameters such as porosity are constant in space. Concentration in resin beads is assumed to be uniform: inside-pore mass transfer is integrated in the global mass transfer coefficient. Local equilibrium is assumed: at the interface, concentration in the mobile phase equals the concentration in equilibrium with the stationary phase (given by adsorption isotherms). The mass transfer in the mobile phase is driven by the concentration gap between the concentration at the interface and the one far from the interface. The axial dispersion in the mobile phase is described by a dispersion coefficient D and uses the local concentration gradient as driving force.

Mass balance in the scale of the bed

To establish the mass balance equation, a small column section, dx , is taken out (Fig. 2-7). By assuming a homogeneous porosity, the void fraction volume is similar, equal to the bed porosity ε . The cross-section for fluid flow is therefore equal to $\varepsilon \cdot S$ where S is the surface area of the cross-section (in m^2). Then, the volume of stationary phase is $(1 - \varepsilon) \cdot S \cdot dx$.

In this section, the general mass balance writes:

$$\text{Input} - \text{Output} = \text{Accumulation} + \text{Reaction} \quad (2 - 13)$$

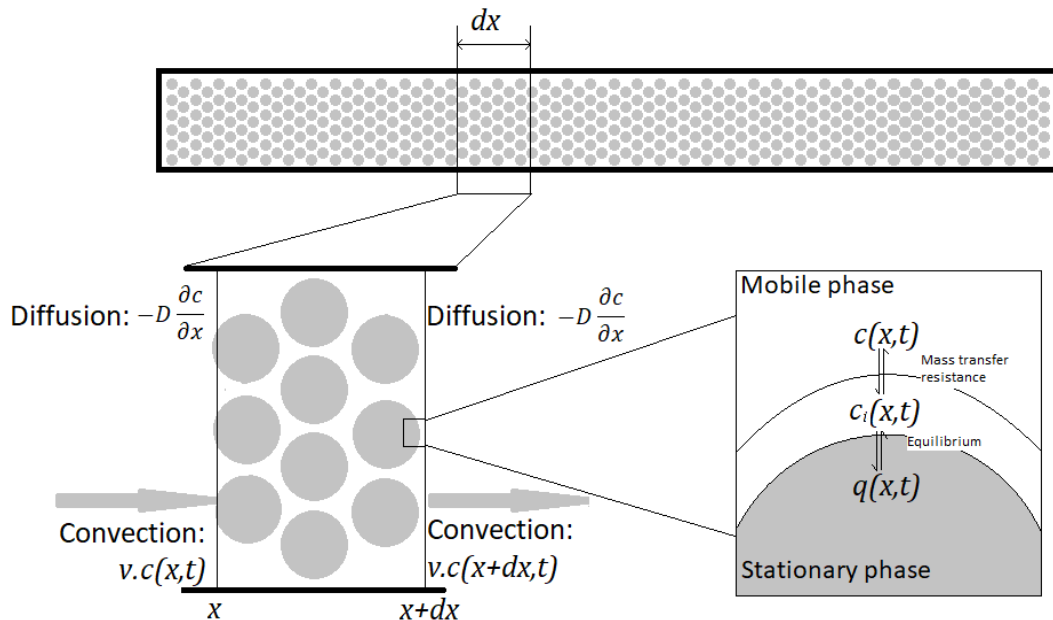


Figure 2-7. The physical model in the scale of bed and resin. D the axial dispersion coefficient (in $m \cdot s^{-2}$), v the interstitial velocity (in $m \cdot s^{-1}$).

The input and output terms refer to the sum of diffusion and convection at position x and $x + dx$ expressed in mol/s:

$$\text{Input} = -D \cdot \frac{\partial c(x, t)}{\partial x} \cdot S \cdot \varepsilon + v \cdot c(x, t) \cdot S \cdot \varepsilon \quad (2 - 14)$$

$$\text{Output} = -D \cdot \frac{\partial c(x + dx, t)}{\partial x} \cdot S \cdot \varepsilon + v \cdot c(x + dx, t) \cdot S \cdot \varepsilon \quad (2 - 15)$$

$$\text{Accumulation} = \frac{\partial q}{\partial t} \cdot S \cdot dx \cdot (1 - \varepsilon) + \frac{\partial c}{\partial t} \cdot S \cdot dx \cdot \varepsilon \quad (2 - 16)$$

Chapter II. Materials and methods

Where v is the interstitial velocity (in m.s^{-1}), c and q are the concentration of component in the mobile phase (in $\text{mol.m}^{-3}_{\text{eluent}}$) and stationary phase (in $\text{mol.m}^{-3}_{\text{resin}}$), D is the axial dispersion coefficient (in $\text{m}^2.\text{s}^{-1}$).

Combining Eq. 2-13 to 2-16, the mass balance in this section of dx becomes:

$$\begin{aligned} -D \cdot \frac{\partial c(x, t)}{\partial x} \cdot S \cdot \varepsilon + v \cdot c(x, t) \cdot S \cdot \varepsilon - \left(-D \cdot \frac{\partial c(x + dx, t)}{\partial x} \cdot S \cdot \varepsilon + v \cdot c(x + dx, t) \cdot S \cdot \varepsilon \right) \\ = \frac{\partial q}{\partial t} \cdot S \cdot dx \cdot (1 - \varepsilon) + \frac{\partial c}{\partial t} \cdot S \cdot dx \cdot \varepsilon + \text{Production} \end{aligned} \quad (2 - 17)$$

The traditional mono-component non-ideal chromatography equation with reaction term is obtained from Eq. 2-17:

$$-F \frac{\partial q}{\partial t} = \frac{\partial c}{\partial t} + v \frac{\partial c}{\partial x} - D \frac{\partial^2 c}{\partial x^2} + NR \quad (2 - 18)$$

Where F is the phase ratio $(1 - \varepsilon)/\varepsilon$ and NR stands for the production or consumption of component due to other chemical reactions (in mol/L.h).

Mass transfer and adsorption at the solid phase (resin)

In the present work, a non-instantaneous mass transfer model was chosen to simulate different mass transfer resistances. Mass transfer resistance between the mobile and stationary phase is driven by molecular diffusion and hydrodynamic properties at the interface (summed in the Sherwood number, depending on Reynolds and Schmidt numbers).

The lumped model was chosen to estimate the mass exchange $R_j^{l \leftrightarrow s}$ from the global mass transfer coefficient k_{aj} of component j (in s^{-1}) between the mobile phase and the stationary phase, due to diffusion inside resin and at its interface:

$$\frac{\partial q}{\partial t} = k_{aj} \cdot (q_j^{eq}(c) - q_j) \quad (2 - 19)$$

Where q_j^{eq} represents the theoretical concentration of component j in the stationary phase (in mol.m^{-3}), which would be in equilibrium with the mobile phase. This equilibrium is calculated from the concentration of all components in the mobile phase, by solving all equilibrium equations (adsorption, ion exchange and acid-basic reactions).

The mass exchange can also be expressed at the liquid side, as:

$$\frac{\partial q}{\partial t} = \alpha_j \cdot (c_j - c_j^i) \quad (2 - 20)$$

Where c_j^i is the concentration of the component j at the interface (in mol.m^{-3}).

Thus, k_{aj} can be estimated from α_j value by assuming a linear equilibrium, whose coefficient K_j is estimated from the adsorption isotherm of component j (cf. section 2.3.2).

$$q_j = K_j \cdot c_j^i \quad q_j^{eq} = K_j \cdot c_j \quad k_a = \frac{\alpha_j \cdot (c_j - c_j^i)}{(q_j^{eq} - q_j)} = \frac{\alpha_j}{K_j} \quad (2 - 21)$$

Chapter II. Materials and methods

For each component, $q^{eq}(c)$ is calculated via the corresponding equilibrium equation, Langmuir equation or ion exchange coefficients depending on the type of interaction between the molecular and the resin surface. The strong anionic resin used in this present work is a styrene-divinylbenzene resin functionalized with quaternary ammonium groups RMe_3N^+ . On the surface of a strong anionic resin conditioned with sulfuric acid, several retention mechanisms could take place:

- The organic acid AH can be attached to HSO_4^- and SO_4^{2-} by a hydrogen bond
- AH can be adsorbed directly to the matrix by van der Waals force
- Ion exchange between base A⁻ and HSO_4^- or SO_4^{2-} fixed on the resin

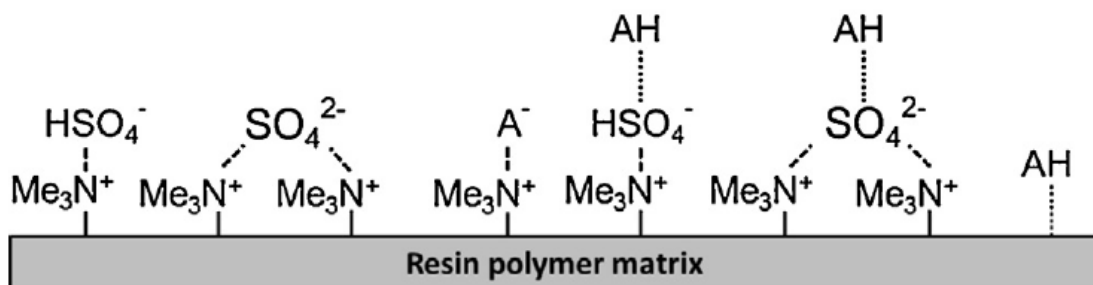


Figure 2-8. Retention mechanisms of a strong anion IEX resin [Lemaire et al. 2016].

Counter-anions SO_4^{2-} or HSO_4^- cover the surface of strong anionic resin in sulfate form (Figure 2-8). Their proportions depend on ion exchange equilibrium and concentration in the mobile phase.

In literature, the adsorption mechanism of organic acid on this type of resin is not well documented. Some researchers have proposed that the adsorption is hypothetically due to the hydrogen bonding [Zhao et al., 2009]. A patent of UOP [Kulprathipanja, 1991] suggested that the molecular form of organic acid was retained only on counter-anions HSO_4^- and SO_4^{2-} . Lemaire et al. [Lemaire et al. 2016] developed these hypotheses in their model, assuming that the interaction was probably hydrogen bonding between the acid hydrogen atom of organic acids and lone electron pairs of sulfate and hydrogen sulfate oxygen atoms.

To describe adsorption, a Langmuir model was chosen, which involves several assumptions [Sircar 2017]:

1. The surface containing adsorption sites is perfectly flat with no corrugation.
2. All adsorption sites are energetically equivalent.
3. Only mono-layer coverage occurs.
4. No interaction between molecules adsorbed on adjacent sites.

Figure 2-9 shows the adsorption of organic acids over strong anionic resin by hydrogen bonding. Some organic acids form more than one hydrogen bond.

Chapter II. Materials and methods

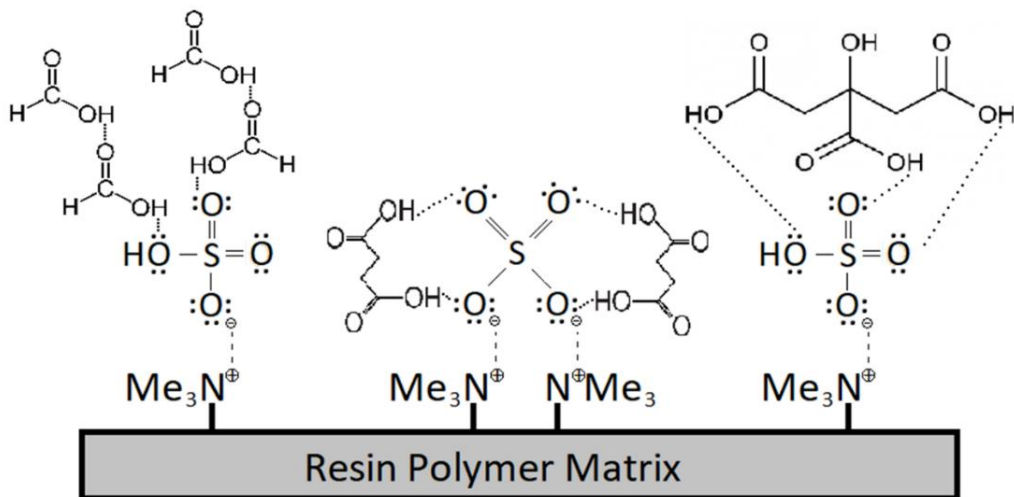
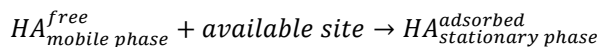


Figure 2-9. Schematic illustration of organic acid adsorption by hydrogen bonding on sulfate or hydrogen sulfate counter-anions. Each SO_4^{2-} or HSO_4^- has eight lone pair electrons.

Generally, Langmuir model assumes a 1st order reaction between the adsorbed molecule (organic acid HA) and the available adsorption site (pair of lone electrons on oxygen atoms):



The kinetics equation is then:

$$q_{\text{HA}} = k_s \cdot c_{\text{HA}} \cdot q_{\text{site}}^{\text{available}} \quad (2 - 22)$$

As first approximation, the adsorption sites on SO_4^{2-} and HSO_4^- were assumed similar. Thus, instead of writing two adsorption equations for SO_4^{2-} and HSO_4^- separately, the total concentration of SO_4^{2-} and HSO_4^- in the stationary phase called $q_{\text{SO}_4}^{\text{tot}}$ (in mol/L) was used. We named N_j the number of pair of electrons that the molecule j takes/covers. Then, $q_{\text{site}}^{\text{available}}$ can be expressed as the total amount of sites minus the amount of occupied sites.

$$q_{\text{HA}} = k_s \cdot c_{\text{HA}} \cdot (N_{\text{tot}} \cdot q_{\text{SO}_4}^{\text{tot}} - N_{\text{HA}} \cdot q_{\text{HA}}) \quad (2 - 23)$$

In the case of a single component model, the Langmuir equilibrium model for component j was described as:

$$q_j = \frac{N_{\text{tot}} \cdot q_{\text{SO}_4}^{\text{tot}} \cdot k_{s_j} \cdot c_j}{1 + N_j \cdot k_{s_j} \cdot c_j} \quad (2 - 24)$$

Where N_{tot} is the number of lone electron pairs on each counter anion ($N_{\text{tot}} = 8$), k_{s_j} the adsorption constant of component j and N_j the number of lone electron pair occupied by each adsorbed molecule.

In the case of a multi-component model, the competitive Langmuir equilibrium model for m components can be described as:

$$q_j = \frac{N_{\text{tot}} \cdot q_{\text{SO}_4}^{\text{tot}} \cdot k_{s_j} \cdot c_j}{1 + \sum_{i=1}^m N_i \cdot k_{s_i} \cdot c_i} \quad (2 - 25)$$

Where k_{s_i} is the adsorption constant (in L/mol) organic acid i .

Chapter II. Materials and methods

The value of $q_{SO_4}^{tot}$ can be estimated from the value of the ion exchange resin capacity q_{max} , which is the concentration of quaternary ammonium groups RMe_3N^+ . The resin supplier gives its estimation (ca. 2.3 eq/L where eq corresponds to equivalent molar charge amount). This value was checked previously as explained in Eq. 2-3.

3.2 Formulation and computational strategy of the continuous model

3.2.1 Formulation in the mobile phase

Eq. 2-18 introduces the mass balance of a mono component system. When organic acid HA is dissolved in H_2SO_4 , five compounds co-exist in the solution: A⁻, H⁺, HA, SO_4^{2-} or HSO_4^- . Each compound has a mass balance equation which involves the mass transfer between the two phases, and acid-base reactions could occur in the mobile phase between these compounds which brings an additional reaction term in the mass balance (NR terms). Thus, the system where one organic acid HA present in H_2SO_4 solution is described by ten equations:

$$\frac{\partial c_{A^-}}{\partial t} + v \frac{\partial c_{A^-}}{\partial x} - D \frac{\partial^2 c_{A^-}}{\partial x^2} = -F \frac{\partial q_{A^-}}{\partial t} + NR_{A^-} \quad (2 - 26)$$

$$\frac{\partial q_{A^-}}{\partial t} = k_a^{A^-} (q_A^{eq} - q_{A^-}) \quad (2 - 27)$$

$$\frac{\partial c_{HA}}{\partial t} + v \frac{\partial c_{HA}}{\partial x} - D \frac{\partial^2 c_{HA}}{\partial x^2} = -F \frac{\partial q_{HA}}{\partial t} + NR_{AH} \quad (2 - 28)$$

$$\frac{\partial q_{HA}}{\partial t} = k_a^{HA} (q_{HA}^{eq} - q_{HA}) \quad (2 - 29)$$

$$\frac{\partial c_{H^+}}{\partial t} + v \frac{\partial c_{H^+}}{\partial x} - D \frac{\partial^2 c_{H^+}}{\partial x^2} = -F \frac{\partial q_{H^+}}{\partial t} + NR_{H^+} \quad (2 - 30)$$

$$\frac{\partial q_{H^+}}{\partial t} = k_a^{H^+} (q_{H^+}^{eq} - q_{H^+}) \quad (2 - 31)$$

$$\frac{\partial c_{SO_4^{2-}}}{\partial t} + v \frac{\partial c_{SO_4^{2-}}}{\partial x} - D \frac{\partial^2 c_{SO_4^{2-}}}{\partial x^2} = -F \frac{\partial c_{SO_4^{2-}}}{\partial t} + NR_{SO_4^{2-}} \quad (2 - 32)$$

$$\frac{\partial q_{SO_4}}{\partial t} = k_a^{SO_4^{2-}} (q_{SO_4^{2-}}^{eq} - q_{SO_4^{2-}}) \quad (2 - 33)$$

$$\frac{\partial c_{HSO_4^-}}{\partial t} + v \frac{\partial c_{HSO_4^-}}{\partial x} - D \frac{\partial^2 c_{HSO_4^-}}{\partial x^2} = -F \frac{\partial q_{HSO_4^-}}{\partial t} + NR_{HSO_4^-} \quad (2 - 34)$$

$$\frac{\partial q_{HSO_4^-}}{\partial t} = k_a^{HSO_4^-} (q_{HSO_4^-}^{eq} - q_{HSO_4^-}) \quad (2 - 35)$$

$q^{eq}(c)$ is calculated by either ion exchange equilibrium or Langmuir adsorption isotherm, which requires c from other equations. Since the proton H^+ does not appear in the stationary phase, the q_{H^+} and $q_{H^+}^{eq}$ are constantly zero. Eq. 2-31 is excluded from the system.

The NR term (production/consumption caused by chemical reactions) are generally expressed by a kinetics equation. For example, in Eq. 2-26, NR_{A^-} represents the dissociation of HA, and might be estimated by a first-order kinetic law towards each reactant (Eq. 2-36), as a first approximation:

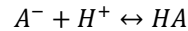
Chapter II. Materials and methods



$$NR_{A^-} = k_+ \cdot c_{HA} - k_- \cdot c_{A^-} \cdot c_{H^+} \quad (2-36)$$

However, it is challenging and time-consuming to find a good kinetic law and estimate its coefficients (k_+ and k_- in this example) for each compound by searching in literature or by performing experiments.

Meanwhile, NR_{AH} in Eq. 2-28 would write:



$$NR_{AH} = k_- \cdot c_H \cdot c_A - k_+ \cdot c_{HA} \quad (2-37)$$

As NR_{AH} is the opposite of NR_{A^-} , NR terms can be removed by combining Eq. 2-26 and Eq. 2-28 and we established the mass balance for the total concentration of A in the mobile phase (c_A^{tot}), in HA or A^- form:

$$\frac{\partial c_A^{tot}}{\partial t} + v \frac{\partial c_A^{tot}}{\partial x} - D \frac{\partial^2 c_A^{tot}}{\partial x^2} = -F * \frac{\partial q_A^{tot}}{\partial t} \quad (2-38)$$

Similarly, equations 2-26 to 2-35 can be combined to get 2 new equations for total SO_4 (indice S) and total acid proton H (indice H) concentration, without any reaction term NR:

$$\frac{\partial c_S^{tot}}{\partial t} + v \frac{\partial c_S^{tot}}{\partial x} - D \frac{\partial^2 c_S^{tot}}{\partial x^2} = -F * \frac{\partial q_S^{tot}}{\partial t} \quad (2-39)$$

$$\frac{\partial c_H^{tot}}{\partial t} + v \frac{\partial c_H^{tot}}{\partial x} - D \frac{\partial^2 c_H^{tot}}{\partial x^2} = -F * \frac{\partial q_H^{tot}}{\partial t} \quad (2-40)$$

Eq. 2-40 could be deducted from Eq. 2-38, 2-39 and electroneutrality Eq. 2-43 and is therefore not independent. Thus, Eq. 2-38 and 2-39, along with Eq. 2-27, 2-29, 2-33 and 2-35, constitute a system of nonlinear and coupled equations. A system of an organic acid present in H_2SO_4 solution is represented by 6 equations. At each time step, these equations give total concentration fields c_A^{tot} , c_S^{tot} and c_H^{tot} .

The concentration of each compound can be estimated using the equilibrium constant of each acid-base reaction. Indeed, these reactions are assumed to be always at an equilibrium state because they are considered to be much faster than all other phenomena.

$$c_A^{tot} = c_{A^-} + c_{HA} \quad (2-41)$$

$$c_H^{tot} = c_{H^+} + c_{HA} + c_{HSO_4^-} \quad (2-42)$$

$$c_{H^+} = 2 \cdot c_{SO_4^{2-}} + c_{HSO_4^-} + c_{A^-} \quad (2-43)$$

$$K_a^{HA} = c_{H^+} * c_{A^-} / c_{HA} \quad (2-44)$$

$$K_a^{HSO_4^-} = c_{H^+} * c_{SO_4^{2-}} / c_{HSO_4^-} \quad (2-45)$$

These five equations form an implicit system. By writing equations in the form of $f(x) = 0$, the system is then solved by a Newton Raphson method:

Chapter II. Materials and methods

$$\mathbf{c} = \begin{pmatrix} c_{A^-} \\ c_{HA} \\ c_{H^+} \\ c_{SO_4^{2-}} \\ c_{HSO_4^-} \end{pmatrix} \quad \mathbf{f}(\mathbf{c}) = \begin{pmatrix} c_{A^-} + c_{HA} - c_A^{tot} \\ c_{H^+} + c_{HA} + c_{HSO_4^-} - c_H^{tot} \\ 2 \cdot c_{SO_4^{2-}} + c_{HSO_4^-} + c_{A^-} \\ c_{H^+} \cdot c_{A^-} - K_a^{HA} \cdot c_{HA} \\ c_{H^+} * c_{SO_4^{2-}} - K_a^{HSO_4^-} \cdot c_{HSO_4^-} \end{pmatrix}$$

The corresponding Jacobian matrix is:

$$J = \begin{pmatrix} 1 & 1 & 0 & 0 & 0 \\ 0 & 1 & 1 & 0 & 1 \\ 1 & 0 & -1 & 2 & 1 \\ c_{H^+} & -K_a^{HA} & c_{A^-} & 0 & 0 \\ 0 & 0 & c_{SO_4^{2-}} & 0 & -K_a^{HSO_4^-} \end{pmatrix}$$

The initial values of \mathbf{c}_0 are concentrations at the previous time step and the total concentrations are those computed at time $t+dt$. The new combination of \mathbf{c}_{i+1} is obtained from the previous combination \mathbf{c}_i by iteration:

$$\mathbf{c}_{i+1} = \mathbf{c}_i - J^{-1} \mathbf{f}(\mathbf{c}_i) \quad (2-46)$$

The Newton-Raphson ensures an order 2 convergence. The infinity norm was adopted for the convergence criterion, with a value equal to 10^{-7} . Thus, after convergence, every element of $\mathbf{f}(\mathbf{c}_i)$ is lower than this value.

3.2.2 Formulation in the stationary phase

In a system where one organic acid HA is dissolved in H_2SO_4 solution, three anions co-exist in both stationary phase and mobile phase: A^- , HSO_4^- , SO_4^{2-} . Therefore, three ion-exchange reactions can occur between two phases while only two of them are independent. The equilibrium is defined by their equilibrium coefficients:

$$K_{HSO_4/A}^{eq} = \frac{c_{A^-} \cdot q_{HSO_4^-}^{eq}}{q_{A^-}^{eq} \cdot c_{HSO_4^-}} \quad (2-47)$$

$$K_{HSO_4/SO_4}^{eq} = \frac{c_{SO_4^{2-}}^2 \cdot q_{HSO_4^-}^{eq}}{q_{SO_4^{2-}}^{eq} \cdot c_{HSO_4^-}^2} \quad (2-48)$$

And the total adsorption sites on the stationary phase reads as:

$$q_{max} = q_{A^-} + q_{HSO_4^-} + 2 \cdot q_{SO_4^{2-}} \quad (2-49)$$

Eq. 2-47 and 2-48 applies only to the theoretical concentration q^{eq} . The real concentration q does not obey these equalities. Meanwhile, Eq. 2-49 remains validated with both q^{eq} and q .

In the mass transfer equations, the four unknown concentrations at equilibrium q_i^{eq} are solved by three equilibrium relations and the definition of maximum ion exchange capacity q_{max}^{ei} :

$$q_{HA}^{eq} = \frac{8 \cdot q_{SO_4^-}^{tot} \cdot k_s \cdot c_{HA}}{1 + N_{HA} \cdot k_s \cdot c_{HA}} \quad (2-50)$$

$$K_{HSO_4/A}^{eq} = \frac{c_{A^-} \cdot q_{HSO_4^-}^{eq}}{q_{A^-}^{eq} \cdot c_{HSO_4^-}} \quad (2-51)$$

$$K_{HSO_4/SO_4}^{eq} = \frac{c_{SO_4^{2-}}^2 \cdot q_{HSO_4^-}^{eq}}{q_{SO_4^{2-}}^{eq} \cdot c_{HSO_4^-}^2} \quad (2-52)$$

Chapter II. Materials and methods

$$q_{max}^{eq} = q_A^{eq} + q_{HSO_4^-}^{eq} + 2q_{SO_4^{2-}}^{eq} \quad (2 - 53)$$

Eq. 2-54 was deducted from equations above to calculate $q_{HSO_4^-}^{eq}$.

$$q_{HSO_4^-}^{eq} = \frac{-B + \sqrt{(B^2 - 4 \cdot A \cdot C)}}{2 \cdot A} \quad (2 - 54)$$

Where:

$$A = \frac{2 \cdot c_{SO_4^{2-}}}{c_{HSO_4^-}^2} \cdot K_{HSO_4/SO_4}^{eq} \quad B = 1 + K_{HSO_4/A}^{eq} \cdot \frac{c_A}{c_{HSO_4^-}} \quad C = q_{max}^{eq}$$

3.2.3 Computational strategy

The CE/SE (conservation element/solution element) [Chang *et al.*, 1991] method was chosen in the present work for its ability to deal with space and time integrals simultaneously. As demonstrated in chapter I (cf. section 3.3.4), we chose to approximate u and f values by a first-order Taylor formula from its center point A.

A zero-order Taylor formula was chosen to approximate the source term p . Finally, following explicit equation is obtained, which enabled u_j^n to be estimated from values of u , f and p at the previous semi-time step:

$$u_j^n = \frac{1}{2} \left[u_{j+\frac{1}{2}}^{n-\frac{1}{2}} + u_{j-\frac{1}{2}}^{n-\frac{1}{2}} \right] - s_{j+\frac{1}{2}}^{n-\frac{1}{2}} + s_{j-\frac{1}{2}}^{n-\frac{1}{2}} + \frac{\Delta t}{4} \cdot \left(p_{j+\frac{1}{2}}^{n-\frac{1}{2}} + p_{j-\frac{1}{2}}^{n-\frac{1}{2}} \right) \quad (2 - 60)$$

where

$$s_{j \pm \frac{1}{2}}^{n-\frac{1}{2}} = \left(\frac{\Delta t}{2 \cdot \Delta x} \right) \cdot f_{j \pm \frac{1}{2}}^{n-\frac{1}{2}} + \left(\frac{\Delta x}{8} \right) \cdot u_{x,j \pm \frac{1}{2}}^{n-\frac{1}{2}} + \left(\frac{\Delta t^2}{8 \cdot \Delta x} \right) \cdot f_{t,j \pm \frac{1}{2}}^{n-\frac{1}{2}}$$

A detailed proof of equation (2-60) is listed in the appendix.

In the case of chromatography convection-diffusion equation, the CE/SE method can be applied to solve the mass balance in the mobile phase by defining:

$$f = v \cdot c - D \cdot \frac{\partial c}{\partial x} \quad u = c \quad p = -F \cdot k_a \cdot (q^{eq} - q) \quad (2 - 61)$$

As a consequence, f , u_t , f_x , then f_t can be deduced from u_x at the mesh point (j,n):

$$f = v \cdot u - D \cdot u_x \quad f_x = \frac{\partial f}{\partial u} \frac{\partial u}{\partial x} = (v \cdot \frac{\partial u}{\partial u} - D \cdot \frac{\partial u}{\partial u \partial x}) u_x \sim v \cdot u_x \quad (2 - 62)$$

$$u_t = p - f_x \quad f_t = \frac{\partial f}{\partial u} \frac{\partial u}{\partial t} = (v \cdot \frac{\partial u}{\partial u} - D \cdot \frac{\partial u}{\partial u \partial x}) u_t \sim v \cdot u_t \quad (2 - 63)$$

These equations tell us that only u and u_x are needed to solve Eq. 2-60. There are many possibilities to calculate the derivative u_x from u . In our model, it is calculated by a modified harmonic mean [Chuanyi *et al.*, 2015]:

$$u_x = \frac{|u_x^+|u_x^- + |u_x^-|u_x^+}{|u_x^+| + |u_x^-|} \quad u_x^- = (u_j^n - u_{j-1}^n) / \Delta x \quad u_x^+ = (u_{j+1}^n - u_j^n) / \Delta x \quad (2 - 64)$$

Chapter II. Materials and methods

u_x^- and u_x^+ are the partial derivative on the left and right side, respectively. The modified harmonic mean equals zero when u_x^- and u_x^+ have opposite signs, and equals the traditional harmonic mean when u_x^- and u_x^+ have the same sign.

Thus, only one variable u is needed to solve the system, which is calculated via Eq. 2-60 with an explicit scheme. Starting from points at time step n , Eq. 2-58 allows us to move to time step $n+1/2$. Points at $n+1$ are then calculated in the same way from points at $n+1/2$.

Meanwhile, the mass balance in the stationary phase were solved separately by a 1st order finite-difference method, at each mesh point (j,n):

$$\frac{q^n - q^{n-1}}{\Delta t} = k_a \cdot (q^{eq} - q^n) \quad (2 - 65)$$

Boundary conditions are used to obtain values of the first and last mesh point (imposed value at inlet and zero derivative at outlet):

$$\frac{\partial c_1^n}{\partial x} = \frac{c_2^n - c_1^n}{dx} = \frac{v}{D} (c_1^n - c_{feed}) \quad (2 - 66)$$

$$\frac{\partial c_{jmax}^n}{\partial x} = \frac{c_{jmax}^n - c_{(jmax-1)}^n}{dx} = 0 \quad (2 - 67)$$

3.3 The discontinuous model

The chromatography elution was also simulated with the discontinuous column model used in a previous work [Lemaire et al. 2016]. In this approach, influence of all dispersion mechanisms such as mass transfer resistance and dispersion is taken into account indirectly by the theoretical plate number NET .

In a discontinuous model, the column is discretized into a series of perfectly stirred reactors which have the same volume V and porosity ε .

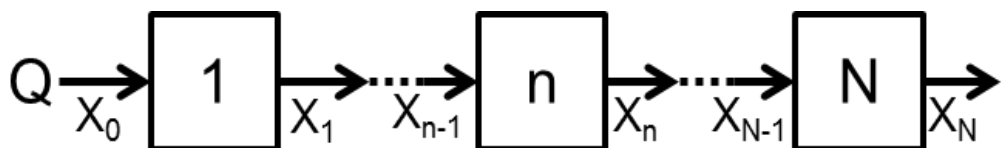


Figure 2-10. Schema of cascade reactor, with Q the flowrate and X_n the concentration in mobile phase of component X at the end of reactor n .

The mass balance is written over the total amount of sulfate, organic acid and acid proton H, as in the continuous model to remove reaction term NR. The concept of cascade reactors assumes a one-way coupling. Therefore, the mass balances express the concentrations in reactor n at time t as a function of concentrations in reactor $n-1$ and time $t-1$. In the case of one organic acid HA present in H_2SO_4 solution, three mass balances are available:

Chapter II. Materials and methods

Mass balance of total SO₄:

$$\begin{aligned} & \varepsilon V \left(\frac{d[c_{HSO_4^-}]_t^n}{dt} + \frac{d[c_{SO_4^{2-}}]_t^n}{dt} \right) + (1 - \varepsilon)V \left(\frac{d[q_{SO_4^{2-}}]_t^n}{dt} + \frac{d[q_{HSO_4^-}]_t^n}{dt} \right) \\ &= Q \left([c_{HSO_4^-}]_t^{n-1} - [c_{HSO_4^-}]_t^n \right) + Q \left([c_{SO_4^{2-}}]_t^{n-1} - [c_{SO_4^{2-}}]_t^n \right) \quad (2-68) \end{aligned}$$

Mass balance of total H:

$$\begin{aligned} & \varepsilon V \left(\frac{d[c_{H^+}]_t^n}{dt} + \frac{d[c_{HSO_4^-}]_t^n}{dt} + \frac{d[c_{AH}]_t^n}{dt} \right) \\ &+ (1 - \varepsilon)V \left(\frac{d[q_{HSO_4^-}]_t^n}{dt} + \frac{d[q_{AH-HSO_4}]_t^n}{dt} + \frac{d[q_{AH-SO_4}]_t^n}{dt} + \frac{d[q_{AH}]_t^n}{dt} \right) \\ &= Q([c_{H^+}]_t^{n-1} - [c_{H^+}]_t^n) + Q([c_{HSO_4^-}]_t^{n-1} - [c_{HSO_4^-}]_t^n) + Q([c_{AH}]_t^{n-1} - [c_{AH}]_t^n) \quad (2-69) \end{aligned}$$

Mass balance of total A :

$$\begin{aligned} & \varepsilon V \left(\frac{d[c_{A^-}]_t^n}{dt} + \frac{d[c_{AH}]_t^n}{dt} \right) + (1 - \varepsilon)V \left(\frac{d[q_{A^-}]_t^n}{dt} + \frac{d[q_{AH-HSO_4}]_t^n}{dt} + \frac{d[q_{AH-SO_4}]_t^n}{dt} + \frac{d[q_{AH}]_t^n}{dt} \right) \\ &= Q([c_{A^-}]_t^{n-1} - [c_{A^-}]_t^n) + Q([c_{AH}]_t^{n-1} - [c_{AH}]_t^n) \quad (2-70) \end{aligned}$$

Where Q is the volumetric flowrate.

In these three mass balances, the left-hand side expression corresponds to the accumulation term in reactor n, and the right-hand side expression represents the transfer by convection. The four unknown concentrations in the stationary phase are obtained from the mass balances of ion exchange sites along with other ion exchange equilibria and adsorption isotherms (Eq. 2-41 to 2-53). These equations form an implicit system, which was solved by the Newton-Raphson method.

4 Simulation of multi-column system: 3C-ISMB process

SMB process is a common purification process in the industry. ISMB is an improved version of SMB process with better performance. Unlike the traditional SMB process, a step of the ISMB consists of two sub-steps (SS) as introduced in the previous chapter. The 3C-ISMB used in this work is a further improvement of ISMB process, which contains three columns instead of four and four sub-steps instead of two.

Figure 2-11 shows the evolution of concentration profile inside a 3C-ISMB system during four sub-steps:

- SS1: The product (volume V_{prod}) is injected to zone 3 and the fast component(F) is collected at zone 3 (Z3).

Chapter II. Materials and methods

- SS2: The eluent (volume V_{elu1}) is injected to zone 1 and the slow component(S) is collected at zone 1.
- SS3: The eluent (volume V_{elu2}) is injected to zone 1 and the fast component is collected at zone 3.
- SS4: All inlet and outlet ports are closed and the mobile phase is just moved (volume V_{loop}) through all column connected in a loop.

Zones are shifted by one column after each step, following the liquid flow direction. As 3C-ISMB is composed of only three columns, a cycle is done after only 3 steps (zones go back to their initial location).

The 3-column architecture is simulated as a unique large column with intermediate inputs and outputs while liquid volume of connection between zones is ignored. During each step, input and output of each column are defined according to their corresponding zone and the current substep. Concentration profiles in each column at the end of a step were saved as initial conditions for the next step. No partial withdraw was present in this system thus, flowrates in each zone were either 0 BV/h, or 0.5 BV/h.

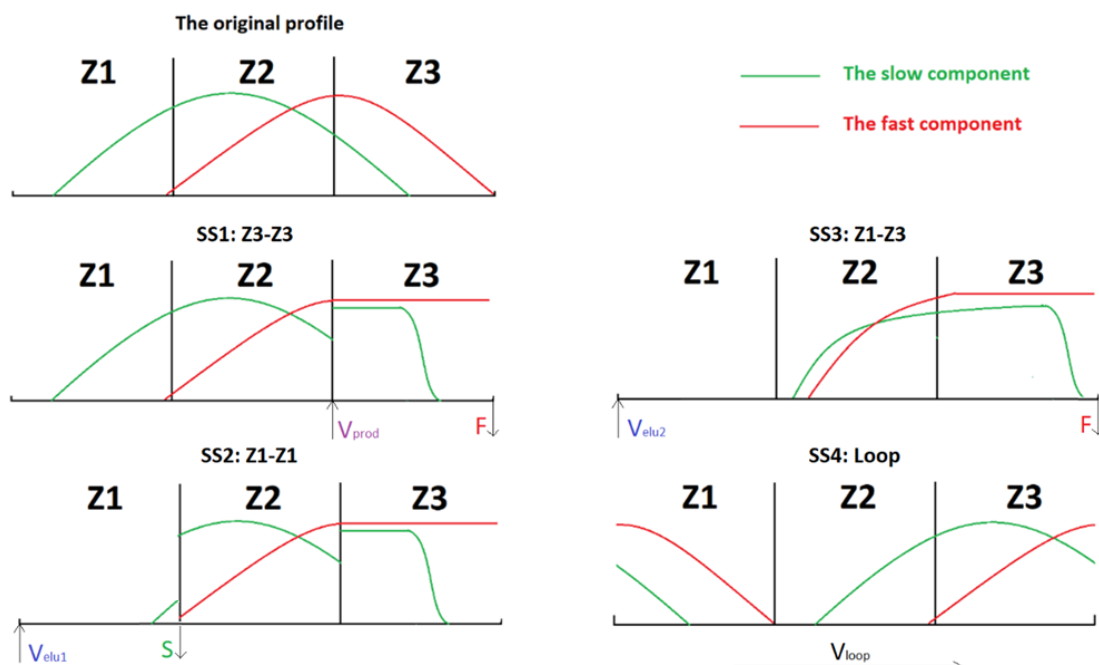


Figure 2-11. A brief process scheme of the 3C-ISMB process studied in the present work.

Performance of an ISMB system could be evaluated from many aspects, one of which is the W/F ratio (Water over Feed volume ratio), which is the volume of eluent used to separate a given volume of product.

$$\frac{W}{F} = \frac{V_{elu1} + V_{elu2}}{V_{prod}} \quad (2 - 71)$$

Another parameter to evaluate ISMB performance is productivity, which is the volume of product which can be treated per hour and per liter of resin:

Chapter II. Materials and methods

$$P_A = \frac{V_{product}}{T_{step} * N_{column} * BV} \quad (2 - 72)$$

Where T_{step} is the step time. N_{column} the number of columns and Q the volumetric flow rate (in BV/h).

Purities of raffinate and extract are usually required as optimization target. During experiments, extract and raffinate are collected continuously during a step. Purity of compound A in the collection (extract or raffinate) is defined by its mean concentration during one cycle:

$$Purity_A = \frac{c_A^{collection}}{\sum c_i^{collection}} \quad (2 - 73)$$

The dilution factor of compound A (F_A) corresponds to the ratio of component concentration in product over its concentration in the corresponding enriched fraction (extract or raffinate). It is an important index which decides the cost of the concentration step after separation:

$$F_A = \frac{c_A^{product}}{c_A^{enriched fraction}} \quad (2 - 74)$$

The recovery rate of compound A (R_A) could be an important index while separating high-value molecule. It is defined by the following ratio:

$$R_A = \frac{c_A^{enriched fraction} \cdot V_{enriched fraction}}{c_A^{product} \cdot V_{product}} \quad (2 - 75)$$

The system needs to be adjusted and optimized to meet separation requirements in terms of purity or recovery rate, and reach the optimal performance in terms of W/F ratio or productivity. The adjustment and optimization will be presented in detail in chapter V.

Chapter III. Estimation of components physico-chemical properties and bed parameters

This chapter presents results of experiments performed to estimate the physico-chemical properties of compounds and resin bed, which are required for the numerical simulation. The model chosen for the study considers Langmuir adsorption, mass transfer rate and axial dispersion. These parameters strongly impact the position and width of chromatography profiles. Thus, experiments were conducted to complete and compare their values found in the literature.

In this study, bed properties are measured by analyzing residence time distribution. Properties of compounds such as coefficients of mass transfer, axial dispersion and adsorption isotherm are measured by frontal analysis and pulse tests. Usual Langmuir and van Deemter equations are chosen as the mathematical expressions to fit experimental results.

1 Bed property determination

1.1 Bed porosity

The bed porosity is the void fraction of the bed (pore volume over total apparent volume). There are however several types of porosities: the interparticle porosity, the intraparticle porosity, the global porosity, and the effective porosity. The effective porosity gives the effective mobile phase volume in the system and is chosen for this work. It was measured by the residence time/volume distribution method [Ariane B., 2021]. Effective porosity includes the active interparticle porosity, plus the volume of connectors. It excludes most of the intraparticle porosity.

Lameloise [Lameloise M.L., 1994] recommends using blue dextran for cationic resins as tracer to determine the effective porosity. This molecule is very large and cannot penetrate pores of beads. However, experience shows that this dye in pure solution is adsorbed by anionic resins. According to Gu [Gu *et al.*, 2013], dextran blue can be used on an anionic resin when it is in a highly concentrated salt solution, to reduce its adsorption.

Since these conditions are rather complicated to implement, we were interested in the use of salts as tracer, considering most would be excluded from resin beads by the Donnan effect [Hirohiko W., & Yuji T., 1982]. Despite that, this method could overestimate the effective porosity because of salts not totally excluded from beads. However, Blanc [Blanc C.L., 2015] has compared porosity measured by injecting blue dextran and NaCl solution with strong cationic and anionic resin. A relative difference of less than 10% was found, which is quite satisfactory. Therefore, for simplicity, we chose to use salts as tracer for the bed of anionic resins to determine their external porosity.

Chapter III. Estimation of components physico-chemical properties and bed parameters

Since the resin was in sulfate form, Na_2SO_4 1 mol/L was chosen instead of NaCl as tracer, and H_2SO_4 solution pH 1.5 as eluent, to avoid ion-exchange, as described in Chapter 2 (section 2.1). Figure 3-1 presents the conductivity evolution (difference between actual and initial conductivity) at column output over the injection time t . The total injection time t_{tot} was corrected to remove the influence of Na_2SO_4 injection time ($t_{\text{Na}_2\text{SO}_4} = 2.4 \text{ min}$) on residence time estimation ($t = t_{tot} - t_{\text{Na}_2\text{SO}_4}/2$).

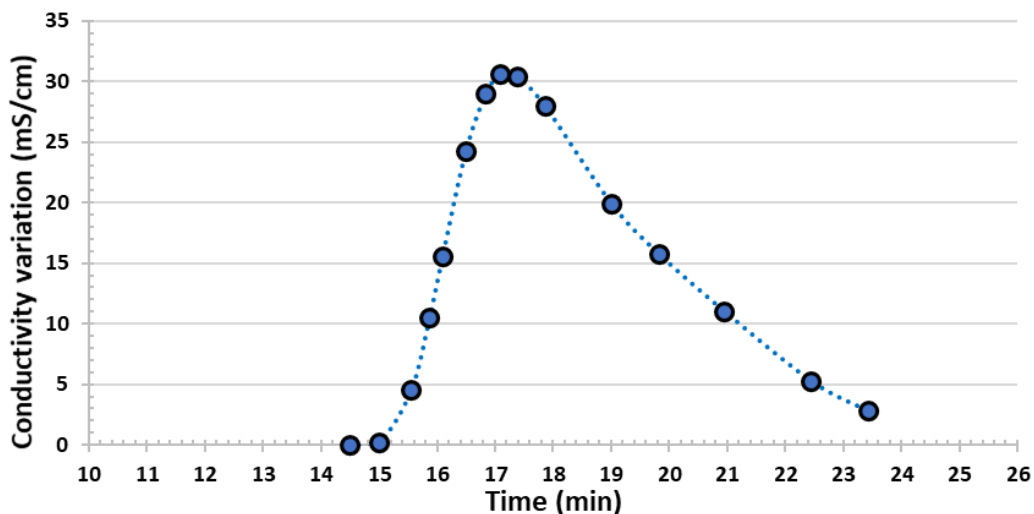


Figure 3-1. Residence time distribution in the system (resin bed + pump + tubing + fitting).

The mean residence time t_s was estimated by following equations:

$$t_s = \int_0^{t_{max}} t \cdot E(t) \cdot dt \quad (3-1)$$

$$E(t) = \frac{S(t)}{\int_0^{\infty} S(t) \cdot dt} \quad (3-2)$$

Where $E(t)$ is the distribution function and $S(t)$ is the conductivity.

As shown in Figure 3-1, the peak is not symmetric and presents a clear tailing. The same tailing was observed again in Figure 3-2. Both tails lasted around 5 minutes, which implies that the potential cause of tailing is the influence of other parts of the system (tubing, fitting and peristaltic pump) on dispersion and asymmetry.

The residence time within the whole system, estimated from Figure 3-1, is $17.4 \pm 0.2 \text{ min}$. Thus, effective mobile phase volume in the system V_{total} is $43.5 \pm 1.5 \text{ mL}$.

To measure the effective mobile phase volume inside other materials V_{other} , the experiment was performed without the column but with the same tubing. Figure 3-2 shows the residence time distribution in the system without the column.

The mean residence time within the system without the column, estimated from Figure 3-2, is $4.8 \pm 0.1 \text{ min}$, which corresponds to V_{other} equals to $12 \pm 0.5 \text{ mL}$. Consequently, the effective porosity of the bed ε is estimated to 0.42 ± 0.015 , according to Eq. 2-2 given in Chapter II.

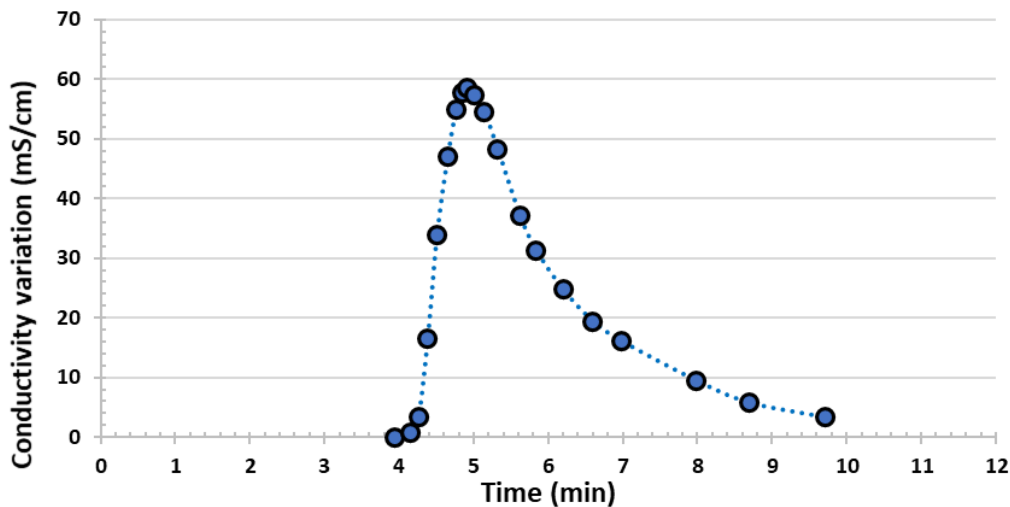


Figure 3-2. Residence time distribution in the system without the column.

To check if the bed is well packed, a small part of the bed was scanned by tomography to obtain the 3D image of the structure inside the column. The resin is initially emerged in eluent (H_2SO_4 pH 1.5). Since the tomograph cannot distinguish resin surface and water, we replaced the mobile phase by air while injecting cold air, then a part of resin was sampled for tomography scan.



Figure 3-3. Part of resin bed (1/4 of a cylinder sample with 2mm of height) scanned by tomography.

Among scanned sample, a small section which is well packed (local porosity varies by less than 5%) was selected for study. The mean bed porosity from the 3D scan is 0.49, which is higher than the bed porosity obtained by residence time distribution (0.42). Indeed the tomography estimates the total bed porosity, whereas the residence time analysis provides the effective bed porosity. The results remain consistent then. One part of the overestimation could also result from resin shrinkage in the air during tomography scan, which lasted almost 1 hour. Consequently, the effective porosity estimation (0.42) was chosen for modeling and simulation purposes.

The tomograph software can also estimate tortuosity from resin bed 3D scan. As introduced in chapter II, the tomograph gave a 3D image of sample void parts, which was divided into 100 layers. The barycenter of each layer was calculated by software, then the tortuosity was defined as the ratio between the total lined-up distance of centroids and the scanned resin bed thickness. The tortuosity given by the software is 1.46. This value will be used during van Deemter curve analysis.

1.2 Resin ion exchange capacity

The resin ion exchange capacity q_{max}^{ei} corresponds to the total amount of ion exchange sites expressed as mol/Lres. q_{max}^{ei} value is estimated to 1.91 ± 0.24 mol/Lres, according to uncertainty range of all parameters (experimental details are given in Chapter II). q_{max}^{ei} will be supposed equal to 2.1 mol/L for simulation in chapters 4 and 5, to get closer to supplier data (2.1 to 2.4 mol/Lres).

2 Frontal analysis

2.1 Glucose and xylose

Frontal analysis and pulse tests were performed with 2 sugars and 5 organic acids, representing main components which can be valorized in hemicellulosic hydrolysates. Results of glucose frontal analysis are shown in Figure 3-4 as example of sugar. Frontal analysis is performed over five stepwise increases of concentration. Results for other compounds are gathered in the annexes.

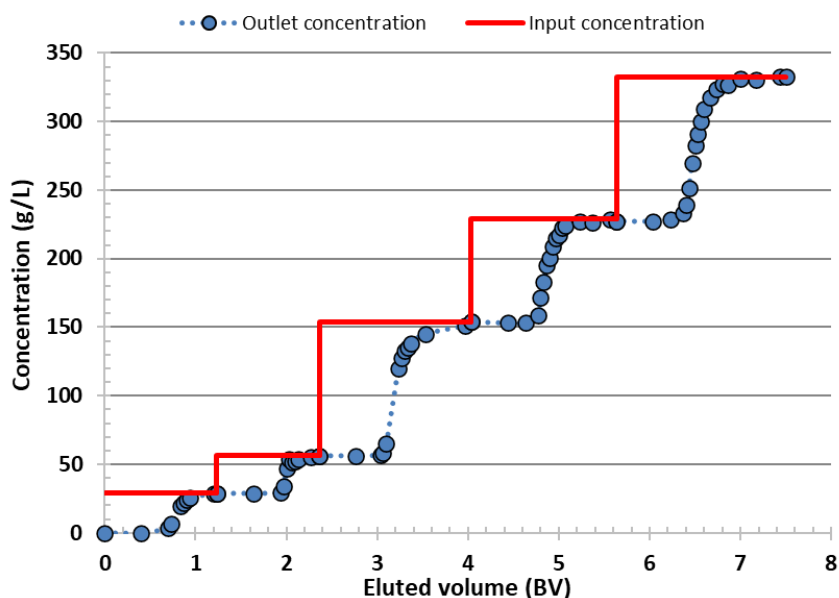


Figure 3-4. Frontal analysis of glucose with UMA 150 resin in sulfate form at pH 1.5 and 20°C.

The isotherm of glucose with UMA 150 resin in sulfate form at pH 1.5 was then deducted as shown in Figure 3-5, by performing mass balance to estimate glucose amount retained in the stationary phase q (expressed as g/L_{res}), once the equilibrium is reached in the whole column (input concentration = output concentration).

Glucose isotherm looks linear. Xylose results are given in the annexes. Sugar adsorption isotherms are linear on ion-exchange resins, as shown in some previous research works [Nobre et al., 2009]. Glucose and xylose properties are quite close as they have a linear isotherm with a similar slope. A linear regression with variance analysis (ANOVA) was performed to estimate the uncertainty range of the line slope corresponding to the affinity coefficient K_s , according to Eq. 3-3. K_s range of glucose and xylose are given in Table 3-1.

$$q_{th} = K_s \cdot c \quad (3-3)$$

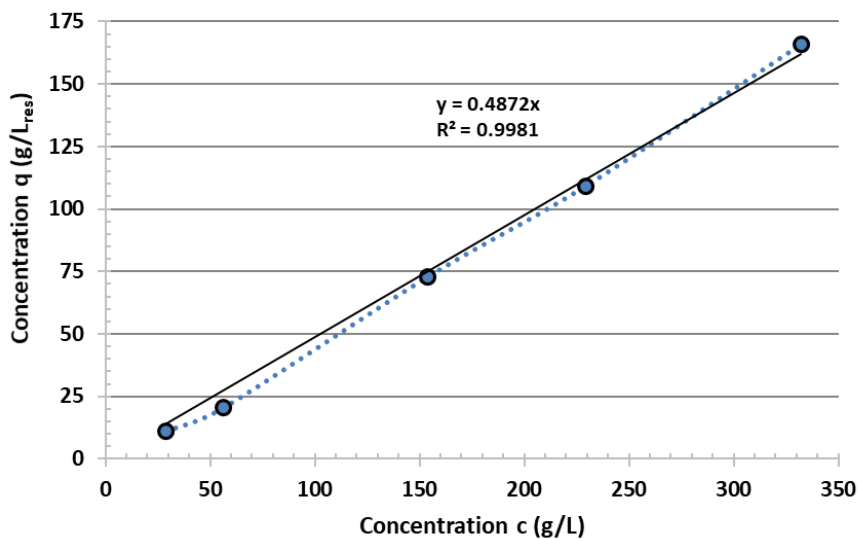


Figure 3-5. Isotherm of glucose and xylose with UMA 150 resin in sulfate form at pH 1.5 and 20°C.

Table 3-1. Uncertainty range of affinity coefficient K_s for glucose and xylose.

Sugar	K_s range (L/L _{res})
Glucose	0.46-0.52
Xylose	0.44-0.49

2.2 Organic acids

2.2.1 Isotherm analysis

The frontal analysis of acetic acid is shown in Figure 3-6 as an example of organic acid.

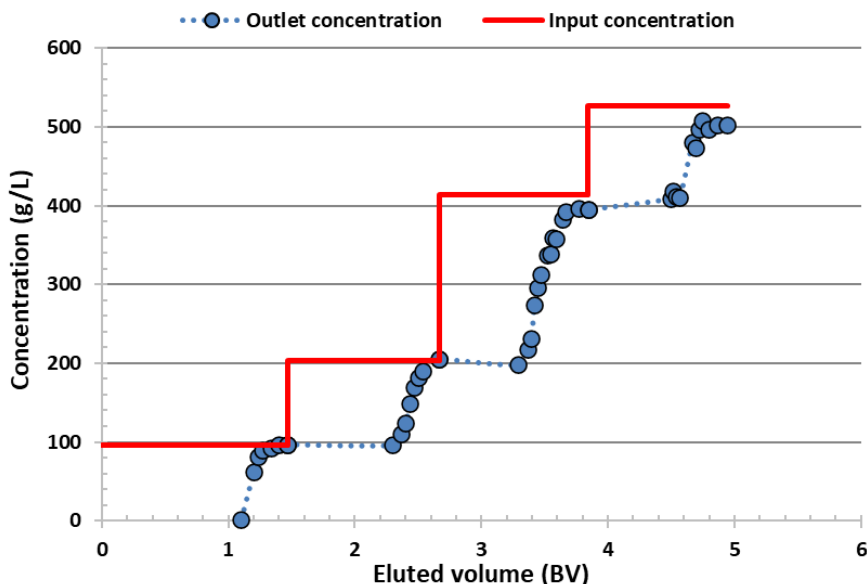


Figure 3-6. Frontal analysis of acetic acid with UMA 150 resin in sulfate form at pH 1.5 and 20°C.

Chapter III. Estimation of components physico-chemical properties and bed parameters

The corresponding isotherm of Figure 3-6 is:

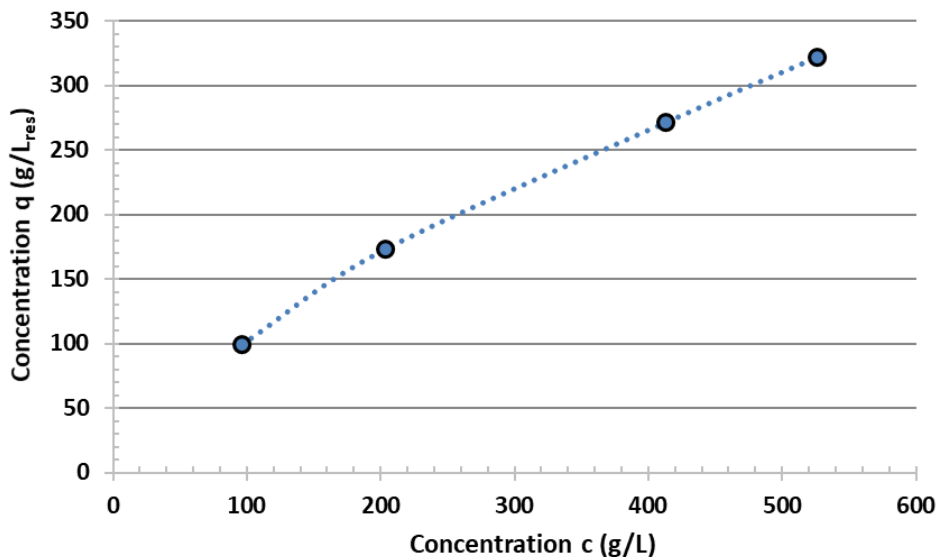


Figure 3-7. Isotherm of acetic acid with UMA 150 resin in sulfate form at pH 1.5 and 20°C.

As we can see in Figure 3-7, the acetic acid isotherm is not linear over the whole concentration range. In Figure 3-8 a linear relation can be found between $1/q$ and $1/c$, which suggest that a Langmuir equation can fit the experimental results:

$$q_{th} = \frac{q_{max} \cdot K_{eq} \cdot c}{1 + K_{eq} \cdot c} \quad (3 - 4)$$

Where q_{max} (in mol/L_{res}) and K_{eq} (in L/mol) are both Langmuir coefficients.

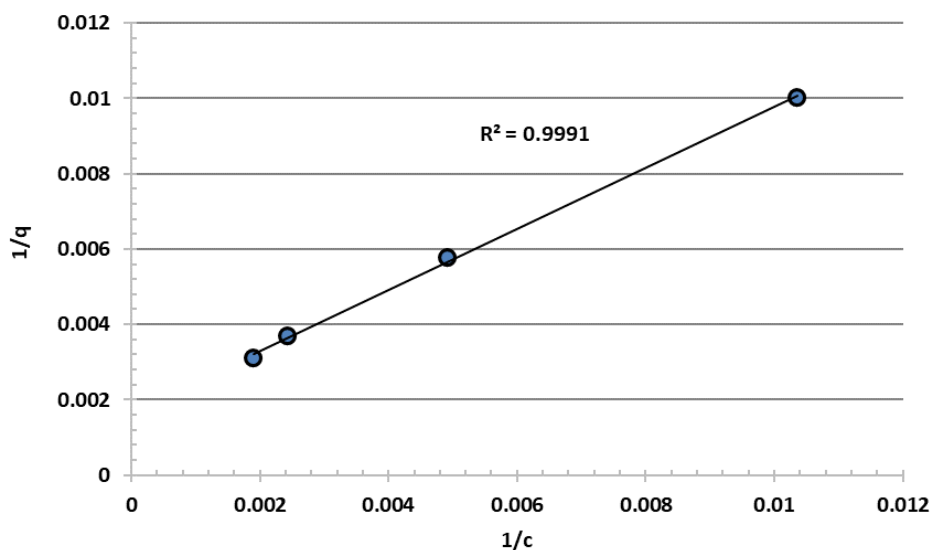


Figure 3-8. Isotherm of acetic acid – linear relation between $1/q$ and $1/c$.

Frontal analysis results and isotherms of other organic acid are shown in the annexes. Like acetic acid, isotherms of other organic acids could be fitted by Langmuir equation (Eq. 3-4), which is often used in research works [Ashfaq et al., 2021, Anasthas et al., 2001]

2.2.2 Langmuir coefficients estimation

Langmuir equation was fitted to experimental points (Figure 3-9) by the least square method detailed in chapter II to get uncertainty range of Langmuir coefficient q_{max} and K_{eq} (Table 3-3).

As introduced in chapter II, organic acid adsorption is probably due to hydrogen bonding between their carboxyl group hydrogen and lone election pairs of sulfate counter-anions on resin surface. Based on adsorption-desorption kinetics as in the Langmuir model, the isotherm could also be expressed as follows:

$$q_{th} = \frac{8 \cdot q_{SO_4}^{tot} \cdot k_s \cdot c}{1 + N_{HA} \cdot k_s \cdot c} \quad (3 - 5)$$

Where $q_{SO_4}^{tot}$ is the total amount of sulfate and hydrogen sulfate counter-anions on resin surface (expressed as mol/L_{res}), k_s is the adsorption coefficient (in L/mol) and N_{HA} is the number of adsorption sites occupied by each organic acid molecule. It is worth remaining that the factor 8 corresponds to the 8 lone electron pairs available per sulfate or hydrogen sulfate counter-anion.

By matching Eq. 3-5 with Eq. 3-4, k_s and N_{HA} can be deduced from q_{max} and K_{eq} values in Langmuir equation:

$$N_{HA} = \frac{8 \cdot q_{SO_4}^{tot}}{q_{max}} \quad (3 - 6)$$

$$k_s = \frac{K_{eq}}{N_{HA}} = \frac{q_{max} \cdot K_{eq}}{8 \cdot q_{SO_4}^{tot}} \quad (3 - 7)$$

Knowing the uncertainty range of q_{max} , K_{eq} and $q_{max} \cdot K_{eq}$, $q_{SO_4}^{tot}$ range is also required to estimate the uncertainty range of N_{HA} and k_s for all organic acids.

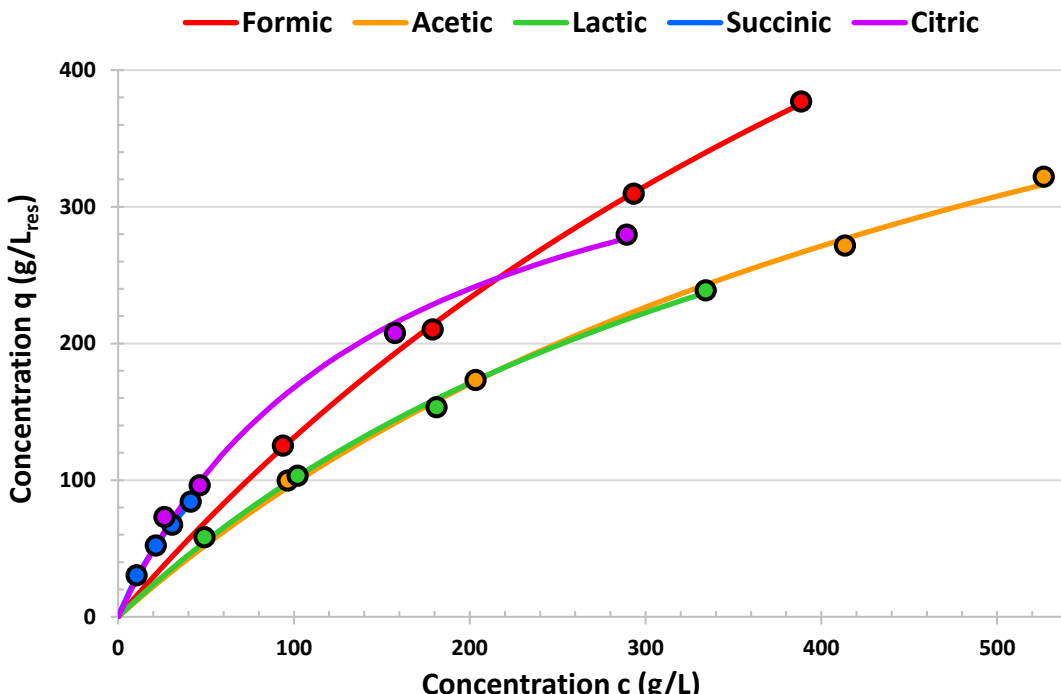


Figure 3-9. Langmuir isotherms of all organic acids with UMA 150 resin in sulfate form at pH 1.5 and 20°C.

Experimental results correspond to points and regression curves correspond to continuous lines.

Chapter III. Estimation of components physico-chemical properties and bed parameters

From eluent composition (pH and concentration of sulfate c_{SO_4} and hydrogen sulfate c_{HSO_4}) and q_{max}^{ei} range ($1.91 \pm 0.24 \text{ mol/L}_{\text{res}}$), $q_{SO_4}^{tot}$ range can be estimated by using ion-exchange and acid-base equilibrium coefficients of sulfate and hydrogen sulfate anions. Actually, $q_{SO_4}^{tot}$ is deduced from the calculation of sulfate amount q_{SO_4} and hydrogen sulfate amount q_{HSO_4} on resin surface (expressed as mol/L_{res}). According to the resin supplier (Appendix III), we consider $K_{SO_4/\text{OH}}^{eq} = 150$ and $K_{HSO_4/\text{OH}}^{eq} = 35$, while HSO₄⁻ pKa is supposed equal to 1.99 in water at 20°C. Table 3-2 gives q_{SO_4} , q_{HSO_4} and $q_{SO_4}^{tot}$ range depending on eluent composition at different pH.

Table 3-2. $q_{SO_4}^{tot}$ range estimation as a function of eluent composition at different pH (H₂SO₄ solution).

pH	1.00	1.25	1.50	1.75	2	2.25
c_{HSO_4} (mmol/L)	83.0	41.2	19.2	8.3	3.3	1.2
c_{SO_4} (mmol/L)	8.5	7.5	6.2	4.7	3.4	2.2
q_{HSO_4} (mol/L _{res})	1.22-1.48	0.86-1.02	0.53-0.61	0.28-0.33	0.14-0.16	0.07-0.08
q_{SO_4} (mol/L _{res})	0.22-0.33	0.40-0.56	0.57-0.77	0.69-0.91	0.76-0.99	0.80-1.03
$q_{SO_4}^{tot}$ (mol/L _{res})	1.44-1.81	1.26-1.58	1.10-1.38	0.98-1.23	0.90-1.15	0.87-1.11

In the present work, eluent pH was fixed around 1.5 so $q_{SO_4}^{tot}$ value is estimated between 1.1 and 1.4 mol/L_{res} ($q_{SO_4}^{tot} = 1.3 \text{ mol/L}_{\text{res}}$ will be supposed for simulation in chapters 4 and 5).

Finally, estimation of q_{max} , K_{eq} , $q_{max} \cdot K_{eq}$, N_{HA} and k_s ranges with UMA 150 resin in sulfate form at pH 1.5 and 20°C are gathered in Table 3-3.

Table 3-3. Langmuir coefficients of five organic acids with UMA 150 resin in sulfate form at pH 1.5 and 20°C.

Organic acid	Molar mass (g/mol)	Acid group number	q_{max} range (mol/L _{res})	K_{eq} range (L/mol)	$q_{max} \cdot K_{eq}$ range (L/L _{res})	N_{HA} range	k_s range (L/mol)
Formic	46	1	18-36	0.035-0.092	1.3-1.7	0.24-0.60	0.12-0.19
Acetic	60	1	9.4-13	0.077-0.14	1.0-1.3	0.65-1.17	0.093-0.15
Lactic	90	1	5.2-8.4	0.13-0.26	1.1-1.4	1.04-2.12	0.097-0.16
Succinic	118	2	1.5-2.7	1.04-2.36	2.8-3.6	3.2-7.3	0.26-0.41
Citric	192	3	1.9-2.7	0.85-1.84	2.3-3.5	3.3-5.9	0.20-0.39

2.2.3 Results interpretation

In Table 3-3, organic acids are listed from the smallest to the largest one in terms of size (molar mass) and number of carboxylic acid groups.

First, we can observe that N_{HA} (number of adsorption site occupied by one organic acid molecule) increases when organic acid size or carboxylic acid group number increases. N_{HA} ranges are comprised between 0.24 and 7.3 which is consistent with the total number of lone electron pairs available for hydrogen bonding on each sulfate or hydrogen sulfate counter-anion (= 8).

Chapter III. Estimation of components physico-chemical properties and bed parameters

Succinic and formic acids have relatively wider N_{HA} range because of the lack of experimental points in the non-linear part of their isotherm (at high-enough concentrations). As the N_{HA} and K_{eq} values are correlated in the linear zone of equilibrium curves, their estimations can be quite inaccurate when it is impossible to obtain enough experimental points in the non-linear zone. Indeed, succinic acid is much less soluble (70 g/L in water at 20°C), meanwhile formic acid is very soluble, but can be significantly adsorbed by the resin (very high q_{max} value). Consequently, it is difficult to estimate accurately q_{max} and K_{eq} separately because both are intricate in their isotherm linear part.

Adsorption coefficient k_s of all organic acids with only one acid group are in the same order of magnitude (0.1 to 0.2 L/mol), whereas k_s of succinic acid (2 acid groups) and citric acid (3 acid groups) are twice as high (0.2 to 0.4 L/mol).

k_s ranges are smaller because they can be estimated directly from ($q_{max} \cdot K_{eq}$) estimation which is more accurate and not affected by the lack of experimental points in the non-linear part of isotherm (at high concentrations).

As shown in chapter II, the model proposed in this work assumes that adsorption is due to hydrogen bonding between carboxylic acid group of organic acid and lone electron pairs of sulfate or hydrogen sulfate counter-anions. Since the total amount of adsorption sites is fixed (8. $q_{SO_4}^{tot}$), if more sites are occupied per molecule (higher N_{HA} value), then fewer molecules can be adsorbed on resin (lower q_{max} value).

According to N_{HA} ranges, possible values that makes sense are assumed to be 0.5 for formic acid, 1 for acetic acid, 2 for lactic acid, 4 for succinic acid and citric acid. Thus, succinic and citric acids occupy more adsorption sites because of their larger molecular size, which can hinder access to free lone pairs (steric hindrance), and their 2 or 3 carboxylic acid groups, which can make as many H bonds with lone pairs. $N_{HA} = 4$ corresponds to 4 lone pairs occupied per succinic or citric acid molecule (cluttered or H-bond), which means up to 2 molecules retained per sulfate or hydrogen sulfate counter-anion.

Inversely, $N_{HA} = 0.5$ for formic acid, which is the smallest acid molecule with only one carboxylic acid group. It corresponds to two formic acid molecules per lone pairs (none cluttered and only single H-bonds), so up to 16 molecules per sulfate or hydrogen sulfate counter-anion.

The formation of formic acid dimers [Agnieszka C., 2007] could explain that up to two formic acid molecules can occupy the same adsorption site (lone pair). This study shows that formic acid molecules can form stable dimers on platinum 111 surface with and without the presence of water. The dimer binding energy is estimated from 3 to 18 kcal/mol depending on dimer structure, which is much stronger than hydrogen bond (around 3 kcal/mol) [Qi Y., 2014].

Acetic acid is also a monoacid but a bit larger than formic acid. $N_{HA} = 1$ corresponds to only one acetic acid molecule per lone pairs (none cluttered and only single H-bonds), so up to 8 molecules per sulfate or hydrogen sulfate counter-anion.

Lactic acid is also a monoacid but much larger than formic acid. $N_{HA} = 2$ corresponds to 2 lone pairs occupied per lactic acid molecule (half cluttered), so up to 4 molecules per sulfate or hydrogen sulfate counter-anion.

Chapter III. Estimation of components physico-chemical properties and bed parameters

Finally, uncertainty ranges of Langmuir coefficients and adsorption coefficient k_s can be refined considering only N_{HA} values which make sense and are listed in Table 3-4.

Table 3-4. Refined Langmuir coefficients assuming only N_{HA} values which make sense for the five organic acids studied with UMA 150 resin in sulfate form at pH 1.5 and 20°C.

Organic acid	Possible N_{HA} value	k_s range (L/mol)	q_{max} range (mol/L _{res})	K_{eq} range (L/mol)	$q_{max} \cdot K_{eq}$ range (L/L _{res})
Formic	0.5	0.12-0.18	18-22	0.058-0.092	1.3-1.7
Acetic	1	0.093-0.14	9.4-11	0.093-0.14	1.0-1.3
Lactic	2	0.097-0.13	5.2-5.5	0.19-0.26	1.1-1.4
Succinic	4	0.26-0.41	2.2-2.7	1.04-1.64	2.8-3.6
Citric	4	0.20-0.39	2.2-2.7	0.85-1.58	2.3-3.5

k_s values of organic acids are linked to the total strength of H-bonds between their carboxylic acid group and lone electron pairs of sulfate or hydrogen sulfate counter-anions. It makes sense that succinic and citric acids have about twice higher k_s value than all monoacids because they can make two or three H-bonds.

3 Pulse tests

3.1 Presentation of van Deemter curves

Pulse tests were performed at different flowrates to obtain the van Deemter curve of compounds, to estimate dispersion coefficients, namely the axial dispersion coefficient D and the mass transfer coefficient k_a . Flowrates vary from 0.1 BV/h to 2 BV/h, which correspond to common operating conditions for preparative chromatography to minimize global dispersion.

As an example, pulse test results with glucose solution are shown in Figure 3-10.

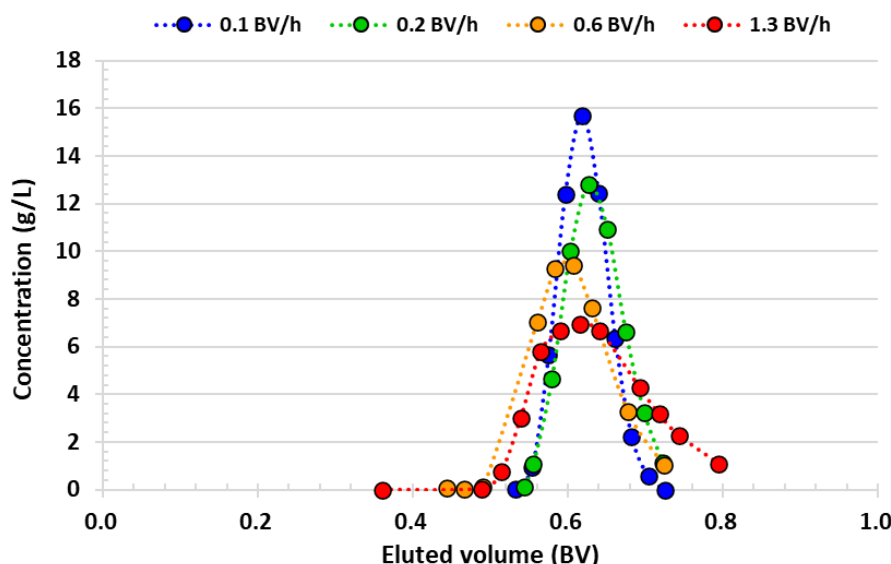


Figure 3-10. Pulse tests of glucose at different flowrates with UMA 150 resin in sulfate form at pH 1.5.

Chapter III. Estimation of components physico-chemical properties and bed parameters

As explained in Chapter II, each peak enables us to estimate HETP (height equivalent to a theoretical plate) as a function of flowrate or interstitial liquid velocity v . The corresponding van Deemter curve of glucose is shown in Figure 3-11:

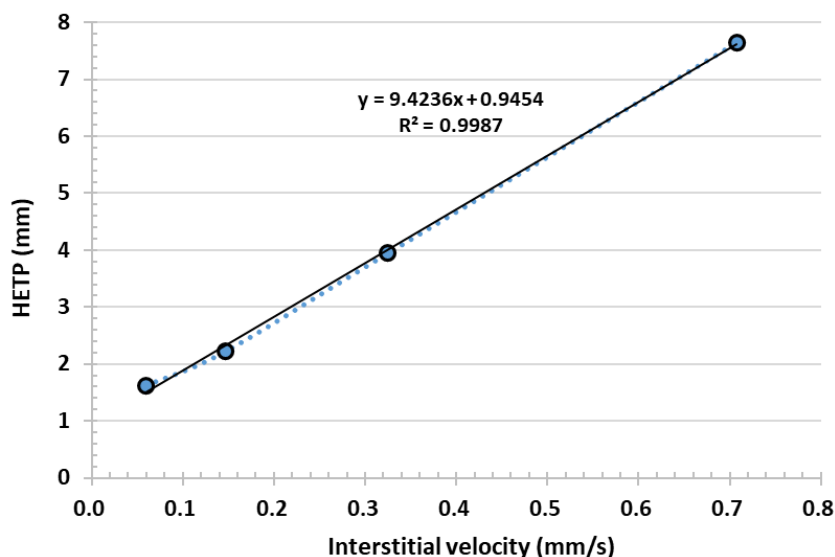


Figure 3-11. Van Deemter curve of glucose with UMA 150 resin in sulfate form at pH 1.5.

Succinic acid pulse tests are shown in Figure 3-12 as an example for organic acids.

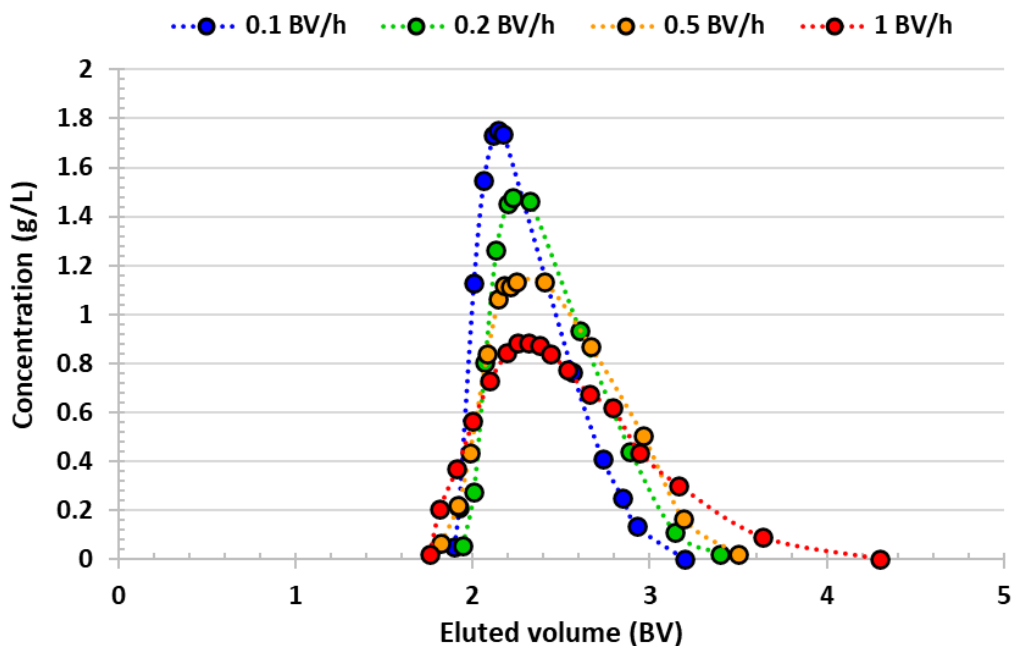


Figure 3-12. Pulse test of succinic acid at different flowrates with UMA 150 resin in sulfate form at pH 1.5.

In the case of succinic and citric acid, the tailing due to ion-exchange (will be explained in chapter IV) increases dispersion on peak right side. Consequently, to avoid or limit ion-exchange influence on HETP estimation, only the left side of the peak was considered to estimate their variance σ^2 .

The corresponding van Deemter curve of succinic acid is shown in Figure 3-13. The linear fit includes all experimental points, even though the first one is obviously not in the linear part of the curve. Its effect on the slope is however minimal.

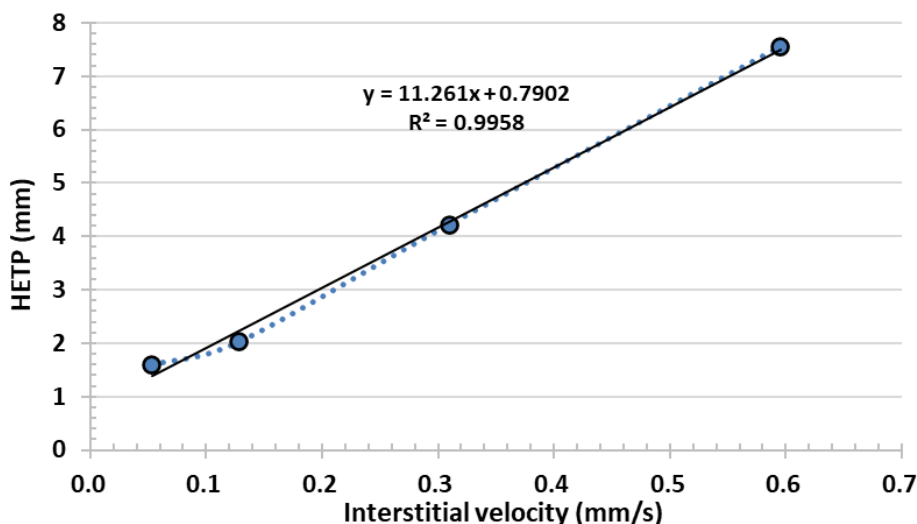


Figure 3-13. Van Deemter curve of succinic acid with UMA 150 resin in sulfate form at pH 1.5.

All pulse tests show that peak width increases with the flowrate. In other words, a higher interstitial liquid velocity leads to a greater dispersion and therefore a larger peak. This trend corresponds to the linear increasing part of van Deemter curve when molecular diffusion (term B) is negligible, and HETP depends almost on mass transfer rate (term C) and mechanical dispersion (term A) according to the usual equation (Eq. 3-8):

$$HETP = A + \frac{B}{v} + C \cdot v \quad (3 - 8)$$

3.2 Estimation of van Deemter coefficients

At first, terms A and C were estimated from experimental points by linear regression, assuming B term to be negligible. Indeed, van Deemter curves of all compounds are almost linear over the whole interstitial velocity range. Variance analysis is performed to estimate uncertainty ranges of A and C , following the same method explained for Langmuir coefficients estimation.

Term B cannot be estimated accurately because of the lack of experimental points in the non-linear part of Van Deemter curve, at very low interstitial velocity (< 0.05 mm/s). Nevertheless, an upper bound for term B , noted B_{up} , can be estimated by variance analysis, depending on A and C . It corresponds to the maximum B value that makes van Deemter equation (Eq. 3-8) deviate too much from experimental points in terms of SSR (Sum of Squared Residuals).

Finally, the range of axial dispersion coefficient D and mass transfer coefficient k_a can be deduced from A , B_{up} and C ranges for all compounds, according to equations from chapter II:

$$D = \frac{A}{2} \cdot v + \frac{B_{up}}{2} \quad (3 - 9)$$

$$k_a = 2 \cdot \left[\frac{\varepsilon \cdot K}{C \cdot (1 + K \cdot F)^2} \right] \quad (3 - 10)$$

Where K is the linear coefficient defined as $K = c/q$, v is the interstitial velocity and $F = \varepsilon/(1 - \varepsilon)$. For glucose and xylose $K = 1/K_s$, and for organic acids it is estimated from the linear part of Langmuir isotherm $K = 1/(q_{max} \cdot K_{eq})$.

Chapter III. Estimation of components physico-chemical properties and bed parameters

Van Deemter curves give the optimum interstitial liquid velocity corresponding to the best separation efficiency (minimum HETP). While comparing van Deemter curves of all compounds, 0.1 BV/h is the optimum flowrate in the investigated range. However, 0.5 BV/h is chosen for all experiments and simulations to get a compromise between separation efficiency and productivity.

Table 3-5 shows the range of van Deemter coefficients for all compounds. D and k_a ranges were estimated considering interstitial liquid velocity equals to 0.23 mm/s, which corresponds to 0.5 BV/h flowrate in our large chromatography column (350 mL bed volume).

According to uncertainty ranges, the impact of mechanical dispersion, represented by term A , seems quite similar for all components. At 0.5 BV/h, mechanical dispersion has a significant impact since it can represent 10% to 60% of global dispersion (HETP) depending on molecule.

Estimation of term C shows that mass transfer rate of lactic and citric acids are twice slower than those of glucose, xylose, acetic acid, and succinic acid transfer rate, which are also three-fold lower than those of formic acid. It makes sense that formic acid, which is the smallest compound, has the faster transfer rate. However, the size is not sufficient to explain all differences: physico-chemical properties also matter. The uncertainty ranges of C are quite narrow for all compounds and result in a quite accurate estimation of mass transfer coefficient k_a (Eq. 3-10).

On the contrary, B , which represents the influence of molecular diffusion, cannot be estimated accurately because it is negligible within the interstitial velocity range. The estimations of B_{up} , the upper bounds of B , are not conclusive due to their high dependence on A and C . However, for any compounds, whatever A and C values within their uncertainty range, B_{up} estimation leads always to a similar estimation of axial dispersion coefficient D (narrow range).

Table 3-5. Van Deemter coefficients for all compounds with UMA 150 resin in sulfate form at pH 1.5.

Compounds	A (10^{-4} m)	B_{up} (10^{-9} m 2 /s)	C (s)	D (10^{-9} m 2 /s)	k_a (10^{-2} L _{res} /L _{bed} /s)
Glucose	7.6-11.4	< 30	9.0-9.9	102-131	2.6-3.2
Xylose	6.6-12.6	< 28	9.8-11.4	91-146	2.3-3.0
Formic acid	9.4-12.3	< 14	3.2-4.0	116-142	6.1-8.5
Acetic acid	8.3-12.0	< 23	8.1-9.1	100-139	2.9-3.5
Lactic acid	1.1-7.5	< 29	19.5-21.3	21-87	1.2-1.5
Succinic acid	4.4-11.4	< 47	10.2-12.3	74-132	1.3-1.9
Citric acid	3.8-13	< 64	19.1-21.8	76-151	0.75-1.1

Table 3-6 shows the theoretical B_{th} value estimated from literature D_m value, together with its influence on dispersion estimation (range of $(B_{th}/2)/D$).

To check the negligible influence of B on the estimation of D (cf. Eq. 3-9), molecular diffusion constant D_m of all compounds were taken from the literature [Alexey et al. 2003, Janet et al. 1999, Ueadaira et al. 1969, Müller 1957], to estimate the theoretical B value according to Eq. 3-11:

Chapter III. Estimation of components physico-chemical properties and bed parameters

$$B_{th} = 2 \cdot \frac{D_m}{\tau} \quad (3-11)$$

Where τ is the bed tortuosity as determined by tomography (1.46).

Table 3-6. Impact of theoretical B values on axial dispersion coefficient D.

Components	D_m (10^{-9} m 2 /s)	B_{th} (10^{-9} m 2 /s)	$(B_{th}/2)/D$
Glucose	0.26	0.36	0.1%-0.2%
Xylose	0.73	1.00	0.3%-0.6%
Formic acid	1.52	2.08	0.7%-0.9%
Acetic acid	1.19	1.63	0.6%-0.8%
Lactic acid	0.82	1.12	0.7%-2.7%
Succinic acid	0.86	1.18	0.5%-0.8%
Citric acid	0.65	0.89	0.3%-0.6%

According to the value of D_m from literature, molecular diffusion represents less than 1% of the axial dispersion coefficient D . Thus, the molecular diffusion is theoretically negligible compared to other dispersion phenomena for the range of flowrate investigated in the present work. In any case, the estimation of D only is required for the simulation and the results show that B_{up} estimated from experimental points results in a similar estimation of D estimation, with a narrow range, for all compounds.

To summarize, estimation of adsorption equilibrium coefficient (N and k_s) were consistent with organic acids adsorption by hydrogen bonding between the hydrogen atom of their carboxylic acid group and one lone electron pair of oxygen atoms of sulfate or hydrogen sulfate counter-anions. Adsorption coefficients showed an evolution with the size / acid group number of molecule. Van Deemter curves showed that in the chosen flowrate range, molecular diffusion could be ignored. Thus, mass transfer resistance is dominant for the peak dispersion.

Chapter IV. Batch chromatography simulation (pulse tests)

Strong anionic resins are often used in sulfate form in chemical or food and feed industries to separate organic acids by chromatography. Development of ion-exchange process by numerical simulation requires more accurate retention model. Some organic acids such as succinic acid and citric acid has an unusual tailing in their chromatography profiles which cannot be explained by usual Langmuir model. In this chapter, the hybrid model presented in chapter II was used to explain this tailing. In addition to Langmuir model to describe adsorption, it considers also organic acid dissociation and ion-exchange of its conjugate base. The model was solved with CE/SE method.

To proceed the simulation, most of the physico-chemical parameters were measured experimentally as shown in the previous chapter. Yet, some parameters required for the simulation, such as the ion exchange constant K^{iex} of some compounds, remain unknown. Moreover, some parameters need to be refined from their uncertainty ranges.

In this chapter, the impact of parameters on the profile were identified by batch chromatography simulation. Parameters such as k_a , D , K^{iex} and Langmuir coefficients were refined by curve fitting. Then, binary mixture pulse test simulations were simulated by both hybrid model and Langmuir model. The improved values of these parameters were also validated and will be used for multi-column process simulation in the next chapter.

1 Influence of k_a , D , K^{iex} and Langmuir coefficients

Before fitting simulation curves to experimental curves, influences of different parameters on the chromatography profile need to be investigated. Generally, mass transfer and axial dispersion coefficients (k_a and D) influence the peak width while K^{iex} and Langmuir coefficients (N_i and k_s) affect the residence time and peak symmetry.

1.1 Influence of global mass transfer coefficient k_a and axial dispersion coefficient D

Figure 4-1 shows the impact of k_a and D on glucose chromatography profile. The simulated curves were obtained with $k_a = 0.05 \text{ s}^{-1}$, $D = 5.10^{-8} \text{ m}^2/\text{s}$ as reference. Reference k_a and D were multiplied and divided by 5 for comparison, which covers uncertainty ranges of k_a and D estimated in Chapter III. Other parameters were identical for glucose pulse test simulation at pH 1.5.

Chapter IV. Batch chromatography simulation (pulse tests)

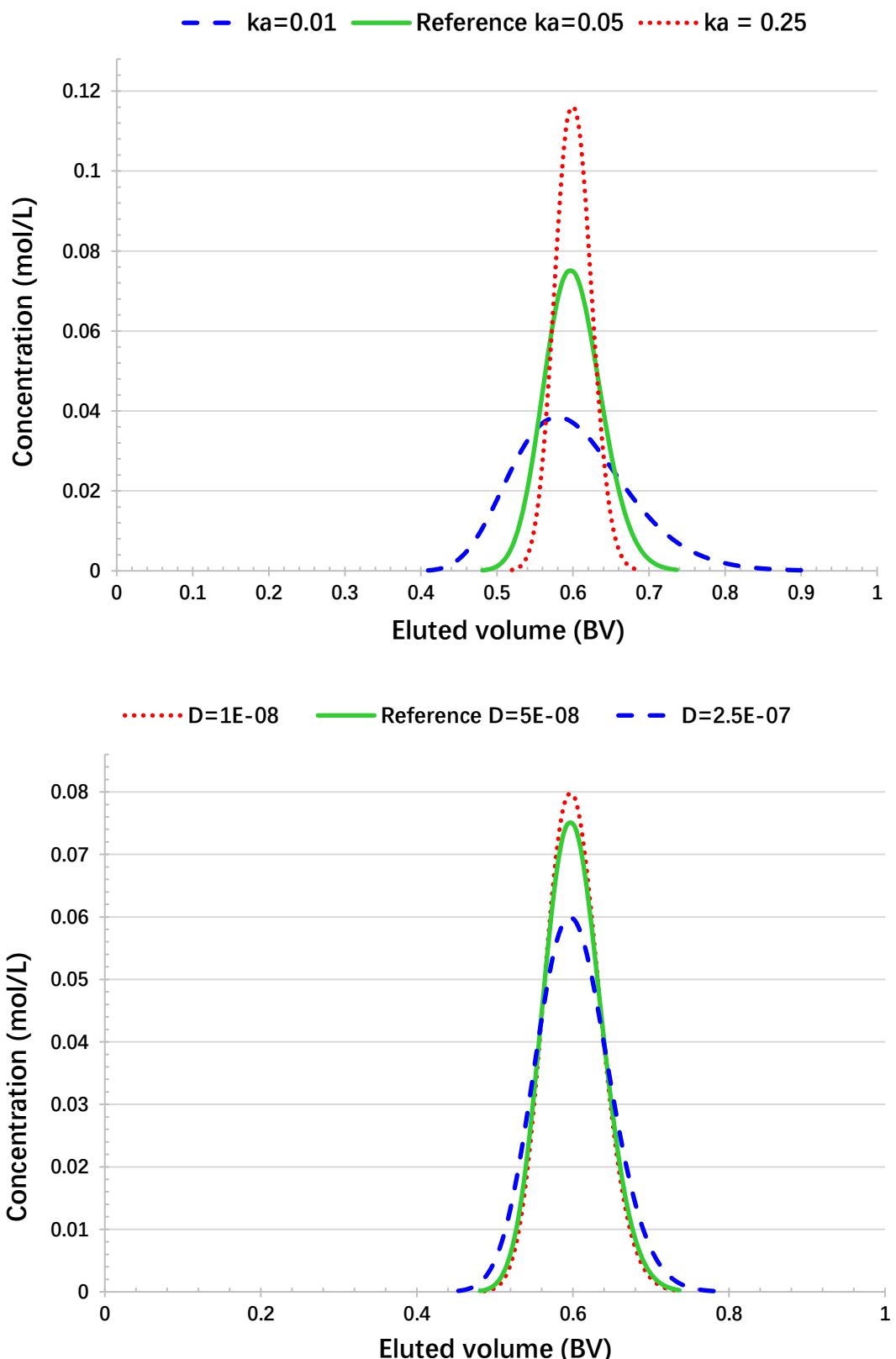


Figure 4-1. Impact of global mass transfer coefficient (A at the top) and dispersion coefficient (B at the bottom) on the chromatography profile.

Chapter IV. Batch chromatography simulation (pulse tests)

Figure 4-1 shows that a higher k_a causes a higher and narrower peak. We can also observe that the variation of D has a relatively lower impact on peak width, which proves that axial dispersion has a lower influence than mass transfer limitation in our operating conditions. Otherwise, these parameters affect neither the mean residence time, nor the peak symmetry. As both k_a and D changes peak width and peak height, an increase of k_a could be theoretically compensated by a decrease of D . Yet, the peak is much more sensitive to variation of k_a within the experimental range. Due to the low sensitivity of D , its mean value estimated from van Deemter curves will be used for all simulations and only k_a value will be refined by curve fitting afterwards.

1.2 Influence of Langmuir coefficients and K^{iex}

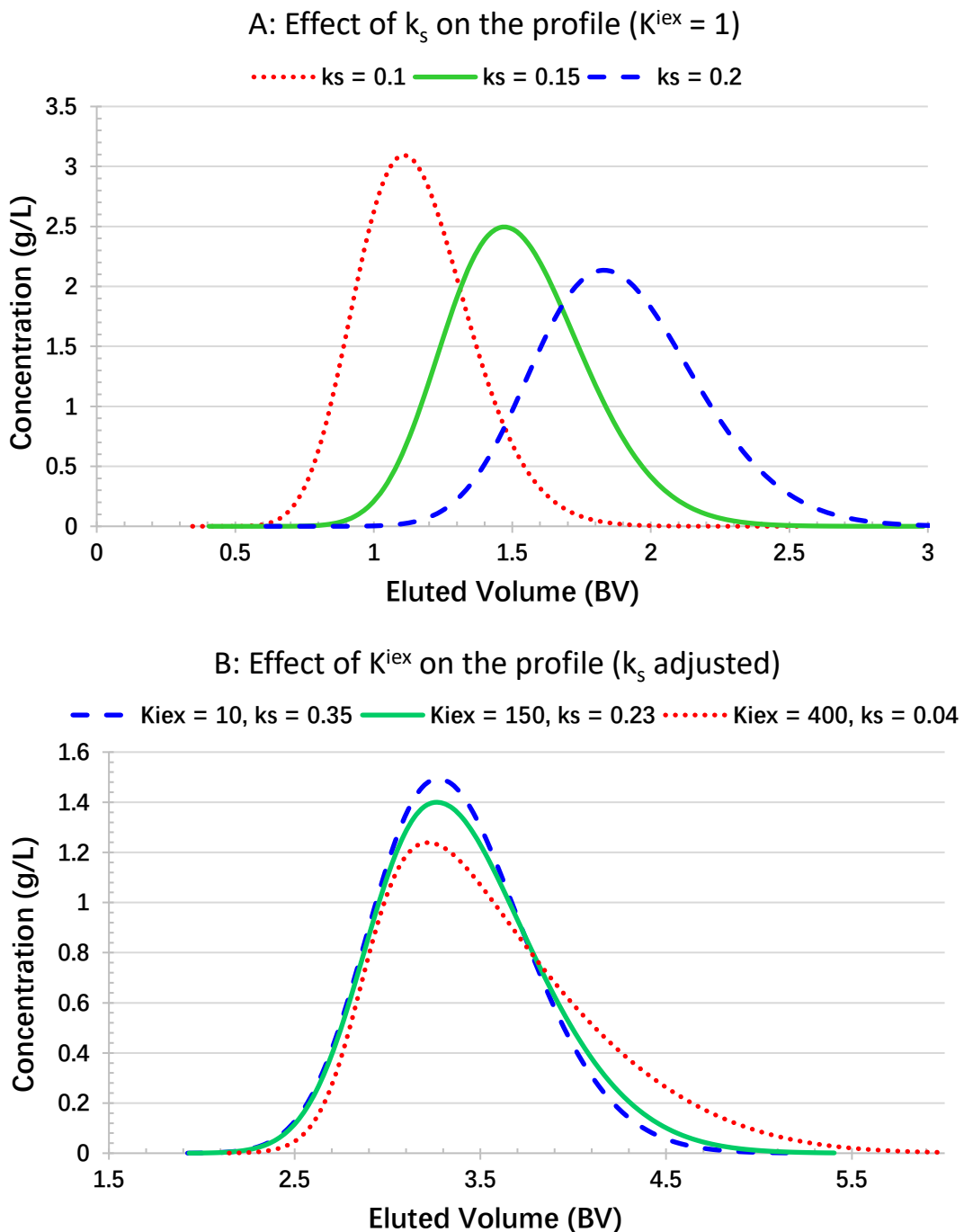
To compare the effect of Langmuir adsorption and ion-exchange on chromatography profiles, citric acid is chosen here as a case study. According to previous researches, citric acid profile can be remarkably affected by ion-exchange with strong anionic resin, which is characterized by a long tailing [Lemaire et al. 2016].

Theoretically, the tailing could be due to a high value of the adsorption affinity k_s or ion-exchange coefficient K^{iex} . Pulse tests with different values of k_s and K^{iex} were simulated. Figures 4-2-A and 4-2-B show the impact of their values on the chromatography profiles. In Figure 4-2-A, K^{iex} is fixed at 1, a negligible value, to focus on the influence of k_s on the profile shape and position. Then, the influence of K^{iex} is compared in Figure 4-2-B. As the objective was to highlight the effect of K^{iex} only on the profile shape, the value of k_s was adjusted for each value of K^{iex} to obtain the same retention volume/time.

As expected, Figure 4-2-A shows that the higher is the adsorption coefficient k_s , the higher is the retention volume. However, the value of the coefficient k_s barely changes the profile shape which remains symmetrical. In comparison, Figure 4-2-B shows that K^{iex} significantly impacts the profile shape by increasing its tailing.

To summarize, the retention volume depends on both K^{iex} and k_s while the profile tailing is influenced almost solely by K^{iex} . Indeed, very high k_s values could also lead theoretically to significant profile tailing, but these values would not be consistent with experimental results, which corresponds to a k_s ranging between 0 and 0.3 L/mol.

The impact of ion-exchange constant K^{iex} depends on the pH of the liquid phase and the pKa of the organic acid. When the pH is much lower than pKa ($\text{pH} < \text{pKa} - 2$), organic acids are mainly in molecular form. In this case, a very small proportion is dissociated into the anionic form, and the peak is less sensitive to the value of K^{iex} .

Figure 4-2. Influence of k_s (A on the top) and K^{iex} (B at the bottom) on organic acid outlet profile.

2 Identification of Langmuir and ion-exchange coefficients

In the present study, K^{iex} was estimated to reproduce the experimental profile tailing obtained in pulse tests of formic, succinic, and citric acids, starting from the resin supplier's estimation. Meanwhile, k_s was adjusted to fit their experimental retention volume. Figure 4-3 gives a curve-fitting example. Initially, k_s was set to the experimental value estimated previously from equilibrium curves (obtained by frontal analysis), considering different possible N values (cf. table 3-5 in Chapter III). The operating conditions of these pulse tests are detailed in Table 4-1.

Chapter IV. Batch chromatography simulation (pulse tests)

Table 4-1. Operating conditions of single component pulse tests.

	Glucose	Xylose	Lactic acid	Acetic acid	Formic acid	Succinic acid	Citric acid
Sample volume (BV)	0.028	0.028	0.028	0.028	0.028	0.02	0.02
Concentration (mol/L)	0.25	0.23	0.32	0.62	0.75	0.57	0.55
Eluent	pH 1.5 H ₂ SO ₄ (0.025 mol/L)						
Flowrate (BV/h)	0.5						

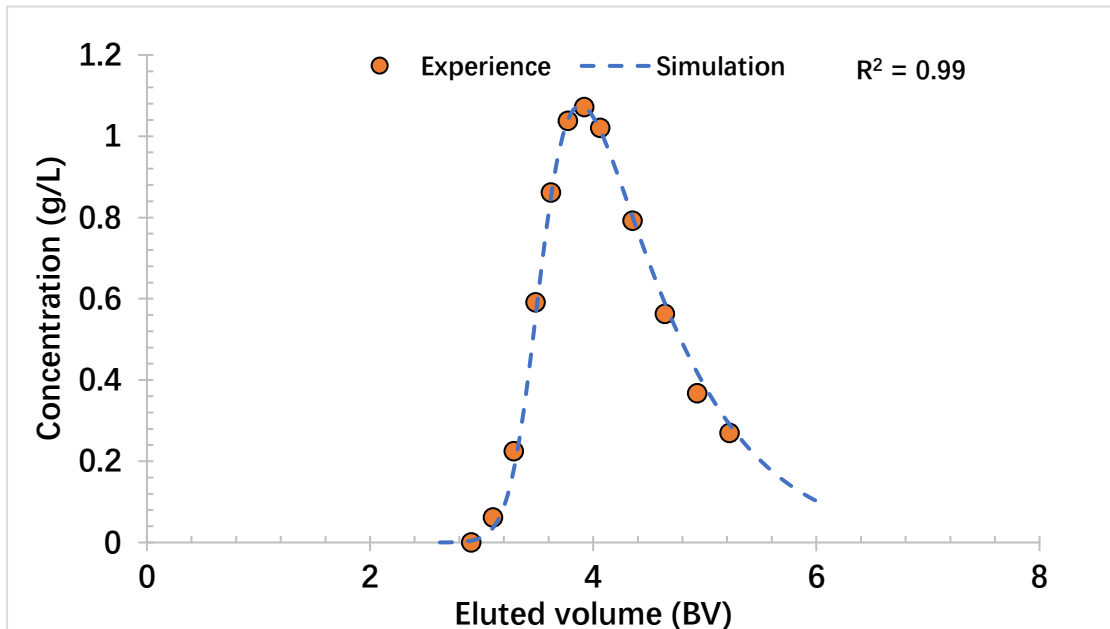


Figure 4-3. Fitting curves to experimental points in the case of citric acid.

The R^2 (R-squared) was calculated to validate fitting quality:

$$R^2 = 1 - \frac{SSR}{SST} \quad (4-1)$$

Where SSR (Sum of Squared Residuals) and SST (Sum of Squared Total) are estimated using following equations:

$$SSR = \sum_i (x_{exp} - x_{th})^2 \quad (4-2)$$

$$SST = \sum_i (x_{exp} - \bar{x}_{exp})^2 \quad (4-3)$$

Where \bar{x}_{exp} corresponds to the mean of experimental values.

Table 4-2 shows the refined estimation of k_a , D which are used for mono-component simulation, along with experimental results from chapter III. The identified value was defined when R^2 reaches its maximum. Curve fitting results and corresponding R^2 are listed in the Appendix.

Chapter IV. Batch chromatography simulation (pulse tests)

Table 4-2. Experimental uncertainty ranges of k_a , D and their refined values.

	k_a identified from pulse tests ($10^{-2} L_{res}/L_{bed}/s$)	k_a identified from van Deemter curves ($10^{-2} L_{res}/L_{bed}/s$)	D identified from van Deemter curves ($10^{-9} m^2/s$)	D identified from pulse tests ($10^{-9} m^2/s$)
Glucose	3.2	2.6-3.2	102-131	110
Xylose	3.4	2.3-3.0	91-146	110
Formic acid	6.1	6.1-8.5	116-142	140
Acetic acid	4.2	2.9-3.5	100-139	110
Lactic acid	1.6	1.2-1.5	21-87	40
Succinic acid	1.3	1.3-1.9	74-132	130
Citric acid	0.6	0.75-1.1	76-151	130

Table 4-2 shows that for most of the compounds, k_a identified from pulse tests appeared in good agreement with their estimation from van Deemter curves as they are both in the same magnitude. The difference of k_a , especially in the case of acetic acid, could be related to the uncertainty of linear coefficient K , or the imprecision of original detailed van Deemter equation. Glucose and xylose have a close k_a because of their similar physico-chemical properties. k_a of organic acids appeared to be associated with their molecular size and acid group number, which shows that the mass transfer is possibly driven by adsorption-desorption and ion-exchange reactions at the interface.

Estimations of k_s and N_i identified from pulse tests are shown in Table 4-3 and compared to first estimation from frontal analysis (cf. Chapter III, section 2).

Table 4-3. The comparison of k_s , N_i between the refined values and experimental results.

	k_s identified from pulse tests	k_s identified from frontal analysis	N_i identified from frontal analysis
Glucose	0.40-0.45	0.46-0.52	--
Xylose	0.45-0.48	0.44-0.49	--
Formic acid	0.2-0.25	0.12-0.18	0.5
Acetic acid	0.10-0.12	0.093-0.14	1
Lactic acid	0.09-0.11	0.097-0.13	2
Succinic acid	0.26-0.28	0.26-0.41	4
Citric acid	0.19-0.21	0.20-0.39	4

In Table 4-3, N_i were imposed to be round values and make sense as explained in chapter III. It shows that with chosen N_i value, k_s values identified from pulse tests match well to values identified from frontal analysis (equilibrium curves). k_s ranges identified from pulse test are at the bottom of ranges identified from frontal analysis, especially for succinic acid and citric acid. It can be explained by the ion-exchange effect during frontal analysis which makes k_s be overestimated. k_s of formic acid matches less well since its adsorption is affected by dimer formation that may be different between pulse tests and frontal analysis: dimer proportions in the mobile and stationary phases may be different during frontal analysis and pulse tests, because concentrations are much lower during pulse tests.

Estimations of K^{lex} from pulse tests are shown in Table 4-4 and compared to the value given by

Chapter IV. Batch chromatography simulation (pulse tests)

the resin supplier.

Table 4-4. Comparison of K^{iex} estimated from pulse tests to the value given by the resin supplier.

	K^{iex} identified from pulse tests	K^{iex} supplier
Glucose	0	0
Xylose	0	0
Formic acid	15±10	30
Acetic acid	45±10	30
Lactic acid	45±10	30
Succinic acid	900±100	--
Citric acid	200±20	220

Table 4-4 shows that K^{iex} ranges identified from pulse tests correspond quite well to supplier data. K^{iex} of succinic acid is around 900 which is much higher than other organic acids but comparable to some organic compounds such as ClO_4^- , CrO_4^{2-} , $C_6H_5SO_3^-$ according to supplier data in appendix.

To prove that the peak tailing is due to K^{iex} and that, within the range of our experiment, it cannot be reproduced by Langmuir adsorption, pulse test simulations were performed with a model which considers only Langmuir adsorption (called the Langmuir model). The simulation results were compared with results simulated with the model proposed in chapter II which considers both Langmuir adsorption and ion exchange (called the hybrid model).

Figure 4-4 presents the comparison for formic, succinic, and citric acids. It highlights that the tailing of succinic and citric acid profiles cannot be reproduced by the Langmuir adsorption model, but only by the hybrid model. It confirms that retention of their corresponding anions by ion exchange must be considered, even if they are poorly dissociated at pH 1.5.

As shown in Figure 4-4, both models can predict the experimental results for formic acid. This is not surprising as its tailing is negligible, with a profile almost symmetrical. The formic acid profile is marginally influenced by ion exchange due to its very low K^{iex} (< 30). Moreover, it is much less dissociated into anions than citric acid because of its higher pKa (3.76 vs. 3.13). Thus, at pH 1.5, only 0.5% formic acid is dissociated, making the ion exchange effect even more negligible.

In comparison, succinic acid has the highest pKa (4.16) but also the highest K^{iex} according to Table 4-4 (900 ± 100). Therefore, despite a low proportion dissociated into anions (0.2% at pH 1.5), the strong retention of succinate anion on resin ion-exchange sites can explain its slight tailing.

Finally, the citric acid profile has the largest tailing because of its lower pKa (3.13) and quite high K^{iex} . Indeed, citric acid is the most dissociated into anions (2.3% at pH 1.5) and citrate anions are strongly retained by ion exchange ($K^{iex} = 200 \pm 20$).

Figure 4-4 confirms that the tailing of succinic and citric acid profiles cannot be reproduced by the Langmuir adsorption model. In contrast, the hybrid model is in good agreement with experimental results. It confirms that organic anions retention by ion exchange must be considered to make predictive simulation, even if they are poorly dissociated at pH = 1.5.

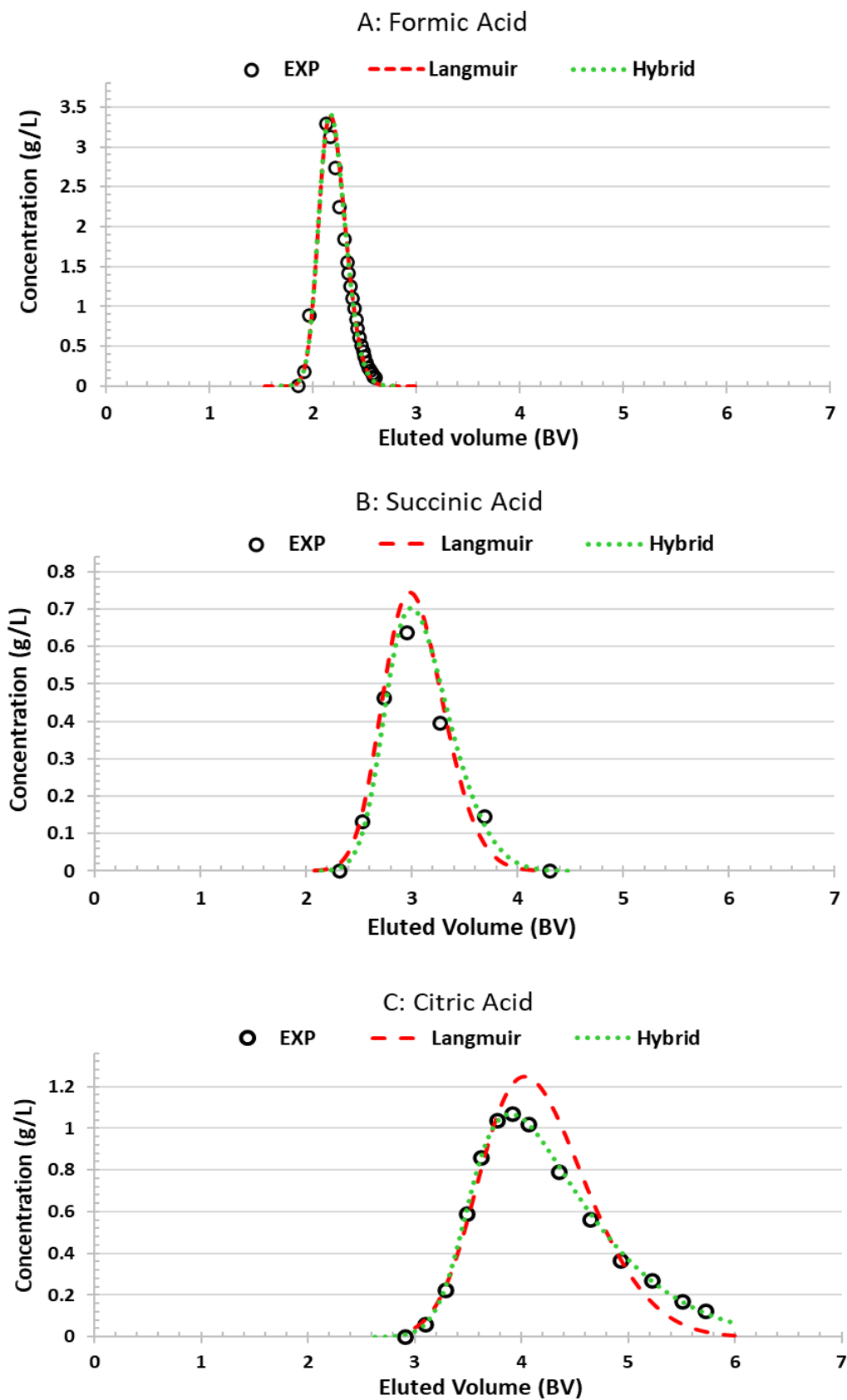


Figure 4-4. Influence of ion-exchange on the outlet profile of formic (A), succinic (B) and citric acids (C).

3 Validation of coefficients for binary mixture and comparison with Langmuir model

To confirm that the hybrid model is more predictive than the model which considers only Langmuir adsorption, a pulse test with a mixture of formic acid and succinic acid was performed experimentally and simulated (Fig. 4-5). Table 4-5 gives parameter values used in both models, whose ranges were estimated previously from experimental data analysis (Table 4-3 and 4-4).

Table 4-5. Parameters used for multi-component pulse test simulation

Model	Organic acid	N_i	k_s used (L/mol)	K^{iex} used	k_a (s ⁻¹)	D (10 ⁻⁷ m ² /s)
With IEX	Formic acid	0.5	0.24	25	0.058	1.4
	Succinic acid	4	0.265	800	0.01	1.3
Only Langmuir adsorption	Formic acid	0.5	0.25	0	0.045	1
	Succinic acid	4	0.44	0	0.01	0.5

Experimental profiles depicted in Figure 4-5 correspond to a pulse test performed with 10 mL pH 1.5 solution, composed of 0.65 mol/L formic acid and 0.267 mol/L succinic acid, eluted with pH 1.5 H₂SO₄ solution at 0.5 BV/h.

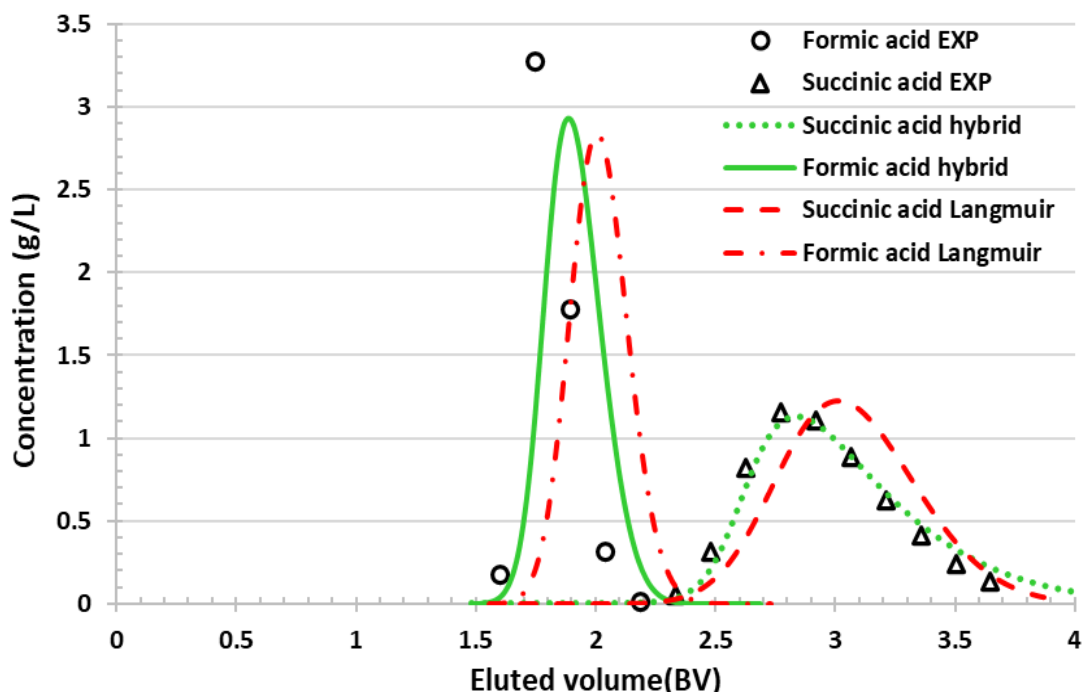


Figure 4-5. Multi-component pulse test to compare predictions of the model which considers only Langmuir adsorption to the hybrid model which also considers ion-exchange.

Chapter IV. Batch chromatography simulation (pulse tests)

Figure 4-5 confirms clearly that the hybrid model predicts the chromatographic profile of both organic acids much better. More specifically, the hybrid model is able to predict the significant tailing of the succinic acid profile, unlike the Langmuir model. Moreover, the mean retention volume of formic acid is better predicted by the hybrid model, even though there is still a slight difference (0.1 BV) compared to experimental points.

The slight discrepancies observed can be due to assumptions and simplifications in the present hybrid model. For example, all adsorption sites were considered equivalent. To be more accurate, adsorption sites on the upper side of SO_4^{2-} and HSO_4^- counter-anions should be considered more accessible than sites closer to the resin matrix.

In addition, formic acid dimer formation was not well considered in this model. We probably underestimated N_{AH} during pulse tests (overestimation of dimer formation), which resulted in an overestimation of formic acid retention volume. What's more, some studies [Neil et al. 1982, Nejad et al. 2019] showed that the original Langmuir competitive equation is not suitable for multi-layer adsorption. Thus, a more accurate model considering different types of adsorption sites might be an interesting approach to better predict the separation of multi-component mixture.

4 Comparison between continuous column model and discontinuous column model

In a previous study a discontinuous model was used by Lemaire et al. [Lemaire et al., 2016] to simulate pulse tests with the hybrid model. The same binary pulse test, depicted in previous section, was also simulated using this discontinuous model. Physico-chemical coefficients were firstly refined from single component curve fitting, then applied to binary pulse test. Table 4-6 summarizes these parameters, knowing that in discontinuous model, the dispersion coefficient D and mass transfer coefficient k_a are not used but dispersion is related to the value of the theoretical stage number NET.

Table 4-6. Parameters used for multi-component pulse test simulation with discontinuous model.

Model	Organic acid	N_i	k_s used (L/mol)	K^{iex} used	k_a (s^{-1})	D ($10^{-7} m^2/s$)	NET
Continuous	Formic acid	0.5	0.24	25	0.06	1.4	--
	Succinic acid	4	0.27	800	0.013	1.3	--
Discontinuous	Formic acid	0.5	0.28	25	--	--	350
	Succinic acid	4	0.24	800	--	--	100

While assuming the same N_i , both models gave similar estimations of k_s and K^{iex} . Succinic acid has smaller k_a and D values than formic acid in the continuous model, corresponding to a global wider dispersion. Consequently, in the discontinuous model, it corresponds to a smaller NET value. NET was set to 225 (the average) for binary separation. Applying coefficients listed above, binary mixture pulse tests results are shown in Figure 4-6.

Chapter IV. Batch chromatography simulation (pulse tests)

Figure 4-6 shows that the continuous column model predicts dispersion better than discontinuous column model. Dispersion of succinic acid was underestimated and dispersion of formic acid was overestimated, which impacted their mean retention time, peak shape and maximum concentration.

The weakness of discontinuous column model is that it imposes the same NET for all compounds. Meanwhile, NET is a essential parameter in discontinuous column model which impacts all other parameters. Thus, even though discontinuous model is more favorable in terms of CPU time, a continuous model was chosen for this study, namely because the dispersion of each compound can be different.

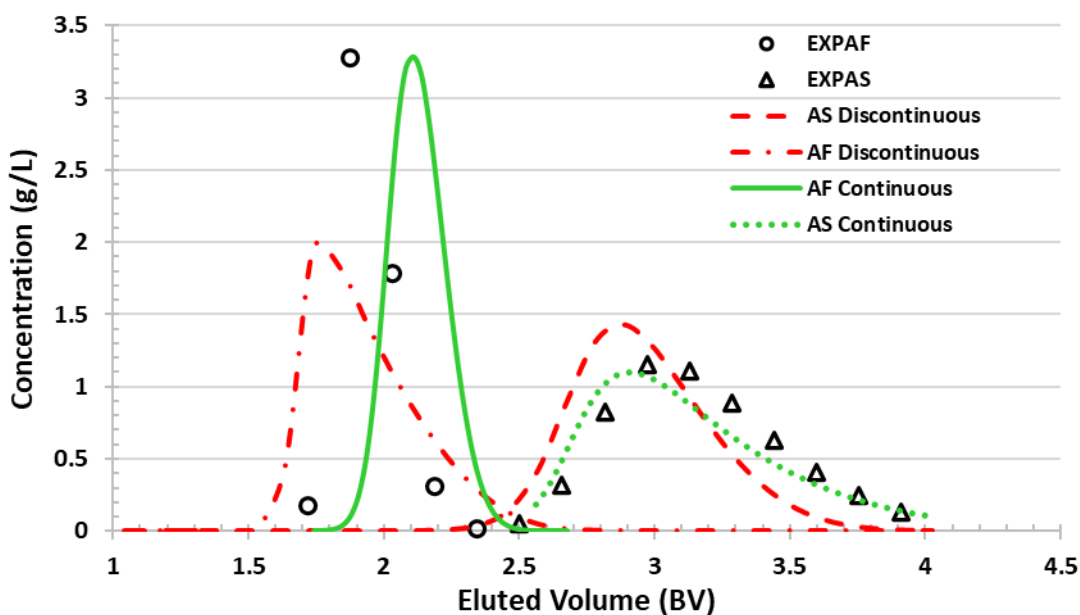


Figure 4-6. Multi-component pulse test to compare predictions of continuous model to discontinuous model.

In conclusion, this chapter confirms that the estimation of adsorption equilibrium coefficient (N_i and k_s) were consistent with the adsorption of organic acids by means of hydrogen bonding between the hydrogen atom of the carboxylic acid group and one lone electron pair of oxygen atoms of sulfate or hydrogen sulfate counter-anions. Our results confirm that the tailing of succinic and citric acid profiles is mainly caused by ion exchange of their very low dissociated fraction, even at low pH (< 1.5). Therefore, organic acid dissociation and ion exchange must be considered to develop a predictive model for succinic and citric acids. The prediction of the hybrid model was successfully validated in the case of a multi-component pulse test. The comparison between discontinuous and continuous column model showed that the discontinuous column model was not sufficient to predict profile dispersion for multi-component separation.

In the next chapter, this hybrid model with continuous column model will be implemented in a multi-column chromatography simulation program to predict and optimize the performance of simulated moving bed technologies.

Chapter V. Multi-column process simulation and development

1 Introduction

Multi-column processes are widely applied in the industry due to their advantages in terms of productivity, eluent consumption and dilution factor, compared to batch chromatography in single column. Simulated moving bed (SMB) chromatography [Broughton *et al.*, 1961] is an excellent alternative to single-column batch chromatography. Its continuous countercurrent operation mode endows it a natural advantage in column efficiency. However, its performance remains to be improved for industrial applications.

Developments of SMB such as ISMB (improved simulated moving bed) have been proposed to enhance its performance in terms of productivity, eluent consumption or dilution factor. These processes usually need to be optimized for better performances. After each optimization step, it could take days before reaching a steady state. Then, numerical simulations is an interesting way to reduce experimental costs in time and materials. An accurate and predictive model is therefore vital for chromatographical process development.

Besides, most SMB-typed processes are limited to binary separation and should be used repeatedly to separate ternary mixtures. The double usage of SMB (such as ISMB in cascade) increases installation and maintenance costs. It is worthwhile to develop a ternary SMB-typed process with less columns and better performances.

In the first part of this chapter, binary separation with 3C-ISMB (three-column ISMB) was simulated with both the hybrid model and Langmuir model mentioned in the previous chapter to show the optimization of the 3C-ISMB process and the importance of developing a precise model. In the second part of this chapter, a 3F4C SSMB (three-fractions-four-columns sequential SMB) process was proposed and applied to a ternary separation (glucose, formic acid, and succinic acid). Its performance was compared with two 3C-ISMB units in cascade to prove its advantages.

2 3C-ISMB simulation for binary separation (formic and succinic acids)

ISMB is commonly used in the sugar industry. A traditional ISMB process contains four zones (generally four columns). However, the fourth zone is just used to ensure purity or concentration of collected products. The 4-column ISMB could be reduced to 3-column ISMB (3C-ISMB) while sacrificing product concentration, meanwhile increasing the productivity defined as the quantity of product treated per hour and liter of resin. 3C-ISMB is chosen for the present study.

A cycle of the 3C-ISMB process contains three steps, and each step consists of 4 substeps as shown in figure 5-1. The optimization of ISMB performances corresponds to adjustments of V_{ssx} (Eluted volume in substep X) to meet separation quality requirements and to achieve maximum productivity and minimum W/F ratio (eluent over product ratio).

2.1 Estimation of V_{ssx} and adjustments of concentration profiles

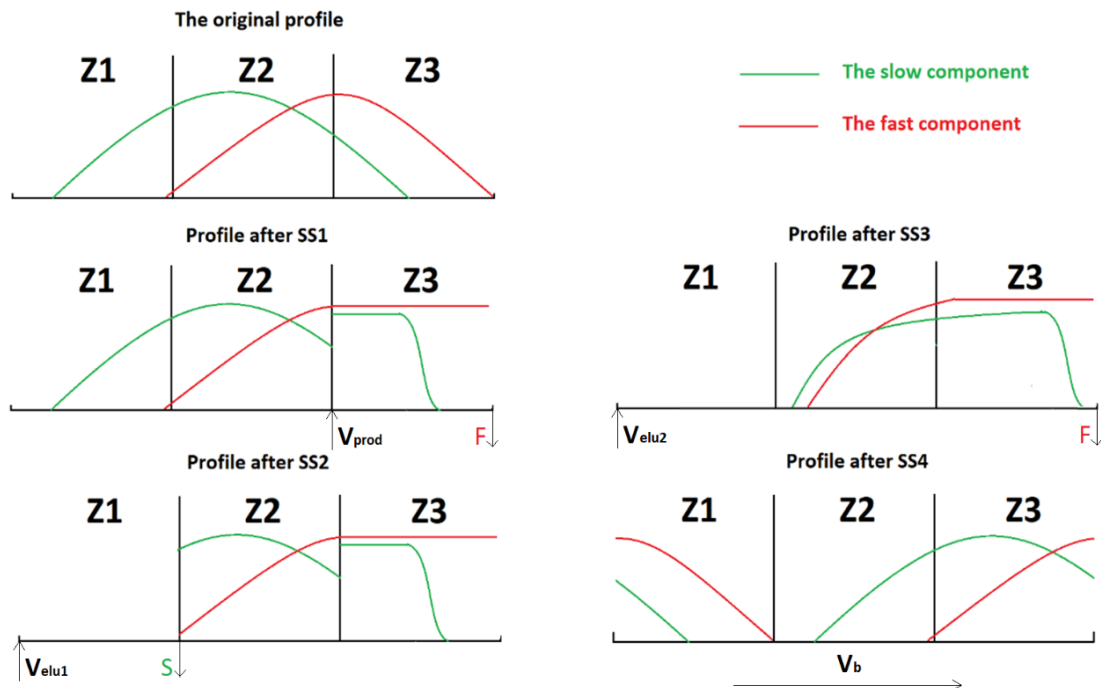


Figure 5-1. Moving of concentration profiles inside a 3C-ISMB system during one step (a simplified diagram).

During the process, the raffinate and extract are collected and analyzed to evaluate the system performance. Since the actual profiles are not visible in the system, the optimization is difficult. This therefore a major advantage of numerical simulation, for which the concentration profiles inside the columns and their evolution are perfectly known. Figure 5-1 shows the displacement of the concentration profiles during one step in an optimized 3C-ISMB system. The concentration profiles after each substep are characterized by the following features of the front and back (right and left side, respectively) of each peak:

- Initially, the fast component front should be close to the zone-3 output so that the fast component can be collected immediately when substep 1 (SS1) begins. The fast component rear is close to the zone-2 input. A little tail of the fast component is tolerated in zone 1, while respecting extract purity demands. The slow component front could be in zones 2 or 3, but it should be close to zone 3 output at the end of substep 3 (SS3). The slow component rear should stay in zone 1, as close as possible to its input to minimize extract dilution.
- During SS1, a volume of product (V_{prod}) is injected into zone 3, pushing the slow component front through zone 3. Meanwhile, the fast component front stays at zone 3 output, since it is the raffinate collection point.

Chapter V. Multi-column process simulation and development

- During SS2 (substep 2), a volume of eluent (V_{elu1}) is injected in zone 1, and the slow component is collected at the zone-1 output (extract). Consequently, the fast component rear should as close as possible to zone-1 output, to ensure the purity of collection,
- During SS3, a volume of eluent (V_{elu2}) is injected into zone 1, and the fast component is collected again at zone-3 output (raffinate). Thus, the injection should stop when the slow component front reaches the zone-3 output.
- During SS4, neither eluent nor product is injected, and neither extract nor raffinate is collected. All columns are connected in series as a loop. A recirculation pump is activated to move a certain volume V_{loop} and shift the slow and fast component profiles until reaching the same initial profiles before SS1 but shifted to the next columns.

At the beginning of each step, the component profiles should be at the same position in each zone as the previous step. The profiles then move exactly one zone during one step. In this work, each zone corresponds to a column, which means that the profiles shift by exactly one column during one step. The breakthrough curve and the elution curve (Figure 5-2) give the volume required to move the front and back of the profiles throughout one column, respectively. The corresponding volumes for the slow (S) and fast (F) components, called V_{min}^S , V_{max}^S , V_{min}^F , V_{max}^F , could be read from the breakthrough curve and the elution curve, respectively (Figure 5-2).

As shown in chapter II, the initial V_{SSx} (eluted volume in substep X) could be initially estimated by performing a frontal analysis with the mixture. Figure 5-2 shows the elution curve and breakthrough curve of a formic acid and succinic acid mixture.

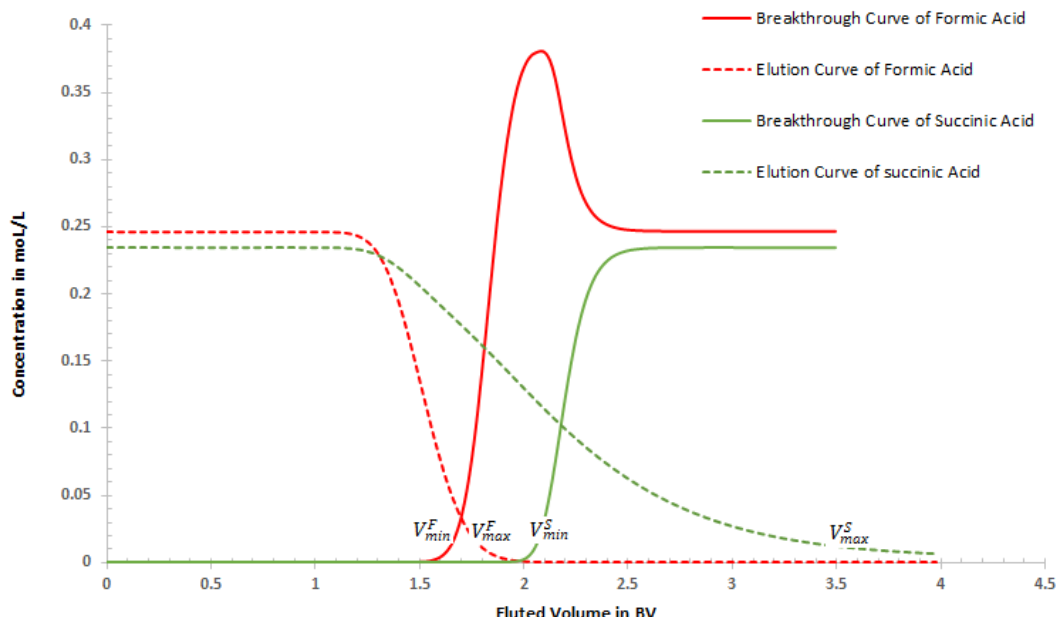


Figure 5-2. Simulated elution curve and breakthrough curve of formic acid and succinic acid., as well as approximative positions of V_{min}^S , V_{max}^S , V_{min}^F , V_{max}^F .

To achieve the ideal tuning corresponding to Figure 5-1, the fast component front should travel throughout zone 1 during SS4 (substep 4). Thus, the eluted volume in zone 1 during only SS4, noted BV_4 , should be equal to:

$$BV_4 = V_{loop} = V_{min}^F = 1.55 \quad (5-1)$$

The fast component rear should travel throughout the zone 2, during a step. Thus, the total eluted volume in zone 2 during a step, noted BV_2 , should be equal to:

$$BV_2 = V_{elu2} + V_{loop} = V_{max}^F = 1.65 \quad (5-2)$$

The slow component front should travel throughout the zone 3, during a step. Thus, the total eluted volume in zone 3 during a step, noted BV_3 , should be equal to:

$$BV_3 = V_{elu2} + V_{prod} + V_{loop} = V_{min}^S = 2.15 \quad (5-3)$$

The slow component rear should travel throughout zone 1, during a step. Thus, the total eluted volume in zone 1 during a step, noted BV_1 , should be equal to:

$$BV_1 = V_{elu1} + V_{elu2} + V_{loop} = V_{max}^S = 3.5 \quad (5-4)$$

Thus, values of V_{ssx} could be deduced from equations above:

$$V_{ss1} = V_{prod} = V_{min}^S - V_{max}^F = 0.5 \quad (5-5)$$

$$V_{ss2} = V_{elu1} = V_{max}^S - V_{max}^F = 1.85 \quad (5-6)$$

$$V_{ss3} = V_{elu2} = V_{max}^F - V_{min}^F = 0.1 \quad (5-7)$$

$$V_{ss4} = V_{loop} = V_{min}^F = 1.55 \quad (5-8)$$

As Figure 5-2 was obtained from simulation in a single column, the real elution and breakthrough curves in the ISMB system might differ slightly. Consequently, the values of V_{ssx} must still be adjusted to improve performances and get closer from the "ideal" profiles shown in Figure 5-1. Eq. (5-5) gives a first estimation of the product volume V_{prod} injected during a step, and the corresponding total eluent volume can be easily deduced from Eq. (5-6) and (5-7):

$$V_{elu1} + V_{elu2} = V_{max}^S - V_{min}^F \quad (5-9)$$

Thus, in Figure 5-2, the product volume V_{prod} corresponds to the distance between the end of the fast component elution curve and the beginning of the slow component breakthrough curve, which must be high enough to get good performance. Besides, the total eluent volume $V_{elu1} + V_{elu2}$ corresponds to the distance between the beginning of the fast component elution curve and the end of the slow component breakthrough curve, which must be as low as possible. Thus, if the slow component has a tailing such as succinic acid, the required eluent volume will be higher.

2.2 System tuning and simulation with the hybrid model

The simulation of 3C-ISMB process is based on the computational model developed in Chapter II for batch chromatography in one column. As explained in this chapter, the 3-column architecture is simulated as a unique, large, column with intermediate inputs and outputs. The physico-chemical parameters of this model are those estimated or refined in chapter IV. Consistently, during each step, input and output of each column are defined according to their corresponding zone and the current substep (Figure 5.1).

Chapter V. Multi-column process simulation and development

Then, zones are shifted by one column after each step, following the liquid flow direction so as to follow component profiles move. As 3C-ISMB is composed of only three columns, a cycle is done after only 3 steps (zones go back to their initial location). Table 5-1 summarizes the input and output configuration of each column during a complete cycle.

Table 5-1. The input and output configuration of each column during a complete cycle.

Substep	Column 1		Column 2		Column 3	
	Input	Output	Input	Output	Input	Output
Step 1	SS1	-	-	-	-	Product Z3 Raffinate Z3
	SS2	Eluent Z1	Extract Z1	-	-	-
	SS3	Eluent Z1	Input Z2	Output Z1	Input Z3	Output Z2 Raffinate Z3
	SS4	Output Z3	Input Z2	Output Z1	Input Z3	Output Z2
Step 2	SS1	Product Z3 Raffinate Z3	-	-	-	-
	SS2	-	-	Eluent Z1	Extract Z1	-
	SS3	Output Z2	Raffinate Z3	Eluent Z1	Input Z2	Output Z1
	SS4	Output Z2	Input Z1	Output Z3	Input Z2	Output Z1
Step 3	SS1	-	-	Product Z3 Raffinate Z3	-	-
	SS2	-	-	-	-	Eluent Z1 Extract Z1
	SS3	Output Z1	Input Z3	Output Z2	Raffinate Z3	Eluent Z1
	SS4	Output Z1	Input Z3	Output Z2	Input Z1	Output Z3

To study the performance of 3C-ISMB for binary separation, a mixture of formic and succinic acid was chosen to highlight the importance of model accuracy. First, 3C-ISMB simulations were performed with the hybrid model discussed in the previous chapter. Details of simulation parameters are listed below in table 5-2.

Table 5-2. Simulation parameters for 3C-ISMB process with binary mixture.

Operating conditions		
Flowrate (BV/h)	0.5	
Eluent	H ₂ SO ₄ (pH 1.5)	
Column (m)	0.7 × 0.25	
Porosity (effective)	0.4	
Simulation parameters		
	Formic acid	Succinic acid
Concentration (moL/L)	0.24	0.24
pKa	3.75	4.16
k _a (s ⁻¹)	0.06	0.013
Dispersion (m ² /s)	1.4E-07	1.3E-07
K ^{iex}	20	800
N	0.5	4
k _s (L/mol)	0.24	0.265

Chapter V. Multi-column process simulation and development

Once the 3C-ISMB simulation program is launched with parameters defined above, about fifteen cycles are required to reach steady state. During experiments, the system is considered in steady state when the mean concentrations of raffinate and extract (over one cycle) remain constant. Contrary to experiments, numerical simulations enable us to visualize the concentration profiles evolution inside the columns during operation. Therefore, the system can also be considered stabilized when the concentration profiles remain identical from one cycle to the next one.

Purity requirements (for instance: >97% for formic acid and >99% for succinic acid) are considered as constraints for optimization, whereas the W/F ratio and the productivity are optimization objectives. Therefore, concentration profiles (locations of front and rear profiles of the slow and fast components) were adjusted by modifying V_{ssx} to increase BV3 and BV4 and decrease BV1 and BV2 as much as possible with respect to purity requirements. For example, the component profiles during each substep shown in Figure 5-3 correspond to the initial V_{ssx} estimation whereas Figure 5-4 depicts the best W/F ratio and productivity obtained after V_{ssx} tuning.

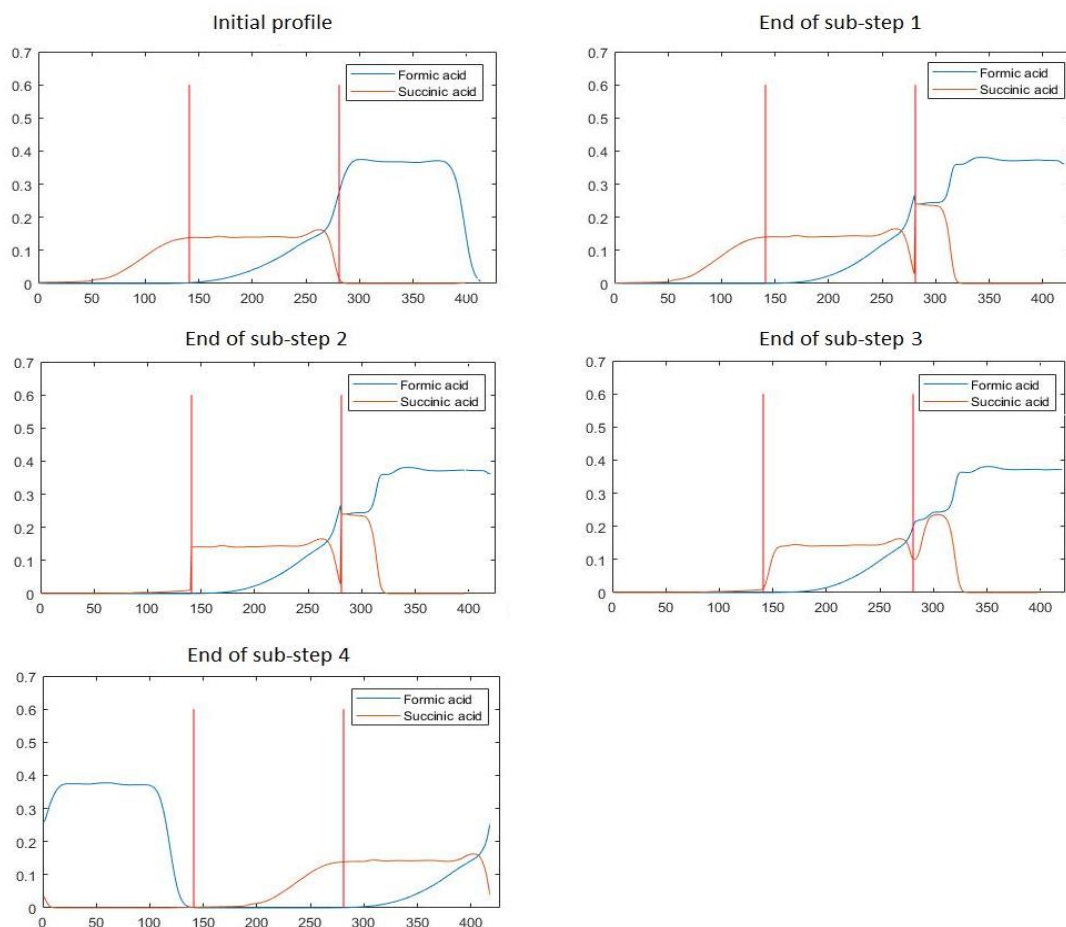


Figure 5-3. Concentration profiles after each substep, with the initial V_{ssx} estimation, in steady state.

In comparison with Figure 5-4, we can see first in Figure 5-3 that succinic acid does not leave zone 3 at the end of SS3. It shows that more formic acid could be collected in the raffinate (zone 3 output) during SS3. Moreover, formic acid purity in the raffinate and succinic acid purity in the extract seems close to 100% in Figure 5-3, while the purity target was only 97% for formic acid

Chapter V. Multi-column process simulation and development

and 99% for succinic acid. This indicates that the initial estimation of V_{ssx} must be adjusted to optimize 3C-ISMB performance in terms of W/F ratio and productivity, which are defined as follows:

$$Prod = \frac{V_{prod}}{3 \cdot \frac{\max(V_{prod}, V_{elu1}) + V_{elu2} + V_{loop}}{Q}} \quad (5 - 10)$$

$$\frac{W}{F} = \frac{V_{elu1} + V_{elu2}}{V_{prod}} \quad (5 - 11)$$

In this case study, the best tuning was $V_{prod} = 0.65$ BV, $V_{elu1} = 2$ BV, $V_{elu2} = 0.05$ BV and $V_{loop} = 1.55$ BV, corresponding to $BV1 = 3.6$ BV, $BV2 = 1.6$ BV, $BV3 = 2.25$ BV and $BV4 = 1.55$ BV. We can notice that the best tuning is quite close to the initial V_{ssx} estimation. V_{elu2} was just decreased from 0.1 to 0.05 while V_{prod} was increased from 0.5 to 0.65. However, it results in a much lower W/F ratio and slightly higher productivity as shown in Table 5-3.

As shown in Table 5-3, the purity of raffinate and extract with the initial V_{ssx} exceeds the purity requirements. Thus, the optimization consisted in increasing the product volume and decreasing the total eluent volume without decreasing too much purities. After adjustments, the W/F ratio was reduced by 25% while the productivity increased by 30%. As a consequence, the dilution factor of raffinate and extract was reduced by 20%.

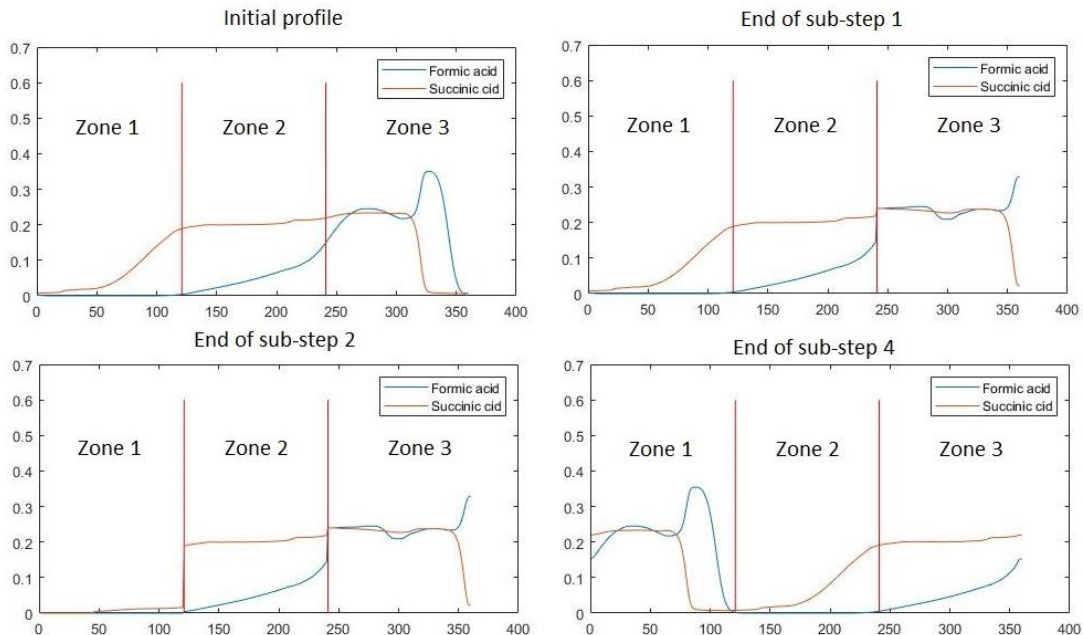


Figure 5-4. Concentration profiles after each substep with the best V_{ssx} tuning, in steady state (profile after sub-step 3 is almost the same as sub-step 2 because V_{elu2} is set to 0.05BV).

Chapter V. Multi-column process simulation and development

Table 5-3. 3C-ISMB performance before and after optimization.

	With initial V_{ssx}	After adjustments	
W/F ratio	3.9	3.15	
Productivity (L_{product}/h/L_{resin})	0.0231	0.0301	
	Raffinate (formic acid)	Extract (succinic acid)	Raffinate (formic acid)
Concentration (mol/L)	0.1958	0.0618	0.2268
Purity (%)	98.64	99.57	96.78
Dilution factor	1.225	3.883	1.058
Recovery rate (%)	97.9	100	100
			Extract (succinic acid)
			0.0744
			99.79
			3.225
			95.4

In both cases, the extract dilution factor remained quite high, due to the large eluent volume during substep 2 (V_{elu1}). However, it could be further reduced because the extract purity is still higher than required (>99%).

Besides, we see that formic acid is not diluted in raffinate (dilution factor around 1) contrary to succinic acid. Indeed, in zone 3, formic acid is released from stationary phase when succinic acid arrives and takes its place. Consequently, formic acid concentration can be even higher in the raffinate than in the product.

In this case study, 3C-ISMB performance is better when almost no eluent is eluted during substep 3 ($V_{elu2} = 0.05$). However, as V_{elu2} is increased, BV_2 increases and the rear of formic acid profile moves further in zone 2. Thus, V_{elu2} could be increased to make all formic acid leave zone 2 after each step, as a result, make zone 2 useless. Consequently, a 2-columns ISMB can also separate both molecules, achieving the same purity requirements with higher productivity (less resin volume), but with a higher W/F ratio, so a higher dilution factor.

2.3 Comparison with Langmuir model

The Langmuir model was discussed in the previous chapter to show that IEX must be considered to improve elution modeling of some organic acids. In this section, a 3C-ISMB is simulated with the Langmuir model for the same binary separation to highlight the discrepancies when IEX is not considered into the multicolumn process model. Thus, simulations were performed with the same operating conditions and physico-chemical parameters refined in Chapter IV when only Langmuir model is considered. Organic acid retention by IEX was neglected ($K^{iex} = 0$).

The initial V_{ssx} estimation from previous section was used to start optimization. Finally, the best tuning was obtained with: $V_{prod} = 0.7$ BV, $V_{elu1} = 1.3$ BV, $V_{elu2} = 0$ BV and $V_{loop} = 1.6$, which corresponds to $BV1 = 2.9$ BV, $BV2 = 1.6$ BV, $BV3 = 2.3$ BV and $BV4 = 1.6$ BV. Figure 5-5 shows the optimized concentration profiles in the system and Table 5-4 summarizes the performances.

Chapter V. Multi-column process simulation and development

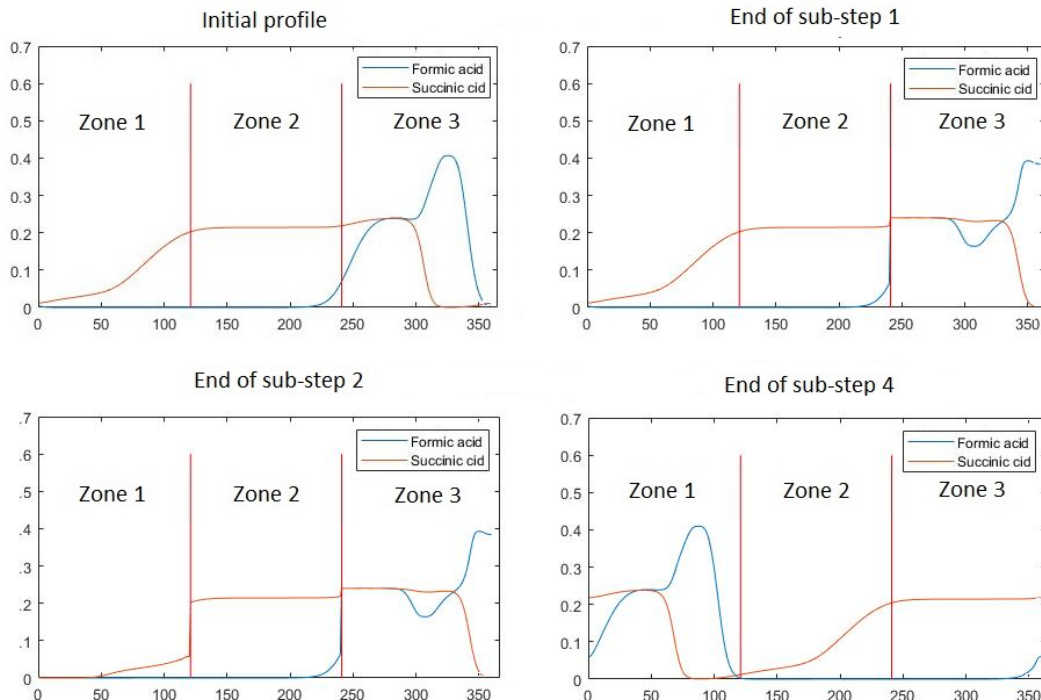


Figure 5-5. Optimized concentration profiles after each substep, in steady state, simulated with Langmuir model.

Table 5-4. 3C-ISBM performance simulated with Langmuir model.

W/F ratio	1.85
Productivity (L_{product}/h/L_{resin})	0.040
	Raffinate (formic acid) Extract (succinic acid)
Concentration (mol/L)	0.0247 0.127
Purity (%)	98.02 99.9
Dilution factor	0.972 1.889

In the previous chapter, it was shown that the Langmuir model cannot reproduce succinic acid tailing. Thus, the eluent volume V_{elu1} , estimated to push succinic acid out of zone 1, is much lower than V_{elu1} predicted by the hybrid model. Consequently, with the same purity requirements, simulation of 3C-ISMB with Langmuir model can overestimate its performance.

Figure 5-6 shows the concentration profiles simulated with the hybrid model but with the best V_{ssx} tuning obtained previously with the Langmuir model. It aims at highlighting bad performances that would be obtained experimentally if V_{ssx} are tuned with the Langmuir model which is less predictive, particularly to simulate succinic acid tailing.

Chapter V. Multi-column process simulation and development

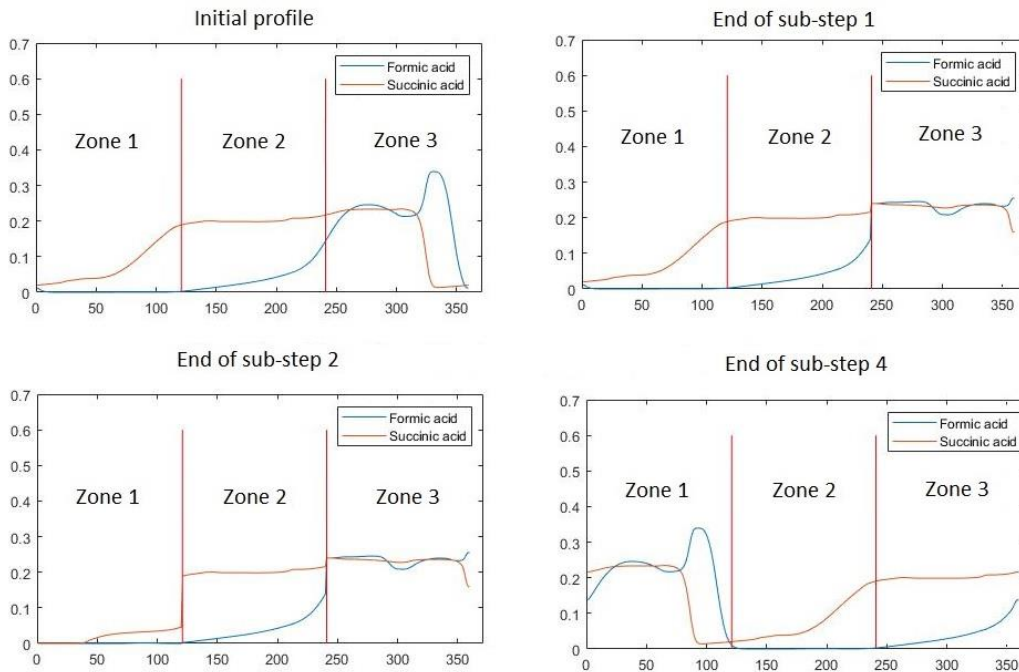


Figure 5-6. Concentration profiles after each substep, in steady state, simulated with the hybrid model, but with the best V_{ssx} tuning obtained from the Langmuir model.

Figure 5-6 shows that concentration profiles would not be well optimized experimentally (predicted here by the hybrid model) if a simple Langmuir model is used for 3C-ISMB simulation. Indeed, succinic acid profiles in Figure 5-6 are poorly located in different zones during substeps, in comparison with Figure 5-5. First, at the end of substep 1, we notice that succinic acid has polluted the raffinate by going out of zone 3.

In addition, the Langmuir model underestimates the succinic acid tailing, so the eluent volume V_{elu1} , resulting in succinic acid remaining in zone 1 after substep 4. As a result, succinic acid will also pollute the raffinate at the end of zone 3 when the next step starts (after a one-zone shifting). Finally, formic acid purity will be lower in the raffinate as can be seen in Table 5-5.

Table 5-5. 3C-ISMB performance with the hybrid model (corresponding to experimental expectation) with the best tuning obtained from simulations with the Langmuir model.

Simulation with hybrid model (experimental expectation)	
W/F ratio	1.85
Productivity ($L_{product}/h/L_{resin}$)	0.0402
	Raffinate (formic acid) Extract (succinic acid)
Concentration (mol/L)	0.241 0.111
Purity (%)	87.3 99.7
Dilution factor	0.997 2.173

3 Development of ternary SMB system (glucose, formic acid and succinic acid)

Nowadays in the industry, some ternary processes with fewer columns have been developed. For instance, there is Japan Organo (JO) process (also termed as pseudo-SMB) [Ju Weon L., 2010], sequential multicolumn chromatography (SMC, also called sequential simulated moving bed SSMB) [Ng et al., 2014], gradient with steady state recycle (GSSR) process [Silva et al., 2010], and capture SMB [Angarita et al., 2015].

Processes such as GSSR are mainly used in high value added molecule production such as protein because of their weak productivity, or high W/F and dilution factor. Their complex settings make optimization difficult. Processes such as SSMB follow counter-current principles as in SMB, therefore, guarantee a better W/F and productivity. Yet, ternary separation by SMB-typed process still needs to be further investigated for economic interests.

3.1 3C-ISMB in cascade

An ISMB unit allows binary mixture separation. Thus, two ISMB units are required to separate ternary mixture containing components A, B, and C (A is the fastest and C is the slowest). Hence, two strategies are possible:

Table 5-6. Two strategies to separate ternary mixture with two ISMB units.

	ISMB n°1	ISMB n°2
Strategy n°1	(A + B) / C	A / B
Strategy n°2	A / (B + C)	B / C

The choice of strategy depends on chromatography profiles of the mixture. In this case study, a mixture that contains 0.1 mol/L glucose, 0.24 mol/L formic acid, and 0.24 mol/L succinic acid is chosen. These components correspond to different types of retention mechanisms: linear adsorption for glucose, Langmuir competitive adsorption for formic acid and Langmuir competitive adsorption plus ion exchange for succinic acid.

Figure 5-7 shows their elution and breakthrough curves. Obviously, strategy n°1 is better in this case because of the larger distance between glucose profile (A) and organic acid profiles (B+C). Thus, both organic acids are separated together from glucose in the first ISMB unit, then separated in the second ISMB unit. For instance, minimum purity requirements were set to 98% for formic acid, 99% for succinic acid and 95% for glucose.

To start optimization of the first ISMB unit, V_{max}^S , V_{min}^S , V_{max}^F and V_{min}^F are estimated from Figure 5-7, to set to initially $BV1 = 4$ BV, $BV2 = 0.77$ BV, $BV3 = 1.5$ BV, and $BV4 = 0.46$ BV. Therefore, $V_{prod} = 0.73$, $V_{elu1} = 3.23$, $V_{elu2} = 0.31$ and $V_{loop} = 0.46$ are set as the starting configuration of the first ISMB unit.

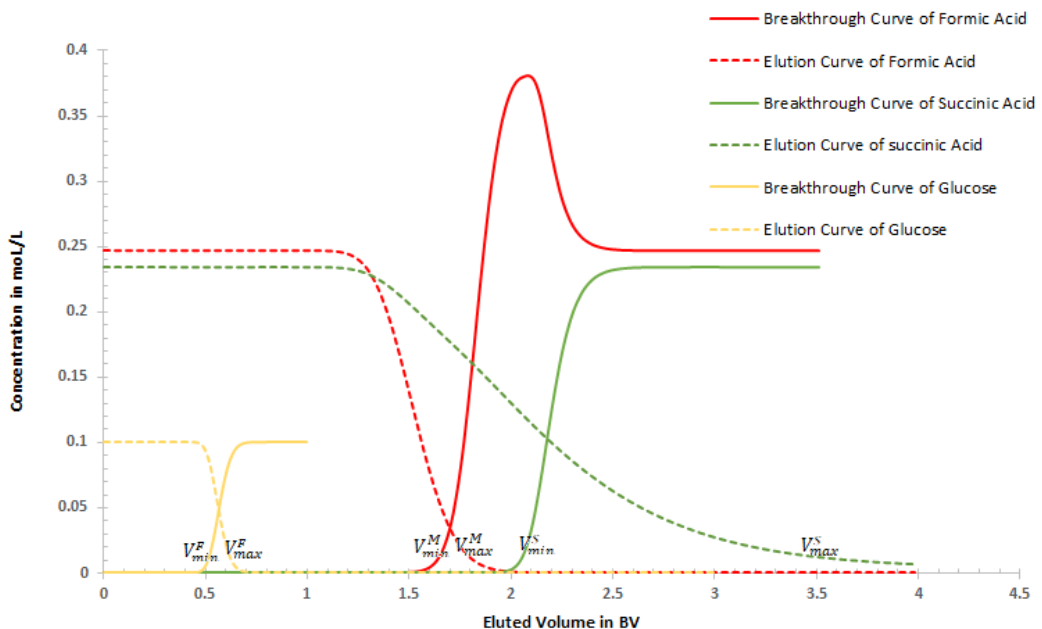


Figure 5-7. Simulated elution and breakthrough curves of glucose, formic acid and succinic acid., and approximative position of V_{min}^F , V_{max}^F , V_{min}^M , V_{max}^M , V_{min}^S and V_{max}^S .

Simulation parameters (operation conditions and physico-chemical parameters) are the same as in the binary mixture simulation (Table 5-2) but in addition the product contains glucose whose parameters are given in Table 5-7.

Table 5-7. Glucose parameters for 3C-ISMB process simulation with ternary mixture.

Glucose	
Concentration (mol/L)	0.1
k_a (s^{-1})	0.03
Dispersion (m²/s)	1E-07
K (L/mol)	0.40

As previously, V_{SSX} were adjusted to optimize 3C-ISMB performance (W/F ratio and productivity) with respect to minimum purity requirements for glucose and both organic acids. The best tuning was $V_{prod} = 1.1$ BV, $V_{elu1} = 2.7$ BV, $V_{elu2} = 0.07$ BV and $V_{loop} = 0.5$ BV, which corresponds to BV1 = 3.27 BV, BV2 = 0.57 BV, BV3 = 1.67 BV and BV4 = 0.5 BV. Figure 5-8 shows concentration profiles after optimization of the first ISMB unit. The performances of the first 3C-ISMB unit are listed in Table 5-8.

Afterward, both organic acids collected in the first ISMB extract must be separated by another 3C-ISMB unit. The simulation started with the same initial V_{SSX} estimation for the binary separation, (Figure 5-2): $V_{prod} = 0.5$ BV, $V_{elu1} = 1.85$ BV, $V_{elu2} = 0.1$ BV and $V_{loop} = 1.55$, which corresponds to BV1 = 3.5 BV, BV2 = 1.65 BV, BV3 = 2.15 BV and BV4 = 1.55 BV.

Chapter V. Multi-column process simulation and development

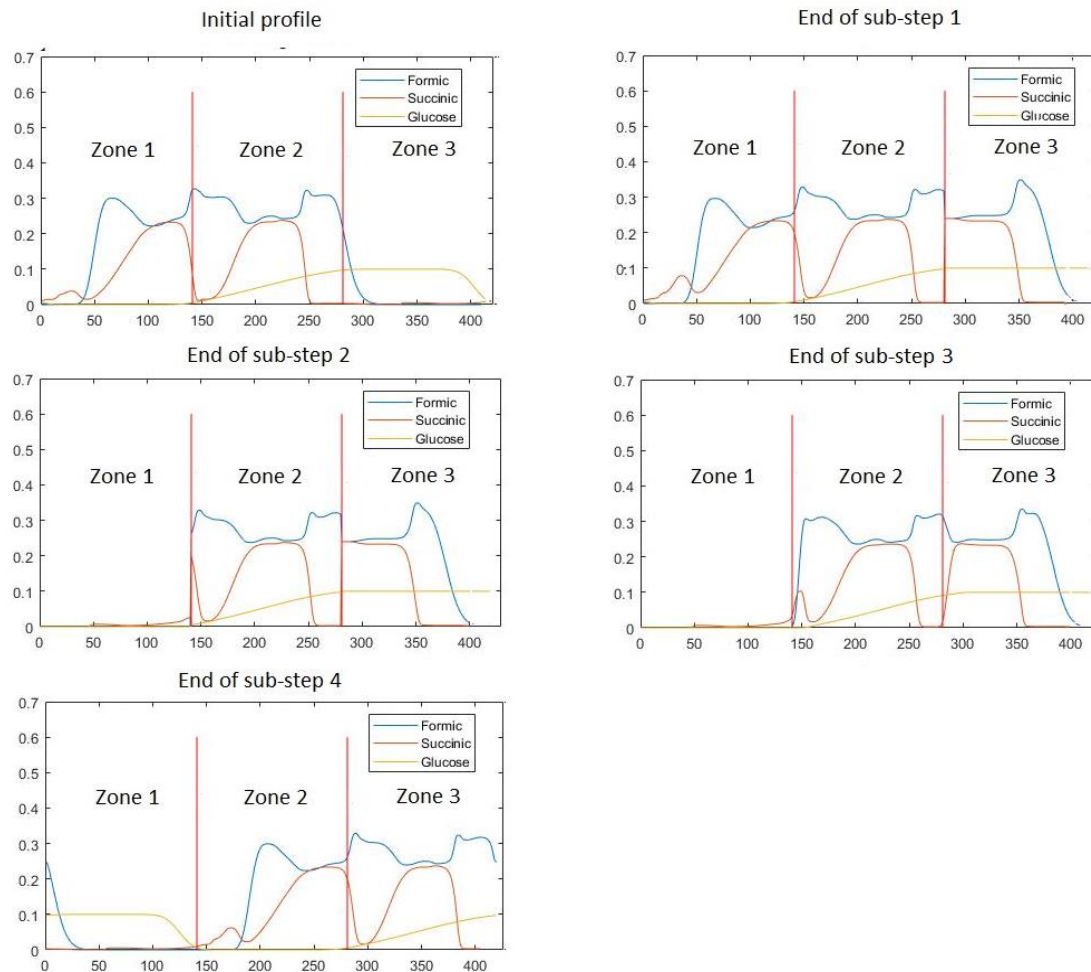


Figure 5-8. Concentration profiles after each substep, in steady state, after optimization of the first 3C-ISMB unit.

Table 5-8. Performance of the first 3C-ISMB unit for ternary separation.

W/F	2.52	
Productivity (L_{product}/h/L_{resin})	0.056	
Raffinate (glucose)	Extract (organic acids)	
Concentration (mol/L)	Formic acid	Succinic acid
0.0936	0.100	0.100
Purity (%)	95.77	50.0
Dilution factor	0.996	2.385
Recovery rate (%)	100	99.6

After optimization, V_{SSX} were adjusted to $V_{prod} = 0.95$ BV, $V_{elu1} = 1.7$ BV, $V_{elu2} = 0.15$ BV and $V_{loop} = 1.6$, which corresponds to BV1 = 3.45 BV, BV2 = 1.75 BV, BV3 = 2.7 BV and BV4 = 1.6 BV. Figure 5-9 shows the profile concentrations after optimization of the second ISMB unit. The performance of the second 3C-ISMB unit is shown in Table 5-9.

Chapter V. Multi-column process simulation and development

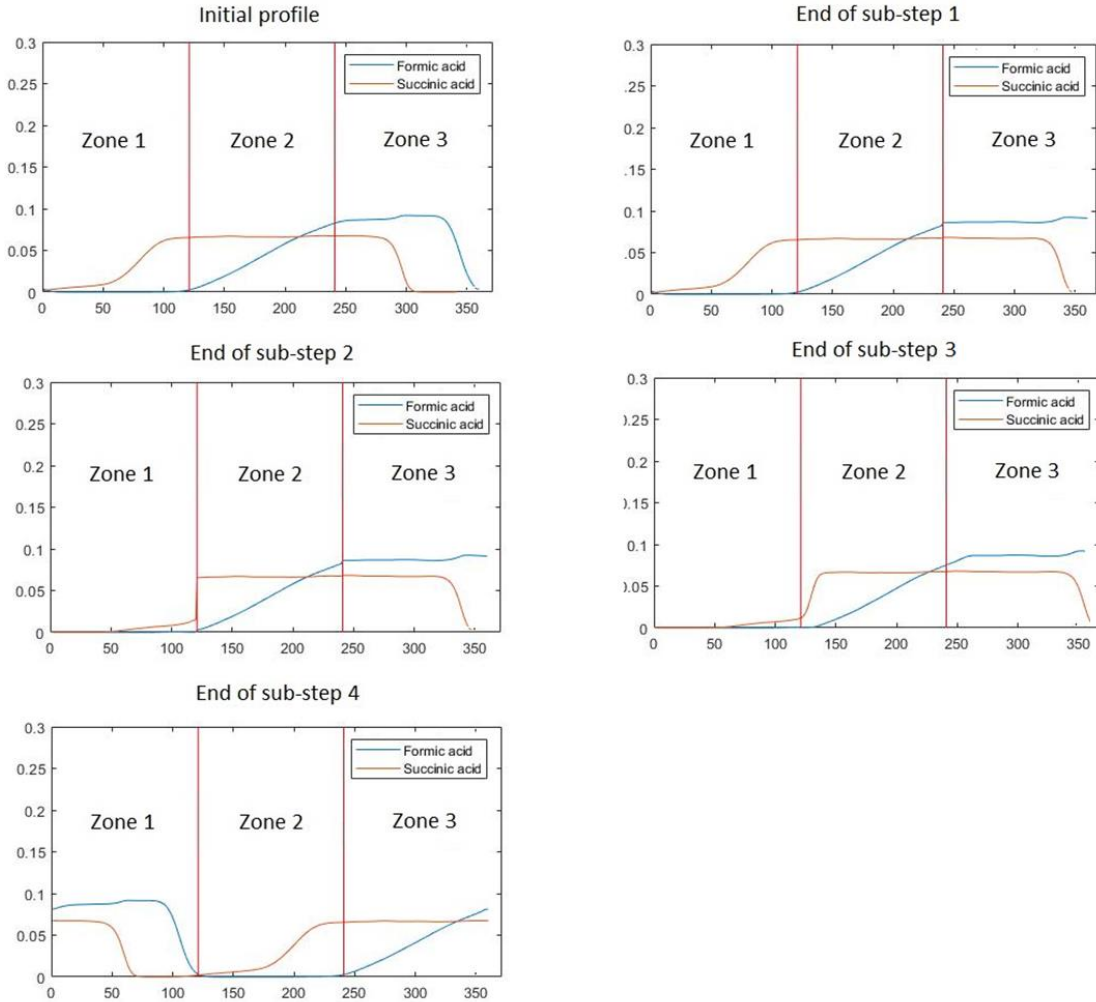


Figure 5-9. Concentration profiles after each substep, in steady state, after optimization of the 2nd 3C-ISMB unit.

Table 5-9. Performance of the second 3C-ISMB unit for ternary separation.

W/F	1.7
Productivity (L_{product}/H/L_{resin})	0.0459
	Raffinate (formic acid) Extract (succinic acid)
Concentration (mol/L)	0.0745 0.0484
Purity (%)	99.4 99.1
Dilution factor	1.176 1.811

To estimate the global performances of 2 ISMB process for ternary separation, the raffinate flowrate from 1st ISMB unit $Q_{raff}^{ISMB\ 1}$ is assumed to be equal to the product flowrate into the 2nd ISMB unit $Q_{prod}^{ISMB\ 2}$. It corresponds to a 2 ISMB process where both ISMB units can work independently thanks to an intermediate tank which collects the raffinate from the 1st unit before entering the 2nd unit. If volume flowrates Q in both units are considered equal (expressed as bed volume per hour), the ratio between $BV^{ISMB\ 1}$ and $BV^{ISMB\ 2}$ (bed volume of 1st and 2nd ISMB unit respectively) can be deduced from their V_{ssx} tuning:

Chapter V. Multi-column process simulation and development

$$\begin{aligned}
 Q_{ext}^{ISBM\ 1} &= Q_{prod}^{ISBM\ 2} \\
 \Leftrightarrow \left(\frac{V_{ext}^{ISBM\ 1}}{V_{step}^{ISBM\ 1}} \right) \cdot Q(in\ BV^{ISMB\ 1}/h) \cdot BV^{ISMB\ 1} &= \left(\frac{V_{prod}^{ISBM\ 2}}{V_{step}^{ISBM\ 2}} \right) \cdot Q(in\ BV^{ISMB\ 2}/h) \cdot BV^{ISMB\ 2} \\
 \Leftrightarrow \frac{BV^{ISMB\ 2}}{BV^{ISMB\ 1}} = \left(\frac{V_{ext}^{ISBM\ 1}}{V_{step}^{ISBM\ 1}} \right) / \left(\frac{V_{prod}^{ISBM\ 2}}{V_{step}^{ISBM\ 2}} \right) \text{ if } Q(in\ BV^{ISMB\ 1}/h) = Q(in\ BV^{ISMB\ 2}/h) \quad (5 - 12)
 \end{aligned}$$

Where $V_{step}^{ISBM\ 1}$ and $V_{step}^{ISBM\ 2}$ are eluted volume corresponding to a step of 1st and 2nd ISMB unit respectively:

$$V_{step}^{ISBM\ 1} = \max(V_{prod}^{ISBM\ 1}; V_{elu\ 1}^{ISBM\ 1}) + V_{elu\ 2}^{ISBM\ 1} + V_{loop}^{ISBM\ 1}$$

$$V_{step}^{ISBM\ 2} = \max(V_{prod}^{ISBM\ 2}; V_{elu\ 1}^{ISBM\ 2}) + V_{elu\ 2}^{ISBM\ 2} + V_{loop}^{ISBM\ 2}$$

Then, the global W/F ratio and productivity can be estimated from the ratio between $BV^{ISMB\ 1}$ and $BV^{ISMB\ 2}$:

$$\begin{aligned}
 Prod_{global}(L_{prod}/h/L_{resin}) &= \frac{\left(\frac{V_{prod}^{ISBM\ 1}}{V_{step}^{ISBM\ 1}} \right) \cdot Q(in\ BV^{ISMB\ 1}/h)}{3 \cdot \left(1 + \frac{BV^{ISMB\ 2}}{BV^{ISMB\ 1}} \right)} \\
 &= \frac{Prod_{ISMB\ 1}(L_{prod}/h/L_{resin})}{\left(1 + \frac{BV^{ISMB\ 2}}{BV^{ISMB\ 1}} \right)} \quad (5 - 13)
 \end{aligned}$$

$$\begin{aligned}
 \left(\frac{W}{F} \right)_{global} &= \left(\frac{V_{elu\ 1}^{ISBM\ 1} + V_{elu\ 2}^{ISBM\ 1}}{V_{prod}^{ISBM\ 1}} \right) + \left(\frac{V_{elu\ 1}^{ISBM\ 2} + V_{elu\ 2}^{ISBM\ 2}}{V_{prod}^{ISBM\ 2}} \right) \cdot \left(\frac{V_{ext}^{ISBM\ 1}}{V_{prod}^{ISBM\ 1}} \right) \\
 &= \left(\frac{W}{F} \right)_{ISMB\ 1} + \left(\frac{W}{F} \right)_{ISMB\ 2} \cdot \left(\frac{V_{ext}^{ISBM\ 1}}{V_{prod}^{ISBM\ 1}} \right) \quad (5 - 14)
 \end{aligned}$$

Table 5-10. Global performance of the 2 ISMB process for ternary separation.

W/F	8.058		
Productivity (L_{product}/h/L_{resin})	0.0127		
	Formic acid	Succinic acid	Glucose
Concentration (mol/L)	0.0745	0.0484	0.0910
Purity (%)	99.4	99.1	96.1
Dilution factor	3.223	4.960	1.099
Recovery rate (%)	96.95	97.41	99.99

As shown in Table 5-10, the global performances of the 2 ISMB process are relatively low in terms of W/F ratio and global productivity, for ternary separation. Compared with 3C-ISMB for binary separation, with the same purity requirements, the W/F is more than doubled, and the productivity is 3-fold lower. Consequently, separated molecules are more diluted.

3.2 A new SSMB ternary separation process (3F4C SSMB)

In this section, an SSMB process based on the design of 4C-ISMB is presented. The new process contains four columns and separates three fractions (named 3F4C SSMB process). Its ternary separation (formic acid, succinic acid, and glucose) was simulated with the hybrid model and compared with the 3C-ISMB in cascade. A patent is under application thus details of the 3F4C SSMB process are not given.

3.2.1 Presentation of the 3F4C SSMB process

The 3F4C SSMB process is a 4-zone SMB-typed process. It resembles ISMB process composed of several substeps and a zone switch at the end of the last substep. This process was conceived thanks to simulation and visualization of each compound profiles inside different zones during substeps of the usual ISMB process. Thus, we observed that the separation of a third component was possible in certain conditions by modifying the substeps sequence.

As for the ISMB process, the system is tuned by adjusting the eluted volume during each substep, noted as V_{ssx} . V_{ssx} are regulated to respect constraints (minimum purity or recovery rate requirements of the three compounds), and to optimize performance such as the W/F ratio, the productivity or dilution factors.

As performed for 3C-ISMB optimization, V_{min} and V_{max} of F, M and S compound, are read from their breakthrough curve and elution curve (Figure 5-7), corresponding to the required volume to move their fronts and rears one column forward after one step. To correctly tune the 3F4C ISMB process, some features must be respected, corresponding to optimization constraints and performance targets.

To evaluate 3F4C SSMB process performance, the ternary separation exemplified in the previous section (glucose, formic acid, and succinic acid) was simulated and optimized. Their breakthrough curves and elution curves were presented in Figure 5-7.

The optimization of 3F4C SSMB process consists in adjusting V_{ssx} to minimize W/F ratio and maximize productivity, meanwhile constraints must be respected to meet purity or recovery rate requirements.

As Figure 5-7 was obtained from simulation in a single column, the real elution and breakthrough curves in the multicolumn system might differ slightly. Consequently, initial estimation of V_{min} et V_{max} of F, M and S compound must be refined by successive iterations to improve performances until reaching optimum profiles.

Table 5-11. Purity requirements for the separation.

Purity requirements		
Glucose	Formic acid	Succinic acid
95%	98%	99%

Simulation results are listed in Table 5-12. The comparison between Table 5-10 and 5-12 shows that the 3F4C SSMB process has much better performance than two ISMB in cascade, for the same purity requirements. The W/F ratio is reduced by almost half, and the productivity is

Chapter V. Multi-column process simulation and development

doubled. Consequently, the 3F4C SSMB process has better dilution factors, namely for formic acid (1.3 instead of 3.2), even though we might note a slight degradation for glucose (1.4 instead of 1.1).

The result shows that both of them can separate ternary mixture with high purity. Ternary separation with two 3C-ISMB units in cascade requires 6 columns in total, whereas 4 columns are sufficient with the 3F4C SSMB process. Moreover, direct separation of three compounds results in smaller dilution factor and better productivity. Economically, its lower W/F ratio reduces eluent consumption, which is important especially when organic or supercritical fluid is used. Its lower dilution factor reduces concentration cost, which is an energy-consuming step. Finally, its lower column number reduces investment and maintenance costs. Therefore, the 3F4C SSMB process is a promising alternative for ternary separation.

Table 5-12. Optimum performance of the 3F4C SSMB process.

W/F ratio	4.95		
Productivity (L_{product}/h/L_{resin})	0.021		
	Formic acid	Succinic acid	Glucose
Concentration (mol/L)	0.1836	0.0751	0.0694
Purity (%)	98.42	98.97	95.79
Dilution factor	1.31	3.19	1.44
Recovery rate (%)	99.9	99.9	99.5

For future work, the 3F4C SSMB process could still be improved, such as removing zone 4 while sacrificing the dilution factor of F. Its performance could also be compared with other 3F processes.

Conclusion and recommendations

In recent years, the simulated moving bed (SMB) chromatographic process has gained popularity with its ability to generate large quantities of highly purified products. The SMB-typed process is a dynamic process that may require many cycles to achieve steady state. A numerical model is therefore an interesting tool to investigate innovative processes or optimize existing ones.

The primary objectives of this research work include i) the prediction of chromatography profile with anion exchange resin and ii) the development of a computational tool to simulate chromatography at the column and system levels, and iii) the development of a 3-fraction multi-column process. To achieve these goals, a systematic study of the experimental design, simulation, and optimization for ion-exchange chromatography and multi-column SMB process was presented.

Organic acid adsorption over strong anionic resin was studied in detail. Results supported the hypothesis that the organic acid adsorption is due to hydrogen bonding between organic acid molecules and sulfate/hydrogen sulfate groups on strong anionic resin. To better account for the liquid-solid equilibrium, a new retention model which combines Langmuir adsorption and ion-exchange, called the hybrid model, was proposed. This hybrid model was imbedded in a lumped model to simulate the process at the column and multi-column scales. The efficient CE/SE (Conservation Element / Solution Element) method was chosen to solve the set of lumped equations.

Experiments were conducted both to determine the keys model parameters and to validate the prediction of the hybrid model. The numerical tool was subsequently used to study the multi-column chromatographical process. This allowed us to propose a new three-fraction SMB-typed process to be developed. For the case-study proposed at the end of the work, this three-fraction process has better performances than the classical process using two steps of two-fraction ISMB in series.

Key results on chromatography profile prediction

It was shown that, on the strong anionic resin, the adsorption isotherms of sugars are linear. On the contrary, isotherms of organic acids are strongly non-linear, but can still be represented by a Langmuir model. Yet, our simulations shown that a simple Langmuir-type adsorption mechanism is not able to explain the tailing behavior of organic acids on strong anion resins. To address this issue, we proposed a complementary mechanism, the so-called hybrid model, which involves ion exchange of the minority dissociated part of organic acids. The results confirm that the tailing of succinic and citric acid profiles is mainly caused by ion exchange of their very low dissociated fraction, even at low pH (< 1.5). Therefore, organic acid dissociation and ion exchange must be considered to get a more predictive model for succinic and citric acids.

Bibliography

The assumption of the hybrid model is that the adsorption of organic acid is due to hydrogen bonding hydrogen bonding between the hydrogen atom of the carboxylic acid group and one lone electron pair of oxygen atoms of sulfate or hydrogen sulfate counter-anions. Therefore, the adsorption equilibrium coefficient (N and k_s) depend on molecular size or acid group number.

The integration of the hybrid model in the continuous column model was successfully validated in the case of a multi-component pulse tests. Compared to the continuous Langmuir model, the hybrid model can predict the important tailing of the succinic acid profile even though there is still a slight difference (0.1 BV) compared to experimental points.

Last important feature of the column model: by using a continuous formulation, the dispersion coefficient can be dependent on the component, which is not possible with a discontinuous model, for which the dispersion is tied to the number of plates, hence equal for all components. This is of utmost importance for the investigation of complex processes, such as a three-phase process.

Key results on the new three-fractions process

Modeling a three-column ISMB process allows concentration profiles inside columns and their evolutions to be generated, which is not possible in experiment. This is therefore a very interesting tool to investigate the effect of operating conditions and tune them to approach the optimum of the process.

The three-column ISMB process has a decent performance while separating binary mixtures, which explains why it is still used in the industry. It is possible to remove some zones under certain separation conditions while sacrificing the dilution factor of F. For ternary mixtures, two three-column ISMB in cascade can separate ternary mixtures with high purity. However, its performance is less attractive for industrial applications.

To overcome this problem, we proposed a three-phase, four-column SSMB process. The process performance depends on the product composition. In the case of separating glucose / formic acid / succinic acid, it is capable of halving eluent consumption and doubling productivity compared to cascade 3C-ISMB. The eluent consumption reduction is important especially when organic or supercritical fluid is used. Its lower dilution factor reduces concentration cost, which is an energy-consuming step. Finally, its lower total column number reduces investment and maintenance costs. The three-fraction, four-column SSMB process seems to be a promising alternative for the ternary separation studied in this work.

Directions for future works

Strong anionic resin UMA 150 was studied in this work. Previous research works [Claire *et al.*, 2015] showed that organic acids could behave differently on other resins, such as strong cationic resin. In addition, a process with mixed resin could have a wider application domain. Studying different resins could contribute to a better comprehension of retention mechanisms.

Bibliography

The present hybrid model could be even more precise if we discard some assumptions and simplifications. For example, adsorption sites on the upper side of SO_4^{2-} and HSO_4^- counter-anions should be considered more accessible than sites closer to the resin matrix. In addition, formic acid dimer formation was not well considered in this model, and lactic oligomer formation was ignored. A new isotherm, instead of Langmuir competitive equation, needs to be employed for multi-layer adsorption. Thus, a more accurate model considering different adsorption types and adsorption-site types might be an interesting approach to better predict the separation of multi-component mixture by chromatography.

The original expression of van Deemter equation was used to predict dispersion coefficients. Yet, other detailed expressions of van Deemter equation are available, and it would be interesting to fit other expressions. For such purpose, additional experiments are necessary at weak flowrate to measure the curved part of van Deemter curve.

It is generally accepted that smaller beads allow for better separation because they lead to more theoretical plates. However, the finer the beads, the higher the pressure drop in the bed, which limits the treatment speed and the productivity of the systems. The choice of the resin granulometry on the system performance would be a complementary research direction for the SMB-typed process optimization.

Equipment such as pump could bring dead volumes, causing an unexpected tailing in the chromatography profile. This impact was ignored during single column pulse test since the product passes these equipments only one single time. However, in a SMB process, product passes through these equipments repetitively which enlarges the impact of dead volumes on the chromatography profile. It is worthwhile to investigate and integrate such impact in the numerical simulation tool.

The three-fraction, four-column SSMB process proposed in this work could be further developed in many other aspects, such as removing some zones while sacrificing the dilution factor of the fast component. Techniques such as temperature/eluent gradient could be implemented to minimize the tailing of succinic acid. With the developed numerical tool, its performance could also be compared with other three-fraction processes such as the Japan Organo process to show its competitiveness.

Bibliography

"Handbook for Monitoring Industrial wastewater". Environmental Protection Agency (USA). August 1973. Retrieved 30 July 2016.

Abunasser N., Phillip W., Ternary separations with one-column Analogs to SMB, Separation science and technology (2005), <https://doi.org/10.1080/01496390500423615>

Adam P., Nicoud R. M., Bailly M., Ludemann-Hombourger O., US Patent 6136198, 2000

Adam, P.R., Nicoud M., and Bailly M., Ludemann- Hombourger O., Process and device for separation with variable-length. U.S. Patent No 6,136,198, 2000.

Agnieszka C.; Anna W.; Adam B. (2007). Viscosity of aqueous solutions of monocarboxylic acids, 130(1-3), 42–47. doi:10.1016/j.molliq.2006.04.008.

Ahmed, Z., Shimonishi, T., Bhuiyan, S.H., Utamura, M., Takada, G. and Izumori, K. Biochemical Preparation of L-Ribose and -L-Arabinose from Ribitol a New Approach. Journal of Bioscience & Bioengineering (1999), 88, 444-450. [https://doi.org/10.1016/S1389-1723\(99\)80225-4](https://doi.org/10.1016/S1389-1723(99)80225-4)

Alan D.,The Oxford Companion to Food. OUP Oxford 3rd Ed. 2014, p. 527. ISBN 978-0-191-04072-6, DOI: 10.1093/acref/9780192806819.001.0001

Anasthas H.M, Gaikar V.G, Adsorption of acetic acid on ion-exchange resins in non-aqueous conditions, Reactive and Functional Polymers, Volume 47, Issue 1,2001, Pages 23-35, ISSN 1381-5148, [https://doi.org/10.1016/S1381-5148\(00\)00066-3](https://doi.org/10.1016/S1381-5148(00)00066-3).

Andrea K., Johnatt O., João M. N., Eduardo D. P., Anthony A. R. D., Luiza H., Chapter 10 - Xylose fermentation to bioethanol production using genetic engineering microorganisms, Genetic and Metabolic Engineering for Improved Biofuel Production from Lignocellulosic Biomass, Elsevier, 2020, Pages 143-154, ISBN 9780128179536, <https://doi.org/10.1016/B978-0-12-817953-6.00010-5>.

Angarita, M., Müller-Späth, T., Baur, D., Lievrouw, R., Lissens, G., Morbidelli, M., 2015. Twin-column CaptureSMB: a novel cyclic process for protein A affinity chromatography. Journal of Chromatography A 1389, 85–95. <https://doi.org/10.1016/j.chroma.2015.02.046>

Anna A., Krzysztof K., Georges G., Theoretical study of the accuracy of the pulse method, frontal analysis, and frontal analysis by characteristic points for the determination of single component adsorption isotherms, Journal of Chromatography A, Volume 1216, Issue 7, 2009, Pages 1067-1083, ISSN 0021-9673, <https://doi.org/10.1016/j.jchroma.2008.12.021>.

Ariane B., Bruno B., Gregory S. P., Residence time distribution in fluidized beds: diffusion, dispersion, and adsorption, Advanced Powder Technology, Volume 32, Issue 5, 2021, Pages 1677-1687, ISSN 0921-8831, <https://doi.org/10.1016/j.apt.2021.03.019>.

Armenante, P. and Kirwan D., MASS TRANSFER TO MICROPARTICLES IN AGITATED SYSTEMS, Chemical Engineering Science 44 (1989): 2781-2796. [https://doi.org/10.1016/0009-2509\(89\)85088-2](https://doi.org/10.1016/0009-2509(89)85088-2)

Bibliography

- Artak E. K., Simple equations to simulate closed-loop recycling liquid–liquid chromatography: Ideal and non-ideal recycling models, *Journal of Chromatography A*, Volume 1423, 2015, Pages 71-78, ISSN 0021-9673, <https://doi.org/10.1016/j.chroma.2015.10.052>.
- Ashfaq A., Israa Othman, Hanifa Taher, Fawzi Banat, Lactic acid recovery from date pulp waste fermentation broth by ions exchange resins, *Environmental Technology & Innovation*, Volume 22, 2021, ISSN 2352-1864, <https://doi.org/10.1016/j.eti.2021.101438>.
- Athalye A.M., Gibbs S.J., Lightfoot E.N., Predictability of chromatographic protein separations. Study of size-exclusion media with narrow particle size distributions, *J. Chromatogr. A*. 589 (1992) 71–85.
- Azevedo, D.C.S., and Rodrigues, A.E.. Fructose-glucose separation in a SMB pilot unit: modeling, simulation, design, and operation. *AIChE J.* 2001, (9): 2042-2051. <https://doi.org/10.1002/aic.690470915>
- Ballerini, D., Les biocarburants: Répondre aux défis énergétiques et environnementaux des transports, Technip (2011). ISBN 2710809699
- Ballesteros, I., Ballesteros, M., Manzanares, P., Negro, M. J., Oliva, J. M., Sáez, F., 2008: Dilute sulfuric acid pretreatment of cardoon for ethanol production. *Biochemical Engineering Journal*. Volume 42, Issue 1, 15 October 2008, Pages 84-91. <https://doi.org/10.1016/j.bej.2008.06.001>
- Barker, P. E. & Ganetsos, G., Fractionation of dextran using repetitive batch chromatography, Separation and Purification Methods, 17 (1) (1988), *Journal of Chemical technology and Biotechnology*, <https://doi.org/10.1002/jctb.280410108>
- Beste, Y.A., Arlt, W., 2002. Side-stream simulated moving-bed chromatography for multicomponent separation. *Chem. Eng. Technol.* 25, [https://doi.org/10.1002/1521-4125\(20021008\)25:10<956::AID-CEAT956>3.0.CO;2-7](https://doi.org/10.1002/1521-4125(20021008)25:10<956::AID-CEAT956>3.0.CO;2-7)
- Bhat, Ramesh M, Vidya, Krishna, Kamath, Ganesh (2001). "Topical formic acid puncture technique for the treatment of common warts". *International Journal of Dermatology*. 40(6): 415–9. doi:10.1046/j.1365-4362.2001.01242.x
- Bienewald, F., Leibold, E., Tužina, P. and Roscher, G. (2021). Vinyl Esters. In Ullmann's Encyclopedia of Industrial Chemistry. https://doi.org/10.1002/14356007.a27_419.pub2
- Bingchang L., Introduction of chromatography model, Publisher of science,2004, Pages 1-15, ISBN 703012846X
- Broughton D.B. & Gerhold C.G., Continuous sorption processes employing fixed bed of sorbent and moving inlets and outlets. US Pat. 2985589, 1961.
- Broughton, D.B., and Gerhold, C.G.. Continuous sorption process employing fixed bed of sorbent and moving inlets and outlets. US Patent 2 985 589. 1961 David Speybrouck,
- Carey G.F., Bruce A.F., Orthogonal collocation on finite elements Chemical Engineering Science Volume 30, Issues 5–6, May–June 1975, Pages 587-596

Bibliography

- Carta, G. Rodrigues, A. E. (1993) Diffusion and convection in chromatographic processes using permeable supports with a bidisperse pore structure. *Chemical Engineering Science* 48(23): 3927-3935. [https://doi.org/10.1016/0009-2509\(93\)80371-V](https://doi.org/10.1016/0009-2509(93)80371-V)
- Chang, S.C., 1995. The method of space-time conservation element and solution element—a new approach for solving the Navier–Stokes and Euler equations. *Journal of Computational Physics* 119, 295–324. <https://doi.org/10.1006/jcph.1995.1137>
- Chen, H.: Chemical composition and structure of natural lignocellulose. In: Chen, H. (ed.) *Biotechnology of Lignocellulose*, pp. 25–71. Springer, Dordrecht (2014). DOI: 10.1007/978-94-007-6898-7_2
- Cherubini F., The biorefinery concept: Using biomass instead of oil for producing energy and chemicals. *Energy Convers. Manage.*, Volume 51, Issue 7, July 2010, Pages 1412-1421, <https://doi.org/10.1016/j.enconman.2010.01.015>
- Chiang, A.S.T., 1998. Continuous chromatographic process based on SMB technology. *AIChE J.* 44, <https://doi.org/10.1002/aic.690440823>
- Ching C.B., Lim B.G., Lee E.J.D., Ng S.C., Preparative resolution of praziquantel enantiomers by simulated counter-current chromatography *J. Chromatography A* (1993) 215. [https://doi.org/-10.1016/0021-9673\(93\)83007-F](https://doi.org/-10.1016/0021-9673(93)83007-F)
- Chuanyi Y., Shaokun T., Yinghua L., Hong-Mei Y., Moses O.T., Combination of space-time conservation element/solution element method and continuous prediction technique for accelerated simulation of simulated moving bed chromatography, *Chemical Engineering and Processing: Process Intensification* 96 (2015), 54-61, <https://doi.org/10.1016/j.cep.2015.07.023>.
- Chung S.F., Wen C.Y., Longitudinal dispersion of liquid flowing through fixed and fluidized beds, *AIChE J.* 14 (1968) 857–866.
- Ciriminna, R., Meneguzzo, F., Delisi, R., Pagliaro, M., 2017. Citric acid: Emerging applications of key biotechnology industrial product. *Chem. Cent. J.* 11, 1–9. <https://doi.org/10.1186/s13065-017-0251-y>
- Claire-Line B., Conception et optimisation d'un procédé innovant pour la purification d'acides organiques issus de biotechnologie, thesis. University Centralesupelec, 2015
- Cretier G., Rocca J. L., Mass Overload in Liquid Chromatography, Experimental Validity of the Haarhoff-Van der Linde Treatment, *Chromatographia* Vol. 18 (1984), Pages 623–627, <https://doi.org/10.1007/BF02261977>
- Cristian G., Guido S., Manfred M., Massimo M. (2010). Optimizing model predictive control of the chromatographic multi-column solvent gradient purification (MCSGP) process, 20(5), 618-629. <https://doi.org/10.1016/j.jprocont.2010.02.013>
- Dąbrowski, A., Hubicki, Z., Podkościelny, P., & Robens, E. (2004). Selective removal of the heavy metal ions from waters and industrial wastewaters by ion-exchange method. *Chemosphere*, 56(2), 91-106. <https://doi.org/10.1016/j.chemosphere.2004.03.006>

Bibliography

- Daniel G. E., John St. Cyr, 2000, Compositions for the storage of platelets, US6790603B2
- Daniel J. Z., Phillip B., Dennis A., Ulesses P. O., Daniel J. S., Javier G., 2017, Tempered xylitol coating for chewing gums, WO2017184926A1
- De Ligny C.L., Coupling between diffusion and convection in radial dispersion of matter by fluid flow through packed beds, Chem. Eng. Sci. 25 (1970)1177–1181
- Dimian, A.C., Kiss, A.A., Novel energy efficient process for acetic acid production by methanol carbonylation, Chemical Engineering Research and Design (2020), doi: <https://doi.org/10.1016/j.cherd.2020.04.013>
- Domb, A.J., Joseph K., David W. Handbook of Biodegradable Polymers. CRC Press. 1st Ed (1998-02-04). p. 275. ISBN 978-1-4200-4936-7, <https://doi.org/10.1201/9780367802219>
- Donald B., Clarence G., Continuous sorption process employing fixed bed of sorbent and moving inlets and outlets, Universal Oil Products Co, US Patent 2985589A (1957)
- Du J., Choi Y., Lee K., Chun B.K., Hong J.H., Chu C.K.. A practical synthesis of L-FMAU from L-arabinose. Nucleosides Nucleotides. 1999 Feb,18(2):187-95. doi: 10.1080/15257779908043066.
- Timmermann E.O., Chirife J., The physical state of water sorbed at high activities in starch in terms of the GAB sorption equation, J. Food Eng. 13 (1991) 171–179.
- Liang-tseng F., Mahendra M., Lee, Yong-Hyun, Cellulose Hydrolysis, Springer-Verlag Berlin Heidelberg (1987), ISBN : 978-3-642-72575-3, DOI: 10.1007/978-3-642-72575-3
- Felinger A, Cavazzini A, Guiochon G. Numerical determination of the competitive isotherm of enantiomers. Journal of chromatography. A. 2003 Feb,986(2):207-225. DOI: 10.1016/s0021-9673(02)01919-2.
- Fellows P. J.: Food Processing Technology. Woodhead Publishing 4th Ed. (2016), p. 197. ISBN 978-0-081-00523-1,
- Fengel D., and Wegener G., Wood: Chemistry, ultrastructure, reactions, Berlin, New York: De Gruyter, 2011. <https://doi.org/10.1515/9783110839654>
- Ganetsos G., Barker P.E., Preparative and Production Scale Chromatography (1992), CRC Press, Page 5-6, ISBN 9781000715682.
- Gao C., Ma C., & Xu P. (2011). Biotechnological routes based on the lactic acid production from biomass. Biotechnology Advances, 29(6), 930-939. <https://doi.org/10.1016/j.biotechadv.2011.07.022>
- Garrett R.H., Grisham C.M. (2013). Biochemistry (5th ed.). Belmont, CA: Brooks/Cole, Cengage Learning. p. 108. ISBN 9781133106296. OCLC 1066452448
- Gibson, L.J., Soc, J.R.: The hierarchical structure and mechanics of plant materials. Interface 9, 2749–2766 (2012), <https://doi.org/10.1098/rsif.2012.0341>
- Giddings J. C., Seager S. L., Strucki L. R., Stewart G. H., Plate Height in Gas ChromatographyAnal.

Bibliography

- Chem. 32, 867 (1960). <https://doi.org/10.1021/ac60163a043>
- Glueckauf, E., Theory of chromatography. Part 9. The “theoretical plate” concept in column separations, Transactions of the Faraday Society (1955), Trans. Faraday Soc. ISBN 10.1039/TF9555100034, <http://dx.doi.org/10.1039/TF9555100034>
- Gritti F., Piatkowski W., Guiochon G. Comparison of the adsorption equilibrium of a few low-molecular mass compounds on a monolithic and a packed column in reversed-phase liquid chromatography J. Chromatogr. A, 978 (2002) 81, DOI: 10.1016/s0021-9673(02)01279-7
- Gu T., Iyer G., Cheng K.S.C., Parameter estimation and rate model simulation of partial breakthrough of bovine serum albumin on a column packed with large Q Sepharose anion-exchange particles, Sep. Purif. Technol. 116 (2013) 319–326. doi:10.1016/j.seppur.2013.06.004.
- Guiochon G., Shirazi D.G., Felinger A., Katti A.M., Fundamentals of Preparative and Nonlinear Chromatography, Academic Press, 2006, pp. 283–286, ISBN0123705371, 9780123705372.
- Gunn D.J., Axial and radial dispersion in fixed beds, Chem. Eng. Sci. 42 (1987)363–373. [https://doi.org/10.1016/0009-2509\(87\)85066-2](https://doi.org/10.1016/0009-2509(87)85066-2)
- Ha S., Larsen R., Masel R.I. Performance characterization of Pd/C nanocatalyst for direct formic acid fuel cells. Journal of Power Sources. (2005). 144 (1): 28–34. doi:10.1016/j.jpowsour.2004.12.031
- Haghghi M., Hossein G., Tabatabaei A., Salehi J. M., Najafi G., Gholami G. H., Ardjmand M., 2013: Lignocellulosic biomass to bioethanol, a comprehensive review with a focus on pretreatment. Renewable and Sustainable Energy Reviews. Volume 27, 2013, Pages 77-93 <https://doi.org/10.1016/j.rser.2013.06.033>
- Halsey J. G., A new multilayer isotherm equation with reference to surface area, J. Am. Chem. Soc. 73 (1951) 2693–2696, <https://doi.org/10.1021/ja01150a076>
- Hariprasad J. S., Kus H., Ajay K. R., Optimization of reactive SMB and Varicol systems, Computers and Chemical Engineering 27 (2003) 1883/1901, doi:10.1016/S0098-1354(03)00159-5
- Hideyuki N., Kayoko T., Shinobu M., Yoko M., Tomoko S., Yoshihiro A., True moving bed chromatography: solid–liquid multi-stage counter-current extraction, Journal of Chromatography A (1999), Pages 61-69, ISSN 0021-9673, [https://doi.org/10.1016/S0021-9673\(99\)00502-6](https://doi.org/10.1016/S0021-9673(99)00502-6).
- High Fructose Corn syrup: Questions and answers, US Food and Drug Administration. 2014-11-05. Archived from the original on 2018-01-25. Retrieved 2017-12-18
- Himmel M.E., (2009). Biomass Recalcitrance: Deconstructing the Plant Cell Wall for Bioenergy. Doi: 10.1002/9781444305418.
- Hirohiko W., Yuji T.. Donnan Exclusion – Ion Exclusion Chromatography. Journal of Liquid Chromatography 1982 , pages 105-119. DOI: 10.1080/01483918208082217
- Holtzapple, M.T., HEMICELLULOSES. Encyclopedia of Food Sciences and Nutrition, 2nd Ed. (2003).

Bibliography

- pp. 3060–3071. ISBN 9780122270550. <https://doi.org/10.1016/B0-12-227055-X/00589-7>
- Hongzhang C., Lan W., Chapter 6 - Sugar Strategies for Biomass Biochemical Conversion, Editor(s): Hongzhang Chen, Lan Wang, Technologies for Biochemical Conversion of Biomass, Academic Press, 2017, Pages 137-164, ISBN 9780128024171, <https://doi.org/10.1016/B978-0-12-802417-1.00006-5>.
- Hongzhang C., Lan W., Chapter 6 - Sugar Strategies for Biomass Biochemical Conversion, Editor(s): Hongzhang Chen, Lan Wang, Technologies for Biochemical Conversion of Biomass, Academic Press, 2017, Pages 137-164, ISBN 9780128024171, <https://doi.org/10.1016/B978-0-12-802417-1.00006-5>.
- Hoppe, H., Ritter, W., Stephen, E. W. C. "The control of parasitic bee mites: Varroa jacobsoni, Acarapis woodi and Tropilaelaps clareae with formic acid". American Bee Journal. (1989).
- Horvath C., Lin H.J., Movement and band spreading of unsorbed solutes in liquid chromatography Journal of Chromatography A (1976), Pages 401-420. DOI: 10.1016/S0021-9673(01)84088-7
- Houghton J., A Mathematical Model for Gas-Liquid Partition Chromatography, Nature-Pages 389–391 (1960). <https://doi.org/10.1038/188389a0>
- Hsu, T. C., Guo, G. L., Chen, W. H., Hwang, W. S., 2010: Effect of dilute acid pretreatment of rice straw on structural properties and enzymatic hydrolysis. Bioresour Technol. Volume 101, Issue 13, July 2010, Pages 4907-4913 <https://doi.org/10.1016/j.biortech.2009.10.009>
- Biao H., & Haiyang L., & Qingfu W., & Yicong T., & Ruirong C., & Jingrong L., & Wenting B., & Lei L., Production and Utilization of L-Arabinose in China. World Journal of Engineering and Technology (2018). 06. 24-36. DOI : 10.4236/wjet.2018.63B004.
- Hur, Jin, Wankat, Phillip, New Design of Simulated Moving Bed (SMB) for Ternary Separations , Industrial & Engineering Chemistry Research - IND ENG CHEM RES (2005), Volume 44, <https://doi.org/10.1021/ie040164e>
- Hyoky, G., Paananen, H., Cotillon, M., Cornelius, G., 1999. FAST separation technology. In: 30th General Meeting of American Society of Sugar Beet Technologists, Orlando, USA
- Isikgor C. Furkan H. Remzi Becer , Lignocellulosic biomass: a sustainable platform for the production of bio-based chemicals and polymers, Polym. Chem., 2015, 6, 4497
- Ismail E., Amin Mo., Francisco J. B., Jorge A. S., Anderson S. S., Seyed Mohammad Bagher Hashemi, Recent advancements in lactic acid production - a review, Food Research International, Volume 107, 2018, Pages 763-770, ISSN 0963-9969, <https://doi.org/10.1016/j.foodres.2018.01.001>.
- Jain H., Mulay S., "A review on different modes and methods for yielding a pentose sugar: xylitol". International Journal of Food Sciences and Nutrition (2014). 65 (2): 135–43. <https://doi.org/10.3109/09637486.2013.845651>
- James A. Kent: Riegel's Handbook of Industrial Chemistry. Springer Science & Business Media, 2013, ISBN 978-3-319-52287-6, p. 938 DOI 10.1007/978-3-319-52287-6

Bibliography

- James, D. H. and Phillips, C. S. G., The chromatography of gases and vapours. Part III. The determination of adsorption isotherms, J. Chem. Soc. (1954), The Royal Society of Chemistry, 1066-1070, <http://dx.doi.org/10.1039/JR9540001066>.
- Jason T., CorradiStanley J., FreySara A., System and process for recovering products using simulated-moving-bed adsorption (2012), Honeywell UOP LLC, US Patent 9017558B2
- Jermann S, Mazzotti M, Three-column intermittent simulated moving bed chromatography: 1. Process description and comparative assessment. Journal of Chromatography A. Volume 1361, September 26 2014, Pages 125-138, <https://doi.org/10.1016/j.chroma.2014.07.101>
- Jermann S., Katsuo S., Mazzotti M., Intermittent Simulated Moving Bed Processes for Chromatographic Three-Fraction Separation, Organic Process Research & Development 2012 16 (2), 311-322, DOI: 10.1021/op200239e
- Jeung K. K. and Phillip C. Wankat, Designs of Simulated-Moving-Bed Cascades for Quaternary Separations, Ind. Eng. Chem. Res. 2004, 43, 1071-1080, <https://doi.org/10.1021/ie020863w>
- Jeung K. K., Yifei Z., and Phillip C. W., Single-Cascade Simulated Moving Bed Systems for the Separation of Ternary Mixtures, Ind. Eng. Chem. Res. 2003, 42, 4849-4860, <https://doi.org/10.1021/ie030373j>
- John H. K., Hugh P. S., B and C terms in the Van Deemter equation for liquid chromatography, Journal of Chromatography A (1983), Volume 282, Pages 297-313, [https://doi.org/10.1016/S0021-9673\(00\)91609-1](https://doi.org/10.1016/S0021-9673(00)91609-1).
- José P. S. A. & Carlos M. S. (2015) Simulated Moving Bed Strategies and Designs: From Established Systems to the Latest Developments, Separation & Purification Reviews, 44:1, 41-73, DOI: 10.1080/15422119.2013.851087
- Ju Weon L., Phillip C. W., Design of pseudo-simulated moving bed process with multi-objective optimization for the separation of a ternary mixture: Linear isotherms, Journal of Chromatography A, Volume 1217, Issue 20, 2010, Pages 3418-3426, ISSN 0021-9673, <https://doi.org/10.1016/j.chroma.2010.03.020>.
- Juichiro Y., Tatsuo Y., Kazuo K., Yoshimasa T., Heiichi S., Katsumi S., Keijiro N., Tsutomu I., Norio T., Masayuki M., Masataka Y., Toshihiko A., Shigeyoshi O., Studies on Erythorbic Acid Production by Fermentation: Part II. Erythorbic Acid Production by Jar Fermentor, Agricultural and Biological Chemistry, Volume 31, Issue 3, 1 March 1967, Pages 340–352, <https://doi.org/10.1080/00021369.1967.10858816>
- Julien L., Claire-Line B., Florence L., Marc-André T., Moncef S., Purification of organic acids by chromatography with strong anionic resins: Investigation of uptake mechanisms. Journal of Chromatography A, Elsevier, 2016, 1458, pp.63-69. ff10.1016/j.chroma.2016.06.057ff. ffhal-01363370f
- Julien L., Claire-Line B., Marc-André T., Dominique P.. Purification des pentoses d'un hydrolysat d'hemicellulose sans neutralisation afin de recycler l'acide sulfurique. XVIème Congrès de la Société Française de Génie des Procédés, Jul 2017, Nancy, France. ffhal-01816518

Bibliography

- Kaczmarski K., Antos D., Fast finite difference method for solving multicomponent adsorption-chromatography models, Computers & Chemical Engineering, Volume 20, Issue 11, 1996, Pages 1271-1276, ISSN 0098-1354, [https://doi.org/10.1016/0098-1354\(95\)00247-2](https://doi.org/10.1016/0098-1354(95)00247-2).
- Kaczmarski K., Use of orthogonal collocation on finite elements with moving boundaries in the simulation of non-linear multicomponent chromatography. Influence of fluid velocity variation on retention time in LC and HPLC, Computers & Chemical Engineering, Volume 20, Issue 1, 1996, Pages 49-64, ISSN 0098-1354, [https://doi.org/10.1016/0098-1354\(95\)00004-L](https://doi.org/10.1016/0098-1354(95)00004-L).
- Kamide, K., Cellulose and Cellulose Derivatives: Molecular Characterization and its Applications, 1st Ed. (2005). Amsterdam: Elsevier. p. 1. ISBN 9780080454443. <https://doi.org/10.1016/B978-0-444-82254-3.X5000-0>
- Karl J.Z., Properties of xylose, Sugar Series, Elsevier, Volume 13, 2000, Page 249, ISSN 0167-7675, ISBN 9780444503510, [https://doi.org/10.1016/S0167-7675\(00\)80044-5](https://doi.org/10.1016/S0167-7675(00)80044-5).
- Karyn M.U., Carolyn R.S., John G.D., Modeling chromatographic dispersion: A comparison of popular equations, Journal of Chromatography A, 1200 (2008) 122–128, <https://doi.org/10.1016/j.chroma.2008.05.073>
- Kim, T.H. Sequential hydrolysis of hemicellulose and lignin in lignocellulosic biomass by two-stage percolation process using dilute sulfuric acid and ammonium hydroxide. Korean J. Chem. Eng. 28, 2156–2162 (2011). <https://doi.org/10.1007/s11814-011-0093-6>
- Kim. J. K., Abunasser, N., and Wankat, P. C., Use of two feed in simulating moving bed for binary separation, Korean J. Chem. Eng. 22, 619-627 (2005).
- Klemm D., Philipp B., Heinze T., Heinze U., et W. Wagenknecht, General Considerations on Structure and Reactivity of Cellulose: Section 2.1–2.1.4, Comprehensive Cellulose Chemistry, Wiley-VCH Verlag GmbH & Co. KGaA, 1998, p. 9 – 29, <https://doi.org/10.1002/3527601929.ch2a>
- Klotz S., Kuenz A., Prüsse U., Nutritional requirements and the impact of yeast extract on the d-lactic acid production by *Sporolactobacillus inulinus*. Green Chem. 2017, DOI:19:4633–41. 10.1039/C7GC01796K
- Knight C.S., Some fundamentals of ion-exchange-cellulose design and usage in biochemistry. Advances in Chromatography, 4, 61-110, 1967.
- Knox J.H., George R.L., Paul A.R., Interaction of radial and axial dispersion in liquid chromatography in relation to the “infinite diameter effect”, Journal of Chromatography A (1976), Volume 122, Pages 129-145, [https://doi.org/10.1016/S0021-9673\(00\)82240-2](https://doi.org/10.1016/S0021-9673(00)82240-2).
- Koch D.L., Brady J.F., Dispersion in fixed Beds, J, Fluid. Mech. 154 (1985)399–427.) doi:10.1017/S0022112085001598
- Kristian M., Samuel L., Eric von L., Jakob K. H., Jens A., ChromaTech: A discontinuous Galerkin spectral element simulator for preparative liquid chromatography, Computers & Chemical Engineering, Volume 141, 2020, 107012, ISSN 0098-1354, <https://doi.org/10.1016/j.compchemeng.2020.107012>.

Bibliography

- Lameloise M.L., Choice of a tracer for external porosity measurement in ion-exchange resin beds, J. Chromatogr. A. 679 (1994) 255–259. doi:[https://dx.doi.org.bibliopam.ecp.fr/10.1016/0021-9673\(94\)80567-9](https://doi.org/10.1016/0021-9673(94)80567-9).
- Lan L., Young-II L., Performance evaluation of the conservation element and solution element method in SMB process simulation, Chemical Engineering and Processing 48 (2009), 878–884, <https://doi.org/10.1016/j.cep.2008.11.003>
- Lars A., Massimo M., A Continuous Multicolumn Countercurrent Solvent Gradient Purification (MCSGP) Process, Biotechnology and Bioengineering, Vol. 98, No. 5, December 1, 2007, DOI 10.1002/bit.21527
- Lauren V., Marcia E., The application of chromatography in the study of off-flavour compounds in pulses and pulse by-products, LWT, Volume 150, 2021, 111981, ISSN 0023-6438, <https://doi.org/10.1016/j.lwt.2021.111981>.
- Lawther, J.M., Sun R., Banks, W.B.: Fractional characterization of alkali-labile lignin and alkali-insoluble lignin from wheat straw. Ind. Crop. Prod. 5, 291–300 (1996) [https://doi.org/10.1016/S0926-6690\(96\)00028-3](https://doi.org/10.1016/S0926-6690(96)00028-3)
- Le Berre C., Serp P., Kalck P. and Torrence G.P. (2014). Acetic Acid. In Ullmann's Encyclopedia of Industrial Chemistry, https://doi.org/10.1002/14356007.a01_045.pub3
- Lee Y.Y., Iyer P., Torget R.W. Dilute-Acid Hydrolysis of Lignocellulosic Biomass. In: Tsao G.T. et al. (eds) Recent Progress in Bioconversion of Lignocellulosics. Advances in Biochemical Engineering/Biotechnology (1999), vol 65. Springer, Berlin, Heidelberg. https://doi.org/10.1007/3-540-49194-5_5
- Lian-Ming S., Francis MEUNIER, Gino BARON, Procédés de séparation à lit mobile ou lit mobile simulé : Adsorption - Procédés et applications, Techniques d'ingénieur, 10 Déc. 2005
- Lloyd R.S., John W.D., Chapter 8 - Liquid-solid chromatography, Editor(s): Salvatore Fanali, Paul R. Haddad, Colin F. Poole, Marja-Liisa Riekola, Liquid Chromatography (Second Edition), Elsevier, 2017, Pages 191-203, ISBN 9780128053935, <https://doi.org/10.1016/B978-0-12-805393-5.00008-7>.
- Lucía F., Global production capacity of acetic acid 2018 & 2023, Statista Jul 6, 2021, <https://www.statista.com/statistics/1063215/acetic-acid-production-capacity-globally/>
- Ludemann H.O. & NICoud R., The "VARICOL" process: A new multicolumn continuous chromatographic process. Separation Science and Technology - SEPAR SCI TECHNOL. (2000) 35. 1829-1862. <https://doi.org/10.1081/SS-100100622>
- Malveda M., Funada C. (2003). "Acetic Acid". Chemicals Economic Handbook. SRI International, <https://web.archive.org/web/20111014162419/http://sriconsulting.com/CEH/Public/Reports/602.5000/>
- Maria M.T., Rykers Lues J.F., Organic Acids and Food Preservation, chapter 2, Nature and composition of organic acids, CRC Press (13 octobre 2010) , P31-32. ISBN-10 : 1420078429
- Martin G., Jason H., Thomas S. M., Fabrice G., Utility of linear and nonlinear models for retention

Bibliography

- prediction in liquid chromatography, Journal of Chromatography A, Volume 1613, 2020, 460690, ISSN 0021-9673, <https://doi.org/10.1016/j.chroma.2019.460690>.
- Martin, A.J.P.; Synge R.L.M., (1941). A new form of chromatogram employing two liquid phases. Biochemical Journal, 35(12), 1358–1368.doi:10.1042/bj0351358
- Martinez F.A.C., Balciunas E.M., Salgado J.M., González J.M.D., Converti A., & De Souza Oliveira R. P. (2013). Lactic acid properties, applications, and production: a review. Trends in Food Science & Technology, 30(1), 70-83. <https://doi.org/10.1016/j.tifs.2012.11.007>
- Martone P., Estevez J., Lu F., Ruel K., Denny M., Somerville C., Ralph J. (Jan 2009). Discovery of Lignin in Seaweed Reveals Convergent Evolution of Cell-Wall Architecture. Current biology: CB. Volume 19, Issue 2, 27 January 2009, Pages 169-175 <https://doi.org/10.1016/j.cub.2008.12.031>
- Masakazu Negawa, Fumihiro Shoji, Optical resolution by simulated moving-bed adsorption technology, Journal of Chromatography A (1992), ISSN 0021-9673, [https://doi.org/10.1016/0021-9673\(92\)87011-V](https://doi.org/10.1016/0021-9673(92)87011-V).
- Masatake Tanimura, Masao Tamura, Takashi Teshima, Method of chromatographic separation (1989), Ryoka Techno Engineering and Construction Co, US Patent 5064539A
- Masuda T., Sonobe T., Matsuda F., Horie M., Process for fractional separation of multi-component fluid mixture, US5198120 A, (1993).
- McCoy M., Chem. Eng. News 78 (25) (2000) 17 (Chiral Business), Morbidelli, M. and M. Mazzotti, "Advances in Simulated Moving bed Chromatography," in "PREP, 15th International Symposium, Exhibit Workshops on Preparative/Process Chromatography Ion Exchange, Adsorption/Desorption Processes & related Separation Techniques," Lecture 201 Washington DC, USA, (2002) pp. 53–54
- Menon V., Rao M., Trends in bioconversion of lignocellulose: Biofuels, platform chemicals & biorefinery concept. Prog. Energy Combust. Sci., Volume 38, Issue 4, August 2012, Pages 522-550, <https://doi.org/10.1016/j.pecs.2012.02.002>
- Michael H., Emmanuelle L., Recent developments in preparative-scale supercritical fluid- and liquid chromatography for chiral separations, TrAC Trends in Analytical Chemistry, Volume 133, 2020, 116090, ISSN 0165-9936, <https://doi.org/10.1016/j.trac.2020.116090>.
- Michel M., KnobDenni J., StanleyTerri J., Vander S., Xiaobo C., Thierry Z., Jacques L., Stephane R. Aromatics production process (2015), Axens SA ExxonMobil Chemical Patents Inc ExxonMobil Chemical Co, US Patent 9708233B2
- Michel S., Guillaume R., 1999, Process of sugarless hard coating and products obtained therefrom, US547859
- Minceva M., and Rodrigues A.E., Two-level optimization of an existing SMB for pxylene separation. Computers and Chemical Engineering, 2005, (29): 2215-2228. <https://doi.org/10.1016/j.compchemeng.2005.08.001>
- Minceva M., and Rodrigues A.E., Modeling and simulation of a simulated moving bed for the

Bibliography

- separation of p-xylene. Ind. Eng. Chem. Res., 2002, (41): 3454-3461.
<https://doi.org/10.1021/ie010095t>
- Mingchuan L., The processing method that a kind of xylitol preserved fruit freezes, 2017, CN107997081A
- Mirabel B., Séparation des protéines par chromatographie préparative. L'actualité chimique, 39-44, Juin-Juillet 1980
- Momoko F., 2017, Composition for hair and hair treatment method, KR20180081452A
- Mónica M., Daphne K., Joaquín G., Gustavo L.G., Bernt N., Marcel O., Continuous adsorption in food industry: The recovery of sinapic acid from rapeseed meal extract, Separation and Purification Technology, Volume 254, 2021, 117403, ISSN 1383-5866, <https://doi.org/10.1016/j.seppur.2020.117403>.
- Mores, S., Souza V., L.P., Irineudo M.J.A., Carvalho J.C., Mello A.F.M., Pandey A., Ricardo S. C., Citric acid bioproduction and downstream processing: Status, opportunities, and challenges, Bioresource Technology (2020), doi: <https://doi.org/10.1016/j.biortech.2020.124426>
- Mosen A., Beet-Sugar Handbook, John Wiley & Sons (2006), Chapter 8, P553, ISBN 0471790982, 9780471790983
- Mota J.P.B., Araújo J.M.M. Theory and Practice of Single-Column Smb Analogs, AIChE J. (2005), Vol. 51, pp. 1641-1653.
- Mueller, A. S., Hamel C., Simulated-moving-bed technology for purification of the prebiotics galacto-oligosaccharides, Separation and Purification Technology, Volume 271, 2021, 118829, ISSN 1383-5866, <https://doi.org/10.1016/j.seppur.2021.118829>.
- Naish P.J., Hartwell S., Exponentially Modified Gaussian functions—A good model for chromatographic peaks in isocratic HPLC. Chromatographia 26, 285–296 (1988). <https://doi.org/10.1007/BF02268168>
- Nallagounder K., 2018, Composés, compositions et méthodes pour la prévention ou le traitement d'affections liées au foie, aux lipides et au glucose, WO2018156513A1
- Nanda S., Maley J., Kozinski J.A., Dalai A.K., Physico-chemical evolution in lignocellulosic feedstocks during hydrothermal pretreatment and delignification. J. Biobased Mater. Bioenerg. 9, 295–308 (2015), <https://doi.org/10.1166/jbmb.2015.1529>
- Nanda, S., Maley, J., Kozinski, J.A., Dalai, A.K.: Physico-chemical evolution in lignocellulosic feedstocks during hydrothermal pretreatment and delignification. J. Biobased Mater. Bioenerg. 9, 295–308 (2015), <https://doi.org/10.1166/jbmb.2015.1529>
- Navarro, A., Caruel, H., Rigal, L., Phemius, P., 1997. Continuous chromatographic separation process: simulated moving bed allowing simultaneous withdrawal of three fractions. J. Chromatogr. A, Volume 770, Issues 1–2, 16 May 1997, Pages 39-50, [https://doi.org/10.1016/S0021-9673\(96\)01073-4](https://doi.org/10.1016/S0021-9673(96)01073-4)
- Ng C., Losso J.N., Marshall W.E., Rao R.M., Freundlich adsorption isotherms of agricultural by-

Bibliography

- product-based powdered activated carbons in a geosmin–water system, *Bioresour. Technol.* 85 (2002) 131–135. [https://doi.org/10.1016/S0960-8524\(02\)00093-7](https://doi.org/10.1016/S0960-8524(02)00093-7)
- Ng C.K., Rousset F., Valery E., Bracewell D.G., Sorensen E., 2014. Design of high productivity sequential multi-column chromatography for antibody capture. *Food and Bioproducts Processing* 92 (2), 233–241.
- Nicoud R.M., Fuchs G., Adam P., Bailly M., Küsters E., Antia F.D., Reuille R., Schmid E., Preparative scale enantioseparation of a chiral epoxide: Comparison of liquid chromatography and simulated moving bed adsorption technology, *Chirality* 5 (1993) 267 <https://doi.org/10.1002/chir.530050415>
- Ninfa A.J., David P.B., Marilee B. (2010). *Fundamental Laboratory Approaches for Biochemistry and Biotechnology*. Hoboken, NJ: John Wiley ISBN: 978-0-470-08766-4
- Nobre C., Santos M.J., Dominguez A., Torres D., Rocha O., Peres A.M., et al., Comparison of adsorption equilibrium of fructose, glucose and sucrose on potassium gel-type and macroporous sodium ion-exchange resins, *Anal. Chim. Acta* 654 (2009) 71–76. doi:10.1016/j.aca.2009.06.043
- Orkomi A.A., Shahrokh M., Simulation and control of multidimensional crystallization processes, *Chem. Eng. Commun.* 201 (2014), 870-895, <https://doi.org/10.1080/00986445.2013.785947>.
- Oswin C., The kinetics of package life. III. The isotherm, *J. Chem. Technol. Biotechnol.* 65 (1946) 419–421. <https://doi.org/10.1002/jctb.5000651216>
- Otani S., Akita S., Iwamura T., Kanaoka M., Matsumura K., Noguchi Y., Sando K., Mori T., Takeuchi I., Tsuchiya T., Yamamoto T., Separation Process of Components of Feed Mixture Utilizing Solid Sorbent [1973], Toray Industries Inc, U.S. Patent 3761533.
- Papathanasiou, M. M., Steinebach, F., Stroehlein, G., Müller-Späth, T., Nascu, I., Oberdieck, R., Pistikopoulos, E. N.. A control strategy for periodic systems – application to the twin-column MCSGP. *Computer Aided Chemical Engineering* (2015), 1505–1510. doi:10.1016/b978-0-444-63577-8.50096-6
- Paul-Dauphin S., Karaca F., Morgan T.J., Probing Size Exclusion Mechanisms of Complex Hydrocarbon Mixtures: The Effect of Altering Eluent Compositions. *Energy & Fuels* (6 Oct 2007). 6. 21 (6): 3484–3489. <https://doi.org/10.1021/ef700410e>
- Pranay G., Kaveh V., Min L., Jens H.V., Charles H., Eric L., Computational fluid dynamic simulation of axial and radial flow membrane chromatography: Mechanisms of non-ideality and validation of the zonal rate model, *Journal of Chromatography A*, Volume 1305, 2013, Pages 114-122, ISSN 0021-9673, <https://doi.org/10.1016/j.chroma.2013.07.004>.
- Pynnonen, B., Simulated moving bed processing: escape from the high-cost box. *Journal of Chromatography A*, 1998, (827): 143-160.
- Qamar S., Yousaf M., The space-time CESE method for solving special relativistic hydrodynamic equations, *J. Comput. Phys.* 231 (2012) 3928-3945, <https://doi.org/>

Bibliography

10.1016/j.jcp.2012.01.039.

Yuanyuan Q., Rongxiu Z., Dongju Z., (2014). Adsorption behaviors of monomer and dimer of formic acid on Pt (111) in the absence and presence of water. *Journal of Molecular Modeling*, 20(6), 2264–4624. doi:10.1007/s00894-014-2264-y

Rajendran A, Paredes G, Mazzotti M (2009) Simulated moving bed chromatography for the separation of enantiomers. *J Chromatogr A* 1216(4):709–738, <https://doi.org/10.1016/j.chroma.2008.10.075>

Ramesh K., Bikram B., Byong-Hun J., Sustainable production and purification of succinic acid: A review of the membrane-integrated green approach, *Journal of Cleaner Production*, Volume 277, 2020, 123954, ISSN 0959-6526, <https://doi.org/10.1016/j.jclepro.2020.123954>

Reutemann W., Kieczka H., (2000). "Formic Acid". Ullmann's Encyclopedia of Industrial Chemistry. doi:10.1002/14356007.a12_013. ISBN 978-3-527-30673-2

Ribeiro A.E., Gomes P.S., Pais L.S., and Rodrigues A.E.. Chiral separation of ketoprofen enantiomers by preparative and simulated moving bed chromatography. *Separation Science and Technology*, 2011, (46): 1726-1739. <https://doi.org/10.1080/01496395.2011.582070>

Robert W., Mark R., John S., Kelly I., Lignocellulosic Biomass to Ethanol Process Design and Economics Utilizing Co-Current Dilute Acid Prehydrolysis and Enzymatic Hydrolysis Current and Futuristic Scenarios, National Renewable Energy Laboratory, <https://doi.org/10.2172/12150>

Rodrigues A.E., Pereira C., Minceva M., Pais L.S., Ribeiro A.M., Ribeiro A., Silva M., Graça N., Santos, J.C. Chapter 6 - Multicomponent Separations by Simulated Moving Bed (SMB)-Based Processes, Editor(s): A.E. Rodrigues, C. Pereira, M. Minceva, L.S. Pais, A.M. Ribeiro, A. Ribeiro, M. Silva, N. Graça, J.C. Santos, *Simulated Moving Bed Technology*, Butterworth-Heinemann, 2015, Pages 145-164, ISBN 9780128020241, <https://doi.org/10.1016/B978-0-12-802024-1.00006-9>.

Rodrigues A., Chenou C., Rendueles V., (1996) Protein separation by liquid chromatography using permeable POROS Q/M particles. *The Chemical Engineering Journal and the Biochemical Engineering Journal* 61(3): 191-201.

Roos Y.H., Water activity and physical state effects on amorphous food stability, *J. Food Process. Preserv.* 16 (1993) 433–447.

Sa Gomes P., and Rodrigues A. E., Outlet stream swing (OSS) and multifeed (MF) Operation of simulating moving beds, *Sep. Sci. Technol.*, 42, 223-252 (2006), <https://doi.org/10.1080/01496390601070125>

Sadighi S., Ahmad A., Shirvani M., Dynamic simulation of a pilot scale vacuum gas oil hydrocracking unit by the space-time CE/SE method, *Chemical Engineering & Technology* 35 (2012), 919-928, <https://doi.org/10.1002/ceat.201100305>

Sadroddin G., Georges G., Comparison of the various kinetic models of non-linear chromatography, *Journal of Chromatography A* (1992), Volume 603, Issues 1–2, Pages 1-11,

Bibliography

[https://doi.org/10.1016/0021-9673\(92\)85340-Y](https://doi.org/10.1016/0021-9673(92)85340-Y).

Saha B.C., in Handbook of Industrial Biocatalysis, ed. C. T. Hou, CRC Press, 2005, ch. Enzymes as Biocatalysts for Conversion of Lignocellulosic Biomass to Fermentable Sugars.

Samsonov G.V., Bakaeva R.M., Sorokina Y.N., Kolomiitsev O.P., Selective adsorption of novobiocin by macroreticular anion exchange resins. Pharmaceutical Chemistry Journal, 7, 424-426, 1973.

Savidan L., La Chromatographie. DUNOD, Paris, 1963.

Schramm H., Kienle A., Kaspereit M., A. Seidel-Morgenstern, Improved operation of simulated moving bed processes through cyclic modulation of feed flow and feed concentration, Chemical Engineering Science, Volume 58, Issues 23–24, 2003, Pages 5217-5227, ISSN 0009-2509, <https://doi.org/10.1016/j.ces.2003.08.015>.

Schramm Henning, Malte Kaspereit, Achim Kienle, Andreas Seidel-Morgenstern, Simulated moving bed process with cyclic modulation of the feed concentration, Journal of Chromatography A, Volume 1006, Issues 1–2, 2003, Pages 77-86, ISSN 0021-9673, [https://doi.org/10.1016/S0021-9673\(03\)00327-3](https://doi.org/10.1016/S0021-9673(03)00327-3).

Se-Hee J., Hee-Geun N., Sungyong M., Optimal design and experimental validation of a modified four-zone SMB process for the separation of a ternary amino acid mixture, Process Biochemistry, Volume 45, Issue 8, 2010, Pages 1288-1298, ISSN 1359-5113, <https://doi.org/10.1016/j.procbio.2010.04.016>.

Seyed O.R., Tingyue G., Empirical correlations for axial dispersion coefficient and Pecletnumber in fixed-bed columns, Journal of Chromatography A, 1490 (2017) 133–137, <https://doi.org/10.1016/j.chroma.2017.02.026>

Shamsul Q., Noreen A., Andreas S., Analysis of general rate model of linear chromatography considering finite rates of the adsorption and desorption steps, Chemical Engineering Research and Design, Volume 111, 2016, Pages 13-23, ISSN 0263-8762, <https://doi.org/10.1016/j.cherd.2016.04.006>.

Shen G., Tao H., Zhao M., Yang B., Wen D., (2009). Effect of hydrogen peroxide pretreatment on the enzymatic hydrolysis of cellulose. Journal of Food Process Engineering. 34. 905 - 921. 10.1111/j.1745-4530.2009.00518.x.

Shen H., Gang W., Liu K., Deliang Z. Numerical simulation of liquid-fueled detonations by an eulerian-lagrangian model. International Journal of Nonlinear Sciences and Numerical Simulation (2012), 13, <https://doi.org/10.1515/ijnsns.2011.102>.

Shubham P.C., Dennis J.M., James E.J., Todd A.W., John G.F., Jr. A., ZacherH., 2000, Catalysts and process for hydrogenolysis of sugar alcohols to polyols, US6291725B1

Silva R.J., Rodrigues R.C., Osuna-Sanchez H., Bailly M., Valéry E., Mota, J.P., 2010. A new multicolumn, open-loop process for center-cut separation by solvent-gradient chromatography. Journal of Chromatography A 1217 (52), 8257–8269. <https://doi.org/10.1016/j.chroma.2010.11.005>

Bibliography

- Simpson H.D., Haufler U.R., Daniel R.M. An Extremely Thermostable Xylanase from the Thermophilic Eubacterium Thermotoga, Biochem. J., 277:413 (1991).
<https://doi.org/10.1042/bj2770413>
- Sindhu R., Binod P., Pandey A., 2016: Biological pretreatment of lignocellulosic biomass - An overview. Bioresource Technology. Volume 199, January 2016, Pages 76-82.
<https://doi.org/10.1016/j.biortech.2015.08.030>
- Siouffi A.M. (2006). About the C term in the van Deemter's equation of plate height in monoliths. Journal of Chromatography A, 1126(1-2), 86–94. doi:10.1016/j.chroma.2006.05.036
- Sircar S., Comments on practical use of Langmuir gas adsorption isotherm model. Adsorption 23, 121–130 (2017). <https://doi.org/10.1007/s10450-016-9839-0>
- Song H., Sadriaj D., Desmet G., & Cabooter D. (2018). Methodologies to determine b-term coefficients revisited. Journal of Chromatography A, 1532, 124–135. doi:10.1016/j.chroma.2017.11.070
- Souhir A., Laurence M., Michel B., Olivier L., The M3C Process: A New Multicolumn Chromatographic Process Integrating a Concentration Step. I—The Equilibrium Model, Separation Science and Technology, 41 (12) 2639-2663 2006
<https://doi.org/10.1080/01496390600829992>
- Stephen B., Emmett P. H., Edward T., Adsorption of Gases in Multimolecular LayersJournal of the American Chemical Society 1938 60 (2), 309-319 DOI: 10.1021/ja01269a023
- Steve T., Beckett's Industrial Chocolate Manufacture and Use. John Wiley & Sons, 5th Ed. 2017, p. 82. ISBN 978-1-118-78014-5, DOI:10.1002/9781118923597
- Stoltz J.F., Rivat C., Geschier C., Colosetti P., Sertillanges P., Tondon J., Regnault V., Purification chromatographique de l'albumine plasmatique humaine à l'échelle pilote. Bio-Sciences, 6, n°4, 103-106, 1987.
- Succinic acid market – growth, trends, covid-19 impact and forecasts (2021-2026), Modor Intelligence (2018).
- Tetsuya K., Masao K., Efficient production of acetic acid from glucose in a mixed culture of Zymomonas mobilis and Acetobacter sp., Journal of Fermentation and Bioengineering, Volume 81, Issue 1, 1996, Pages 42-46, ISSN 0922-338X, [https://doi.org/10.1016/0922-338X\(96\)83118-7](https://doi.org/10.1016/0922-338X(96)83118-7).
- Thomas B., Dietmar B., Horst W.D., Armin F., Günther S., Sakayu S., Hideaki Y., Biotechnology, in: Ullmann's Encyclopedia of Industrial Chemistry, 7th Edition, Wiley-VCH, 2011. ISBN 978-3-527-32943-4. Volume 6, p. 48
- Thomas H., Polysaccharides I: structure, characterisation and use., 1958. Berlin: Springer. 2005. ISBN 978-3-540-31583-4. DOI: 10.1007/b136812
- Torget R., Walter P., Himmel M., Grohmann K., Dilute-acid pretreatment of corn residues and short-rotation woody crops, Appl. Biochem. Biotechnol., 28/29:75 (1991).

Bibliography

- Torget R., Werdene P., Himmel M., Grohmann K., Dilute acid pretreatment of short rotation woody and herbaceous crops, *Appl. Biochem. Biotechnol.*, 24/25:115 (1990).
- Torgny F., Patrik F., Jörgen S., Chapter 24 - Modeling of preparative liquid chromatography, Editor(s): Salvatore Fanali, Paul R. Haddad, Colin F. Poole, Marja-Liisa Riekola, *Liquid Chromatography (Second Edition)*, Elsevier, 2017, Pages 573-592, ISBN 9780128053935, <https://doi.org/10.1016/B978-0-12-805393-5.00024-5>.
- Tsai A.M., Englert D., Graham E.E., Study of the dynamic binding capacity of two anion exchangers using bovine serum albumin as a model protein. *Journal of Chromatography*, 504, 89-95, 1990.
- Ur-Rehman S., Mushtaq Z., Zahoor T., Jamil A., Murtaza M.A., Xylitol: a review on bioproduction, application, health benefits, and related safety issues. *Critical Reviews in Food Science and Nutrition* (2015). 55 (11): 1514–28. <https://doi.org/10.1080/10408398.2012.702288>
- Uttam Kumar Jana, Naveen Kango, Applications of Fungal Hemicellulases, *Encyclopedia of Mycology*, Elsevier, 2021, Pages 305-315, ISBN 9780323851800, <https://doi.org/10.1016/B978-0-12-819990-9.00058-5>.
- Van Deemter J.J., Zuiderweg F.J., Klinkenberg A., Longitudinal diffusion and resistance to mass transfer as causes of nonideality in chromatography, *Chemical Engineering Science*, Volume 5, Issue 6, 1956, Pages 271-289, ISSN 0009-2509, [https://doi.org/10.1016/0009-2509\(56\)80003-1](https://doi.org/10.1016/0009-2509(56)80003-1).
- Vanderwiel J.P., Continuous recovery of bioproducts by adsorption. Thesis, Academie Boeken Centrum, De Lier, The Netherlands, 1989.
- Vedeneeva V.V., Dobrynina O.V., Momot N.N., Samsonov G.V., Dynamics of the processes of anion-exchange sorption and desorption of phenoxyethylpenicillin. *Pharmaceutical Chemistry Journal*, 3, 121-124, 1974.
- Vera G.M., Rodrigues A.E., Separation of ternary mixtures by pseudo-simulated moving bed chromatography, *Journal of Chromatography A* (2001), Volume 939, Issues 1–2, Pages 23-40, ISSN 0021-9673, [https://doi.org/10.1016/S0021-9673\(01\)01335-8](https://doi.org/10.1016/S0021-9673(01)01335-8).
- Vincent D. R., Charanjit R.B., 1999, Nasal delivery of xylitol, Xlear Inc, US6599883B1
- Vincent O., Marlène B., Pierre-Yves P., Jérôme P., Sugarcane bagasse mild alkaline fractionation and production of purified fractions by pulse chromatography with water, *Industrial Crops and Products*, Volume 125, 2018, Pages 370-378, ISSN 0926-6690, <https://doi.org/10.1016/j.indcrop.2018.09.019>.
- Vinicio V.S., Rodrigues A.E., Loureiro J.M., Ribeiro A.M., Idelfonso B.R., Transient analysis of true/simulated moving bed reactors: A case study on the synthesis of n-Propyl propionate, *Computers & Chemical Engineering*, Volume 137, 2020, 106820, ISSN 0098-1354, <https://doi.org/10.1016/j.compchemeng.2020.106820>.
- Wei L., Dong H., Pan H., Hu X., Zhu J., Study on the mechanism of the deflagration to detonation transition process of explosive, *Journal of Energetic Materials* 32 (2014) 238-251.

Bibliography

<https://doi.org/10.1080/07370652.2013.825347>

Wenbiao Y., 2012, Herbal tea containing L-arabinose, CN102987028A

Wingren C., Hansson U.B., CHROMATOGRAPHY: LIQUID | Partition Chromatography (Liquid–Liquid), Editor(s): Ian D. Wilson, Encyclopedia of Separation Science, Academic Press, 2000, Pages 760-770, ISBN 9780122267703, <https://doi.org/10.1016/B0-12-226770-2/01801-9>.

Wooley R., Ma Z., Wang N.H.L., A nine-zone simulating moving bed for the recovery of glucose and xylose from biomass hydrolyzate. Industrial Eng. Chem. Res. 1998. 37, 3699-3709, <https://doi.org/10.1021/ie9800896>

Wyman C.E., 20 years of trials, tribulations, and research progress on bioethanol technology: Selected key events along the way, Appl. Biochem. Biotechnol., 91-93:5 (2001). DOI: 10.1385/abab:91-93:1-9:5

Xiaoguang H., A preparative method for the production of yogurt of xylitol. 2016 CN107771939A.

Xiaoling Z., Zehui Z., Yafan C., Yubin Z., Yue Z., Youhui G., Zongjun C., Xiaofen W., Accelerated biomethane production from lignocellulosic biomass: Pretreated by mixed enzymes secreted by Trichoderma viride and Aspergillus sp., Bioresource Technology, Volume 309, 2020, 123378, ISSN 0960-8524, <https://doi.org/10.1016/j.biortech.2020.123378>.

Yaskovich G.A., KOZNEVA E.P., EL'KIN G.E., VOROB'EVA V.Y., SAMSONOV G.V., Kinetics of sorption of the desoxyribonuclease of actinomyces streptomycini from a native solution with KMT carboxyl cation-exchange resin. Pharmaceutical Chemistry Journal, 12, 631-634, 1974.

Yoshihiro N., Hideki Y., 2004, Blood sugar level rising inhibitor, JP2005289847A

Young-II L., Sten-Bay J., A fast and accurate numerical method for solving simulated moving bed (SMB) chromatographic separation problems, Chemical Engineering Science, Volume 59 (2004), 1931-1947, <https://doi.org/10.1016/j.ces.2003.12.026>

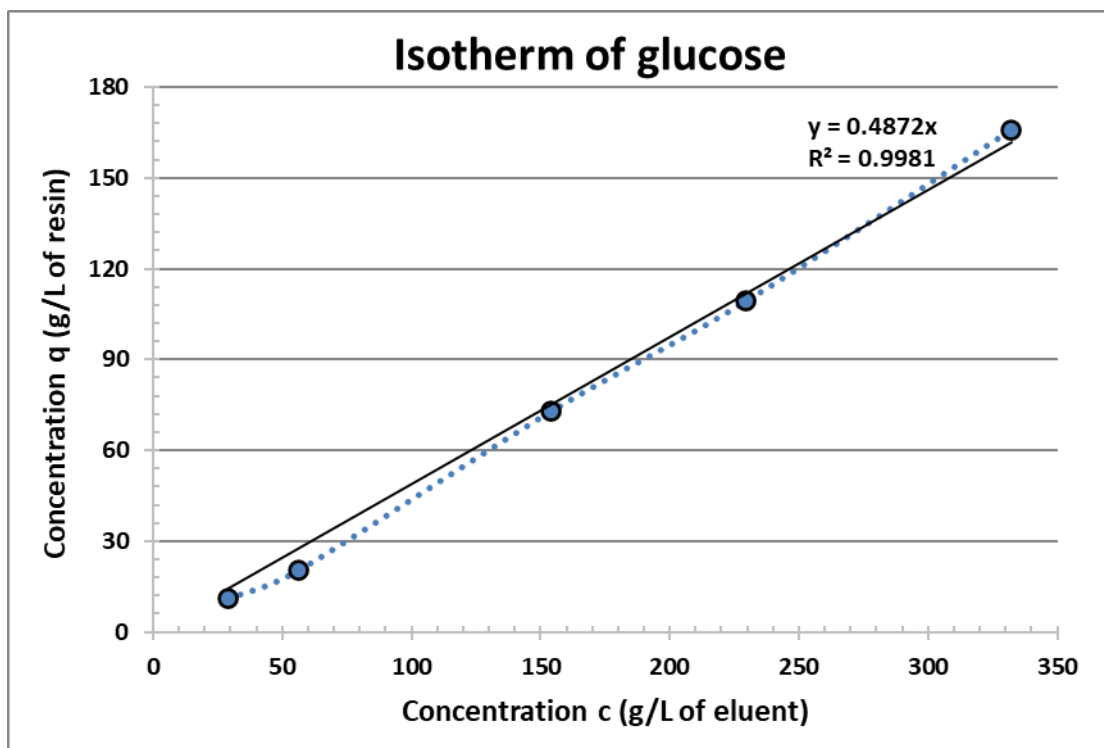
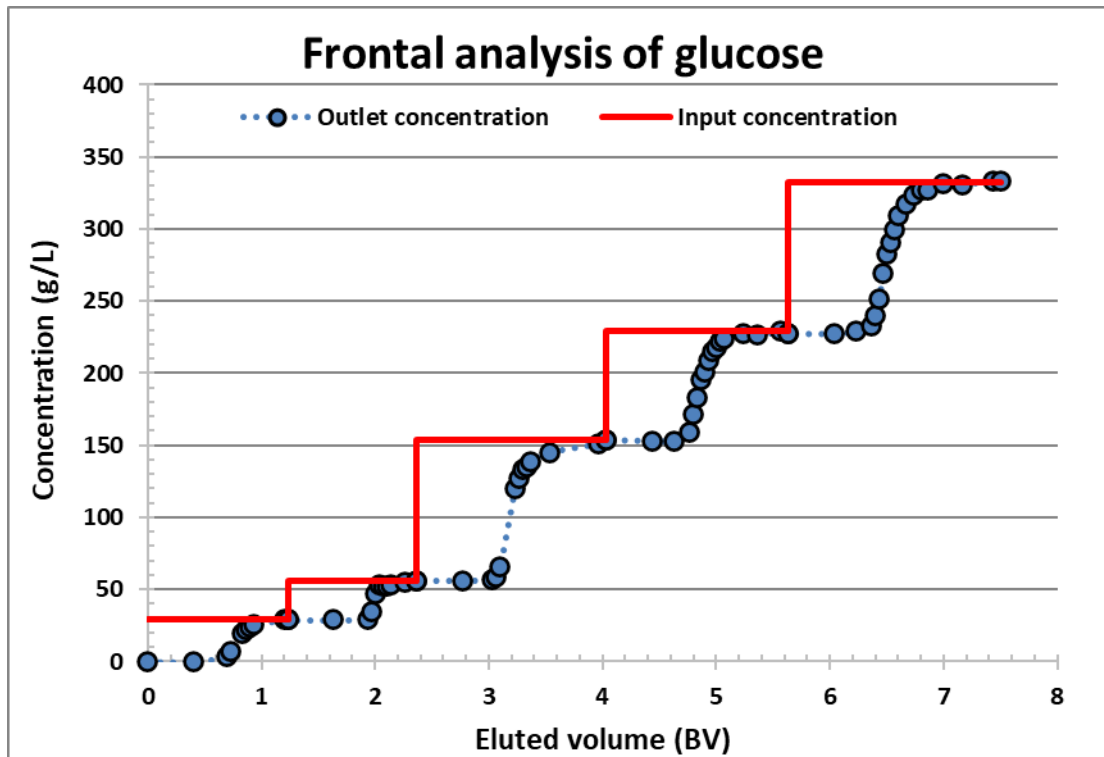
Zhang, Z., Mazzotti M., Morbidelli M., PowerFeed Operation of Simulated Moving bed Units: Changing the Flowrates During the Switching Interval, J. Chromatography A, 1006(1–2), 87–99 (2003). [https://doi.org/10.1016/S0021-9673\(03\)00781-7](https://doi.org/10.1016/S0021-9673(03)00781-7)

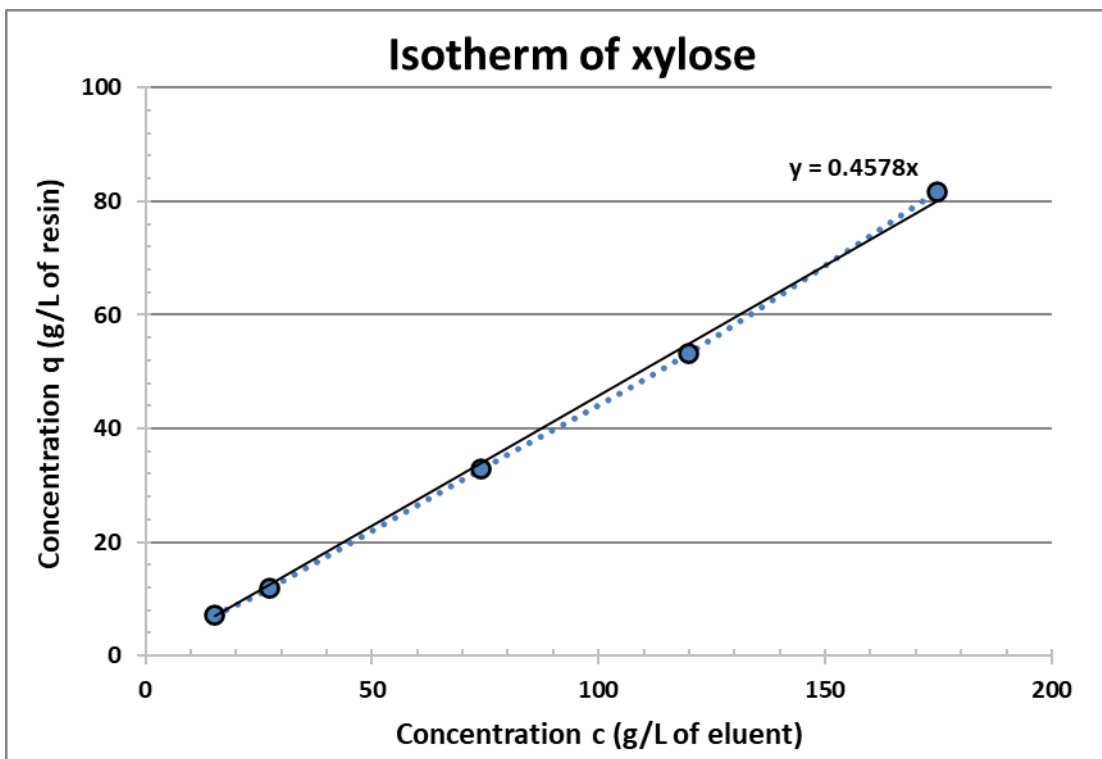
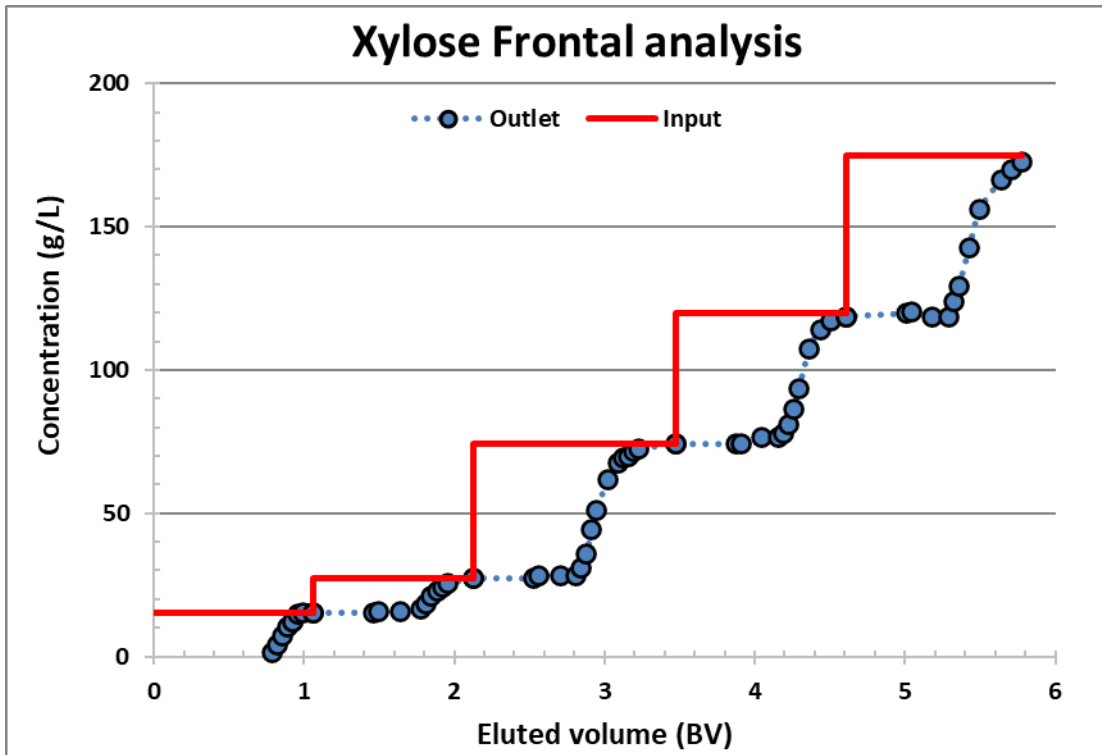
Zhao-wen L., Guo-Hua C., Yi-fan C., Synthetic process of telbivudine, an antivirus agent, Chinese Journal of Medicinal Chemistry 2009-01

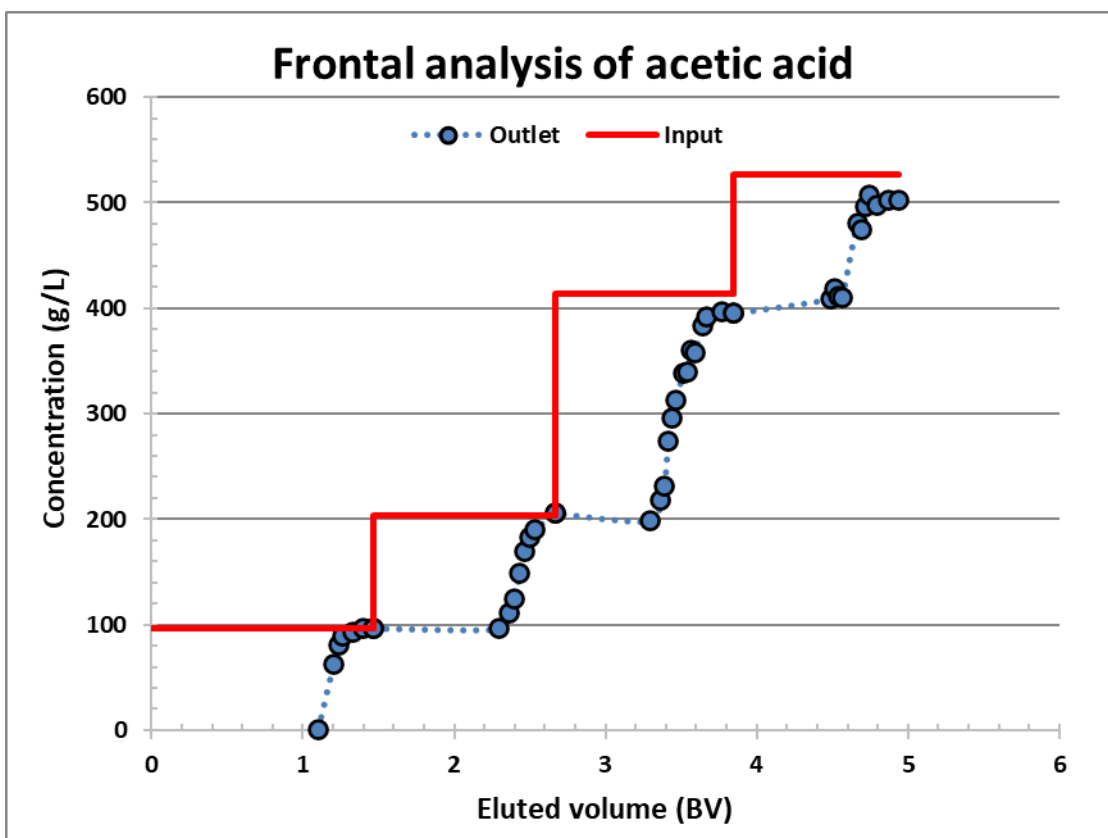
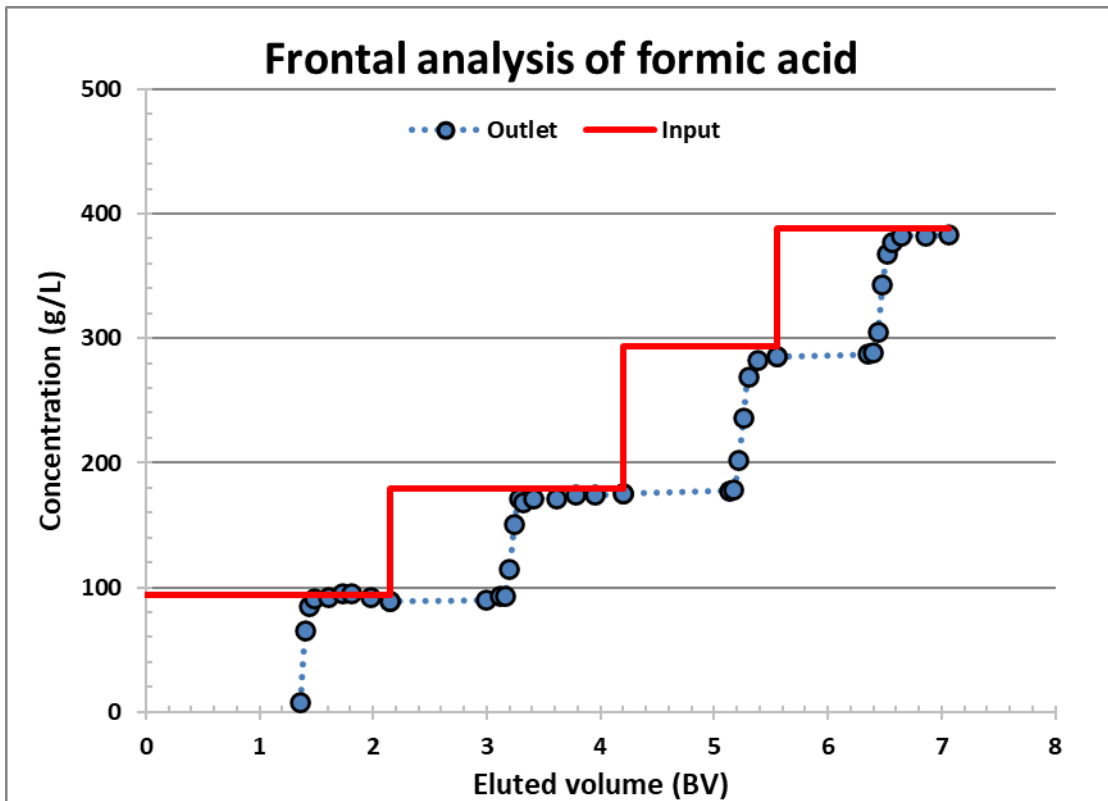
Appendices

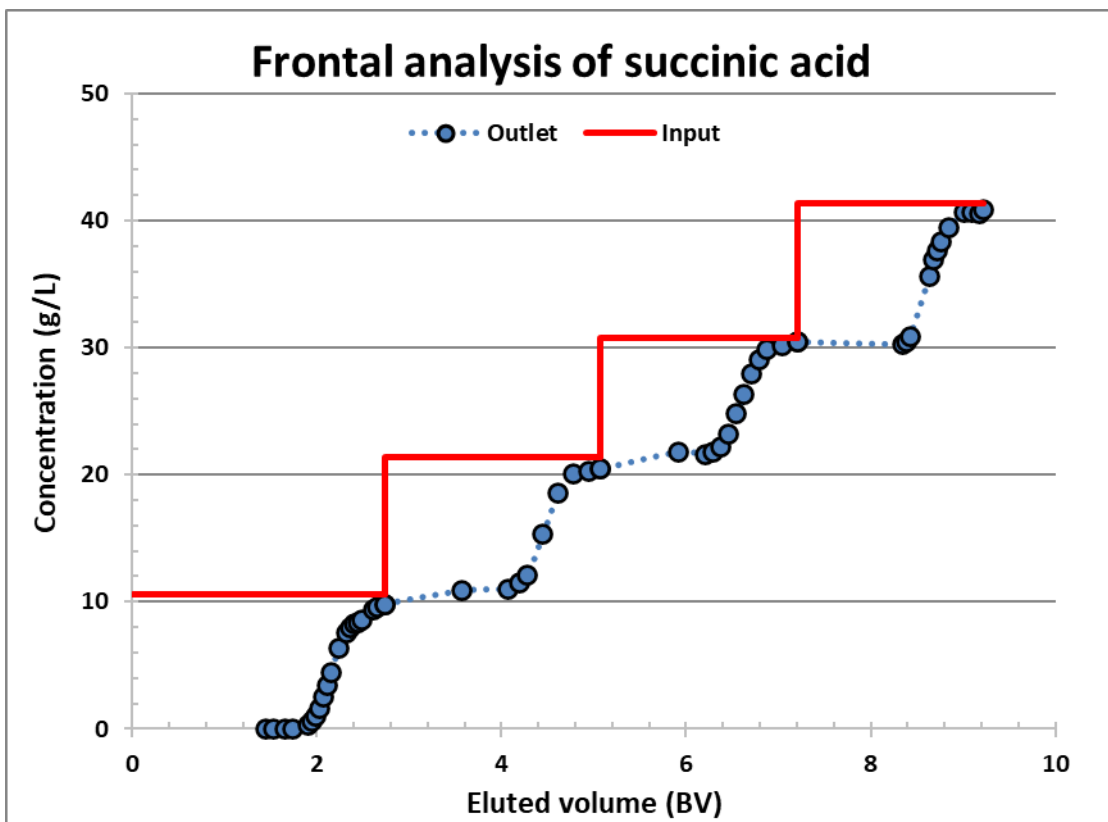
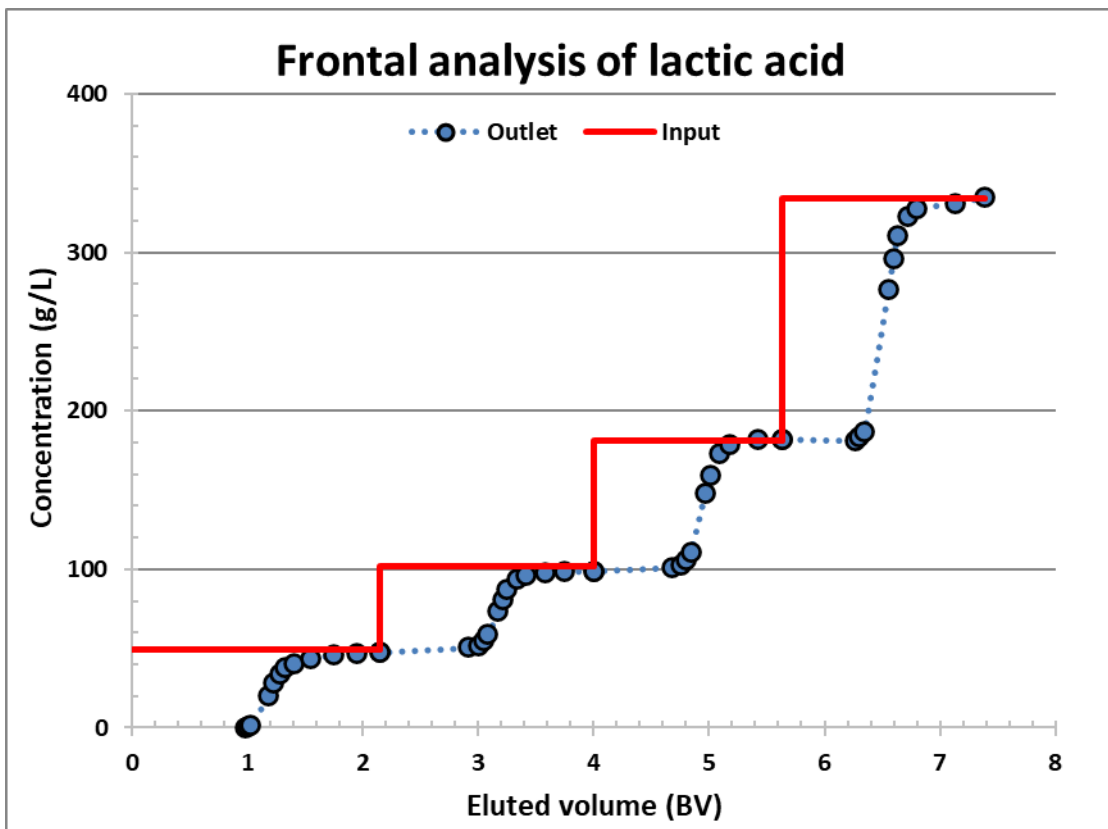
Appendix I:

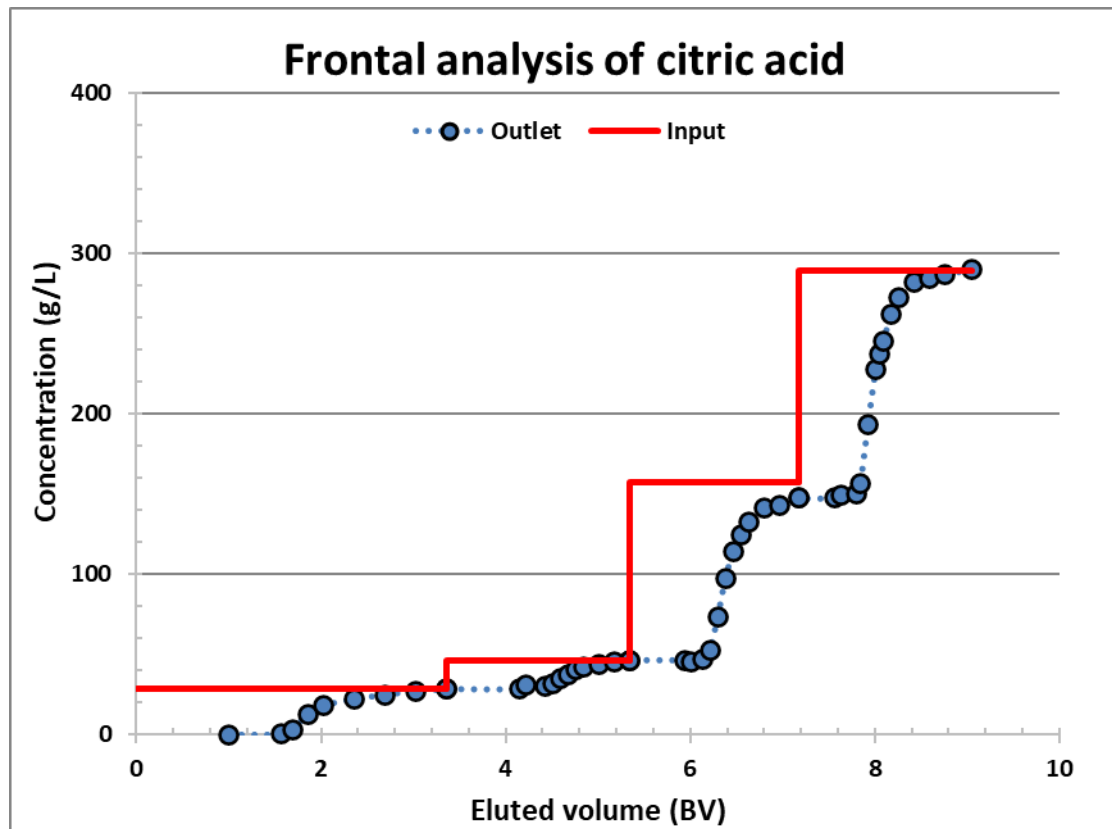
Frontal analysis curves and isotherms





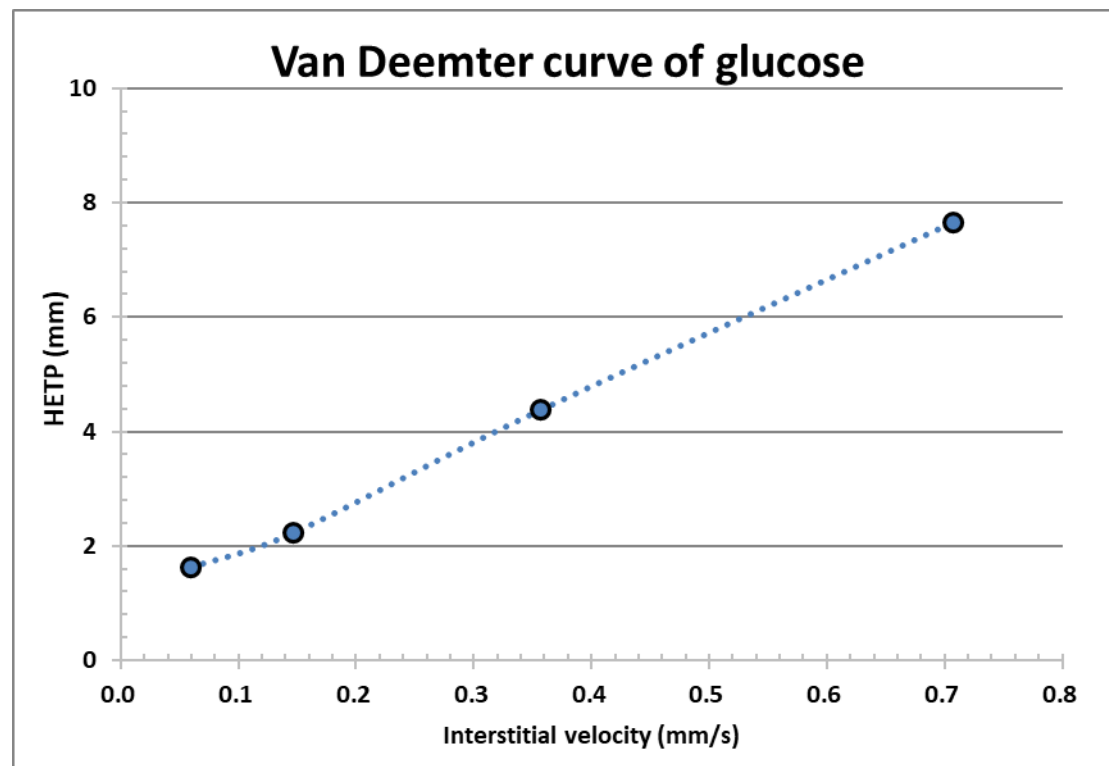
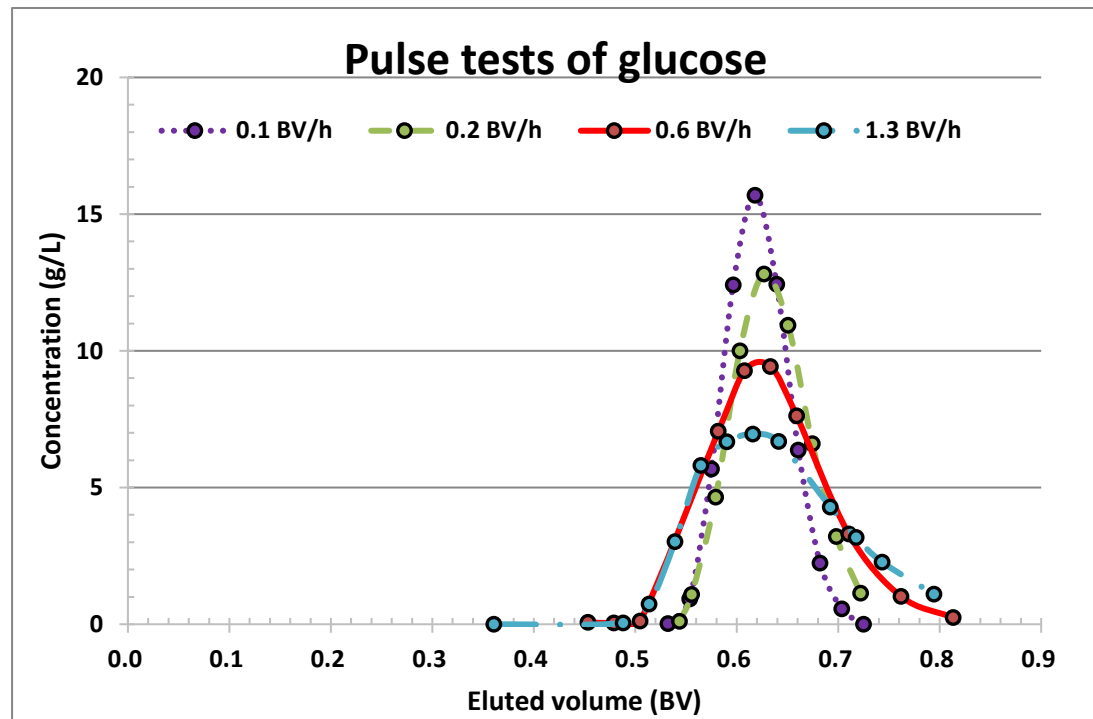


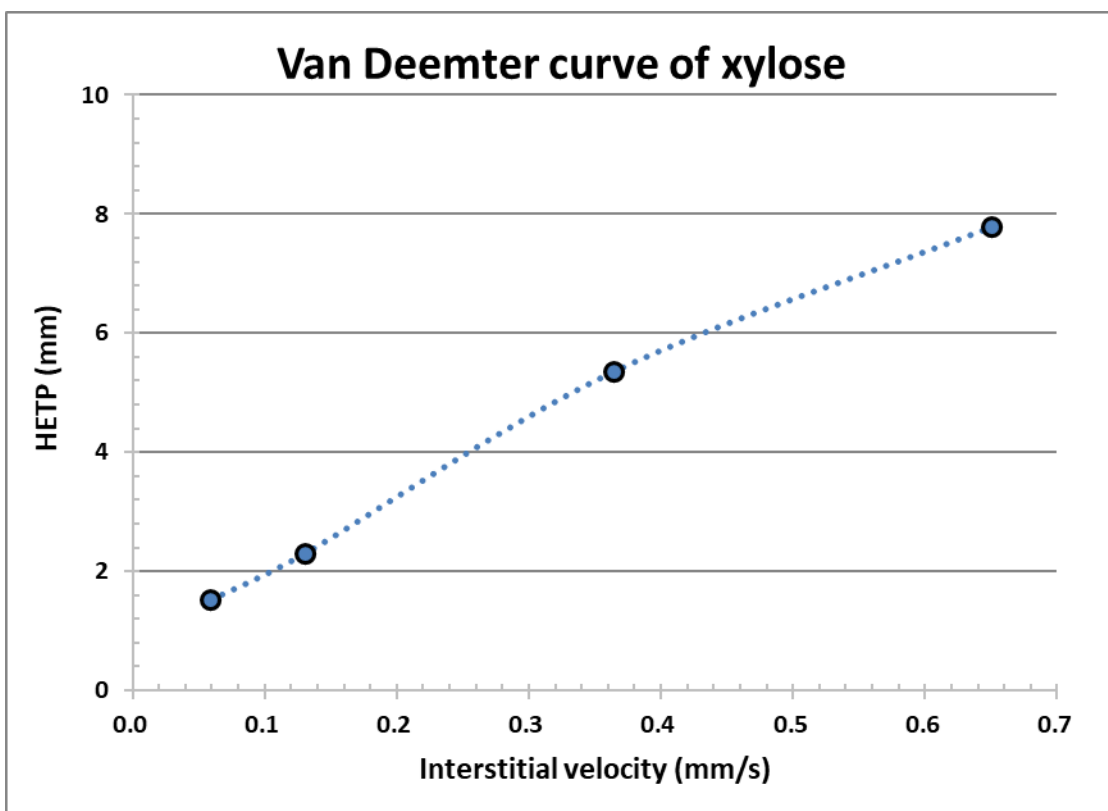
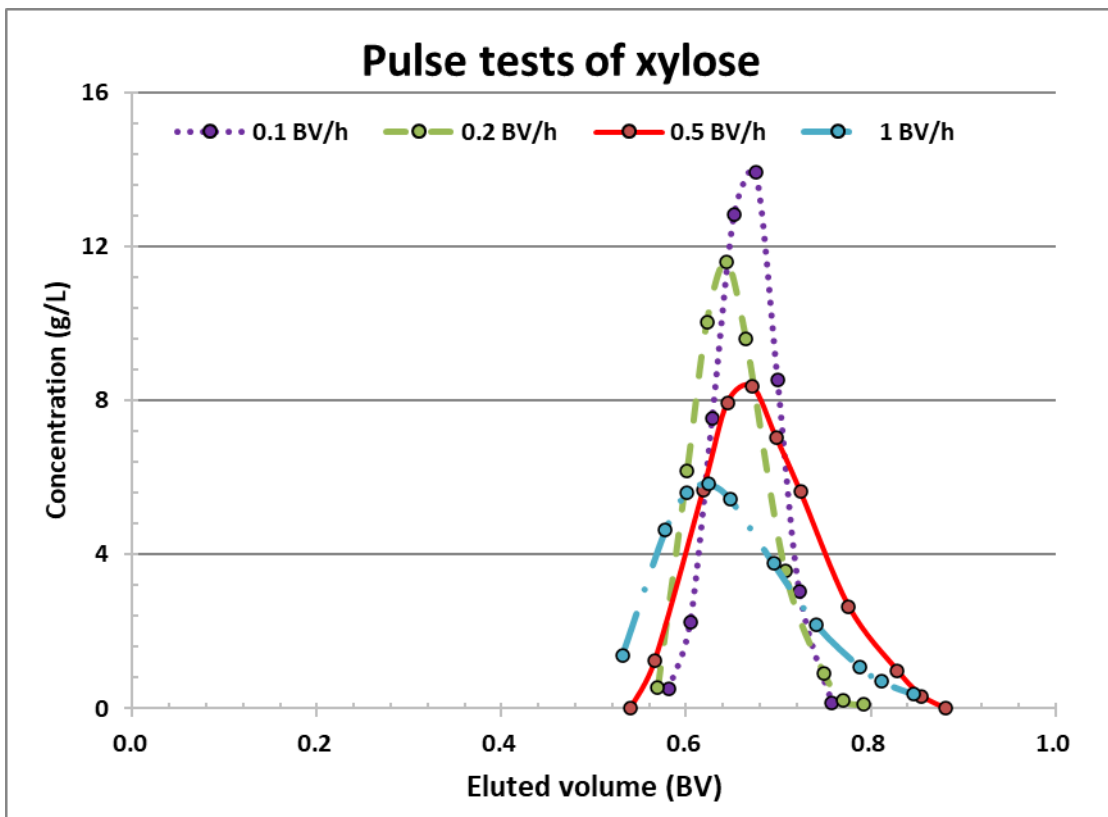


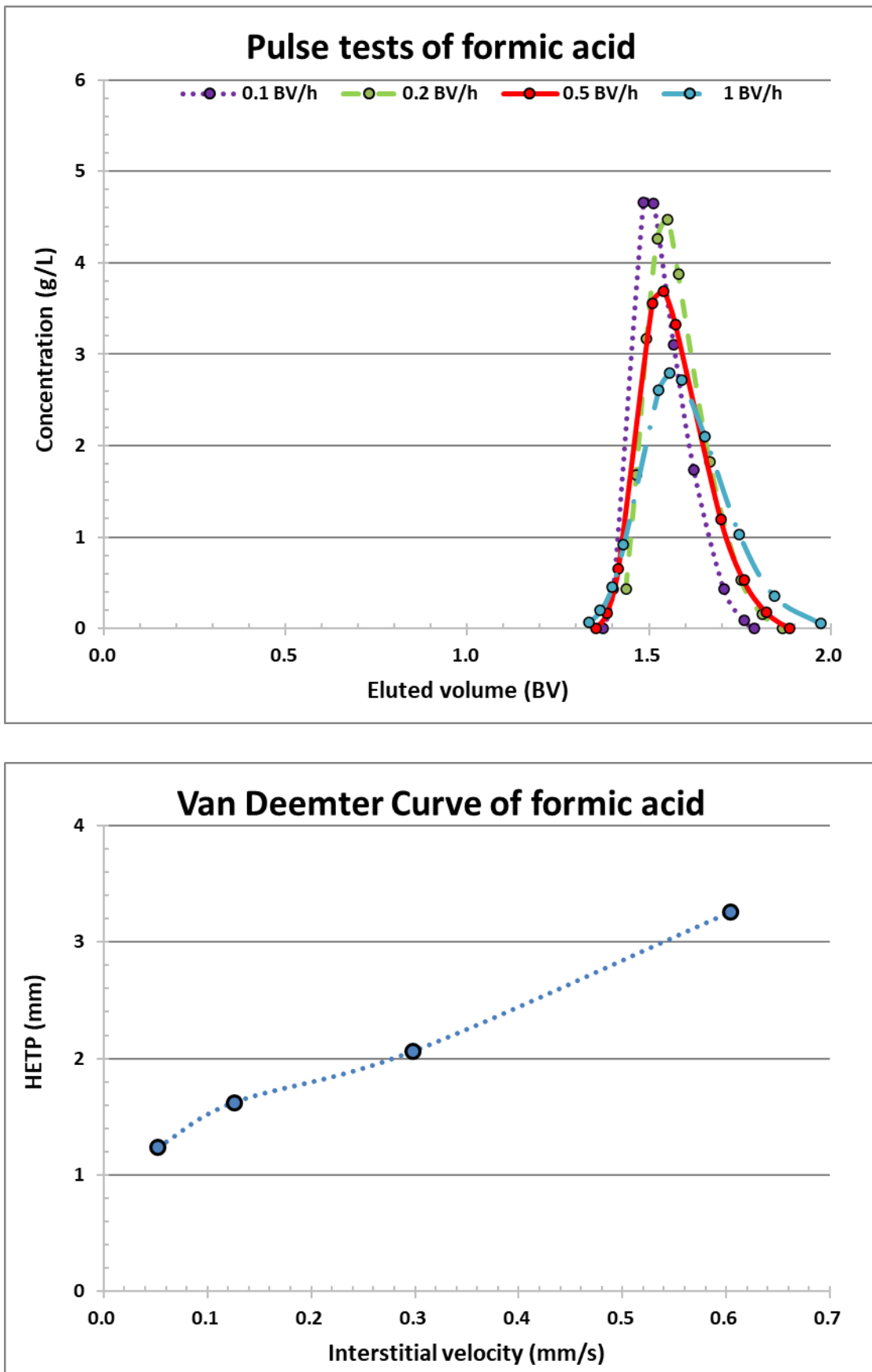


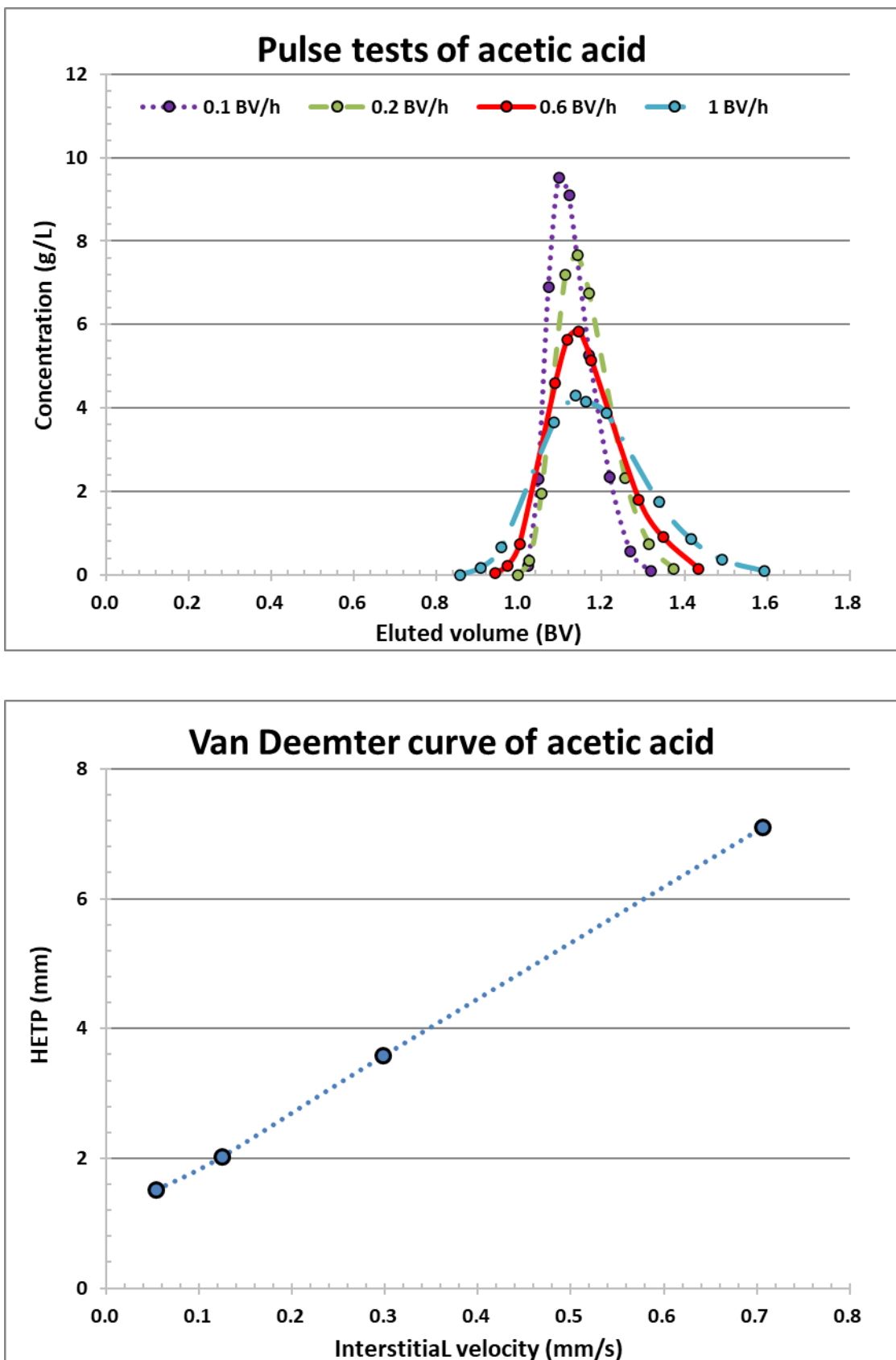
Appendix II:

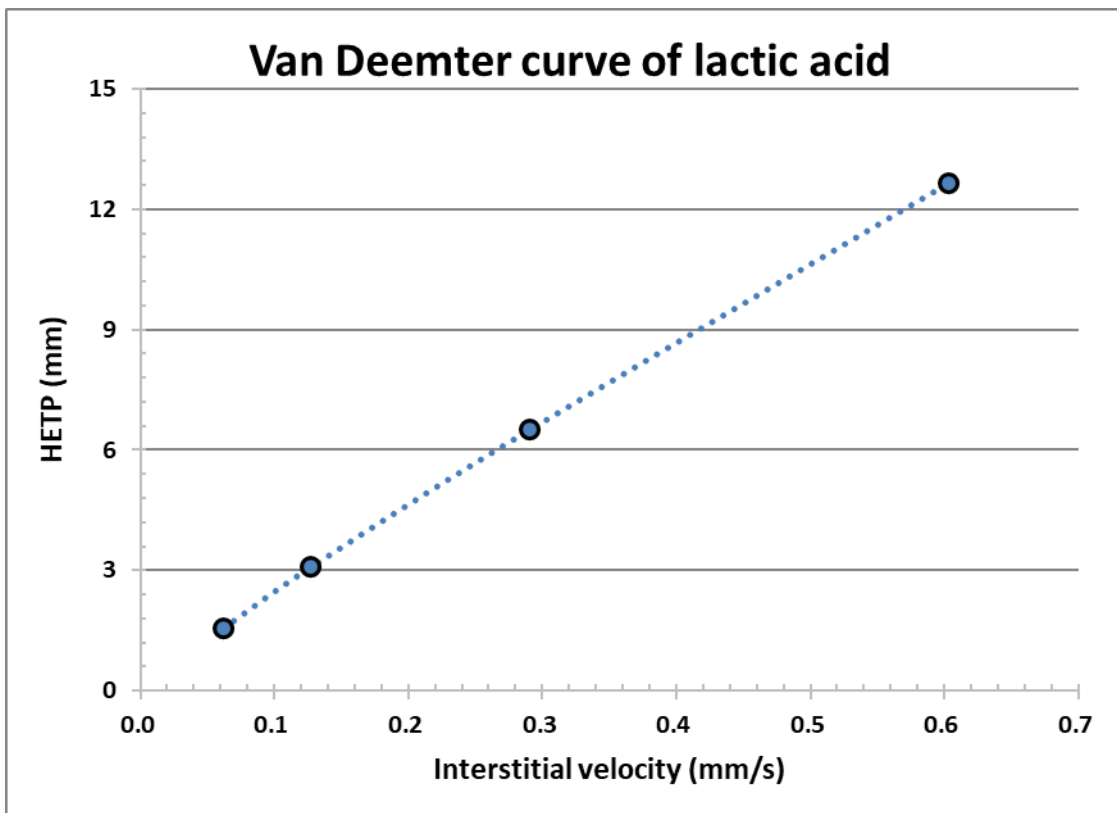
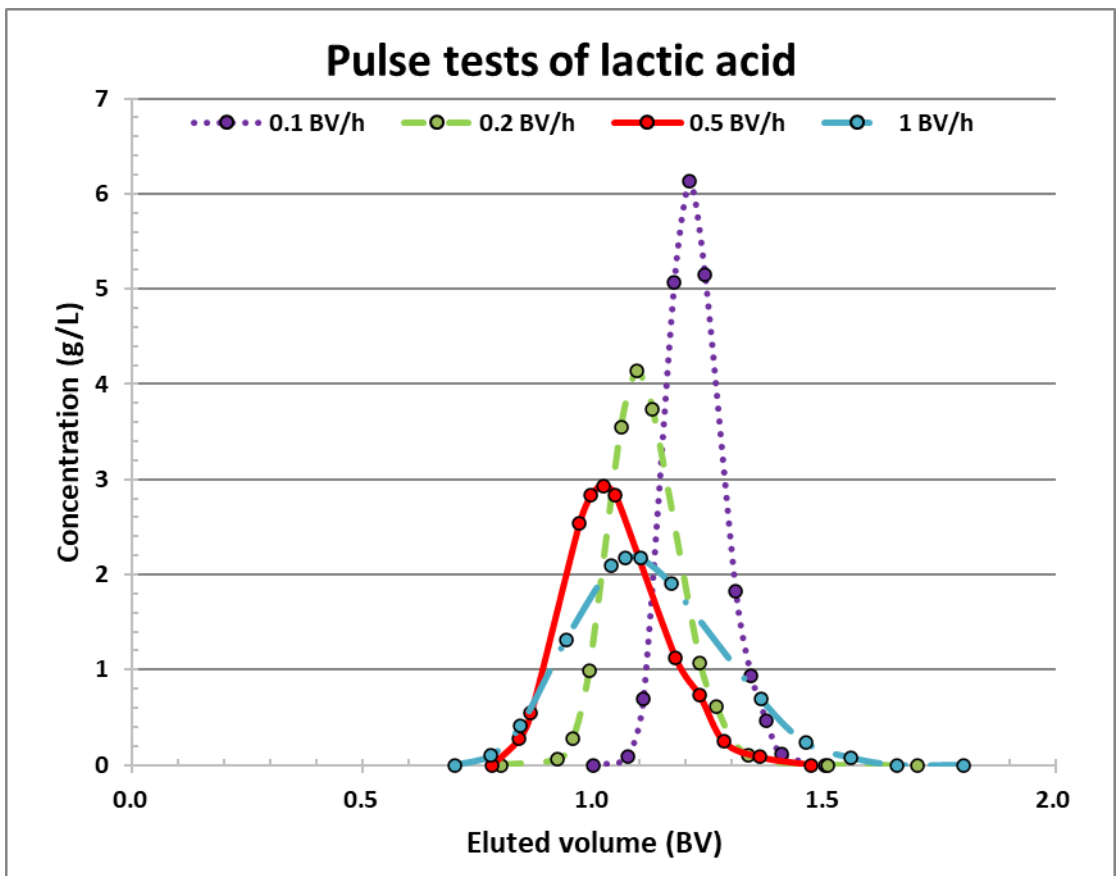
Pulse tests and van Deemter curves:

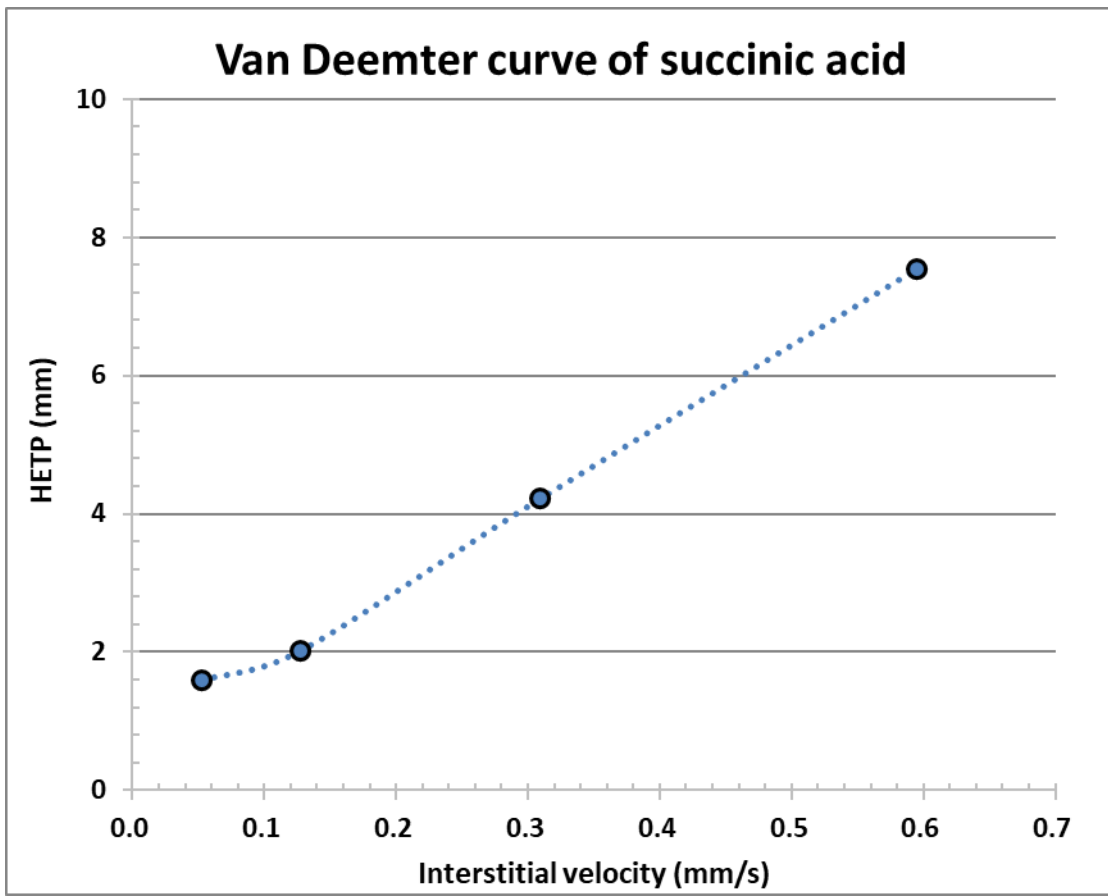
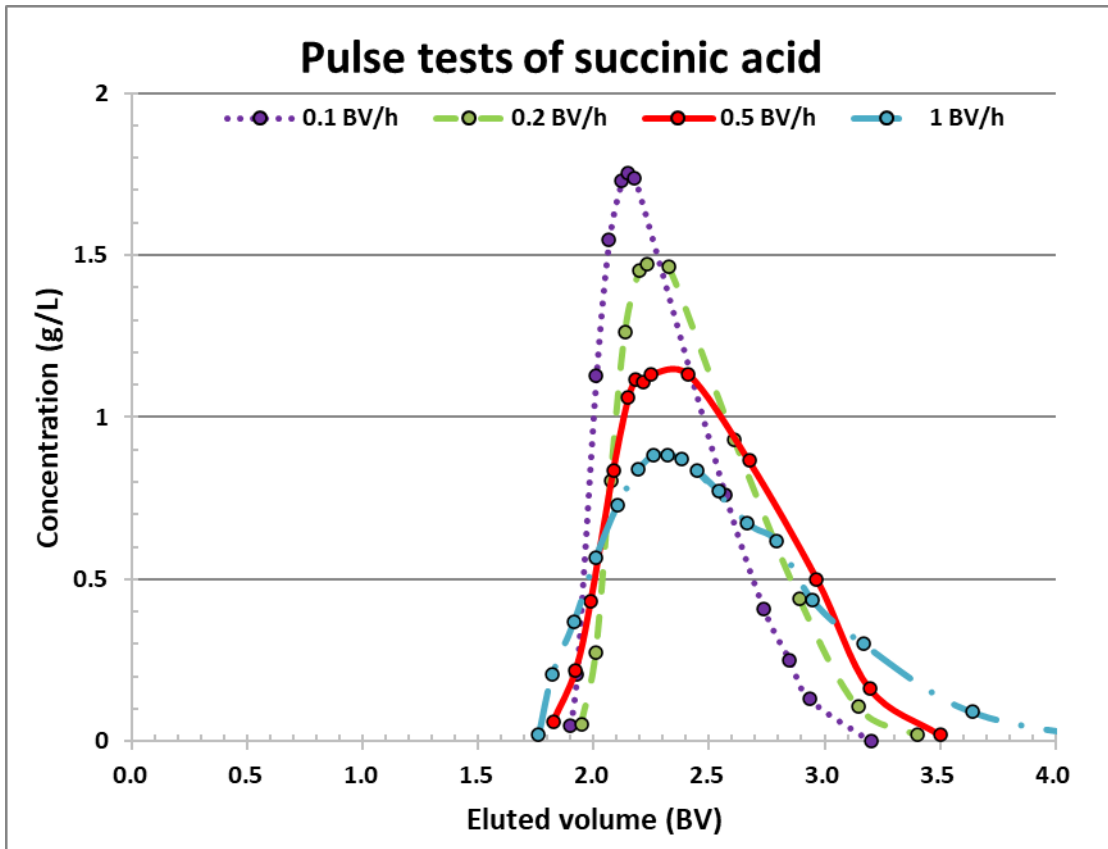


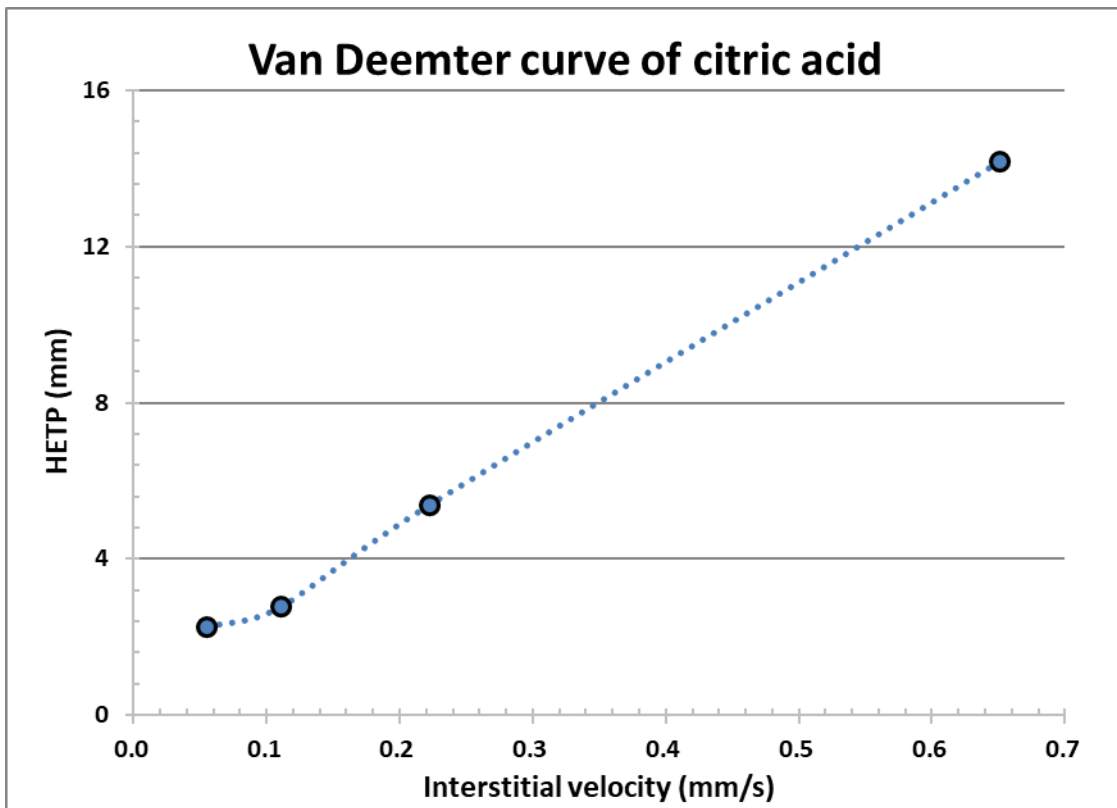
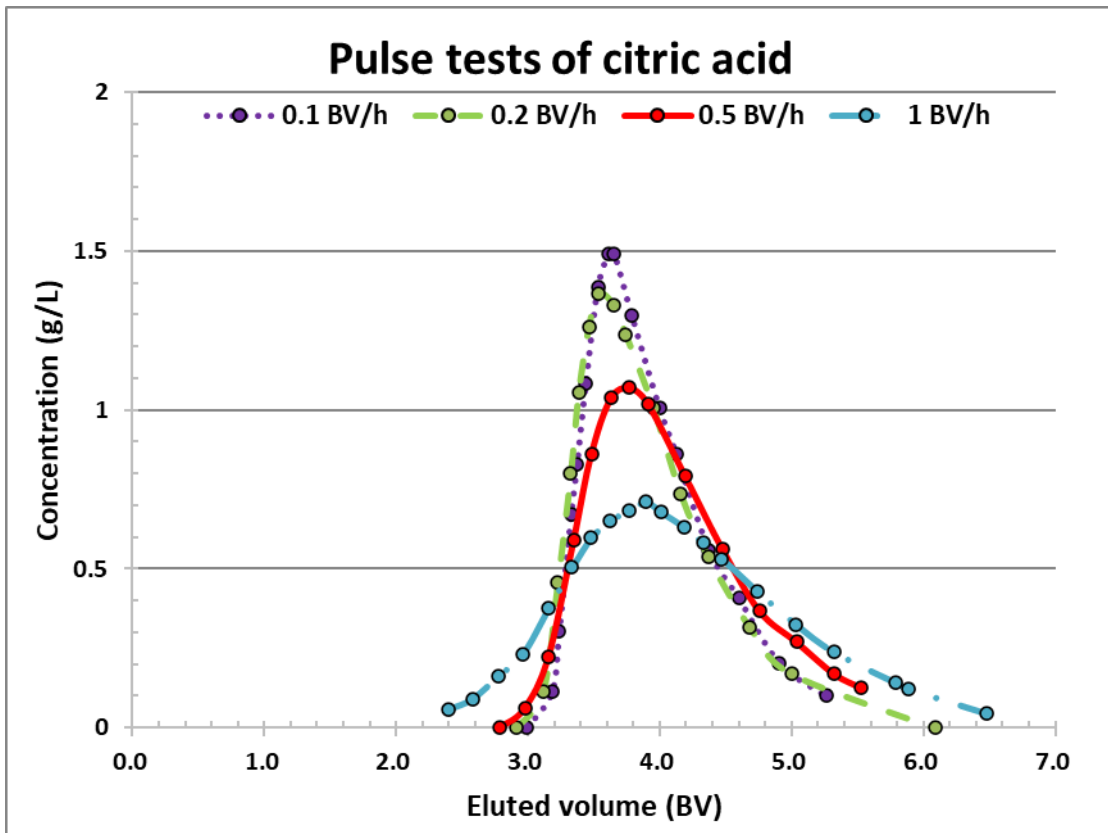












Appendix III:

SBA (strong base anion) resin selectivity coefficients

Ion	Type 1	Type 2
$HSiO_3^-$	<1.0	<1.0
OH^-	1.0	1.0
F^-	1.6	0.3
$CH_3CH_2COO^-$	2.6	0.3
CH_3COO^-	3.2	0.5
$HCOO^-$	4.6	0.5
$H_2PO_4^-$	5.0	0.5
IO_3^-	5.5	0.5
HCO_3^-	6.0	1.2
Cl^-	22	2.3
NO_2^-	24	3
BrO_3^-	27	3
HSO_3^-	27	3
CN^-	28	3
HSO_4^-	35	9
Br^-	50	6
NO_3^-	65	8
ClO_3^-	74	12
Phenate	110	27
SO_4^{2-}	150	/
I^-	175	17
SeO_4^{2-}	280	/
Citrate	220	23
ClO_4^-	>500	/
CrO_4^{2-}	1700	/
$C_6H_5SO_3^-$	>500	75

Source: Ion Exchange Resins Selectivity, DuPont, Form No. 45-D01458-en, Rev. 2 November 2019;
DOWEX™ Ion Exchange Resins Technical Information, Form No. 177-01755-0207

Appendix IV:

CE/SE method proof

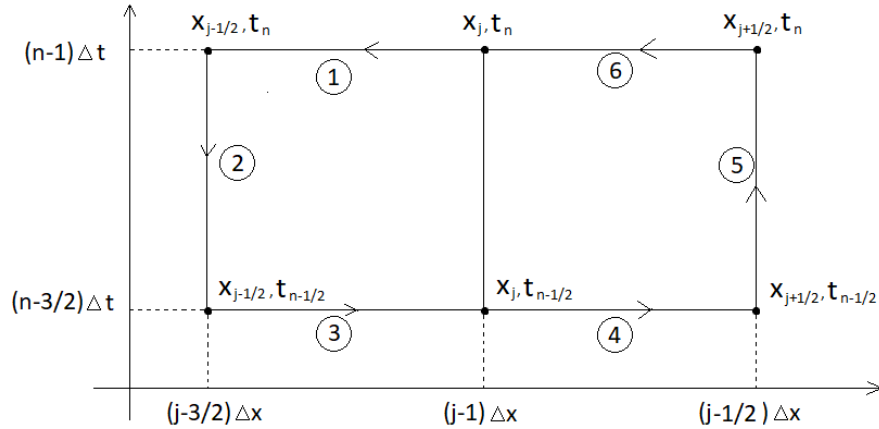


Figure 1. Integral steps for the linear integral term

For PDE like

$$\frac{\partial u}{\partial t} + \frac{\partial f}{\partial x} = p$$

The Green's theorem tells that the line integral along a closed curve ∂C of a function equals to the integral of the derivative over the corresponding plane region ∂D :

$$\oint_{\partial C} (-u \cdot dx + f \cdot dt) = \iint_{\partial D} \left(\frac{\partial u}{\partial t} + \frac{\partial f}{\partial x} \right) \cdot dx \cdot dt = \iint_{\partial D} p \cdot dx \cdot dt$$

Starting from point (j,n) , the $\oint_{\partial C} (-u \cdot dx + f \cdot dt)$ is the sum of integral over 6 segments counterclockwise as shown in figure above:

$$\oint_{\partial C} (-u \cdot dx + f \cdot dt) = ① + ② + ③ + ④ + ⑤ + ⑥ = \iint_{\partial D} p \cdot dx \cdot dt$$

Integrals over each segment are calculated separately.

In this work u and f values were approximated by a first-order Taylor formula from its center point (j,n) :

$$u^*(x, t) \sim u_j^n + u_{x_j}^n \cdot (x - x_j) + u_{t_j}^n \cdot (t - t_n)$$

$$f^*(x, t) \sim f_j^n + f_{x_j}^n \cdot (x - x_j) + f_{t_j}^n \cdot (t - t_n)$$

Meanwhile, a zero-order Taylor formula was chosen to approximate the source term p , which means that p value was treated as a constant in each solution element:

$$p^*(x, t) \sim p_j^n$$

Appendices

Integral (1) :

$$\begin{aligned}
 \int_{(j-1)\Delta x}^{(j-\frac{3}{2})\Delta x} -udx + fdt &= \int_{(j-1)\Delta x}^{(j-\frac{3}{2})\Delta x} -udx = \int_{(j-1)\Delta x}^{(j-\frac{3}{2})\Delta x} -(u_j^n + u_{x_j}^n \cdot (x - x_j) + u_{t_j}^n \cdot (t - t_n))dx \\
 &= \int_{(j-1)\Delta x}^{(j-\frac{3}{2})\Delta x} -(u_j^n + u_{x_j}^n \cdot (x - (j-1)\Delta x))dx \\
 &= -u_j^n \cdot \int_{(j-1)\Delta x}^{(j-\frac{3}{2})\Delta x} dx - u_{x_j}^n \cdot \int_{(j-1)\Delta x}^{(j-\frac{3}{2})\Delta x} (x - (j-1)\Delta x)dx = \frac{\Delta x}{2} \cdot u_j^n - \frac{\Delta x^2}{8} \cdot u_{x_j}^n
 \end{aligned}$$

Integral (2) :

$$\begin{aligned}
 \int_{(n-1)\Delta t}^{(n-\frac{3}{2})\Delta t} -udx + fdt &= \int_{(n-1)\Delta t}^{(n-\frac{3}{2})\Delta t} fdt = \int_{(n-1)\Delta t}^{(n-\frac{3}{2})\Delta t} f_{j-\frac{1}{2}}^{n-\frac{1}{2}} + f_x^{n-\frac{1}{2}} \cdot (x - x_{j-\frac{1}{2}}) + f_t^{n-\frac{1}{2}} \cdot (t - t_{n-\frac{1}{2}}) dt \\
 &= \int_{(n-1)\Delta t}^{(n-\frac{3}{2})\Delta t} f_{j-\frac{1}{2}}^{n-\frac{1}{2}} + f_t^{n-\frac{1}{2}} \cdot (t - t_{n-\frac{1}{2}}) dt \\
 &= f_{j-\frac{1}{2}}^{n-\frac{1}{2}} \cdot \int_{(n-1)\Delta t}^{(n-\frac{3}{2})\Delta t} dt + f_t^{n-\frac{1}{2}} \cdot \int_{(n-1)\Delta t}^{(n-\frac{3}{2})\Delta t} (t - (n - \frac{3}{2})\Delta t) dt \\
 &= -\frac{\Delta t}{2} \cdot f_{j-\frac{1}{2}}^{n-\frac{1}{2}} - \frac{\Delta t^2}{8} \cdot f_t^{n-\frac{1}{2}}
 \end{aligned}$$

Integral (3) :

$$\begin{aligned}
 \int_{(j-\frac{3}{2})\Delta x}^{(j-1)\Delta x} -udx + fdt &= \int_{(j-\frac{3}{2})\Delta x}^{(j-1)\Delta x} -udx \\
 &= \int_{(j-\frac{3}{2})\Delta x}^{(j-1)\Delta x} -(u_{j-1/2}^{n-1/2} + u_{x_{j-1/2}}^{n-1/2} \cdot (x - x_{j-1/2}) + u_{t_{j-1/2}}^{n-1/2} \cdot (t - t_{n-1/2}))dx \\
 &= \int_{(j-\frac{3}{2})\Delta x}^{(j-1)\Delta x} - \left(u_{j-1/2}^{n-1/2} + u_{x_{j-\frac{1}{2}}}^{n-\frac{1}{2}} \cdot (x - x_{j-\frac{1}{2}}) \right) dx \\
 &= -u_{j-\frac{1}{2}}^{n-\frac{1}{2}} \cdot \int_{(j-\frac{3}{2})\Delta x}^{(j-1)\Delta x} dx - u_{x_{j-\frac{1}{2}}}^{n-\frac{1}{2}} \cdot \int_{(j-\frac{3}{2})\Delta x}^{(j-1)\Delta x} (x - (j - \frac{3}{2})\Delta x) dx \\
 &= -\frac{\Delta x}{2} \cdot u_{j-\frac{1}{2}}^{n-\frac{1}{2}} - \frac{\Delta x^2}{8} \cdot u_{x_{j-\frac{1}{2}}}^{n-\frac{1}{2}}
 \end{aligned}$$

Appendices

Integral (4):

$$\begin{aligned}
 \int_{(j-1)\Delta x}^{(j-1/2)\Delta x} -udx + fdt &= \int_{(j-1)\Delta x}^{(j-1/2)\Delta x} -udx \\
 &= \int_{(j-1)\Delta x}^{(j-1/2)\Delta x} -(u_{j+1/2}^{n-1/2} + u_{x_{j+1/2}}^{n-1/2} \cdot (x - x_{j+1/2}) + u_{t_{j+1/2}}^{n-1/2} \cdot (t - t_{n-1/2})) dx \\
 &= \int_{(j-1)\Delta x}^{(j-1/2)\Delta x} -\left(u_{j+1/2}^{n-1/2} + u_{x_{j+1/2}}^{n-1/2} \cdot (x - x_{j+1/2})\right) dx \\
 &= -u_{j+1/2}^{n-1/2} \cdot \int_{(j-1)\Delta x}^{(j-1/2)\Delta x} dx - u_{x_{j+1/2}}^{n-1/2} \cdot \int_{(j-1)\Delta x}^{(j-1/2)\Delta x} (x - (j - \frac{1}{2})\Delta x) dx \\
 &= -\frac{\Delta x}{2} \cdot u_{j+1/2}^{n-1/2} + \frac{\Delta x^2}{8} \cdot u_{x_{j+1/2}}^{n-1/2}
 \end{aligned}$$

Integral (5):

$$\begin{aligned}
 \int_{(n-\frac{3}{2})\Delta t}^{(n-1)\Delta t} -udx + fdt &= \int_{(n-\frac{3}{2})\Delta t}^{(n-1)\Delta t} fdt = \int_{(n-\frac{3}{2})\Delta t}^{(n-1)\Delta t} f_{j+1/2}^{n-1/2} + f_{x_{j+1/2}}^{n-1/2} \cdot (x - x_{j+1/2}) + f_{t_{j+1/2}}^{n-1/2} \cdot (t - t_{n-1/2}) dt \\
 &= \int_{(n-\frac{3}{2})\Delta t}^{(n-1)\Delta t} f_{j+1/2}^{n-1/2} + f_{t_{j+1/2}}^{n-1/2} \cdot (t - t_{n-1/2}) dt \\
 &= f_{j+1/2}^{n-1/2} \cdot \int_{(n-\frac{3}{2})\Delta t}^{(n-1)\Delta t} dt + f_{t_{j+1/2}}^{n-1/2} \cdot \int_{(n-\frac{3}{2})\Delta t}^{(n-1)\Delta t} (t - (n - \frac{3}{2})\Delta t) dt = \frac{\Delta t}{2} \cdot f_{j+1/2}^{n-1/2} + \frac{\Delta t^2}{8} \cdot f_{t_{j+1/2}}^{n-1/2}
 \end{aligned}$$

Integral (6):

$$\begin{aligned}
 \int_{(j-\frac{1}{2})\Delta x}^{(j-1)\Delta x} -udx + fdt &= \int_{(j-\frac{1}{2})\Delta x}^{(j-1)\Delta x} -udx = \int_{(j-\frac{1}{2})\Delta x}^{(j-1)\Delta x} -\left(u_j^n + u_{x_j}^n \cdot (x - x_j) + u_{t_j}^n \cdot (t - t_n)\right) dx \\
 &= \int_{(j-\frac{1}{2})\Delta x}^{(j-1)\Delta x} -\left(u_j^n + u_{x_j}^n \cdot (x - x_j)\right) dx \\
 &= -u_j^n \cdot \int_{(j-\frac{1}{2})\Delta x}^{(j-1)\Delta x} dx - u_{x_j}^n \cdot \int_{(j-\frac{1}{2})\Delta x}^{(j-1)\Delta x} (x - x_j) dx = \frac{\Delta x}{2} \cdot u_j^n + \frac{\Delta x^2}{8} \cdot u_{x_j}^n
 \end{aligned}$$

The p in the source term is approximated by zero order Taylor's formular at point $(x_{j-1/2}, t_{n-1/2})$ and $(x_{j+1/2}, t_{n-1/2})$

$$\iint_{\partial D} p \cdot dx \cdot dt = \frac{\Delta x \Delta t}{4} \left(p_{j-\frac{1}{2}}^{n-1/2} + p_{j+\frac{1}{2}}^{n-1/2} \right)$$

Appendices

By summing up ① to ⑥ we have :

$$\begin{aligned}
 \oint_{\partial C} (-u \cdot dx + f \cdot dt) &= ① + ② + ③ + ④ + ⑤ + ⑥ \\
 &= \frac{\Delta x}{2} \cdot \mathbf{u}_j^n - \frac{\Delta x^2}{8} \cdot u_{x,j}^{n-\frac{1}{2}} - \frac{\Delta t}{2} \cdot f_{j-\frac{1}{2}}^{n-\frac{1}{2}} - \frac{\Delta t^2}{8} \cdot f_t_{j-\frac{1}{2}}^{n-\frac{1}{2}} - \frac{\Delta x}{2} \cdot u_{j-\frac{1}{2}}^{n-\frac{1}{2}} - \frac{\Delta x^2}{8} \cdot u_{x,j-\frac{1}{2}}^{n-\frac{1}{2}} \\
 &\quad - \frac{\Delta x}{2} \cdot u_{j+\frac{1}{2}}^{n-\frac{1}{2}} + \frac{\Delta x^2}{8} \cdot u_{x,j+\frac{1}{2}}^{n-\frac{1}{2}} + \frac{\Delta t}{2} \cdot f_{j+\frac{1}{2}}^{n-\frac{1}{2}} + \frac{\Delta t^2}{8} \cdot f_t_{j+\frac{1}{2}}^{n-\frac{1}{2}} + \frac{\Delta x}{2} \cdot u_j^n + \frac{\Delta x^2}{8} \cdot u_{x,j}^n \\
 &= \Delta x \cdot \mathbf{u}_j^n - \frac{\Delta x}{2} \cdot u_{j-\frac{1}{2}}^{n-\frac{1}{2}} - \frac{\Delta x}{2} \cdot u_{j+\frac{1}{2}}^{n-\frac{1}{2}} - \frac{\Delta t}{2} \cdot f_{j-\frac{1}{2}}^{n-\frac{1}{2}} - \frac{\Delta t^2}{8} \cdot f_t_{j-\frac{1}{2}}^{n-\frac{1}{2}} - \frac{\Delta x^2}{8} \cdot u_{x,j-\frac{1}{2}}^{n-\frac{1}{2}} \\
 &\quad + \frac{\Delta x^2}{8} \cdot u_{x,j+\frac{1}{2}}^{n-\frac{1}{2}} + \frac{\Delta t}{2} \cdot f_{j+\frac{1}{2}}^{n-\frac{1}{2}} + \frac{\Delta t^2}{8} \cdot f_t_{j+\frac{1}{2}}^{n-\frac{1}{2}} = \iint_D p \cdot dx \cdot dt = \frac{\Delta x \Delta t}{4} \left(p_{j-\frac{1}{2}}^{n-\frac{1}{2}} + p_{j+\frac{1}{2}}^{n-\frac{1}{2}} \right)
 \end{aligned}$$

After some arrangements the following expression which allows us to obtain value of u_j^n from known values at point $(x_{j-1/2}, t_{n-1/2})$ and $(x_{j+1/2}, t_{n-1/2})$.

$$\begin{aligned}
 u_j^n &= \frac{1}{2} \cdot \left(u_{j-\frac{1}{2}}^{n-\frac{1}{2}} + u_{j+\frac{1}{2}}^{n-\frac{1}{2}} \right) + \left(\frac{\Delta t}{2\Delta x} \cdot f_{j-\frac{1}{2}}^{n-\frac{1}{2}} + \frac{\Delta x}{8} \cdot u_{x,j-\frac{1}{2}}^{n-\frac{1}{2}} + \frac{\Delta t^2}{8\Delta x} \cdot f_t_{j-\frac{1}{2}}^{n-\frac{1}{2}} - \right) \\
 &\quad - \left(\frac{\Delta t}{2\Delta x} \cdot f_{j+\frac{1}{2}}^{n-\frac{1}{2}} + \frac{\Delta x}{8} \cdot u_{x,j+\frac{1}{2}}^{n-\frac{1}{2}} + \frac{\Delta t^2}{8\Delta x} \cdot f_t_{j+\frac{1}{2}}^{n-\frac{1}{2}} \right) + \frac{\Delta t}{4} \cdot (p_{j-\frac{1}{2}}^{n-\frac{1}{2}} + p_{j+\frac{1}{2}}^{n-\frac{1}{2}})
 \end{aligned}$$

Figure 2 shows the mesh grill used in the program. Every dotted rectangle represents an application of the equations demonstrated above. To obtain values at point (x_j, t_n) from points at (x_{j-1}, t_{n-1}) and (x_{j+1}, t_{n-1}) , intermediate points are firstly calculated. Values at (x_j, t_n) is obtained from two neighbor intermediate points.

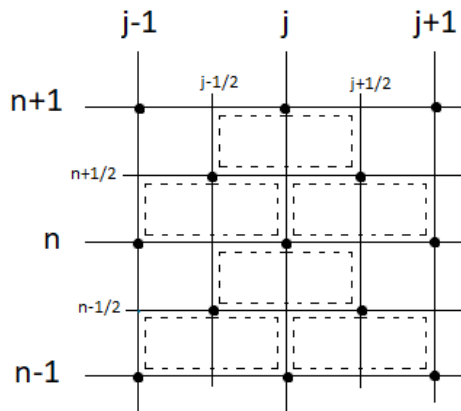
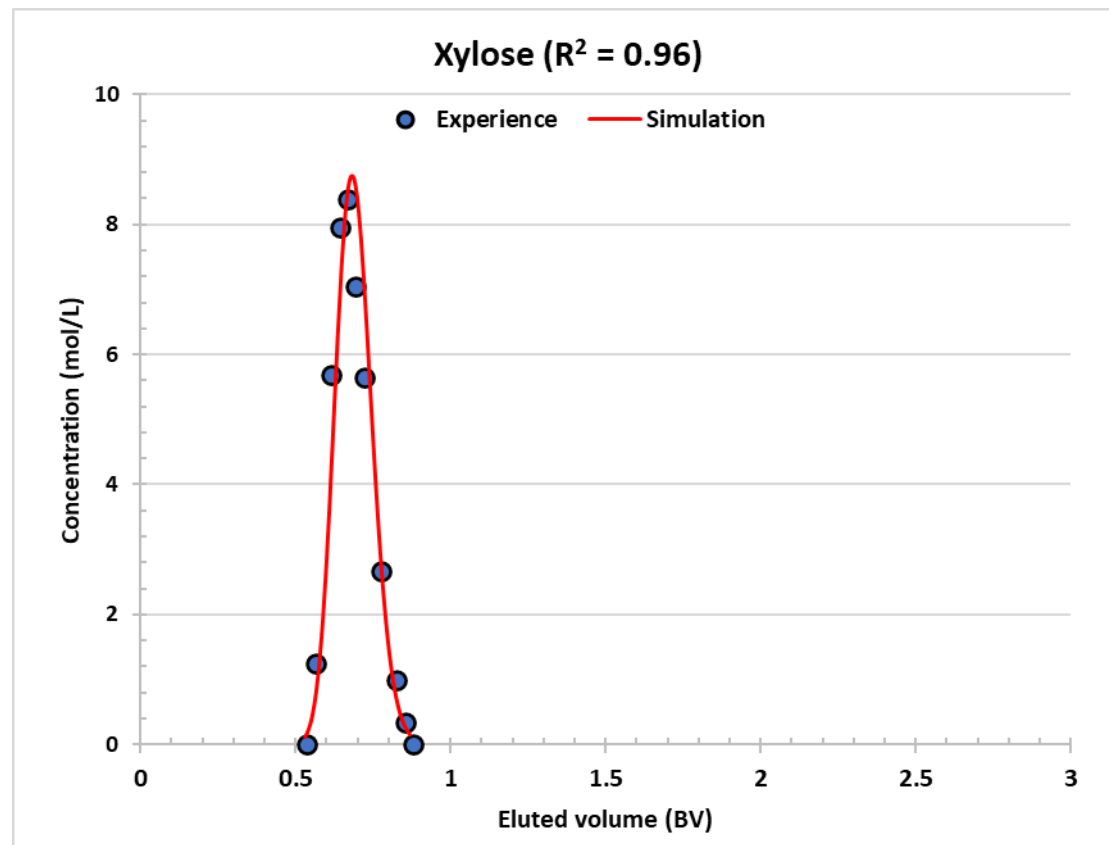
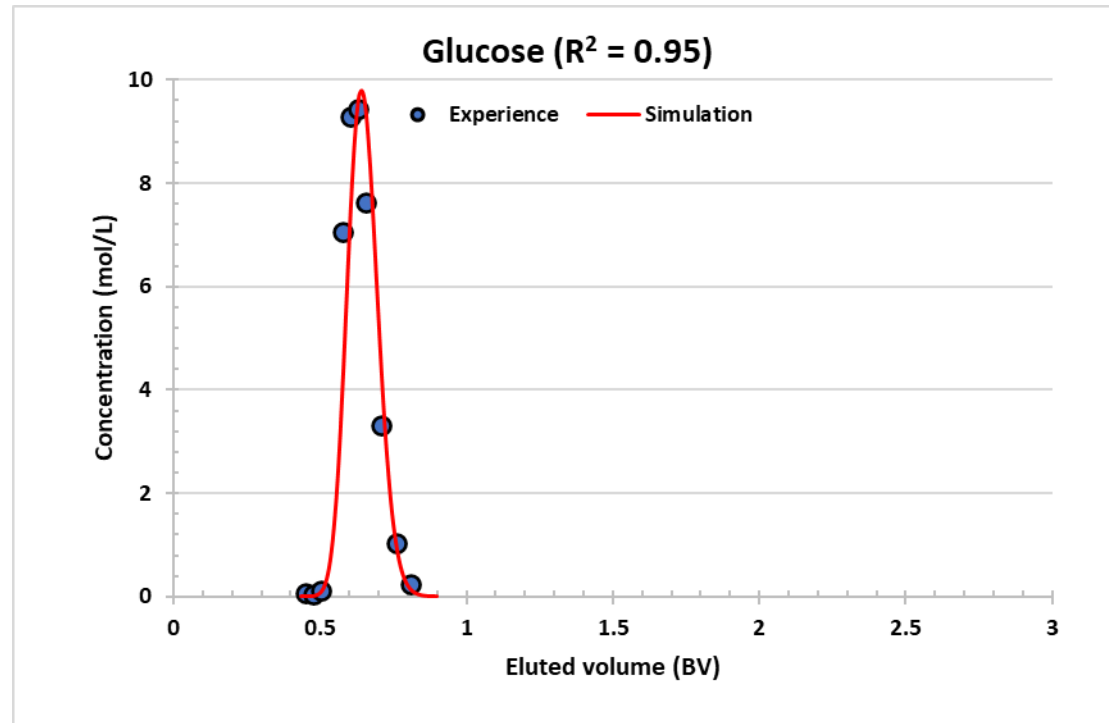


Figure 2. Conservation elements and solution elements in the mesh grill

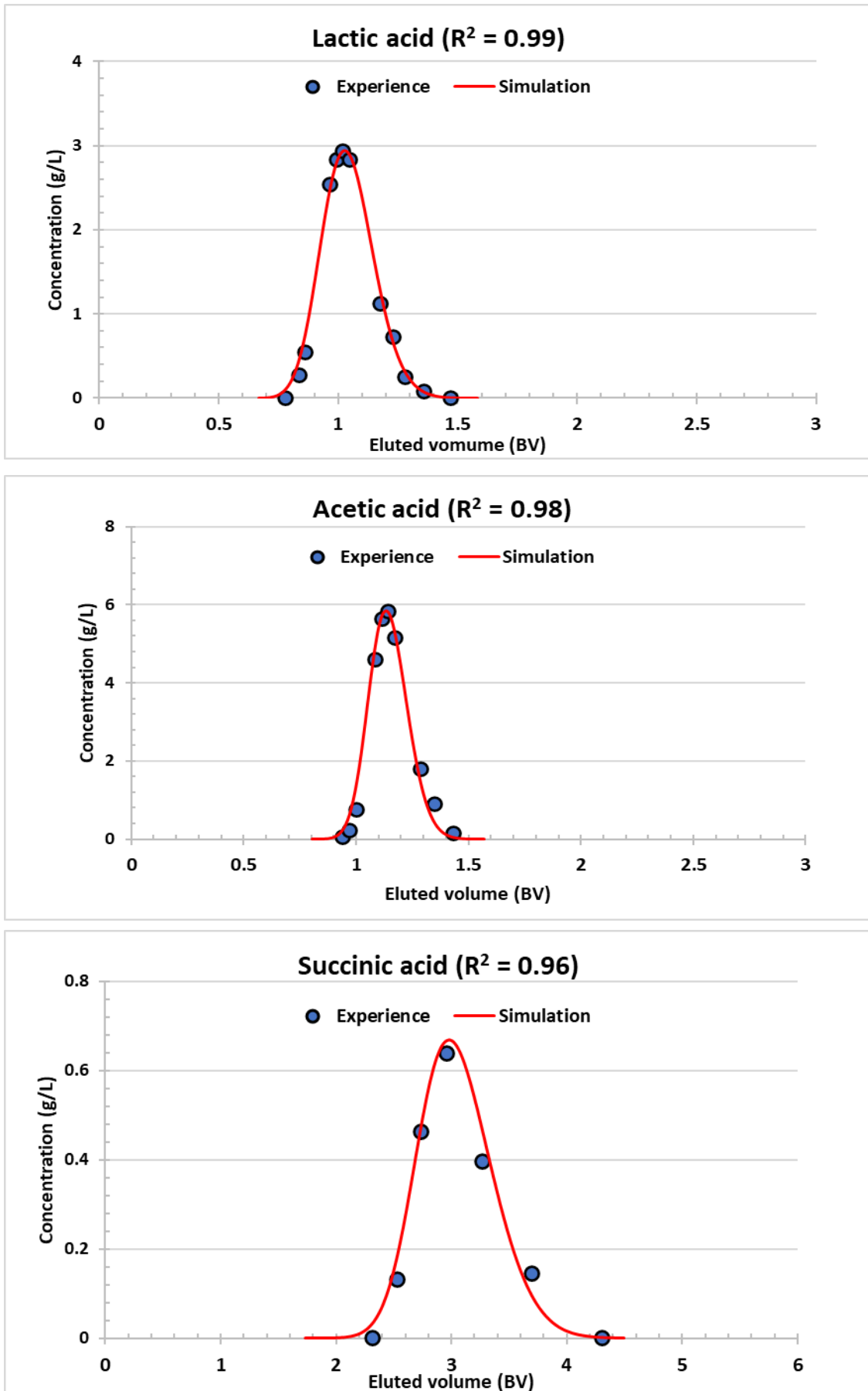
Dotted points are mesh points used during simulation, noticing that by introducing intermediate points, mesh point amount was multiplied by four. However, only 1/3 of intermediate points participated in the calculation.

Appendix V:

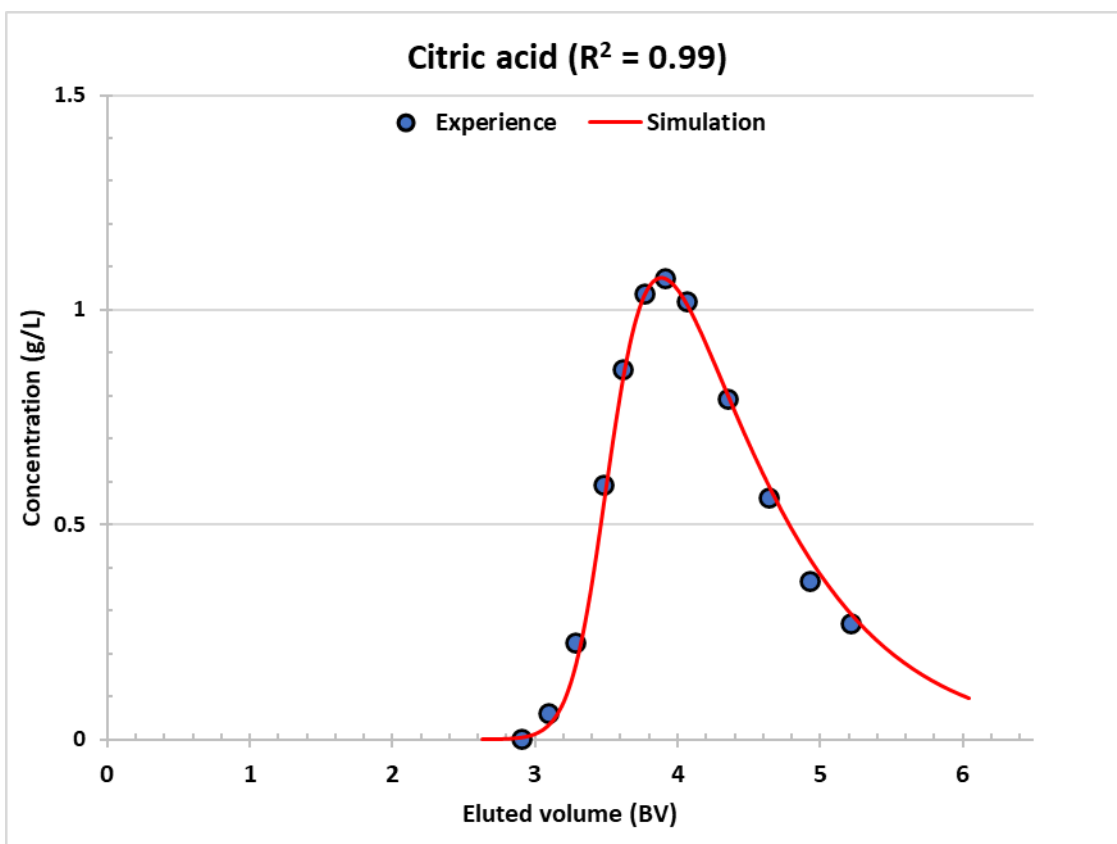
Curve-fitting results



Appendices



Appendices



Appendix VI:

Synthèse de la manuscrit

La chromatographie préparative telle que le SMB est la solution ultime lorsque les techniques de séparation classiques telles que la distillation, l'extraction liquide-liquide, la filtration sur membrane ou la cristallisation ne sont pas suffisamment sélectives ou consomment trop d'énergie, de produits chimiques ou de solvants. Cependant, son application s'accompagne toujours de trois facteurs limitants : une faible productivité, une consommation d'élution élevée et un taux de dilution élevé.

Cette étude vise à évaluer l'utilisation de la chromatographie préparative dans la conception d'un procédé chromatographique multi-colonnes avec une résine échangeuse d'ions anionique forte. Cette étude s'est principalement concentrée sur deux sucres (glucose et xylose) et cinq acides organiques (acides formique, acétique, lactique, succinique et citrique), qui sont des produits valorisables pendant l'hydrolyse et la fermentation de l'hémicellulose.

Le chapitre I comporte 3 parties : Une présentation de la biomasse lignocellulosique, de sa composition et des traitements qui lui sont appliqués. Un état de l'art des techniques de chromatographie et des méthodes mises en oeuvre pour caractériser les colonnes et une présentation d'architectures de procédés de chromatographie préparative. La modélisation de la chromatographie est ensuite détaillée, en commençant par la description du transfert de matière dans deux types de colonnes (continue et discontinue).

Le chapitre II décrit tout d'abord les méthodes et dispositifs expérimentaux mis en oeuvre pour déterminer les paramètres qui sont requis dans les simulations. Dans ce chapitre, un modèle d'adsorption de Langmuir plus détaillé est proposé sur la base de nos travaux théoriques précédents, en supposant que l'adsorption est due à une liaison hydrogène entre les acides organiques et les anions sulfates. Le modèle de Langmuir plus détaillé a ensuite été couplé à un modèle d'échange d'ions pour prédire le profil chromatographique des acides organiques. Les bilans massiques ont été résolu par la méthode CE/SE (conservation element / solution element).

Le chapitre III présente les résultats expérimentaux concernant les propriétés physico-chimiques des composants et les caractéristiques du lit. Des expériences ont été réalisées pour compléter et valider ce modèle (appelé modèle hybride) : Une première étude sur la résine anionique forte a été menée pour mesurer la porosité du lit et la capacité maximale d'échange d'ions. Sa porosité issue de la tomographie a été comparée à la porosité calculée à partir de la distribution du temps de séjour. Ensuite, l'étude thermodynamique de l'adsorption de deux sucres et de cinq acides organiques en solution pure a été réalisée. Elle a révélé un comportement très différent pour les deux types de composés : l'adsorption des sucres est assez linéaire, tandis que celle des acides organiques est fortement non linéaire et suit l'équation de Langmuir.

Appendices

L'influence de la vitesse sur la dispersion et le transfert de masse entre deux phases a été étudiée. Il a été montré que l'efficacité de la colonne diminue linéairement avec la vitesse d'élution, selon le modèle de van Deemter. Les coefficients de dispersion et de transfert de masse ont alors été déduits à partir des paramètres de l'équation de van Deemter.

Le chapitre IV présente des simulations de la colonne de chromatographie et plus spécifiquement des profils de concentration simulés lors d'injection. Des injections avec des solutions synthétiques pures et mixtes ont été étudiées pour évaluer l'influence des paramètres sur les profils chromatographiques, tels que les coefficients de Langmuir, les constantes d'équilibre d'échange d'ions, les coefficients de transfert de masse, etc. Ces valeurs ont ensuite été identifiées par curve-fitting, et le modèle hybride a été validé par une séparation binaire.

Le chapitre V porte sur le développement d'architectures de procédés multi-colonnes de type SMB séquentiel. Le modèle hybride a ensuite été utilisé pour simuler un procédé 3C-ISMB (3 columns improved simulated moving bed) pour la séparation binaire. Le même procédé a également été simulé avec Langmuir modèle pour comparaison. Les résultats ont montré que le modèle de Langmuir n'est pas adapté aux procédés multi-colonnes en présence d'acides organiques avec trainée. Ensuite, la séparation ternaire avec deux ISMB en cascade a été simulée par le modèle hybride.

Enfin, un nouveau procédé 3F4C SSMB (three fractions four columns sequential simulated moving bed) a été optimisé et simulé avec le modèle hybride. Ses performances ont été comparées à celles de deux ISMB en cascade. Les résultats ont montré les performances (productivité, consommation d'éluant et facteur de dilution) du nouveau procédé 3F4C SSMB est mieux.

Ce travail vise à développer un outil numérique fiable qui est censé être implémenté dans un programme de simulation de chromatographie multi-colonnes pour prédire et optimiser les performances des technologies de lit mobile simulé. Nous avons ainsi montré que le modèle hybride prédit les profils chromatographiques et les performances des procédés multi-colonnes avec une meilleure précision. Avec l'aide de cet outil, nous avons également développé un nouveau procédé à lit mobile simulé qui peut séparer trois fractions simultanément avec seulement quatre colonnes (brevet en préparation).